KU LEUVEN

FACULTY OF SCIENCE

UNIVERSITEIT GENT

FACULTY OF SCIENCES

Characterization of spatially variable riverbed hydraulic conductivity using Electrical Resistivity Tomography (ERT) and Induced Polarization (IP)

Sien BENOIT

Supervisor: Prof. Dr. Ir. M. Huysmans
KU Leuven – Vrije Universiteit Brussel

Co-supervisor: Prof. Dr. Ir. F. Nguyen
KU Leuven – Université de Liège

Mentor: Gert Ghysels
Vrije Universiteit Brussel

Thesis presented in fulfillment of the requirements for the degree of Master of Science in Geology (Ghent – Leuven)

Academic year 2016-2017

Preface

This dissertation is about the characterization of heterogeneous hydraulic conductivity in riverbeds with use of two geo-electrical methods, ERT and IP. It frames within research on river – groundwater interaction, a currently, hot topic in the hydrogeological world. I wrote this thesis as a completion of my MSc of Geology and worked on it during the academic year of 2016 – 2017. I enjoyed exploring and deepening into hydrogeological and geophysical research, which, I believe, will also benefit in my future professional career. Therefore, I want to kindly thank my supervisor Prof. Marijke Huysmans and co-supervisor Prof. Frédéric Nguyen for introducing me in the subject, helping me to give direction to the project, for their feedback and tips, which made me learn and improve my understanding in these specific fields.

I am very thankful to Gert Ghysels, who helped me with data analyses, assisted in the geophysical field work and provided data of his own hydrogeological field work. I strongly appreciate how he was always ready with fast and clear answers on my – sometimes overload of – questions. Thanks goes to Thomas Hermans, who helped with data acquisition and inversion of geophysical data. I would also like to thank Kevin Gommers. Because our subjects were closely related, it was very useful to have each other's help and second opinion. We could work together in the data acquisition and for some data analyses, as well as support one another when things did not work out how we hoped for. I am grateful to Gaël Dumont and Eric Van Beek for helping in preparation of or during the field work.

Special thanks go to Tuur Benoit and Lien Decruy for proofreading my dissertation and providing me useful tips and feedback. Of course, I would like to express my profound gratitude to my parents, Lode Benoit and Door Sercu, who gave me unqualified support during my complete studies. They encouraged me in hard periods, listened to my stories and issues, and supported me in all my decisions. They always helped to look for solutions, and kept me always enthusiastic. Likewise, I want to thank my brothers Tuur, Jef and Sus, as well as my sisters-in-law, Lien and Sarah, for their feedback during the making of this thesis. Moreover, they gave me mental support and were always ready to listen or to give advice.

I would also like to acknowledge my fellow geology students, who became close friends throughout these five years I stayed in Leuven. Together, we experienced an unforgettable time in the lovely city of Leuven. I am also thankful to my friends of secondary school. In our weekly meet-ups, we could all relieve our worries about our thesis, support each other and especially, relax, chat and forget our work for a moment. Also other close friends, such as Sofie Messely and Elias Strassmann, were important to me during this year of thesis work. They let me release my issues, frustrations or satisfaction with my work. Thanks goes to my friends I met during my Erasmus semester in Zürich. The few reunions provided unforgettable weekends between weeks of hard work. In addition, five months of experience abroad gave me insight into which domains of geology most appeal to me, leading me to the thesis I have written, and which I hope you enjoy reading.

Sien Benoit

Leuven, 6 June 2017

Summary

This Master's thesis is about the characterization of spatial variability of hydraulic conductivity (K) in a riverbed using electrical resistivity tomography (ERT) and induced polarization (IP). Hydraulic conductivity is an important hydrogeological parameter, which describes how easily water flows through the pore space in sediment. It can be very heterogeneously distributed, not only on a wide scale, but also on a local scale such as a riverbed. Therefore, visualization of the spatial distribution of K in riverbeds is important because it can improve the understanding of river – groundwater interaction, as well as groundwater models. In this thesis, two geo-electrical methods are investigated in their capability to characterize hydraulic conductivity in a riverbed. Hence, a link between electrical properties of the subsurface and hydraulic conductivity is sought. If correlation is present, the extent of application is examined, by assessing its predictability.

The site of investigation in this study is 25 m long and 15 m wide and is situated in the Aa river, a lowland river in Northern Belgium. The riverbed is mainly composed of sand, with variable amounts of clay and organic matter. First, slug tests are performed to obtain hydraulic conductivity data. Next, ERT and IP measurements are made, which result in inverted profiles of resistivity (ρ), chargeability (M) and normalized chargeability (MN) in the riverbed. Resistivity is a measure for how difficult electrical current can flow through the medium. Chargeability describes how well electrical energy can be stored in the subsurface. Normalized chargeability is obtained by dividing chargeability by resistivity. In this way, it is made independent of bulk conductive properties. Lastly, drillings are performed in the riverbed to obtain lithological information. After data acquisition, linkage of hydrogeological, geo-electrical and lithological data is performed via data extraction. For this purpose, four methods for data extraction are tested in their effectiveness. The most relevant method determined in this study, is to extract data at a similar scale as the influential area of the applied methods. In this case, data from ERT and IP profiles are averaged within a window of length 1.5 m in the direction of the measured profiles (i.e. the direction perpendicular to the stream) and a height of < 1.5 m around a central point location. The obtained value is assigned to this central point, which corresponds to a point location of a specific slug test measurement. Because slug test measurements are performed at two consecutive depth intervals of 25 cm, the harmonic average of K at these two depths is considered, to make comparison with averaged geo-electrical data meaningful.

Heterogeneity of hydraulic conductivity in the riverbed is confirmed: K values vary between 0.11 m/d and 11.39 m/d in the study site. Hydraulic conductivity is low along the left bank and it can be supposed low close to the right bank as well, where penetration of a piezometer was not possible or slug tests took too much time. Sediments close to the banks are composed of sand, intermingled with clay and organic matter. In the middle and right half of the river, hydraulic conductivity is high. Sediments in these parts of the river are composed of sand with few clay or organic material.

Inverted models of resistivity, chargeability and normalized chargeability show values which are in correspondence with typical ranges for sand or clayey sand. Resistivity varies between < 60 – > 145 Ωm, chargeability varies between 0 – > 85 mV/V and normalized chargeability between 0 – > 1 mS/m. Chargeability and normalized chargeability are generally low in the middle and right half of the study site, while high values occur in the left half. However, patterns of resistivity are rather diagonally structured: low ρ is present upstream and in the right half of the river, and high ρ occurs downstream and along the left bank of the river section. Hence, point maps and maps interpolated by ordinary kriging show the clearest correlation between hydraulic conductivity and chargeability and between hydraulic conductivity and normalized chargeability. Also, some correspondence in patterns between hydraulic conductivity and resistivity can be observed. Moreover, for all geo-electrical parameters, correlation with K is negative, meaning that low values of K correspond to high values of M, MN or ρ and vice versa.

Further, scatterplots of hydraulic conductivity versus chargeability, normalized chargeability and resistivity all reveal decreasing trends. Linear, log-linear, linear-log or log-log regressions are fit to these

plots, resulting in significant relations for all expected correlations. However, linear fits are weak: the adjusted R^2 is 0.35 for K vs. ln(M), 0.14 for K vs. ln(MN) and 0.12 for ln(K) vs. ρ. Quite some scatter occurs around the linear regressions, indicating that these regressions cannot be used as predictive models.

Furthermore, geostatistical analyses with variograms show that all parameters, i.e. K, ρ, M and MN, have ranges of similar magnitudes: ca. 10 – 12 m. Ranges of directional variograms of hydraulic conductivity and normalized chargeability indicate that spatial influence of these parameters is larger in the direction of the stream compared to the perpendicular direction. This is because water flow causes longitudinal arrangement of sediments and their properties in the river. However, the opposite is true for chargeability and resistivity, where ranges are larger in the direction perpendicular to the river in contrast to the parallel direction. This is a consequence of smoothing in inversions of ERT and IP profiles. Profiles are made perpendicular to the stream, leading to more dependency of values within the profiles than between separate profiles. In addition, clusters in the investigated river section can be delineated using several methods. This is done by visual comparison between point maps of K and ρ, M and MN or by principal component analysis (PCA) or cluster analysis (CA). Consequently, zonation results in minimization of variability of hydraulic conductivity within clusters in the riverbed.

The strongest correlation between hydraulic conductivity and chargeability or normalized chargeability can be explained by the fact that all three parameters are strongly determined by interconnected pore space area. Clay content and compaction, which determines pore volume, both influence hydraulic conductivity and chargeability, but in a reverse manner. Normalized chargeability is less influenced by changes in porosity due to normalization with resistivity. Clay content and porosity also determine resistivity, but their effects can compensate for one another. Moreover, dependency of resistivity on clay content is variable with the lithological dominance in the subsurface. Increased clay and organic matter content can result in decreasing pore connection, which increases resistivity, but clay can also enhance electrical current flow by its electrical double layers (EDLs). Therefore, correlation between hydraulic conductivity and resistivity is more changeable.

In conclusion, ERT and IP cannot be used in a predictive way for K determination, since no predictive model with limited scatter could be obtained. Despite that, correlation between hydraulic conductivity and resistivity, chargeability or normalized chargeability is useful for qualitative linkage on the local scale of the studied riverbed in the Aa river.

List of Abbreviations and Symbols

K	Hydraulic conductivity [LT^{-1}] – Horizontal hydraulic conductivity [LT^{-1}] from section 2
K_h	Horizontal hydraulic conductivity [LT^{-1}]
K_v	Vertical hydraulic conductivity [LT^{-1}]
K_{mean}	Harmonic mean of hydraulic conductivity depth measurements [LT^{-1}]
ERT	Electrical Resistivity Tomography
IP	Induced Polarization
SIP	Spectral Induced Polarization
ρ	Electrical resistivity [$VA^{-1}L$]
ρ_a	Apparent electrical resistivity [$VA^{-1}L$]
σ	Electrical conductivity [$AV^{-1}L^{-1}$]
M	Chargeability [VV^{-1}]
M_a	Apparent chargeability [VV^{-1}]
MN	Normalized chargeability [$AV^{-1}L^{-1}$]
OD	Outer Diameter [L]
STA	Slug Test Analysis
EDL	Electrical Double Layer
ϕ	Porosity [-]
RMS	Root-mean-squared
k	Geometric factor [-]
DOI	Depth Of Investigation [L]
h	Lag distance [L]
γ	Semi-variance
Ln	Natural logarithm
OM	Organic Matter
R^2	Coefficient of determination [-]
p	p-value [-]
PCA	Principal Component Analysis
CA	Cluster Analysis
UPGMA	Unweighted Pair Group Method with Arithmetic mean = Unweighted average linkage agglomerative clustering method

Table of Contents

List of Figures

Appendices

List of Tables

Appendices

1. Introduction

Hydraulic conductivity (K) is a very important, though very variable, parameter in hydrogeology. It is a property of sediments and rocks that describes how easily fluids can move through the pore space. Also in riverbed sediments, heterogeneity of hydraulic conductivity is significant (e.g. Calver, 2001). It determines, together with the local hydraulic gradient, water exchange fluxes between river and groundwater. Because riverbed hydraulic conductivity is difficult to measure directly, it is often assumed to be homogeneous in a riverbed when applied in groundwater models. However, spatial variations over several orders of magnitude can occur and are, hence, often neglected. This can lead to a systematic underestimation of net river-aquifer exchange fluxes, especially in local studies (Kalbus et al., 2009).

Interaction between river and groundwater receives more and more attention in current hydrological research. Therefore, spatial heterogeneity of hydraulic conductivity is of special interest. At present, Gert Ghysels investigates the interaction of river and groundwater, and more specifically the role of spatial heterogeneity of riverbed conductivity, in his PhD at the Vrije Universiteit Brussel (VUB). In this context, this Master's thesis aims to investigate if geophysical measurements are a useful tool for the characterization of hydraulic conductivity of riverbed sediments.

Electrical resistivity tomography (ERT) and induced polarization (IP) are two geophysical methods which provide results from electrical current injection along a profile. From ERT, resistivity (ρ) of the subsurface is obtained and with IP, chargeability (M) of the subsurface is the target. By dividing chargeability by resistivity, normalized chargeability (MN) is obtained. This is a measure for polarizability of sediments, without influence of the bulk medium. ERT and IP are widely used in land surveys for engineering applications, e.g. groundwater table or soil moisture content investigation, fault investigation, etc. Their application on water bodies has been restricted due to the conductive water layer that limits sensitivity in depth. Application and design of electrical resistivity tomography and induced polarization in river surveys is currently investigated in the Master's thesis of Kevin Gommers (2017) at KU Leuven.

The main objective of this Master's thesis is to test to which extent ERT and IP can be used to characterize spatial variability of riverbed hydraulic conductivity. Correlation between sediment electrical resistivity, chargeability or normalized chargeability and hydraulic conductivity is sought. Accordingly, several methods will be assessed and limitations will be considered. Aim is that subsequent research can make use of the investigated relationships so that the characterized heterogeneity of hydraulic conductivity of riverbed sediments can be applied in groundwater models to improve their accuracy.

Two fields sites have been investigated and are situated in the Aa river, located in the Nete catchment in northern Belgium. Firstly, slug tests at point locations along several profiles across the river are performed, resulting in direct measurements of K. Subsequently, ERT and IP measurements along those profiles are made to obtain, respectively, electrical resistivity and chargeability of the riverbed sediments. Combining these two parameters leads to normalized chargeability. Floating electrodes are used to measure at the river water level. Afterwards, ERT and IP data are inverted with RES2DINV using special boundary conditions e.g. to fix the resistivity of the water. To find correlation between inverted resistivity, chargeability or normalized chargeability profiles and directly measured K values, statistical and geostatistical analyses are performed with use of R and SGeMS.

Previous studies have focused on spatial variation of hydraulic conductivity in riverbeds using conventional K measurement methods (e.g. Chen et al., 2008; Sebok et al., 2014). Also studies with application of ERT on rivers have been performed, but with the aim to characterize the riverbed and subsurface sediment geometry (e.g. Clifford & Binley, 2010; Crook et al., 2008). However, research combining ERT and IP measurements to characterize spatial variability of hydraulic conductivity in riverbeds has not yet been published. That is why this Master's thesis will focus on the relationship between electrical resistivity, chargeability, normalized chargeability and hydraulic conductivity in riverbed sediments.

1.1. GEOGRAPHICAL AND GEOLOGICAL SITUATION

A study site in the Aa river (Belgium) has been investigated with hydrogeological and geophysical measurements. The Aa river is situated in Flanders and is a tributary of the Kleine Nete river, which flows via the Grote Nete into the Scheldt river in the province of Antwerp (Figure 1). The Aa is a typical Flemish lowland river with an average slope of 0.48 ‰ and has a total length of 36.7 km (Anibas et al., 2011). Its catchment area is 235 km², which is 15 % of the Nete basin. The average stream discharge of the Aa river is 2.55 m³/s (Waterinfo, 2017) and is controlled by weirs across the river (Figure 2) and the growth of macrophytes in summer (Bal & Meire, 2009). The change in water level is determined by rain fall, opening or closing of the weirs. Rarely, peak discharges occur. The cross section of the Aa river is rectangular with a flat river bottom. It is fed by several ditches in its catchment area. Also on a larger scale, the Kleine Nete has originated from a lot of small brooks fed by rain. In the 1960's, the Aa was stretched and canalized for agricultural purposes, as this is the main land use in the drainage area of the Aa.

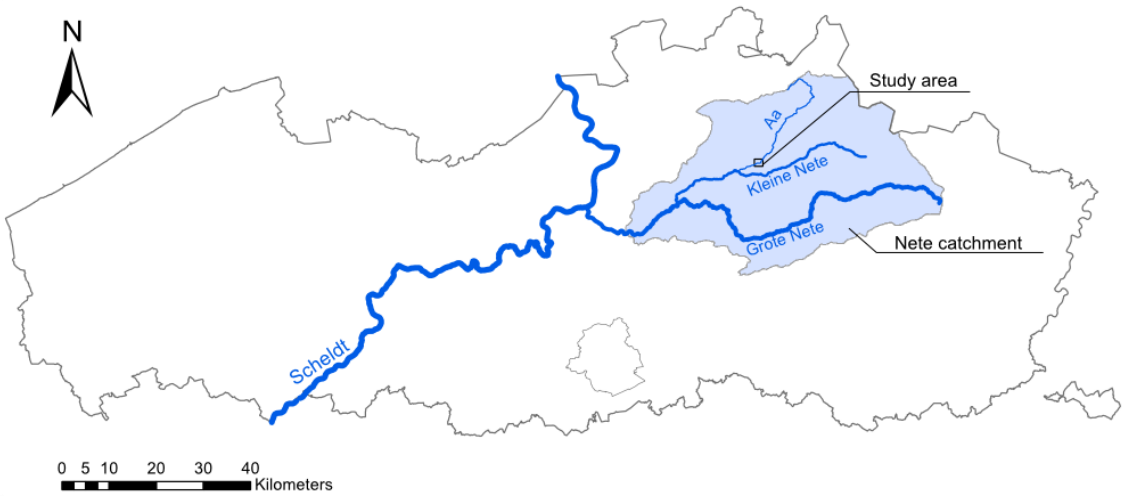

Figure 1 Situational map of the study area in the Nete river catchment in Flanders (modified after Anibas et al., 2009).

The investigated field site is located at 5.5 km from the mouth of the Aa in the Kleine Nete river, at the border of the communes of Lille, Vorselaar and Herentals and is indicated in Figure 2. The Aa river flows at this location in WSW direction, has a depth of 0.20 m – 0.70 m and an average width of 15 m. The length of the study site is 25 m. The groundwater level in the study area is shallow and occurs only 1 m below the land surface (Anibas et al., 2011). At the different moments of the measurement surveys, the water level of the river was between 9.7 mTAW and 10.0 mTAW.

The sediment type in the river is dominantly sand. The riverbed consists of fine to medium sand with varying fractions of organic material, especially in the banks of meanders (Anibas et al., 2011). It is compacted along the banks and looser in the middle of the river with sometimes pool and riffle structures. Below the riverbed sediments, Tertiary formations are present (Figure 3). The Formation of Kasterlee, which is composed of fine sands with clay fractions, overlies the Formation of Diest, which consists of heterogeneous sand with gravel layers and glauconite (DOV, 2016). Together with the Formation of Berchem, which lies below the Formation of Diest, these geological units form an unconfined aquifer of 80 m thick (Anibas et al., 2016). The underlying aquitard is the Formation of Boom. When hydraulic conductivities of the Formation of Diest and the Formation of Kasterlee are parametrized in groundwater models, values of 9.8 m/d and 12.5 m/d are assigned to these formations, respectively (Woldeamlak, 2007).

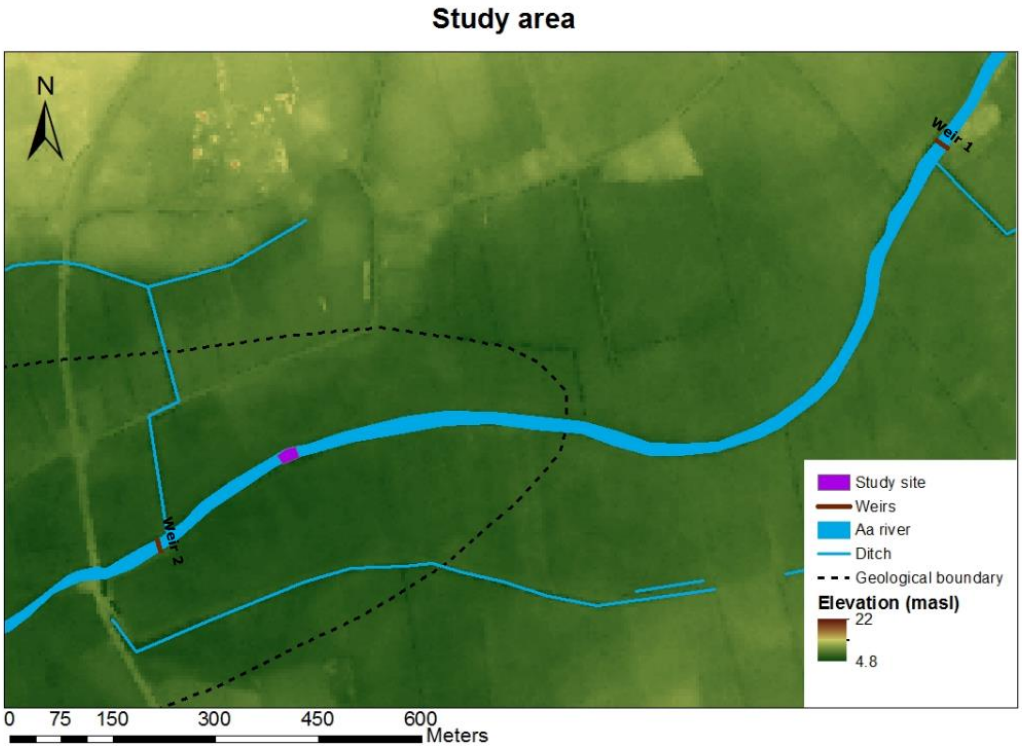

Figure 2 Digital Elevation Map (DEM) of the area surrounding the field site. The geological boundary between the Formation of Kasterlee (southwest corner) and the Formation of Diest is indicated (modified after Anibas et al., 2011).

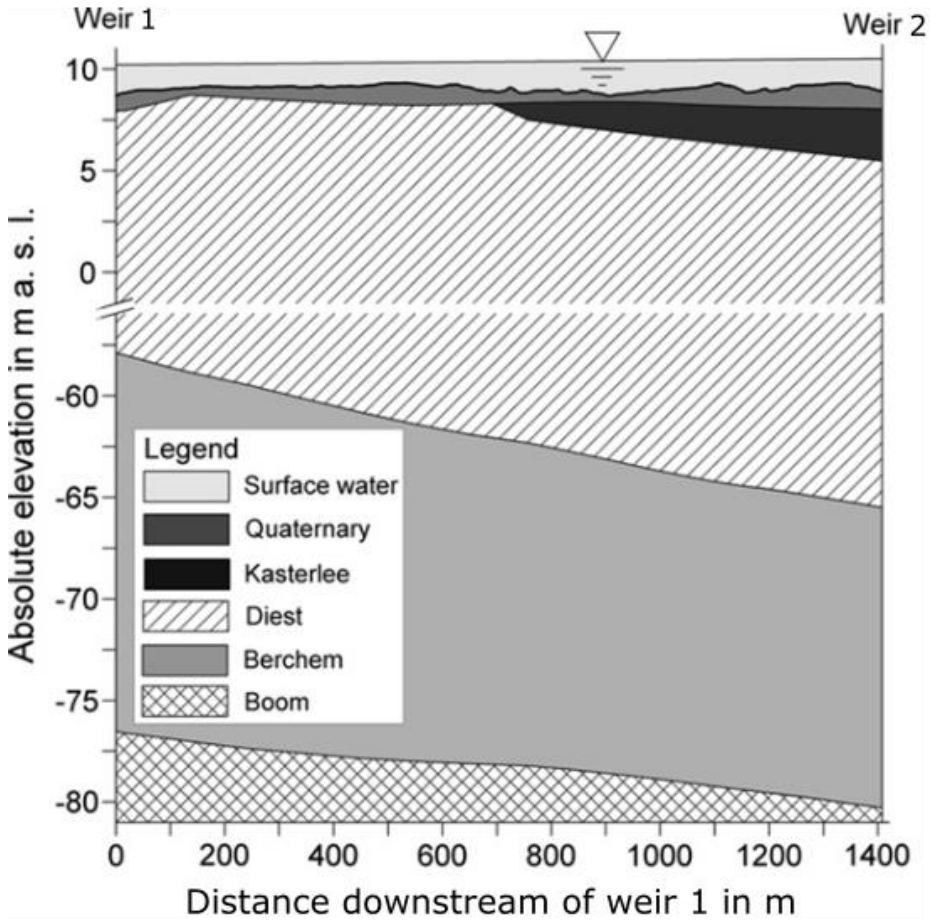

Figure 3 Geological cross-section below the Aa river between the two weirs in the study area (DOV, 2010).

1.2. HETEROGENEITY OF HYDRAULIC CONDUCTIVITY IN RIVERBEDS

Variation of hydraulic conductivity K occurs on different scales. On a local scale, such as a riverbed, it can be interesting to characterize spatial variation of K to improve analyses of flow and transport processes through the riverbed. Calver (2001) summarized permeability data of river sediments and concluded that K ranges from values smaller than 10^{-9} m/s to values higher than 10^{-2} m/s, with a dominance in values between 10^{-7} m/s and 10^{-3} m/s. Both horizontal hydraulic conductivity K_h and vertical hydraulic conductivity K_v show spatial variation in a riverbed, although K_v is less variable in space according to Kennedy et al. (2008). However, Chen et al. (2008) found variations of K_v over four to five orders of magnitude in the same vertical profile and over different locations. Spatial variation in hydraulic conductivity is due to the influence of the sedimentary and geomorphological environment as well as the method of determination, including scale, size and imprecision of the applied method (Calver, 2001; Kalbus et al., 2006; Landon et al., 2001). In addition, groundwater fluxes, sediment turnover, hyporheic fluxes and activity of interstitial and benthic fauna influence hydraulic conductivity in a riverbed (Kalbus et al., 2009).

Sebok et al. (2014) investigated the influence of river morphology on hydraulic conductivity in a riverbed. They found that K_h is the highest in the inner bend of a stream and K_v is the highest in the outer bend and near the middle of the channel. Deposition of sand and erosion are given as explanations for these observations. This is because sand is less compacted in the inner bend and the organic layer is removed in the outer bend and middle of the channel. They also stated that more heterogeneity of hydraulic conductivity is present in a channel bend than in a straight channel because of the more dynamic environment in the former. Within the bend, hydraulic properties vary more across the stream than along it. Sebok et al. (2014) also concluded that K_v is strongly related to the thickness of the organic layer in the subsurface.

Besides spatial variation of hydraulic conductivity in riverbeds, also temporal changes occur. Opposite to what was found for spatial variability of K_h and K_v, vertical hydraulic conductivity is more susceptible to temporal changes than horizontal hydraulic conductivity. Temporal changes can be attributed to sedimentary and scouring processes on the upper layer of the stream bed (Sebok et al., 2014), as well as to changes in water viscosity and biogeochemical processes (Genereux et al., 2008).

Many analytical solutions (e.g. Butler et al., 2001; Hunt, 1999) and numerical models (e.g. the River package in MODFLOW of McDonald & Harbaugh (1988)) assume a homogeneous low K riverbed, used in a conductance term characterizing the riverbed. Kalbus et al. (2009) showed that this assumed homogeneity leads to strong homogenization of water fluxes through the streambed, to such an extent that it is unlikely to occur in natural environments. The assumption of a homogeneous low K streambed can therefore only be applied for calculations of average water budgets on a regional scale (Kalbus et al., 2009). The reason why a low K is usually chosen, is because clogging often occurs in a riverbed. This can be due to deposition of fine-grained sediment and organic matter (e.g. Sophocleous et al., 1995), siltation around macrophytes (e.g. Wharton et al., 2006) or bacterial growth and microfilms (e.g. Boulton et al., 1998). However, this is not always valid. Also high permeability compared to the underlying sediment can occur in the streambed (Chen et al., 2008) and streambed sediments are not always distinguishable from the underlying material (Chen, 2005).

Characterization of spatial variability of hydraulic conductivity in riverbeds is important because of its effect on the interaction between river and groundwater (Kalbus et al., 2009). These river – groundwater interactions influence water resource management, water quality and functioning of the riparian ecosystem. Therefore, it is necessary to measure hydraulic conductivity for simulation of 3D flow between river and aquifer near the interface. In addition, it also determines contaminant transport and biogeochemical modelling in the hyporheic zone. The hyporheic zone is the interface between a river and aquifer where groundwater and surface water mix. Different processes occur in this specific zone

such as transport, degradation, transformation, precipitation and sorption of substances. Chen et al. (2008) showed that a low K_v layer in the hyporheic zone affects streamflow depletion depending on its depth, thickness, K_v value, length and width within the channel and extension into the aquifer along both sides of the river.

Water exchange between river and groundwater in a streambed can be downward or upward, in a losing or gaining stream reach respectively. If downwelling occurs, first vertical flow from the river into the sediment will be dominant, followed by dominantly horizontal flow towards the aquifer. If upwelling occurs, horizontal flow from the aquifer to the riverbed is dominant in a first stage, continued with vertical flow to the river. This upward moving water can be groundwater, but also re-emerging surface water that was stored in the pores of the river sediment. These water exchanges in the riparian zone are subjected to seasonal variations (Kalbus et al., 2006) and determined by natural hydrologic processes (e.g. Chen & Chen, 2003; Chen et al., 2008) or man-induced processes such as pumping (e.g. Sun & Zhan, 2007). Furthermore, geomorphological features can cause pressure variations and consequently, variations in water exchange fluxes (Hutchinson & Webster, 1998; Thibodeaux & Boyle, 1987), as well as relocation of sediment grains on the streambed (Elliott & Brooks, 1997).

Kalbus et al. (2009) found that the influence of the aquifer on groundwater fluxes through the streambed is larger than the influence of the streambed itself. They showed, similar to Sebok et al. (2014), that an increase in spatial heterogeneity of hydraulic conductivity results in a higher proportion of high fluxes through the riverbed. The highest fluxes occur where vertical hydraulic conductivity and the vertical hydraulic gradient are high because in this case, there is no organic sediment layer present (Sebok et al., 2014).

1.3. METHODS FOR HYDRAULIC CONDUCTIVITY DETERMINATION

Several methods exist to determine hydraulic conductivity in riverbeds, both direct and indirect methods. Nonetheless, uncertainty on obtained K values is often large because of the large variability of K. The uncertainty depends on the scale, size and imprecision of the method used (Calver, 2001). Hydraulic conductivity values can be obtained from field assessments, laboratory experiments or numerical modelling. An overview of methods is given by Landon et al. (2001) and Kalbus et al. (2006) and is summarized in the following paragraphs.

Mostly, field measurements are used to determine hydraulic conductivity. Many techniques exist with their own advantages and limitations. A first set of methods are permeameter tests, which are used to obtain vertical conductivity K_v of the riverbed. In a falling head permeameter test, water is added to a target displacement and when the water level falls, the displacement over time is recorded. In contrast, the water level in a constant head permeameter test is maintained by constantly adding water. The volume required for this, determines the resulting K_v value. For both types of permeameter tests, the Hvorslev (1951) or Darcy equation can be applied to calculate K_v. However, the latter is less accurate than the Hvorslev equation, although in sediments deeper than 0.3 m, the implementation of a permeameter test with the Hvorslev equation is not advised. With an in-situ permeameter test using a standpipe, not only vertical hydraulic conductivity is measured, but also horizontal and oblique hydraulic conductivity can be measured using an L-shaped or inclined pipe respectively. Permeameter tests are quick and easy to apply, and K_v can be directly measured in the streambed. They are useful to investigate the heterogeneity of streambeds.

A second regularly implemented field method is a slug test. Horizontal hydraulic conductivity is obtained by comparing the recovery of the head after a fast change in water level and theoretical models, such as the equation of Bouwer & Rice (1976) or Hvorslev (1951). It is a simple, quick and inexpensive method and is useful when pumping tests are not possible e.g. because of a low K formation. There is

also no need to remove or add water. A limitation of slug tests is the development of a low K skin around the filter. This is the largest source of error in slug tests because it results in ambiguous response values and imperfections. Repeated measurements are therefore recommended to detect such low K skins. Nonetheless, slug tests are useful in process studies and to investigate heterogeneity of hydraulic conductivity.

A third field method is a pumping test. In this test, the drawdown in a piezometer is recorded in function of time during pumping at a constant rate. This results in a K value that is averaged over a large subsurface volume. Disadvantages are boundary conditions, the prohibitive cost and the prerequisite for a pumping well and at least one observation well. A special type of pumping test is the piezo-seep meter, in which vertical hydraulic conductivity is measured in a restricted area of a pan. This test is useful when investigating the spatial distribution of K in a shallow streambed. It has a smaller test radius than a normal pumping test, is inexpensive, easy to apply, and tests can be performed at many locations at a time. Another possibility is a seepage meter. These hydraulic gradient measurements use the Darcy equation after measurement of the downward seepage flux from a measurement bag. However, reliability of this method is questioned by Landon et al. (2001).

Laboratory measurements are a second way to examine hydraulic conductivity. These measurements are indirect methods of hydraulic conductivity determination. For example, grain size analysis can be performed. Several empirical relations exist between statistical grain size parameters and K, such as described by Hazen (1893), Schlichter (1905), Terzaghi (1925), Beyer (1964), Shephard (1989) and Alyamani & Sen (1993). Grain size analysis results in a bulk hydraulic conductivity of the sediment core. Moreover, the result is an estimation from disturbed material, while pore space geometry is as important as grain size for the value of K. Hence, grain size analysis is not representative of true hydraulic properties of the subsurface. It can nonetheless be used as a first estimation of hydraulic conductivity.

Finally, numerical modelling schemes exist to indirectly obtain hydraulic conductivity of the streambed. Calver (2001) stated that pooled data can serve as a guide for starting values for the model. Because numerical models average hydraulic conductivity in space and are applied over a larger spatial scale than field and laboratory measurements, the outcomes of hydraulic conductivity are within a more conservative range. Sanchez-León et al. (2016) used hydraulic tomography with tracer tests to resolve the spatial distribution of the 3D hydraulic conductivity field. They combined several pumping tests with different well configurations and inverted the results. Spatial variability of K was obtained from kriging based on pilot points.

The choice of a specific method for K determination depends on the objective of the project and, consequently, the scale of investigation. Also, the vertical location of low K sediment is important in the decision for a method (Landon et al., 2001). Point measurements are useful to detect heterogeneity of hydraulic conductivity and therefore, to determine spatial variation of exchange processes and flow paths between groundwater and surface water (Kalbus et al., 2006). However, areas between locations remain unknown, which can lead to the neglect of extreme values. On the other hand, integrating measurements over large sample volumes provides reliable averages of K, but cannot be used to characterize spatial heterogeneity of hydraulic conductivity in riverbeds (Kalbus et al., 2006). In view of this, it would be ideal to combine multiple methods to obtain results at multiple scales.

1.4. GEOPHYSICAL METHODS IN RIVERS

In recent years, research has been performed on the usefulness of geophysical methods on rivers. Techniques that are usually used on land surface are adjusted to be applicable on water surfaces. Marine or lacustrine methods have already existed for a long time, but environmental application of methods on small scale water surfaces, such as rivers, has only recently been investigated. The methods used in this thesis project are electrical resistivity tomography (ERT) and induced polarization (IP). For both methods, electrical current is injected in the subsurface between two electrodes and the

voltage difference between two other electrodes is measured. This signal is used to determine resistivity and chargeability of the subsurface, with respectively ERT and IP.

Implementation of ERT and IP in rivers can be used in several applications. First of all, ERT is used to characterize the stream channel sediment structure and hydrostratigraphy (Clifford & Binley, 2010; Crook et al., 2008) and to find the transition between the riparian zone and the stream channel (Crook et al., 2008). Nyquist et al. (2008) used ERT to map groundwater discharge because ERT results can be interpreted in order to find variation in porosity and pore fluid conductivity, as well as the amount of clay in the saturated zone. Crestani et al. (2015) used the contrasting resistivity of a saline tracer to map solute evolution through an aquifer, which can be used to assess hydraulic conductivity. Other applications are flow and transport monitoring in the vadose zone (al Hagrey & Michaelsen, 1999; Chen et al., 2008; Dailey et al., 1992) and estimation of hydraulic properties (Binley et al., 2002). The IP method is used to map saline intrusions, find clay layers or detect organic or inorganic contaminants (Attwa & Günther, 2013; Slater & Lesmes, 2002). Kruschwitz et al. (2010) used IP for pore size determination.

Crook et al. (2008) described different configurations that can be used with ERT on stream surfaces. Electrodes can be floating on the water surface, can be submerged within the water column or can be physically embedded in the riverbed with the possibility to insulate the upper part of the electrodes to avoid contact with river water. Electrodes can also be hung in boreholes to obtain higher resolution at depth. In this case, there is need for boreholes along the river. Protocols that can be applied in an ERT and/or IP survey are the same as on land. The most common protocols are the dipole-dipole electrode configuration and Wenner electrode configuration (Figure 8 in section 2.3). The first one provides a good horizontal resolution with high sensitivity at shallow depths, while the latter has a good vertical resolution with high sensitivity relatively deeper in the subsurface (Clifford & Binley, 2010). Other protocols are the gradient array, which is a variation of the Wenner array, and the pole-pole electrode configuration. The latter has a great depth of penetration with respect to the length of the measured profile (Crook et al., 2008). Similar as for land surveys, data inversion is required after data acquisition. With this, depth of investigation (DOI) or sensitivity analyses provide essential information about the effective depth of penetration, which is required for data interpretation and error analysis (Edwards, 1977; Spitzer, 1998). Especially in this study, where ERT and IP are applied on a water surface, the depth of penetration should be sufficiently deep into the riverbed in order to examine it at least to the depth of the slug test measurements.

An important advantage of ERT and IP is that they are non-invasive methods to obtain information about electrical properties of the subsurface, such as its architecture or particular features. Geologic materials have a broad range of resistivity values varying between 10^{-2} – 10^{6} Ωm. ERT and IP are useful in challenging terrain where it is difficult to obtain direct information on the subsurface or where there is a complex stream environment (Crook et al., 2008). Moreover, these methods are most effective when there is a strong contrast in electrical conductivity between groundwater, sediments and surface water (Nyquist et al., 2008).

Despite this, one of the main limitations in an ERT and IP survey on a river is the presence of the water layer. Because of its high electrical conductivity compared with sediments underneath, which are the focus of investigation, measurement sensitivity is degraded (Crook et al., 2008). Resolution also decreases with increasing distance from the electrodes and due to poor electrode coverage at the end of profiles, recovery at those locations is less accurate (Crook et al., 2008). Because of the reduction of sensitivity with depth and the smoothness constraint applied in inversions, ERT and IP images are often smeared (Clifford & Binley, 2010).

Besides ERT and IP, other geophysical methods have also been tested and applied on water surfaces in recent years. Binley et al. (2013) applied a multi-measurement and multiscale program for the characterization of spatial variability of water fluxes at the groundwater – surface water interface. They performed an electromagnetic (EM) survey, in addition to sediment core analysis, slug tests and other methods. In particular, EM was used to map variation in sediment properties beneath rivers and to

identify contrasts in groundwater sources due to changes in pore water conductivity. GPR is another method applicable on rivers. It is used for example to map scour surfaces and trough cross bedding in riverbeds (Cardenas & Zlotnik, 2003) or to monitor one or two dimensional infiltration experiments in the vadose zone (Finsterle & Kowalsky, 2008; Jadoon et al., 2010; Looms et al., 2008).

In general, geophysical methods are useful in water borne surveys to obtain hydrological properties of interest from the inversion of geophysical data (Crestani et al., 2015). They provide spatial information on subsurface properties and processes (Crook et al., 2008). As opposed to conventional measurements of hydrogeological parameters, all geophysical methods are non-invasive. This avoids coring or destructive drilling in the riverbed (Clifford & Binley, 2010). In addition, geo-electrical methods provide a continuous image of the subsurface instead of point measurements which are often not densely enough spaced to catch the complete spatial or temporal variability of the parameter of interest (Crook et al., 2008). In addition, geophysical results are valuable because they complement conventional measurements and since they also help to identify optimal locations for further investigations (Clifford & Binley, 2010). Conditions for applicability are a distinct contrast in geophysical properties of hydrological units and sufficient resolution and sensitivity of the method to capture these contrasts (Clifford & Binley, 2010). Despite this, hydrogeological properties or states are not measured directly, which results in the need of petrophysical relationships for interpretation. Therefore, this thesis project aims to investigate such a petrophysical relation between hydraulic conductivity and electrical resistivity, chargeability and normalized chargeability for riverbed sediments.

1.5. RELATIONS BETWEEN GEOPHYSICS AND HYDRAULIC CONDUCTIVITY

The relation between geophysical and hydrogeological properties of sediments and rocks has been the focus of several research projects throughout the last 70 years. This is because relationships are expected between hydraulic conductivity K and electrical conductivity σ, which have common properties: water flow and electrical current are both channelized through the interconnected pore space in sediments, and K and σ are both related to parameters which are measures of interconnected pore volume and interconnected pore space (Revil & Cathles, 1999; Schön, 1996). Slater (2007) made a review of past research on relationships between electrical properties and hydraulic conductivity. Despite the similarities between K and σ, he stated that there exists no direct, universal relationship due to different dependencies of these parameters to sediment properties. On the one hand, hydraulic conductivity K is related to effective porosity and geometry of the pore space (Attwa & Günther, 2013). On the other hand, resistivity, the inverse of conductivity, is related to pore volume, in other words the amount of electrolyte providing conduction, and to pore surface area properties, more specifically the electrical double layer EDL of clay minerals, which are important current flow paths. Therefore, resistivity is limited in K estimation and Slater (2007) suggested that IP and SIP (Spectral Induced Polarization) measurements provide better relations with K. The reason for this would be because chargeability and normalized chargeability only depend on the interconnected pore surface area. This factor also controls K: connectivity of pore space is of primary importance for water flow through sediments.

Estimations of such petrophysical relationships can be used to convert geophysical images to spatial distributions of hydrogeological properties with addition of direct measurements (Slater, 2007). Furthermore, joint inversions have been applied in recent research. In a joint inversion, geophysical and hydrological data are inverted simultaneously. However, hydrologic and geophysical data sets are mostly function of different physical quantities, which hampers the implementation of joint inversions (Slater, 2007).

Purvance & Andricevic (2000) found a linear-log correlation between hydraulic conductivity K and electric conduction σ' (the real part of the complex electric conductivity σ*). This correlation is positive if the interconnected pore volume and thus the electrolyte dominates the electrical current, such as in

gravel and sand. It is negative if electrical current is dominated by interconnected pore surface area, such as in clay and fine silt:

$$K = a(\sigma')^b \tag{1.1}$$

where a and b need to be estimated based on comparison between geo-electrical measurements and hydraulic conductivity measurements (Purvance & Andricevic, 2000). Resistivity – hydraulic conductivity relations for aquifers have been published by several authors, mostly empirically derived and for regional application. Kelly (1977) found empirical relations between the formation factor F (described in section 2.3 and equation (2.8)) and K, and between resistivity ρ and K in an aquifer. Kazakis et al. (2016) found a linear relation between aquifer hydraulic conductivity and normalized resistivity, similarly as Yadav & Abolfazli (1988).

Other geophysical methods have also been applied to find correlations. For example, electromagnetic induction (EM) was used to characterize moisture content in the soil, which can be related to hydraulic conductivity (Farzamian et al., 2015). Salako & Adepelumi (2016) combined ERT and GPR to characterize hydraulic conductivity of different subsurface layers. Di Maio et al. (2014) combined the use of Archie and Van Genuchten models for prediction of hydraulic conductivity from laboratory sediment resistivity measurements. Other studies used ERT as a monitoring tool. Crestani et al. (2015) monitored a tracer injected in an aquifer. Studies in 2015 (Farzamian et al.) and 2016 (Chou et al.) used ERT to monitor water injection in an unsaturated zone, which was then used in characterization of hydraulic conductivity distribution in the soil.

Weller et al. (2015) stated that IP and SIP measurements provide better relations with hydraulic conductivity K because they are only related to surface conductivity and surface area of the interconnected pore network. Several authors have sought a relation between K and relaxation time τ (Hördt et al., 2007; Kruschwitz et al., 2010; Scott & Barker, 2003). Relaxation time τ is the time it takes for ions to return to their equilibrium position after current is cut off. Binley et al. (2005) found a positive correlation, Titov et al. (2010) established a local empirical relationship and Attwa & Günther (2013) also related K and τ, but found that correlation was weak. Single frequency models for K estimation from IP measurements are proposed by Börner et al. (1996) and Slater & Lesmes (2002). Slater (2007) stated a general dependence of geo-electrical measurements and hydraulic conductivity K:

$$K = \frac{a}{F(\sigma'')^c} \tag{1.2}$$

where F is the formation factor and σ" is the imaginary part of the complex electrical conductivity σ*, which is measured with IP in frequency domain. σ" characterizes polarization during IP measurements.

To summarize, the use of geophysical methods in riverbeds to characterize hydraulic conductivity has mostly been applied in indirect ways. GPR can provide extra information in a 3D characterization of heterogeneity of K in channel bend deposits (Cardenas & Zlotnik, 2003). However, there has not yet been research on the relation between hydraulic conductivity and electrical resistivity, chargeability and normalized chargeability measured with geophysical methods, in field applications on a local scale such as in riverbeds. That is why the goal of this thesis project is to investigate this topic to provide more insight in the usefulness of ERT and IP in local groundwater – surface water interaction studies.

1.6. OBJECTIVES

The main objective of this Master's thesis is to investigate if ERT and IP are capable to characterize the spatial variability of hydraulic conductivity in a riverbed and if so, to which extent. To achieve this, a significant correlation between hydraulic conductivity K and electrical resistivity ρ is sought, as well as between hydraulic conductivity K and chargeability M and normalized chargeability MN. Hydraulic conductivity is measured in a direct way with slug tests. Resistivity and chargeability are measured with

the geophysical methods ERT and IP, respectively, and a combination of both is used to calculate normalized chargeability. First, it is investigated if ERT and IP can be applicable on rivers, which is profoundly discussed in the Master's thesis of Kevin Gommers (2017). Then, the ability to predict spatial K distribution using ERT and IP is investigated.

To this end, spatial patterns, both on point scale, spatially averaged and on interpolated maps, trends in scatterplots as well as linear models are determined in a comparative analysis of hydraulic conductivity, resistivity, chargeability and normalized chargeability. Possible correlations between these parameters, on a local scale in a riverbed, are the central subject of this dissertation. In addition, it is judged if ERT and IP can serve, at this location, as a predictive tool in hydrogeologic settings. The outcome of this project can be used in groundwater – surface water interaction studies, which aim at improving groundwater models for more strategic water management.

2. Methodologies and theory

Several methods are applied for the investigation of a link between hydraulic conductivity and geo-electrical properties in a riverbed, both in the field as during processing and analysis of the data. In the field, slug tests and geo-electrical measurements (ERT and IP), as well as riverbed drillings, are performed. The acquired raw data are later processed to obtain the parameters of interest, i.e. hydraulic conductivity K from slug tests, electrical resistivity ρ from ERT measurements, chargeability M from IP measurements and normalized chargeability MN from a combination of ERT and IP. For this purpose, the Bouwer & Rice (1976) method is used for slug tests and inversions are performed with the raw ERT and IP data. Drillings are executed in the riverbed to recover lithological data. To evaluate the link between hydrogeological and geo-electrical data, spatial patterns as well as general statistics of K, ρ, M and MN are analyzed. Statistical methods involve descriptive statistics, linear regressions, principal component analysis and cluster analysis. In addition, geostatistical analyses are performed to have an idea about the distance of influence of each parameter and to obtain continuous images of point maps. To do this, variograms and ordinary kriging are applied. With all these methods, it is the purpose to detect zones or patterns in the data and, if present, correlation between hydraulic conductivity and geo-electrical parameters.

2.1. FIELD SETUP

A schematic overview of the field setup for slug test measurements, ERT and IP measurements and riverbed drillings is shown in Figure 4. For both the slug test and ERT/IP survey, the same profiles across the river are measured, except for the first one, which was not measured by ERT and IP. Eight and seven profiles are measured, respectively with slug tests and with ERT and IP, with a spacing of approximately 3 m between the profiles. The names of the profiles are equal for all methods.

Slug tests measurements are performed at six point locations per profile at two different depths. These depth intervals are 20 – 45 cm and 45 – 70 cm in the riverbed. Point locations are separated by approximately 2 m. If it was not possible to measure at one location, a point location in between two points is measured. Reference points indicating the profiles in the field are measured with GPS during the slug test survey. For ERT and IP measurements, 25 to 28 electrodes are positioned on the water surface. The spacing between the electrodes is 0.50 m. Drillings are performed at eight locations in the study site, more specifically, at locations close to the banks and in the middle of the river. Their exact distances from the banks are indicated in Figure 4.

The different field methods have been executed in different periods throughout the year. The slug test survey was performed in August and September 2016, ERT and IP were measured in December 2016 and riverbed drillings were executed in May 2017.

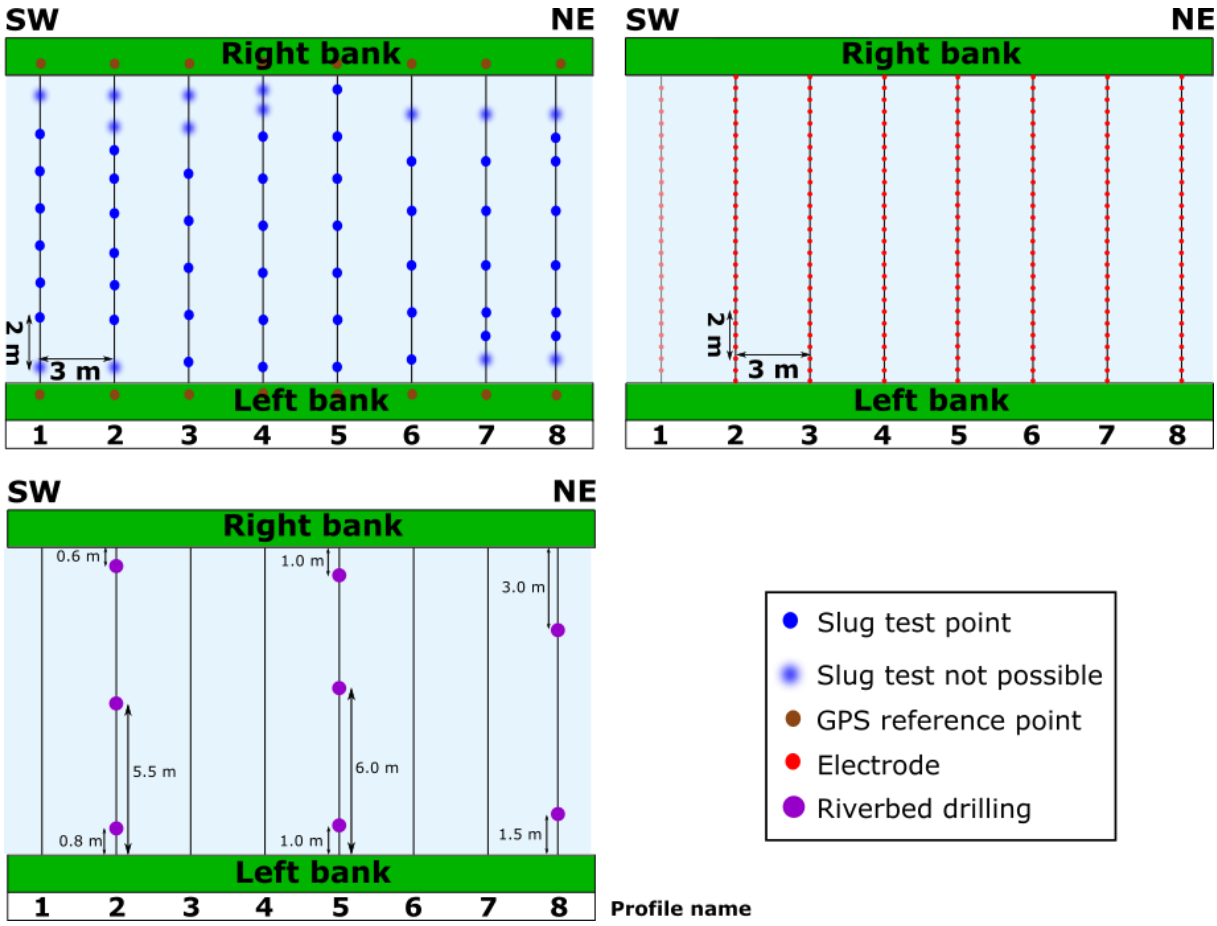

Figure 4 Schematic overview of the field setup of slug test measurements (upper left), the ERT and IP survey (upper right) and riverbed drillings (down left).

2.2. SLUG TESTS

A slug test is a field method to obtain horizontal hydraulic conductivity K_h at point locations by measuring the recovery of the head in a piezometer after near-instantaneous disturbance of the equivalent water level (Butler, 1998; Landon et al., 2001). This method is quick, easy to implement and inexpensive. It is the most common method for in situ estimation of hydraulic conductivity in shallow, often unconfined formations (Butler, 1998). Besides easy implementation in high K formations, it could also be useful in low K formations where pumping tests are not applicable (Butler, 1996). Nonetheless, long equilibration times in low K formations can also hamper measurements. Furthermore, it is important to recognize a low K skin that can form around the filter of the well (Butler, 1996). Therefore, repeated tests are required to either mobilize the low K skin, if present, or at least recognize its presence (Butler, 1996). Because slug tests are the only applied method in this dissertation, 'hydraulic conductivity K' will be used to indicate horizontal hydraulic conductivity K_h, unless ambiguity occurs.

To perform the slug tests, a mini-piezometer (OD = 3.7 mm) is pushed into the riverbed sediments (Figure 5). Water exchange between the piezometer and sediments occurs through a well screen of 25 cm with a slot size of 0.65 mm that is welded to a drive point at the lower end and a stainless-steel pipe at the upper end (Figure 5 A). A GW1600 Pneumatic Slug Test Kit (Geoprobe Systems) is used to measure the hydraulic head in the piezometer with a small-diameter pressure transducer (Figure 5 A).

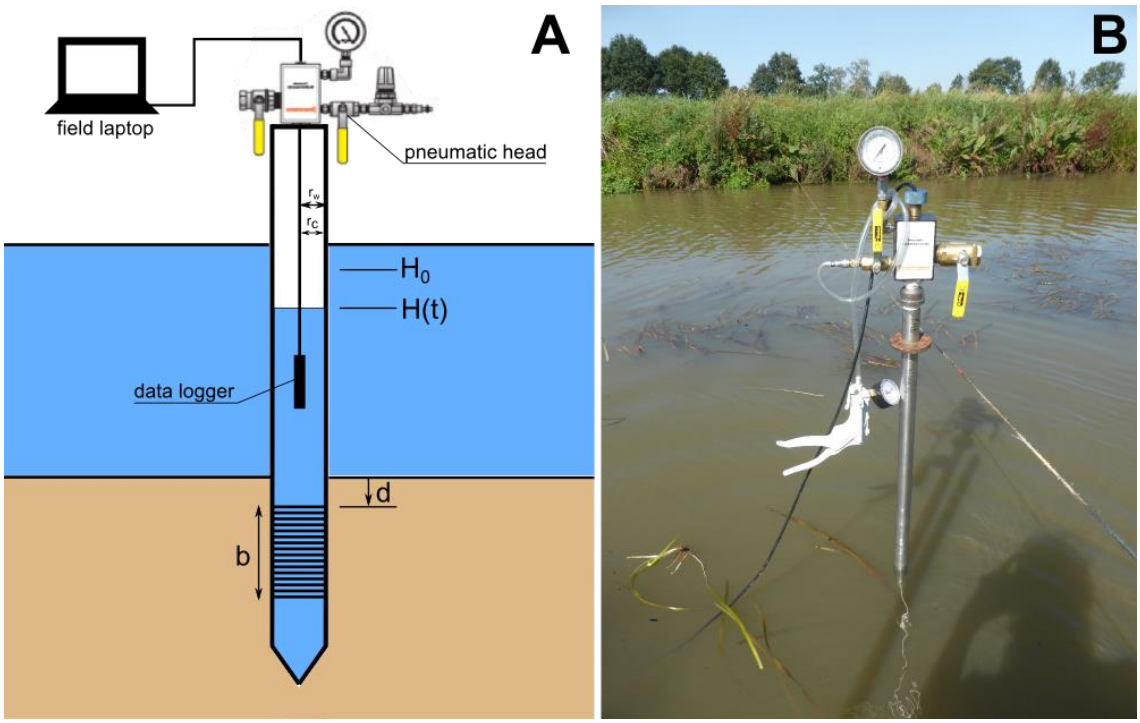

Figure 5 (A) Rising head slug test setup with indication of parameters used in the slug test analysis. The values of these parameters are given in Table 1. (B) Slug test setup in the field.

Pneumatic rising-head slug tests are performed. Such a test is composed of several steps (Figure 6). Before initiation, the mini-piezometer is driven into the riverbed sediment until the well screen is at the depth of investigation, i.e. 20 – 45 cm deep or 45 – 70 cm deep. First, air pressure is increased in the piezometer by manual pumping. This pushes the hydraulic head down, while increasing the total pressure, expressed in cm H_2O, in the piezometer (Figure 6). After equilibration of the head, pressure is quickly released and the hydraulic head recovers to the static level. This is measured by the pressure transducer and visualized in real-time on the connected laptop (Figure 5 A). Processing to obtain hydraulic conductivity from the recovery curve is performed using Slug Test Analysis (STA) software (Geoprobe systems). At several locations repeated tests are performed to test the presence of a low K skin and, with this, the value of the slug test measurements. Repeated tests are analyzed with visual inspection of normalized head vs. log t plots: tests at the same location should produce (almost) equal curves.

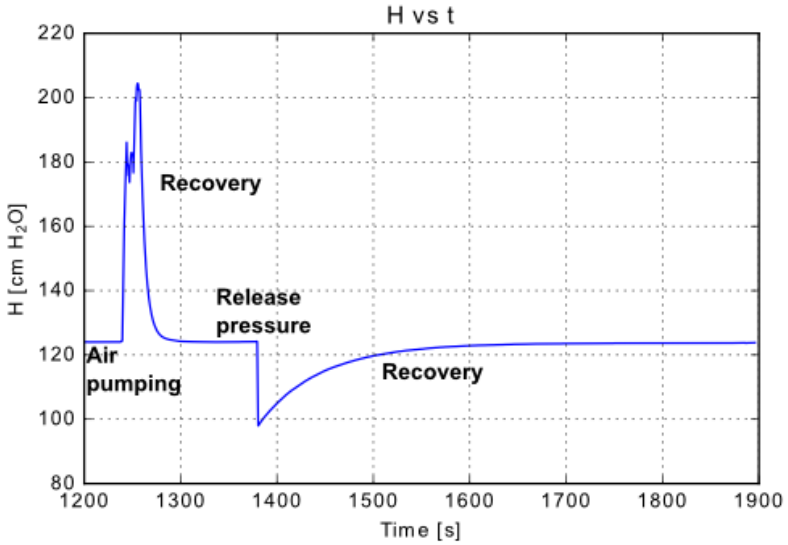

Figure 6 Course of the hydraulic head in the piezometer during a slug test.

Recovery of the hydraulic head (Figure 6) is analyzed using the Bouwer & Rice (1976) method, modified for anisotropy by Zlotnik (1994). This method is applicable in unconfined aquifers (Butler, 1996), as is the case in the present survey where an unconfined sand aquifer of ca. 80 m thick is present. Bouwer & Rice (1976) and Zlotnik (1994) found that

$$\ln\left(\frac{H(t)}{H_o}\right) = -\frac{2K_h bt}{r_c^2 \ln\left(\frac{R_e}{r_w^*}\right)} \tag{2.1}$$

where H(t) is the hydraulic head at time t [L], H_0 the initial hydraulic head at time t = 0 s [L], b is the effective screen length [L], r_c is the effective well casing radius [L], corrected for the radius of the transponder, R_e is the effective radius of the slug test [L] and $r_w^* = r_w \left(\frac{K_z}{K_h}\right)^{\frac{1}{2}}$ is the effective well radius [L], corrected for anisotropy. The values of these parameters in this survey are given in Table 1 and are indicated in Figure 5 A.

First, a plot of the natural logarithm of the normalized hydraulic head versus time is created, which is subsequently fit to a straight line. The slope of this fitted line is the negative inverse of the time lag T_0. This is the time at which a normalized head of 1/e is obtained. Then, the horizontal hydraulic conductivity can be calculated:

$$K_h = \frac{r_c^2 \ln\left(\frac{R_e}{r_w^*}\right)}{2bT_0} \tag{2.2}$$

For wells that end above the lower impermeable boundary, the second term of the numerator can be calculated as follows:

$$\ln\left(\frac{R_e}{r_w^*}\right) = \left[\frac{1}{\ln\left(\frac{d+b}{r_w^*}\right)} + \frac{A + B\left(\ln\left[\frac{B_t - (d+b)}{r_w^*}\right]\right)}{\frac{b}{r_w^*}}\right]^{-1} \tag{2.3}$$

where d is the z-position of the top of the well screen (positive direction downwards) [L] and B_t is the aquifer thickness [L]. The values of these parameters are given in Table 1 and indicated in Figure 5 A. A and B are empirical coefficients, which are dimensionless and calculated with the following formulas:

$$A = 1.4720 + 3.537 * 10^{-2}\left(\frac{b}{r_w^*}\right) - 8.148 * 10^{-5}\left(\frac{b}{r_w^*}\right)^2 + 1.028 * 10^{-7}\left(\frac{b}{r_w^*}\right)^3 - 6.484 * 10^{-11}\left(\frac{b}{r_w^*}\right)^4 + 1.573 * 10^{-14}\left(\frac{b}{r_w^*}\right)^5 \tag{2.4}$$

$$B = 0.2372 + 5.151 * 10^{-3}\left(\frac{b}{r_w^*}\right) - 2.682 * 10^{-6}\left(\frac{b}{r_w^*}\right)^2 - 3.491 * 10^{-10}\left(\frac{b}{r_w^*}\right)^3 + 4.738 * 10^{-13}\left(\frac{b}{r_w^*}\right)^4 \tag{2.5}$$

Table 1 Values of the parameters of the slug tests, indicated in Figure 5 A.

Parameter	Value
b (cm)	25
r_c (cm)	1.658
R_e (cm)	1.535
r_w (cm)	1.535
K_z/K_h	0.1
B_t (cm)	8000

Butler (1996) found that the best fit of the recovery curve is in the interval [0.20; 0.30] of $\ln\left(\frac{H(t)}{H_o}\right)$, which is therefore used for the calculation of K_h. If the test response does not recover up to 0.20, the interval [0.30; 1.00] is used. However, one must be aware that due to storage effects there is often not a good fit in the very beginning of the test.

The volume that is influenced by a slug test measurement in the riverbed has a height of at least 25 cm, which is the effective length of the screen. How wide the influence, or slug test radius, goes, is not exactly known and can be variable depending on the surrounding sediment. Butler (1998) stated that the width of the influential volume is dependent on the dimensionless storage parameter α, which is a function of the specific storage. The smaller this α, the larger the representative volume of the slug test. Because specific storage is different in every point location, the slug test radius also differs from point to point. Butler (1998) also stated that slug tests are representative for relatively small volumes, but in reality, this volume can be larger than expected. This is for example claimed by Ramey et al. (1975), who stated that the slug test radius can be up to several hundreds of the effective screen radius. In this study, this would result in a slug test radius of 1.6 m or more. On the other hand, Barker & Black (1983) predicted the value of the slug test radius based on the value of α. As this value is not known in this study, the slug test radius cannot be predicted with this method. In any case, a lot of uncertainty is connected to the influential volume of a slug test and therefore, an exact slug test radius cannot be given.

Slug test measurements are performed in eight profiles, with approximately six points per profile. A schematic view of the field setup is shown in Figure 4. GPS coordinates of the slug test point locations are determined based on the measurement of the GPS coordinates of a point on the left bank and on the right bank (Figure 4), and measurement of the distances between successive points in each profile and between the measured GPS points and the first or last slug test point in the profile. A GNSS Leica Geosystem is used for the measurement of GPS coordinates. Goniometric calculations in the projected Belgian Lambert 1972 coordinate system are performed using the right bank coordinate as a starting point. The left bank coordinate is used to check the accuracy of the calculations. A correction is applied for each calculated point based on the difference in calculated and measured left bank coordinate.

2.3. ELECTRICAL RESISTIVITY TOMOGRAPHY (ERT)

Electrical resistivity tomography (ERT) is a geophysical method to map resistivity (ρ) of the subsurface. For an electrical resistivity survey, four electrodes are positioned on a line, symmetrical around a common midpoint. Two electrodes serve as current or source electrodes and inject DC current. Two other electrodes are potential or receiver electrodes, measuring a potential difference which depends on the transmitted current, the position of all electrodes and the resistivity distribution in the ground (Christensen & Christiansen, 2015). If the distance between the current electrodes increases, deeper parts in the subsurface can be reached.

This setup is repeated many times with multiple combinations of electrode pairs. This results in apparent resistivity values at several locations in the subsurface under the measured profile. Apparent resistivity is resistivity of a homogeneous half space that would yield the measured resistance. It is thus different from true resistivity of the inhomogeneous subsurface. Nevertheless, it can be visualized in a pseudosection and used as a data quality check. A pseudosection is a plot of the apparent parameter values (e.g. resistivity) below the center of each electrode configuration at a depth proportional to the length of the configuration. Apparent resistivity ρ_a [$VA^{-1}L$] is related to resistance of the subsurface (the ratio of measured potential difference ΔV [V] and injected current I [A]) via the geometrical factor k, which is dependent on the geometry of the electrode configuration:

$$\rho_a = k * \frac{\Delta V}{I} \tag{2.6}$$

Factors that contribute to conductivity of the subsurface, which is the inverse of resistivity, are pore water, conductive solids (e.g. metal oxides, metal sulphides, graphite) and the electrical double layer (EDL) of clay minerals (Christensen, 2000). Conductivity of pore water is dependent on the type and concentration of dissolved ions (salinity), temperature and, to a minor extent, pressure (Christensen, 2000). The relation between formation conductivity σ_f [$AV^{-1}L^{-1}$] and pore water conductivity, porosity ϕ, saturation S_w, and EDL is described in Archie's law (1942):

$$\sigma_f = \frac{\sigma_w}{F} + \sigma_s \tag{2.7}$$

$$F = a\varphi^{-m}S_w^{-n} \tag{2.8}$$

where σ_w is the pore water conductivity [$AV^{-1}L^{-1}$], σ_s is the EDL conductivity [$AV^{-1}L^{-1}$], F is the formation factor, a the saturation coefficient, m is the cementation factor and n is the saturation exponent. In view of this, ERT can be used to distinguish between geological materials such as sand and clay, between saturated/unsaturated materials or between salt and fresh water (Christensen, 2000). Qualitatively, a relation between electrical resistivity and hydraulic conductivity can be made: high resistivity may represent sandy deposits and thus high hydraulic conductivity, while low resistivity may represent clay, corresponding to low hydraulic conductivity (Christensen, 2000). However, porosity determining the amount of water in the pores also has a strong influence on the value of ρ. So, this qualitative statement is only valid in extremal cases of dominating sand or clay.

The ABEM Terrameter LS1 is used for the geo-electrical measurements. This is a state-of-the-art data acquisition system for self-potential (SP), resistivity and time-domain induced polarization (ABEM Instrument AB, 2012). The device and including tools are shown in Figure 7. As mentioned earlier, a multi-electrode method is applied with the purpose to map vertical and lateral resistivity variation in the riverbed. Resistivity in the third direction, perpendicular to the profile, is assumed invariant.

Figure 7 ABEM Terrameter LS instrument and all its utensils (ABEM Instrument AB, 2012).

The dipole – dipole configuration in time-domain is used in the field survey (Figure 8 A). This electrode configuration is useful to characterize lateral variations and to detect small scale features (Christensen & Christiansen, 2015). It has a high resolution in shallow parts of the subsurface. A disadvantage is that

it is susceptible to noise. The Wenner electrode configuration (Figure 8 B) is less susceptible for this, but is less sensitive to small scale features, as it is more robust and more effective in characterization of vertical variations (Christensen & Christiansen, 2015). Other electrode configurations, such as the gradient array, pole – pole or Schlumberger array, also have their advantages and limitations, but are in this small-scale survey less relevant. Because of the limited depth of investigation of this study (slug tests are only up to 70 cm deep), the dipole – dipole configuration is preferred. The geometric factor k for the dipole – dipole configuration is defined by

$$k = \pi n a(n+1)(n+2)(n+3) \tag{2.9}$$

where a is the length of the current or potential dipole and n is a multiple of this length a so that n*a is the distance between the two dipoles (Figure 8 A).

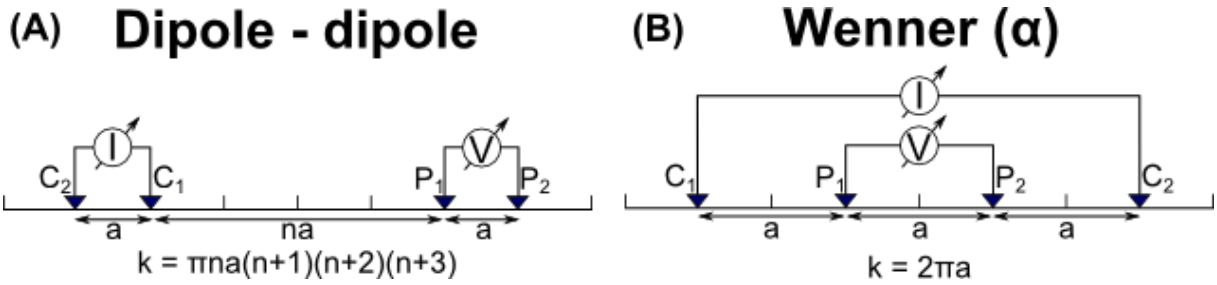

Figure 8 Arrangements of the electrodes for the (A) dipole - dipole array and (B) Wenner (α) array and their geometric factors k (modified after Loke et al. (2013)).

During the dipole – dipole data acquisition, an electrode spacing of 0.5 m is used and an acquisition time of 1.5 s and 1.7 s is implemented. Current between 10 mA and 200 mA was injected in a measuring cycle of a positive current pulse, a double negative pulse and again a positive pulse. The field setup of the ERT survey is schematically shown in Figure 4. Because four electrodes are used per measurement and the distance between the electrodes is 0.5 m or a multiple from this between the electrode dipoles, the length of the influential volume of ERT measurements is at least 1.5 m. The height and width of the volume of sediments influencing a measurement is not exactly known. If electrodes are separated at a wider distance, measurements go deeper. Consequently, the volume of influence will be longer, higher and wider with increasing electrode pair spacing.

Different from conventional ERT measurements, where electrodes are planted in sediments on land, electrodes in this field survey are floating on the water surface using foam along the electrode cable (Figure 9). The water depth at each electrode is measured with a measuring stick to incorporate these values in later inversions. To visualize this, linear interpolation between point locations is performed to obtain a continuous map of the bathymetry. Also, water conductivity is measured to use as a priori information in the inversions. The effectiveness of ERT for shallow riverbed measurements is dependent on the ratio of the resistivity of the water layer and resistivity of riverbed sediments. Sensitivity is shallow if resistivity of the sediments is large in comparison to that of surface water (Clifford & Binley, 2010). Other possibilities for aquatic geoelectric surveys could be to bring the electrodes in contact with the riverbed or to trail submerged electrodes along the riverbed (Crook et al., 2008).

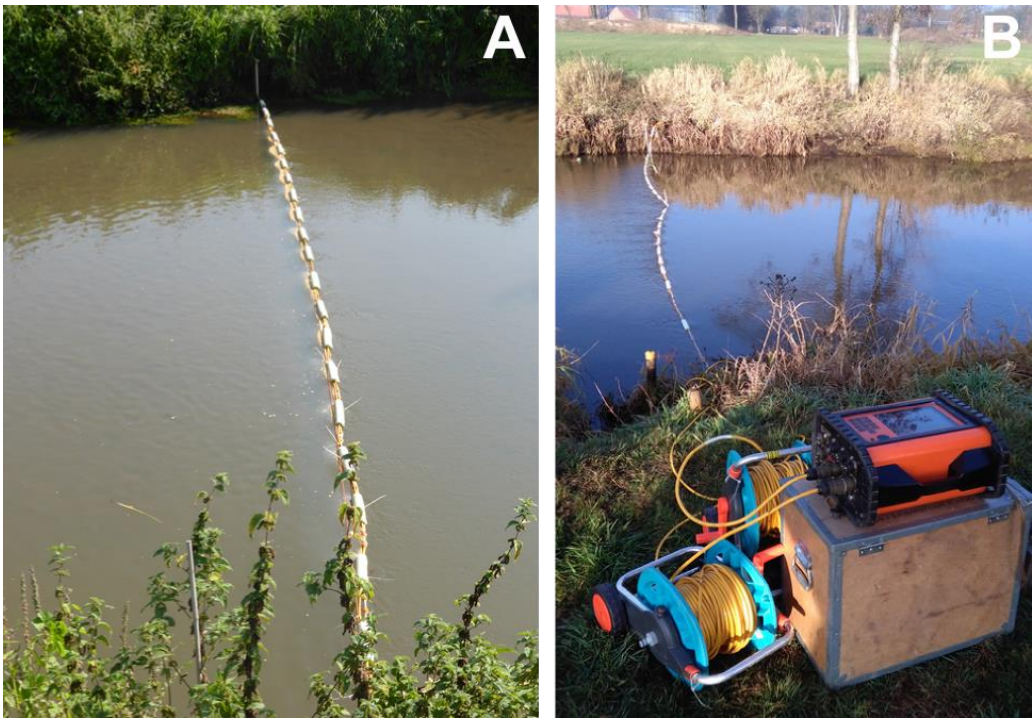

Figure 9 (A) Electrode cable floating on the water surface during data acquisition. (B) ABEM Terrameter and floating electrodes during data acquisition.

After data acquisition, apparent resistivity data need to be converted to real resistivity data. This is an inverse problem as one must find a model from a set of discrete data. It can be clarified by solving the forward problem for a series of models and compare the results of each with the measured data to find the best model (Christensen & Christiansen, 2015). A non-linear smoothness-constrained least-squares optimization technique is used iteratively to find the resistivity of the model blocks (deGroot-Hedlin & Constable, 1990; Loke et al., 2003). The goal of the inversion is to find the optimal model parameters m such that (Groetsch, 1999):

$$d = G(m) \tag{2.10}$$

with d being the observed data, m the model parameters and G being the forward, non-linear operator, describing the equations that relate d and m. To limit the difference between observed data and predicted data, the objective function needs to be minimized. The objective function ϕ representing the L2-norm is defined as:

$$\phi = ||d - Gm||_2^2 \tag{2.11}$$

To minimize the objective function, a Gauss-Newton approach is applied in the inversions executed in this thesis. This involves regularization or damping and a smoothing constraint. In addition, other constraints can be incorporated in this approach, such as the thickness and resistivity of the water layer.

First, an initial model is made and the model response is calculated. Then, the root-mean-squared (RMS) error is calculated as follows

$$RMS = \sqrt{\frac{1}{N} * \sum_{i=1}^{N} \frac{(d_i - G_{ij}m_j)^2}{(d_i)^2}} \tag{2.12}$$

where $d = ln\rho_{a,i}^{data}$ with $\rho_{a,i}^{data}$ is the apparent resistivity measured at point i, where $G_{ij}m_j = ln\rho_{a,i}^{response}$ with $\rho_{a,i}^{response}$ is the apparent resistivity calculated based on the model output at point i after iteration j, and N is the number of measurements. Next, the model parameters are changed according to the

smoothness constraints and in such a way that the RMS is reduced to obtain a better fitting model. The model response is calculated again and also the other steps are repeated until the RMS is lower than the estimated error level of the data (1 %) or until the RMS is not decreasing anymore with more than 5 %.

To perform the inversions, RES2DINVx64 version 4.06 is used. This is a computer program that performs rapid 2D and 3D resistivity and IP inversions using the least-squares method to determine a model of the subsurface for data obtained from electrical imaging surveys (Dahlin, 1996; Loke et al., 2003). It can be used for all conventional and non-conventional electrode configurations. Inversions of land, aquatic or cross-borehole surveys can be performed with this program (Loke, 2015). Rectangular model blocks are used. Because sensitivity decreases with increasing distance from the electrodes, the size of the model blocks increases with depth and towards the beginning and end of the profile (Loke, 2015). Hence, settings are adjusted so that the thickness of the model layers increases with depth with a factor of 1.05. The thickness of the first layer is set at 34 % of the electrode spacing. A finite element method with trapezoidal elements is used and an isotropic model is assumed. Before inversion, outliers in the pseudosection are removed during quality control. Since an aquatic survey is executed, water depths below the floating electrodes are incorporated and the measured water conductivity is fixed in the inversions, assuming a sharp change across the water bottom boundary. Also, an extended model is imposed. The initial damping factor applied is 0.15 and increases in depth with a factor of 1.10. It is adjusted to the sensitivity of the model, e.g. higher damping factors are applied at the sides of the model.

The result of an inversion is a model representing resistivity of the subsurface along the profile. One must be aware that the recovered resistivity variation is damped compared to reality as smoothing is applied during inversion (Christensen & Christiansen, 2015). In addition, lateral variations in the third dimension, perpendicular to the profiles, are assumed constant. In reality, there are inhomogeneities in the third direction which influence the resulting patterns in the profiles.

During data acquisition and processing several errors can occur. Possible errors during data acquisition are poor electrode contact, random device errors or external effects (Crook et al., 2008). That is why stacking of at least two and maximum three measurements are performed so that the coefficient of variation between repeated measurements is below 1 % (ABEM Instrument AB, 2012). To analyze acquisition errors, reciprocal measurements could be performed. These are measurements with the same electrode setup but with the current electrodes as the potential electrodes and vice versa. This is discussed in detail in the Master's thesis of Gommers (2017). Another error source is the variation of resistivity in the direction perpendicular to the profile (Christensen & Christiansen, 2015). Furthermore, the RMS error will never be zero after data processing and it is important to be aware that a model is a simplification of reality, always including errors to a certain limit.

The depth of investigation is determined by means of two extra inversions of the data using background reference models with different reference resistivity values (Oldenburg & Li, 1999). One inversion model uses a low reference resistivity of 0.1 times the average apparent resistivity of the data and the second inversion model uses a high reference resistivity of 10 times the average apparent resistivity. Areas where these inverted models look similar are well constrained by the data because, despite the enforced reference resistivity, the models are still comparable. Areas where these inverted models deviate from each other are areas of which little information is obtained from and the reference resistivity consequently has a considerable influence on the resulting model. The index describing the difference between these two models is the DOI index. The closer to 0, the more the model is constraint by the data. The closer to 1, the more the model is constraint by the reference models and therefore, the less reliable the model is in these areas.

Kevin Gommers (2017) investigates in his Master's thesis the design and assessment of ERT and IP in the same study site as this thesis. In his work, an in-depth analysis of DOI and sensitivity are described. 3D inversions of the ERT and IP data are performed and compared with the 2D inversions.

2.4. INDUCED POLARIZATION (IP)

Induced polarization (IP) is a geophysical method which maps chargeability of the subsurface. Chargeability is the degree to which the subsurface can store electrical charge via diffusion polarization mechanisms at mineral grain – pore fluid interfaces. This is usually via accumulation of local charge gradients in electrical double layers (EDLs) of clay minerals (Slater, 2007). IP has the purpose to distinguish changes in lithology and pore fluid.

IP is measured and inverted together with the ERT data. The same field setup is used (Figure 4) with a dipole – dipole electrode configuration (Figure 8) and 0.5 m spacing between the electrodes. Again, for each measurement two pairs of electrodes are operational. Instead of the potential difference measured with ERT, the decaying residual voltage after cut-off of the applied current is measured between the two receiver electrodes. This results in a pseudosection of the apparent chargeability M_a [VV^{-1}] which can be inverted to real chargeability M [VV^{-1}]. Chargeability is defined as the ratio of the residual voltage V_s integrated over a time window Δt after termination of an applied current and the voltage V_p measured at some time during application of the current:

$$M = \frac{\int_{\Delta t} V_s dt}{V_p} * \frac{1}{\Delta t} \tag{2.13}$$

Chargeability is closely related to resistivity, which is a function of porosity and saturation, salinity and clay content, as shown in equations (2.7) & (2.8) (Slater & Lesmes, 2002). Chargeability is thus dependent on bulk conduction and surface polarization mechanisms. To remove the effect of bulk conduction, normalized chargeability MN [$AV^{-1}L^{-1}$] can be calculated. This is chargeability weighted by resistivity:

$$MN = M/\rho \tag{2.14}$$

It is consequently not dependent on bulk conduction mechanisms, such as porosity and pore water properties, but only on the magnitude of surface polarization properties of the material. These are mainly surface conductivity and specific surface area of the sediments (Weller et al., 2015). Normalized chargeability is accordingly used to detect changes in structural properties, more specifically in variability of clay content (Slater & Lesmes, 2002). More clay leads to more surface area and surface conductivity. This creates more polarizability and thus a higher normalized chargeability (Slater & Lesmes, 2002; Titov et al., 2010). Another way to express chargeability is relaxation time (Attwa & Günther, 2013; Titov et al., 2010). This is the time it takes to equilibrate to the background potential difference between the electrodes.

As IP data acquisition and processing occurs simultaneously with ERT data acquisition, the same methods and settings are applied. For both, the ABEM Terrameter LS1 is used (Figure 7) with the dipole – dipole array (Figure 8) and the electrodes floating on the water surface (Figure 9). A time-domain waveform of one positive and one negative current pulse is injected. The residual voltage is measured in 12 consecutive windows of 0.10 – 0.30 s, in such a way that the window length increases in time. The first time window starts recording 0.05 s after the current is switched off. The total chargeability is measured as the average of values measured in all the time windows. In addition, because the same electrode configuration is applied as for ERT, also the influential volume of IP is the same. The length is thus at least 1.5 m, but height and width are not known and variable, depending on the distance between the dipoles.

The inverse problem for IP is the same as for ERT: the best model of chargeability below the profile is sought by iteratively calculating the forward model and comparing calculated apparent chargeability with measured data to improve the model. The same non-linear smoothness-constrained least-squares method is used as for ERT, specified in equations (2.10) & (2.11) (deGroot-Hedlin & Constable, 1990; Loke et al., 2003). The same inversion parameters and model dimensions are implemented in the

program RES2DINV (Dahlin, 1996; Loke et al., 2003). The IP model damping factor used is 0.25. The RMS error is calculated as in equation (2.12). Error, DOI and sensitivity analyses are performed during ERT processing and also apply to IP data. In IP processing and interpretation, it is assumed that chargeability is invariant perpendicular to the profile.

2.5. RIVERBED DRILLING

To link the results of slug tests, ERT and IP to lithological differences, drillings are performed in the riverbed. A riverbed auger is used to recover sediment. This is a hollow, metal tube of 80 cm long, which is closed at the bottom with a valve (Figure 10). The valve hinges towards the inside of the tube. The tube is pushed into the sediment to the desired depth. The valve closes when the tube with sediment is pulled up and sediment material is recovered by holding the auger upside down. Locations where drillings are performed are indicated in Figure 4 and described in section 2.1.

Figure 10 Pictures showing the riverbed auger with indication of the length and the closing valve.

2.6. LINKAGE OF SLUG TEST RESULTS WITH ERT AND IP RESULTS

The main objective of the thesis is to compare slug test estimations of horizontal hydraulic conductivity with resistivity, chargeability and normalized chargeability in the riverbed. Therefore, results of all methods should be linked to each other to make comparison valuable. In a first step, profiles of the slug test survey should be related to those of the ERT and IP survey, as shown in Figure 11. In a second step, geo-electrical data corresponding to the point measurements of K should be extracted from the continuous 2D profiles, obtained from ERT and IP inversion.

Connection of slug test profiles to ERT and IP profiles is based on GPS coordinates measured during the slug test survey. Measured profiles are indicated in the field, so that profiles are measured at the

same location. However, the exact start and end of the ERT and IP profiles are not known because no GPS coordinates or distances from the banks have been measured during the geo-electrical survey. GPS coordinates of the electrodes in the ERT & IP profiles are therefore calculated based on the GPS coordinates of the slug tests measurements. The ERT profiles are longer than the slug test profiles: the first and last electrode of the survey are laid on the water surface immediately next to the banks, while the first and last slug test point locations in each profile are at a certain distance from the banks (Figure 11). Accordingly, the slug test profiles fit within the length of the ERT profiles, as these latter represent the whole width of the river. Next, it is assumed that the first and last slug test point are located at equal distance from the left and right bank, equivalently from the first and last electrode, respectively. In this way, the GPS coordinates of every electrode can be calculated. Changes in the water level can however change the width of the river asymmetrically due to differences in the slope at the right and left bank respectively. The assumption of a symmetric fit of a slug test profile in an ERT profile can therefore lead to small errors in the calculations. That is why the coordinates of reference points on the right bank are calculated as well, to verify the difference in calculated and measured GPS coordinates. This error is subdivided over the calculated electrode coordinates as a correction term.

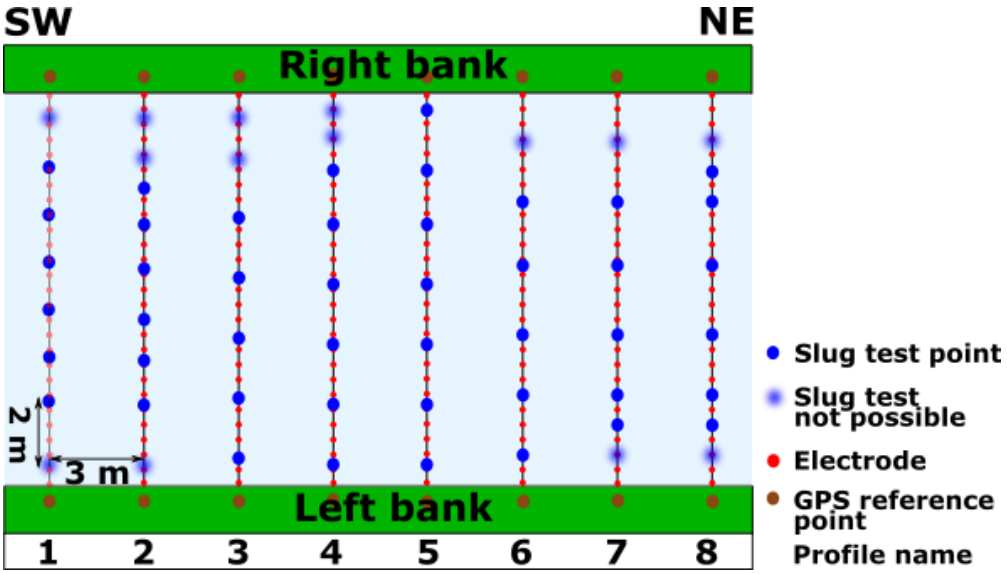

Figure 11 Linkage of slug test profiles and geo-electrical profiles.

Because slug test results are point measurements of hydraulic conductivity, corresponding point locations (exact, or spatially averaged) need to be extracted from the ERT & IP profiles. Therefore, slug test points need to be located within the geo-electrical profiles first. The 'ERT coordinates', i.e. the distance displayed in an ERT or IP profile (between 1 – 14 m), of the slug test measurements are calculated based on the distance between the first electrode and the slug test point:

$$x_{E1-S} = \sqrt{(X_{E1} - X_S)^2 + (Y_{E1} - Y_S)^2} \tag{2.15}$$

where $x_{E1\text{-}S}$ is the distance [L] between the first electrode in the water E1 and a slug test point S, X and Y are GPS coordinates [L]. This distance calculated for each slug test point is then added to the ERT coordinate of the first electrode in the profile (i.e. 0.25 m less than the start of the profile display, e.g. Figure 24). Again, because of the error in the measured distances between the slug test points, ERT coordinates of the slug test point locations need to be corrected. This is done by subdividing the error, i.e. the difference in the calculated and real ERT coordinate of the last electrode, between the slug test points depending on the distance from the first electrode:

$$corrected\ ERT\ coordinate = uncorrected\ ERT\ coordinate + error * \frac{distance\ to\ E1}{total\ distance\ of\ profile} \tag{2.16}$$

The depth of the slug test in the ERT profile is calculated by adding the water depth, measured at the moment of ERT measurements, to the average slug test depth.

The next step is to extract geo-electrical data from the ERT and IP profiles at the same location of the slug test points. To do so, several methods at different extraction scales are tested and compared, summarized in the following paragraphs and Table 2, as well as visually shown in Figure 12.

Table 2 Overview of the type of methods used for data extraction of hydraulic conductivity and geo-electrical parameters.

Method	Type of comparison	Window	Number of iterations
Method 1	Point comparison	Point	Last iteration
Method 2	Areal comparison	Square of 50 cm	Last iteration
Method 3	Areal comparison	Rectangle of 1.5 m	Last iteration
Method 4	Areal comparison	Rectangle of 1.5 m	Third iteration

First, point comparison is performed. Values of exactly corresponding point locations are compared to each other. A grid with a point spacing of 6 cm is overlain on the continuous ERT and IP profiles to enable extraction of the geo-electrical values. With this method, single values of resistivity, chargeability and normalized chargeability are compared with the point measurements of hydraulic conductivity (Figure 12). An advantage is that all K values can be compared to a geo-electrical value and an average of the two depths does not need to be considered. However, it should be kept in mind that a point measurement of K is assumed to be situated in the middle of the interval over which the slug test was performed, i.e. at 32.5 cm depth for the shallow interval and 57.5 cm depth for the deep interval. Point extraction is consequently very local and there is a large probability that not exactly corresponding points are compared due to errors in GPS or ERT coordinate linkage. There are also errors because the K value at the middle of the depth interval is taken instead of considering the whole depth interval and because geophysical properties are only representative for a certain volume and not for a single location.

Secondly, comparison of hydrogeological and geo-electrical parameters is based on areal comparison. Several values around the corresponding point locations and within the profiles, are considered in one single value, by averaging over a certain area. This is done because the measurement scale of the applied methods is larger than a point location in a grid of 6 cm x 6 cm. Slug tests are performed with a filter of length 25 cm, but the influencing slug test radius cannot be predicted exactly and is dependent on surrounding sediment. The length of the area influencing ERT and IP measurements is stated to be at least 1.5 m, but the height and width of influence are unknown (section 2.3 & 2.4). Because of the uncertainties in different directions, the scales of the methods are difficult to compare and by averaging values over different areas, it is therefore investigated which scale makes both methods comparable. Volume comparison is however not possible, because only 2D inversions are analyzed in this thesis.

Therefore, a second method for comparison is done based on averaged geo-electrical parameters over a square with a side of 50 cm (Figure 12). The arithmetic mean of five values is considered: the central corresponding point location, as used in method 1, and points at 25 cm to the left, right, above and below the central point. In this way, it is possible to compare all measured K values, both depths considered separately, with corresponding ρ, M and MN values.

The third method uses a rectangle of 1.5 m length around a central corresponding point location. All grid values of a geo-electrical parameter are averaged in a rectangle with sides at 75 cm to the left, right and below the central point (Figure 12). Because of limited depth of K measurements, the upper side of the rectangle is situated at the water level, which is less than 75 cm above the central point. Because this rectangle incorporates both depths of hydraulic conductivity measurements, values at separate depths are averaged to one value of K per locality. Consequently, the central point in this method is situated at a depth of 45 cm below the riverbed (Figure 12), instead of at 32.5 cm and at 57.5 cm below the riverbed. The harmonic, arithmetic and geometric mean of K are tested for comparison.

The fourth method for comparison is the same data extraction method as the third one, but with use of inversion results after three iterations (Figure 12). Because the RMS error is already low for all profiles after three iterations, it is interesting to check if further development of the model actually results in better correspondence between hydraulic conductivity and geo-electrical parameters. With fewer iterations, subsurface structures are not yet clearly aligned and are thus more smoothed.

These four types of comparison are analyzed to find the optimal method for correlation between hydraulic conductivity and geo-electrical parameters. The best method is used for further in-depth analyses and comparisons.

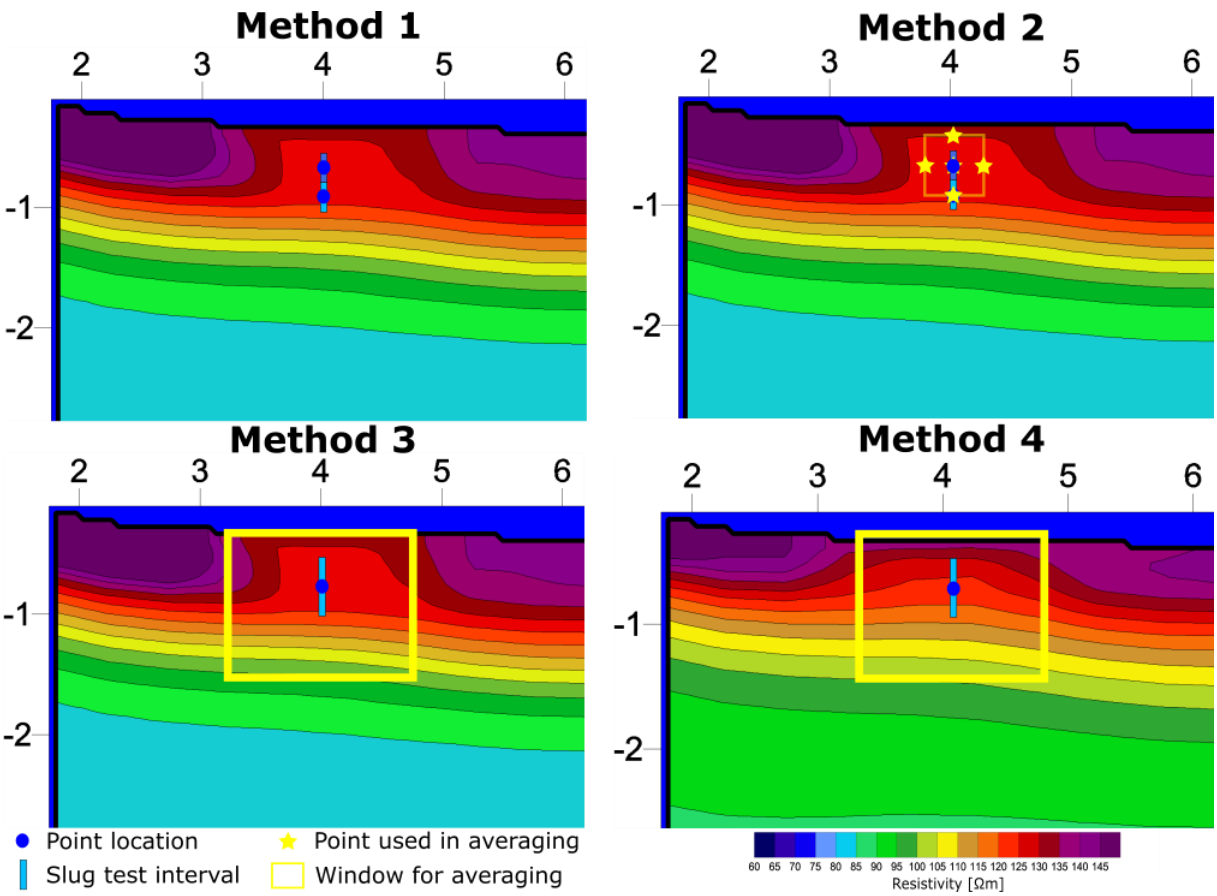

Figure 12 Visualization of data extraction methods from geo-electrical profiles.

After data extraction, points of hydraulic conductivity and geo-electrical parameters can be meaningfully correlated with each other. With use of GPS coordinates, calculated for the point data, point maps can also be made for resistivity, chargeability and normalized chargeability. This is done either for data at the separate depth intervals (for method 1 and 2) or for all data (for method 3 and 4). These point maps are then compared to those of hydraulic conductivity data, at both depth intervals (for method 1 and 2), harmonically averaged (for all methods) or arithmetically and geometrically averaged (for method 3). It is investigated if similar patterns or groups of points can be recognized and how correlations occur.

In addition, scatterplots of point data are made. Hydraulic conductivity data is plotted against resistivity, chargeability or normalized chargeability data. This is done for datasets containing all data, for subdatasets with only data of a depth interval or with harmonically averaged data. All scatterplots have been investigated without transformations, with a (natural) logarithmic transformation of one of the parameters or with both parameters transformed. Trends in the scatterplots are visually assessed.

2.7. STATISTICS

Several statistical analyses are performed. On the one hand, descriptive statistics are performed to obtain general information on the distribution and magnitude of the parameters. On the other hand, statistical analyses investigating the correlation between the parameters are executed. The purpose is to check the significance of relations between hydraulic conductivity and geo-electrical parameters. For all statistical calculations, Rstudio (Rstudio, 2015) is used.

2.7.1. DESCRIPTIVE STATISTICS

First, descriptive statistics are performed on the acquired hydraulic conductivity data, resistivity, chargeability and normalized chargeability data. Measures of central tendency and dispersion are calculated to evaluate the order of magnitude, variation and range of the variables. Histograms, Shapiro-Wilk tests and possibly transformations are made to analyze the distribution of the variables. This statistical analysis is performed for all K, ρ, M and MN values, for values at the separate depth intervals and for harmonic mean K values at each point location. The harmonic mean of K is calculated because low K values have a considerable influence on vertical flow through the riverbed. Independent samples t-tests are performed to test the significance of differences between two groups (e.g. between the two depth intervals).

2.7.2. LINEAR REGRESSION

When hydraulic conductivity and geo-electrical parameters are compared, scatterplots of K versus resistivity, chargeability and normalized chargeability are created. After visual analysis of the plots, linear models are fit to the data. A line is estimated through the points using the least squares method (Chambers, 1992). This method minimizes the residual sum of squares RSS, calculated as

$$RSS = \sum_{i=1}^{N} (y_i - (ax_i + b))^2 \tag{2.17}$$

with y_i is the i^{th} value of the variable to be predicted, x_i is the i^{th} value of the explanatory variable, a is the estimate of the slope and b is the estimate of the intercept. The explanatory variable x, in this study, is hydraulic conductivity. The y variables are resistivity, chargeability or normalized chargeability. The resulting equation of the fit is then given as

$$y = ax + b \tag{2.18}$$

The p-value for both estimates is considered significant if its value is below 0.05. Especially the p-value of the slope is of importance for assessment of correlations. Also, the adjusted R^2 is calculated for each model. This is the proportion of the variance explained by the linear model, i.e. the coefficient of determination R^2, corrected for the number of parameters p. Also, the number of samples n is taken into account:

$$adjusted\ R^2 = 1 - (1 - R^2)\frac{n-1}{n-p-1} \tag{2.19}$$

95 % confidence intervals C.I. are calculated for the estimate of the slope as follows

$$95\ \%\ C.I. = [a - 1.96 * s.e.; a + 1.96 * s.e.] \tag{2.20}$$

with a is the estimate of the slope and s.e. is the standard error on this estimate. The confidence intervals are smallest in the center of the fitted line and widen further away from the center.

When linear regressions are fit to point data in scatterplots, it is assumed that the relationship between the variables is linear, that residuals are normally distributed and that the variance across the regression line is homogeneous.

2.7.3. PRINCIPAL COMPONENT ANALYSIS (PCA)

A principal component analysis PCA is performed on the multivariate dataset with n objects, i.e. the point locations, and four variables: hydraulic conductivity, resistivity, chargeability and normalized chargeability. The concept of a PCA, described by Mardia et al. (1979), is to rotate the original system of axes (assigned to the variables) so that new axes are defined orthogonal to one another. These new axes are called principal components. Axes are numbered and successive axes represent successive dimensions of maximum variance of the scatter of points. The results of a PCA are new positions of the objects in a coordinate system of principal component axes instead of in a coordinate system of axes with the variables.

The mathematical calculation of a PCA is the eigenanalysis of the dispersion matrix S:

$$S = (n-1)^{-1} {Y'}_c Y_c \tag{2.21}$$

with n is the number of objects and Y_c is the column-centered and standardized matrix of dataset Y. The results of the eigenanalysis are eigenvectors, which are the principal axes, and eigenvalues, which give the amount of variance of the data along the corresponding principal axis. Principal axes, or principal components PCs, are orthogonal to each other. The first PC explains the largest part of the variance in the dataset. The second PC explains the second largest part, etc.

The components of the eigenvectors in the principal component system are the loadings of the variables (K, ρ, M and MN) in this new coordinate system. The coordinates of the objects, here the point locations, in the PC coordinate system are called the scores of the objects. Loadings and scores are plotted in a biplot. This is a plot of PC 1 versus PC 2 with the loadings of the variables plotted as arrows and the scores of the objects plotted as dots. The scores are given on the left and bottom axis, while the values of the loadings are given on the top and right axis. The type of biplot used in this dissertation is a correlation biplot. This means that the angles between the variables and/or objects reflect their mutual correlation, but the distances between objects cannot be interpreted as approximations of Euclidean distances in multidimensional space. With use of a PCA, clusters or groups in the dataset can be recognized. Points plotting within a similar angle to certain variables show more correlation than points which are connected by large angles.

2.7.4. CLUSTER ANALYSIS (CA)

A cluster analysis (CA) is a quantitative way to classify objects in a multivariate dataset. Next to this quantitative method for clustering, clustering of data points based on visual comparison between hydraulic conductivity and one or more geo-electrical variables is conducted. Although this visual clustering is subjective, it provides clusters which are continuous in space.

A quantitative cluster analysis is performed with four hierarchical cluster methods: single linkage agglomerative clustering, complete linkage agglomerative clustering, unweighted average linkage agglomerative clustering (Unweighted Pair Group Method with Arithmetic mean, UPGMA) and Ward's minimum variance method, described by Everitt (1974). For all methods, a distance matrix must be calculated first. This matrix contains the distances between objects, calculated as the sum of squared difference between two objects. This yields one value for each pair of points in an n x n matrix. The resulting clusters are visualized graphically in a dendrogram, indicating the distance, or 'height', at which objects are aggregated. It shows thus the cluster topology.

Single linkage agglomerative clustering constructs clusters by grouping first the two closest objects, then the second closest objects or pair of objects, etc. Aggregation results in continuously increasing groups until all objects are part of the same cluster.

The concept of complete linkage agglomerative clustering is that fusion of two clusters depends on the most distant pairs of objects. An object only joins a cluster if it is linked to all the objects already member of that cluster.

The unweighted average linkage agglomerative cluster method (UPGMA) first groups two objects which are closest to each other. Then, distances from that pair to all other objects are calculated as the average of distances between the individual points of the pair and the other objects. This process is continued until all objects belong to the same cluster.

Ward's minimum variance method minimizes the sum of squared distances between the centroids of clusters. If there are no clusters yet, all objects are their own cluster and the distance to their centroid is 0.

To evaluate which clustering method is best, two measures can be used as an indication. The first one is cophenetic correlation. This is the Pearson's correlation coefficient, calculated between the original distance matrix and the cophenetic matrix. The cophenetic matrix contains all cophenetic distances, which are the distances where two objects become a member of the same cluster. The higher cophenetic correlation, the better the cluster method.

Another measure to find the optimal cluster method is the Gower distance. This is the sum of squared differences between the original and cophenetic distance between the objects. The clustering method with the lowest Gower distance indicates the most optimal method.

2.8. GEOSTATISTICS

Exploratory geostatistical analyses are performed for hydraulic conductivity values (all K values, K values at separate depths and harmonically averaged K values), extracted resistivity, chargeability and normalized chargeability data, or possibly for transformations of these data. These will be compared to each other to find a spatial relation between hydraulic conductivity and one or more geo-electrical parameters.

First, variograms are made using SGeMS (Remy, 2004). A variogram is a plot of the semi-variance and the distance or 'lag' h [L] between two points x_i and x_{i+h} [L]. The semi-variance of a variable Z is defined as

$$\gamma(h) = \frac{1}{2N} * \sum_{i=1}^{N} [Z(x_i) - Z(x_i + h)]^2 \tag{2.22}$$

where N is the number of measurements (Gelhar, 1993). Each point on a variogram corresponding to a certain lag, comprises thus a number of measurements or pairs. The larger the number of pairs for a certain lag, the more representative and reliable the point on the variogram. When a fit is sought between points on the variogram, focus is put on lags with the largest number of pairs. Lags with 10 pairs or less are considered not to be reliable. First, omnidirectional variograms are constructed to explore the overall spatial continuity of a variable. Then, directional variograms are made to detect the degree of spatial correlation and directional anisotropy. It can also reveal trends in cross sections. Directional variograms are made parallel and perpendicular to the river flow direction.

Figure 13 shows an example of a variogram. The semi-variance is small for small lags and increases with increasing lag. From a certain lag, the semi-variance becomes independent of the lag. This lag distance is called the 'range'. It is an indication of the distance of spatial dependence. In other words,

the range shows to which distance of a certain point, another point is still influenced by the value of the variable at this point. Next, the sill of a variogram is the maximum value of the semi-variance and is, in theory, similar to the variance of the variable itself. Mostly also a nugget is present in a variogram. This is a deviation of the semi-variance from zero when h = 0 because of variability at a smaller scale than the scale of the measurement or due to measurement errors. It gives information on the importance of small scale variation or uncertainty. Further, in directional variograms, the tolerance angle (angle away from the viewing line, indicating which points are incorporated in the variogram) is set to 22.5° for hydraulic conductivity data and 45° for geophysical data, while this is 90° in all omnidirectional variograms. Because data in a variogram is often not straightforward to plot on a curve, multiple lags and lag separations are used in such a way that points comprising a lot of pairs are considered more reliable. The most optimal values for the range, sill and nugget are considered in further analyses.

To obtain values for the range, sill and nugget of a variogram, a model is fit to the lag points. Spherical models are most used for this purpose, but for very smoothly varying data, Gaussian models often give a better fit. Model fits are based on visual inspection and trial-and-error for good correspondence between the data and the model.

Variograms are made for obtained hydraulic conductivity data and for resistivity, chargeability and normalized chargeability data. By comparing their ranges, similarities in spatial dependence of the variables can be detected.

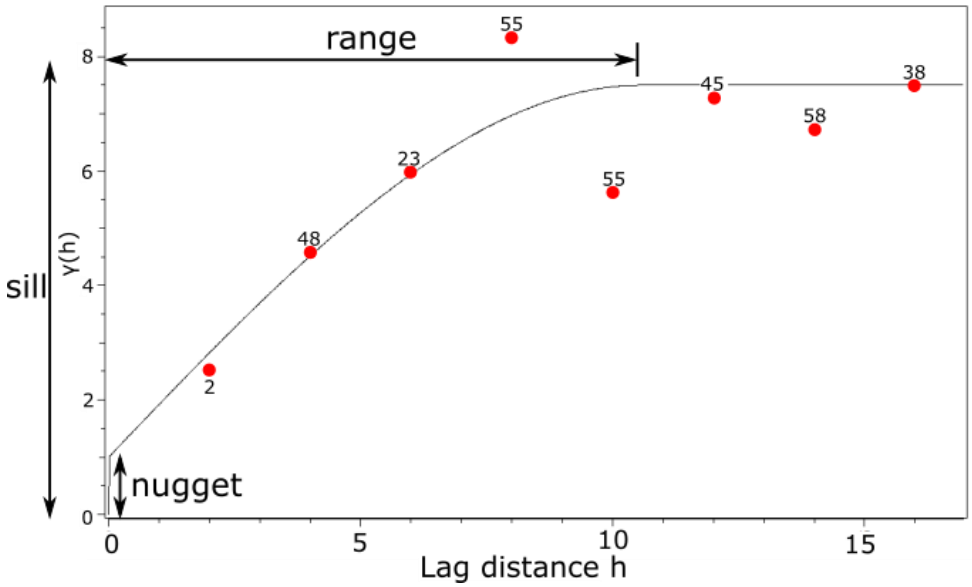

Figure 13 Example of a variogram of K values in the shallow depth interval. The range, sill and nugget are indicated. Numbers represent the number of pairs for a specific lag.

Using the obtained variograms, ordinary kriging is performed to interpolate a variable between point values. To do this, also SGeMS (Remy, 2004) is used. A spatially continuous image is the result and provides another means to compare the spatial distribution of hydraulic conductivity and geo-electrical parameters with one another. Kriging is finding the optimal weights λ_i using semi-variances calculated from the variogram model (Oliver & Webster, 1990). Estimates of unknown points are weighted linear combination of the values of known points within a certain search window (Myers, 1992):

$$Z^*(x) = \sum_{i=1}^{N} \lambda_i(x) * Z(x_i) \tag{2.23}$$

where $Z^*(x)$ is the estimated value of the variable at point x and $Z(x_i)$ is the true value of the variable at point x_i. The applied search window is a circular ellipsoid with a radius of 10 m including minimum 2 and maximum 12 data points in the search ellipsoid.

In ordinary kriging, there is only a constant unknown mean in the search ellipsoid of x (Myers, 1992). Therefore, two criteria should be fulfilled (Oliver & Webster, 1990). First, the model should be unbiased. This is the case when the sum of the weights equals 1 ($\sum \lambda_i = 1$). The second criterion states that the variance of the estimate should be minimal:

$$\frac{1}{N} * \sum_{i=1}^{N} (Z_i^*(x) - Z_i(x))^2 = minimal \tag{2.24}$$

Solving this optimization system results in the following kriging system, which includes the variogram model previously calculated:

$$\begin{bmatrix} \hat{\lambda} \\ \varphi \end{bmatrix} = \begin{bmatrix} Var_{x_i} & 1 \\ 1^T & 0 \end{bmatrix}^{-1} * \begin{bmatrix} Cov_{x_i,x} \\ 1 \end{bmatrix} = \begin{bmatrix} \gamma(x_1,x_1) & \cdots & \gamma(x_1,x_n) & 1 \\ \vdots & \ddots & \vdots & \vdots \\ \gamma(x_n,x_1) & \cdots & \gamma(x_n,x_n) & 1 \\ 1 & \cdots & 1 & 0 \end{bmatrix}^{-1} * \begin{bmatrix} \gamma(x_1,x^*) \\ \vdots \\ \gamma(x_n,x^*) \\ 1 \end{bmatrix} \tag{2.25}$$

where Var_{x_i} is the variance of x_i [L²], $Cov_{x_i,x}$ is the covariance of x_i and x [L²], $\gamma(x_i, x_j)$ is the semi-variance between point x_i and x_j and φ is the Lagrange-multiplicator. This is valid when the variable is intrinsic, which means that the variable is stationary and the variogram is constant over the domain (Oliver & Webster, 1990). An important advantage of kriging as interpolation method is the fact that also the associated error variance on the estimate Z*(x) is calculated. This is a linear combination of the semi-variance between the unknown point and known points (Oliver & Webster, 1990). The error variance is low close to known points while it becomes larger at increasing distances from known points.

2.9. THEORY FOR CORRELATION BETWEEN HYDRAULIC CONDUCTIVITY, RESISTIVITY, CHARGEABILITY AND NORMALIZED CHARGEABILITY

Interpretation of ERT and IP profiles is not straightforward since resistivity, chargeability and normalized chargeability are dependent on several factors. The influence of these factors to a specific value is variable. Therefore, profiles of the three geo-electrical variables should be interpreted together, with results of riverbed drillings in consideration.

In sedimentary environments, bulk resistivity is mainly dependent on pore water. Porosity, temperature and salinity of pore water are thus influencing factors of subsurface resistivity (Christensen, 2000) (Table 3). The higher the porosity, the more water in the pore space, the more conductive the medium. Temperature and salinity of pore water are inversely proportional to resistivity of the medium (Table 3). Hayley et al. (2007) stated a resistivity decrease of 1.8 – 2.2 % per degree Celsius increase in water temperature. The effect of salinity and temperature is important if differences in the subsurface are strong enough. Also clay and organic matter (OM) content are influencing factors of resistivity (Chen et al., 2008). The electrical double layer (EDL) associated with these materials enhances electrical flow through sediment and reduces consequently resistivity (Slater, 2007). However, fine particles of clay and organic matter can also decrease pore volume in sands, leading to higher resistivity.

Chargeability and normalized chargeability are measures for the degree of storage of electrical charge in the subsurface. They are mainly controlled by surface polarization mechanisms. These mechanisms are interconnected surface area and surface conductivity. The most important surface polarization mechanism is the EDL associated with clay and organic material. Chargeability can also be influenced by bulk conduction properties, such as pore volume and pore water properties (Slater & Lesmes, 2002). The larger the porosity, the more water can be present between the sediment grains. Because water is hardly chargeable, it decreases chargeability (Table 3). In addition, the magnitude of polarization decreases with increase of water conductivity, related to salinity and temperature (Slater & Lesmes,

2002; Titov et al., 2010) (Table 3). By normalizing chargeability with resistivity, this dependency on bulk conduction disappears. Hence, almost only surface properties of the sediment are of importance for the value of normalized chargeability (Slater & Lesmes, 2002). Electrical surface conduction is dominated by accumulation of local charge gradients in the EDL at the mineral – pore water interface (Slater, 2007). More clay and organic matter result thus in a higher surface conductivity. Moreover, small, platy particles increase specific surface area, enhancing the effect of the EDL. Consequently, the higher the clay content, the more chargeable the sediment.

Differences in chargeability and normalized chargeability can be used to distinguish large temperature and salinity effects from lithological effects. Furthermore, groundwater generally has a higher salinity than river water and its temperature is less fluctuating (Nyquist et al., 2008). In winter, temperature of groundwater is higher than temperature of surface water and in summer, the opposite is true. As ERT and IP measurements are performed in winter, conductivity of surface water is assumed to be lower than conductivity of groundwater in this study (Table 4), because temperature and salinity of surface water are assumed to be lower than those of groundwater.

Table 3 Overview of the influence of clay and organic matter (OM) content, pore volume, salinity and temperature on riverbed resistivity, chargeability and normalized chargeability. Relations in italic indicate their limited influence.

	Clay and OM content	Pore volume	Salinity	Temperature
Low ρ	High	High	High	High
High ρ	Low	Low	Low	Low
Low M	Low	High	High	High
High M	High	Low	Low	Low
Low MN	Low	*Low*	*High*	*High*
High MN	High	*High*	*Low*	*Low*

In accordance to the above described factors, resistivity and normalized chargeability can be linked to certain lithologies. Sand is more resistive and less chargeable than clay and organic matter. Several ranges for sediments in the riverbed can be assumed. Table 4 gives an overview of these assumed ranges based on ranges found in literature (Appendix A). These values are indicative and in no way stringent. According to Anibas et al. (2011), the riverbed is composed of fine sand with organic matter and clay in varying contents.

Table 4 Indicative ranges of resistivity and normalized chargeability for sediment and groundwater. Ranges are based on literature (Appendix A), with a wide tolerance for range limits.

	Resistivity [Ωm]	Normalized chargeability (mS/m)
Sand	40 – 250	0.01 – 0.025
Sand & clay	20 – 160	0.10 – 0.25
Clay	1 – 100	> 0.50
Peat, organic matter	10 – 70	-
Fresh water	3 – 120	-
Groundwater	10 – 40	-

Hydraulic conductivity is determined by pore space geometry and effective porosity (Attwa & Günther, 2013). Interconnected pore space area is thus of primary importance for K. Clay and organic matter consequently decrease hydraulic conductivity by blocking pore connections. Moreover, decreasing porosity could make water flow through sediments more difficult.

Because clay and organic matter content strongly determine both hydraulic conductivity and chargeability or normalized chargeability, correlation between both is expected to be relatively direct. Additionally, opposite dependence of chargeability and hydraulic conductivity on both clay content and porosity, make correlation between both probable. Resistivity is also influenced by both surface properties of the sediment, and porosity and pore water properties. But opposed to chargeability, compensation of effects can occur, making the expectation of correlation between hydraulic conductivity and resistivity more variable. The importance of one or the other factor in the value of resistivity is dependent on the amount of clay or other fine particles. Purvance & Andricevic (2000) found a linear-log relation between hydraulic conductivity and the real part of electric conduction. This relation is negative in clay and silt, where electrical current flow is dominated by interconnected pore surface area properties. In sand and gravel sediments, the linear-log relation is stated to be positive, because the effect of pore volume dominates. Attwa & Günther (2013) stated that for sandy, clayey soils, a negative correlation exists between hydraulic conductivity and resistivity on a local scale, while this is positive on a large scale e.g. of an aquifer. Also Kazakis et al. (2016) identified a negative linear relation between K and ρ.

3. Results

In this section, results of data acquisition and analyses are presented. First, results of the individual methods are given, i.e. of the slug test analysis, electrical resistivity tomography (ERT), induced polarization (IP) and riverbed drilling at the field site. The obtained data, more specifically hydraulic conductivity K for slug tests, resistivity ρ for ERT, chargeability M for IP and normalized chargeability MN for both ERT and IP, are shown and statistically analyzed. Also, patterns in space and depth are considered and the results of geostatistical analyses are shown. The latter include variograms and kriging. Next, a comparison of all data is performed for correlation between hydraulic conductivity and these geo-electrical data. Relations between K and geo-electrical data are explored using visual comparison, as well as statistically by point and area comparison.

3.1. SLUG TEST ANALYSIS

Horizontal hydraulic conductivity is measured using slug tests along eight profiles at the field site (Figure 4). Per profile, K_h is measured at approximately six point locations at two different depths. The first depth interval is between 20 and 45 cm below the riverbed and the second depth interval is between 45 and 70 cm below the riverbed. The Bouwer & Rice method (1976) is used to calculate horizontal hydraulic conductivity values. If repeated tests are performed, the average value is used in further analysis. Similarly as stated in section 2.2, horizontal hydraulic conductivity will be referred to as hydraulic conductivity, and abbreviated by K instead of K_h, unless ambiguity can occur. In addition, it must be remarked that measurements that were planned to make near the right bank, and some near the left bank, were not possible to execute because of two reasons: either the riverbed could not be penetrated with the piezometer or the measurement took too much time. This is the case for all profiles except for profile 5 (Figure 4). Moreover, not all measurements in the deep depth interval could be performed because of the same reasons. This was the case for 10 points, all situated in proximity of the banks.

Mean horizontal hydraulic conductivity in the study area is 4.24 m/d with a standard deviation of 3.07 m/d. The data does not follow a normal or lognormal distribution (Figure 14 A & B). All measured data of K range between 0.11 m/d and 11.39 m/d, which corresponds to 1.27×10^{-6} m/s and 1.32×10^{-4} m/s, respectively. Hydraulic conductivity varies thus over two orders of magnitude in a small study area of 25 m x 15 m.

Considering only the K values measured in the shallow depth interval of 20 – 45 cm, average hydraulic conductivity is 5.74 m/d with a standard deviation of 2.78 m/d. K values vary between 0.79 m/d and 11.23 m/d and have a normal distribution (Figure 14 C). In the deeper depth interval of 45 – 70 cm the mean hydraulic conductivity is 2.37 m/d with a standard deviation of 2.31 m/d. Minimum and maximum measured K are 0.11 m/d and 11.39 m/d, respectively, at this depth and values are lognormally distributed (Figure 14 D). Spatial distribution of K values at shallow and deep depth is visualized in Appendix B Figure 1 and Figure 2, respectively. There seems to be a striking difference in the magnitude of K between the two depth intervals, with high K values occurring at shallow depth and low K values deeper in the riverbed. An independent samples t-test confirms that there is a significant difference in means of K between the shallow and deep depth interval. This is also visualized in Figure 15 where in each profile hydraulic conductivity between 20 – 45 cm is higher than hydraulic conductivity between 45 – 70 cm.

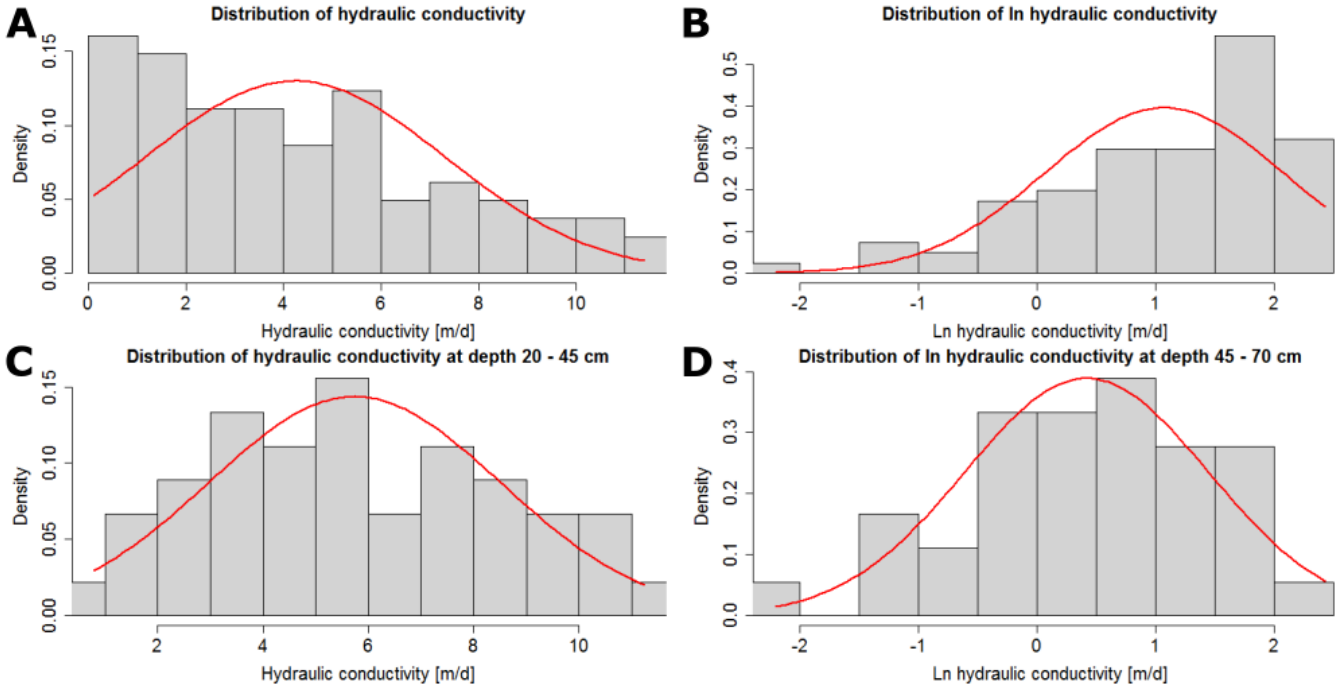

Figure 14 Frequency distribution of (A) all hydraulic conductivity data, (B) the natural logarithm of all hydraulic conductivity data, (C) hydraulic conductivity in the shallow depth interval, (D) the natural logarithm of hydraulic conductivity in the deep depth interval.

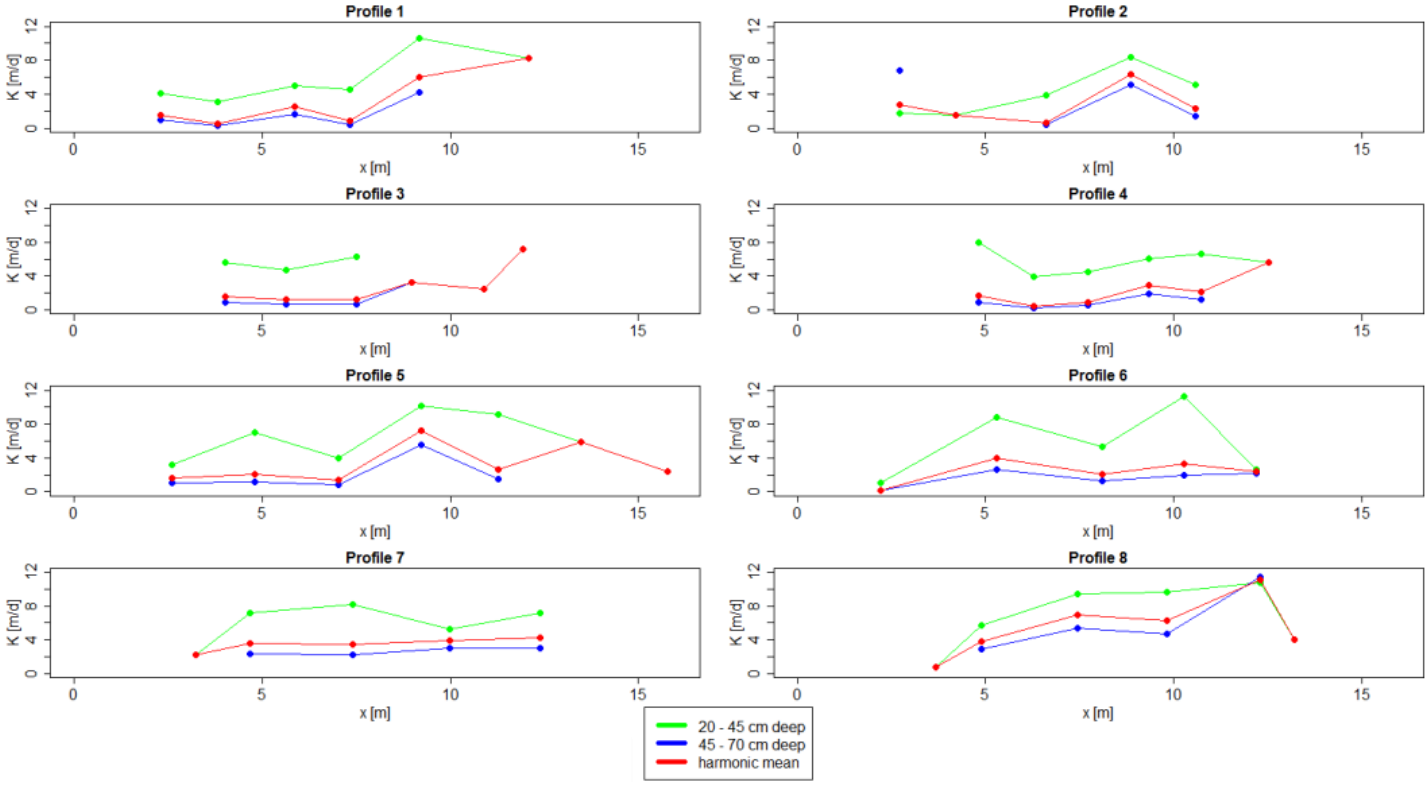

Figure 15 Variation of hydraulic conductivity with distance along the profiles. Distance x increases from left to right bank.

The spatial distribution of hydraulic conductivity is shown in Figure 16. This figure also shows that high hydraulic conductivities are present at shallow depth and low values are measured in the deeper depth

interval. In general, there is a pattern of high values in the right part and upstream in the middle of the river, while low values occur along the left bank and downstream in the middle. This pattern is more expressed when harmonic means of the two depth measurements at each point location are considered. The harmonic mean is the type of average which is most representative for cases of vertical flow through sediments. This is because low hydraulic conductivity has a considerable influence on flow through the riverbed. The map of average conductivity values shows that a visual subdivision in zones is possible (Figure 17). In section 3.4.7, a cluster analysis will be performed to visualize and quantify several possibilities of zonation. First, a high K_{mean} zone, indicated by the red polygon in Figure 17, is situated in the right part of the river and across the river at the upstream end of the study area. Average K_{mean} in this zone is 4.66 m/d with a standard deviation of 2.24 m/d. Values vary between 2.09 m/d and 11.10 m/d and are lognormally distributed. A low K_{mean} zone is situated at the left-hand side of the riverbed and towards the middle in the downstream part of the study area. Values of low K_{mean} vary between 0.20 m/d and 2.77 m/d and have an average value of 1.40 m/d with a standard deviation of 0.73 m/d. Low K_{mean} is normally distributed.

Repeated tests have been conducted to check for reproducibility of the results, to detect low K skins or to confirm bad measurements where they were suspected, e.g. when the initial displacement of the water level was too small. Two or three repeated tests are performed at eight distinct locations. These measurements are performed on exactly the same location and depth after water in the piezometer re-equilibrated, without removal and reintegration of the slug test apparatus. The error between repeated measurements is calculated as the difference between the maximum and minimum measured K value divided by the average K value of repeated tests at that location. Repeating errors vary between 2 % and 40 %. They are 15 % on average with a standard deviation of 14.32 %. The reason for this relatively high error level is because repeated tests are mainly performed at locations where a first measurement was assessed not to be reliable enough. A lot of repeated tests were executed in a previous campaign on the same river and with the same setup. These yielded low errors (6.52 % on average with 5.95 % standard deviation), which allows the assumption of the absence of a low K skin for slug test measurements in this section of the Aa river. By visual inspection of normalized head vs. log(t) plots, the accuracy of repeated tests is assessed. Repeated tests showing equal or very similar curves in the log(t) versus normalized head plots, are maintained in the analysis using the average K value of the repeated measurements at that location. Curves of repeated tests that are deviating from each other in the log(t) versus normalized head plots, cannot be considered as reliable and are therefore not incorporated in further analyses.

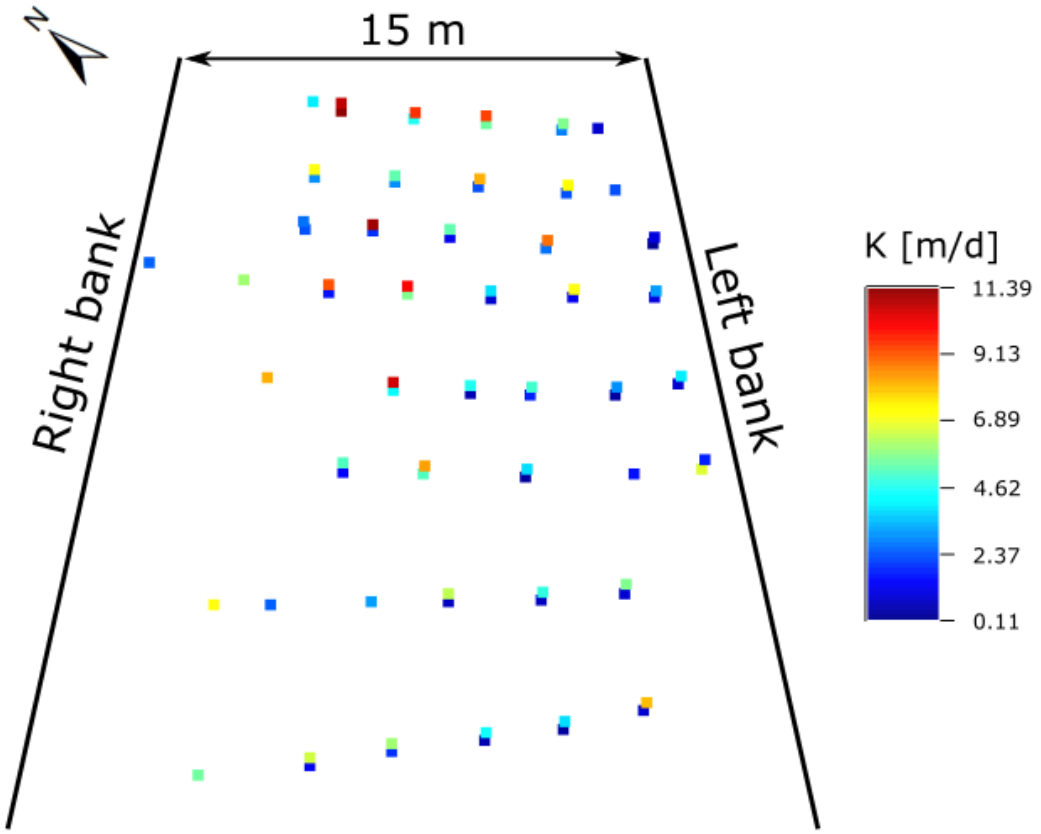

Figure 16 3D view of hydraulic conductivity distribution in the field site.

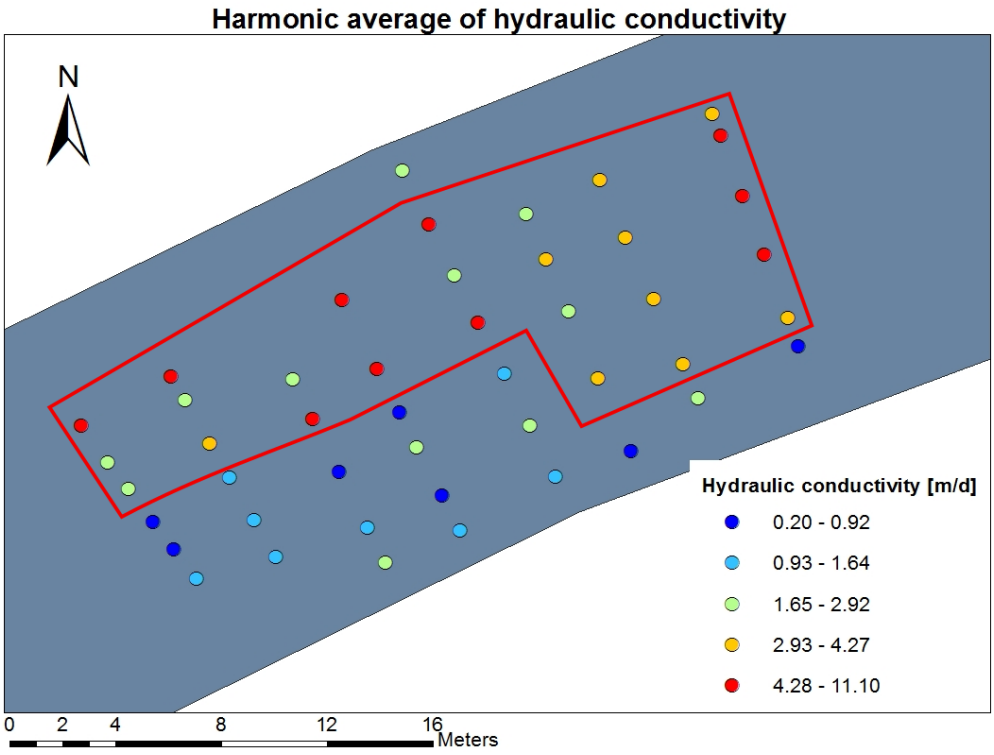

Figure 17 Spatial distribution of the harmonic mean of hydraulic conductivity values. The red polygon indicates a zone of high K.

Variograms are made for all collected K-data, for the shallow depth interval (20 – 45 cm), the deep depth interval (45 – 70 cm) and harmonic mean data of K at these depths. For each of these datasets an omnidirectional variogram is made, as well as a directional variogram parallel to the river and one perpendicular to the river flow direction. Directional variograms are made with a tolerance angle of 22.5° for all variograms, except for those of harmonic mean data. These directional variograms have a tolerance angle of 45°. Models are fit to the lag points based on trial-and-error and visual inspection of the plots.

Considering all hydraulic conductivity data, the range of the omnidirectional variogram is 8.10 m (Figure 18 A). This means that the K value of any point within a distance of 8.10 m from a certain point is correlated to hydraulic conductivity at this specific point. The directional variogram parallel to the river has a range of 8.80 m (Figure 18 B) and perpendicular to the river the range is 5.10 m (Figure 18 C). The range of the variogram parallel to the river is thus strikingly larger than the range of the variogram perpendicular to the river. Consequently, there is more mutual influence of hydraulic conductivity in the direction of the stream compared to the direction across the stream. The sill of these variograms varies between 9.50 (m/d)² and 9.61 (m/d)². This is similar to the variance of the K data, which is 9.41 (m/d)² (Figure 18). Nuggets change between 4 (m/d)² and 6 (m/d)². The nugget for the omnidirectional variogram is rather variable and is therefore uncertain. In all cases, nuggets have a relative large contribution to the sill.

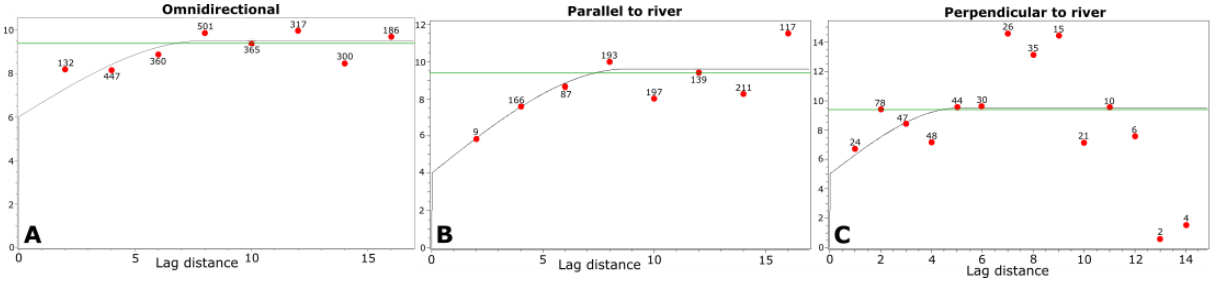

Figure 18 Variograms based on all hydraulic conductivity data (A) omnidirectional, (B) parallel to the river and (C) perpendicular to the river. The vertical axis indicates the semi-variance [(m/d)²]. The variance of the data is shown with a green line. Numbers at each point indicate the number of pairs for that lag.

Next, only hydraulic conductivity data of the shallow depth interval are used to build variograms. The range of the omnidirectional variogram is 8.60 m, 10.50 m of the variogram parallel to the river and 5.10 m of the variogram perpendicular to the river (Appendix C Figure 5). In other words, the range of the parallel directional variogram is more than twice as much as the range of the perpendicular directional variogram. In the shallow level in the riverbed, spatial dependence of hydraulic conductivity is therefore clearly larger in the flow direction than perpendicular to the stream. The sill of the variograms varies between 7.30 (m/d)² and 9.25 (m/d)², which comprises the variance of K data at this depth (i.e. 7.72 (m/d)²). The nuggets are 1 (m/d)² to 4.5 (m/d)² (Appendix C Figure 5).

Variograms for the deep depth interval are made with log transformed K data of this depth because of the lognormal distribution of this variable (Figure 14 D). The range of the omnidirectional variogram is 11 m (Appendix C Figure 6 A). Similar to variograms in the shallow interval, the range of the parallel directional variogram is approximately twice the range of the perpendicular directional variogram, i.e. 9.00 m and 4.65 m respectively. However, there is a lot of scatter and therefore uncertainty in the variogram parallel to the river (Appendix C Figure 6 B). The sill varies hardly (1 (m/d)² - 1.15 (m/d)²) and the nugget is small for directional variograms (0.10 (m/d)²), while it is higher (0.45 (m/d)²) and rather uncertain for the omnidirectional variogram (Appendix C Figure 6). Comparing both depths, hydraulic conductivity at shallow depth has a slightly further influence than hydraulic conductivity at deeper depth in the riverbed, based on the obtained variogram models.

Variograms for depth-averaged hydraulic conductivity are also constructed (Figure 19). In general, the ranges of the variograms are larger compared to these of all data or data per depth. The omnidirectional variogram has a range of 12 m, which is equal to the range of the variogram in the direction parallel to

the river. The range of the variogram perpendicular to the river is 11 m. Values of the ranges are, in other words, all rather similar, which could also be influenced by the uncertainty in the variograms. The sill of the variograms varies between 6 (m/d)² and 8 (m/d)², which is close to the variance of 6.11 (m/d)². The sill of the variogram parallel to the river is the closest to the variance of K_{mean} and shows the best fit. All variogram models are spherical and nuggets are approximately between 1.5 (m/d)² and 2.5 (m/d)².

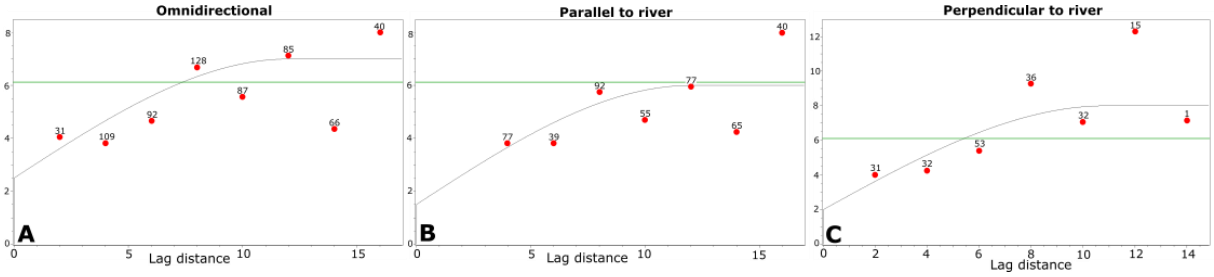

Figure 19 Variograms based on depth-averaged hydraulic conductivity data (A) omnidirectional, (B) parallel to the river and (C) perpendicular to the river. The vertical axis indicates the semi-variance [(m/d)²]. The variance of the data is shown with a green line. Numbers at each point indicate the number of pairs for that lag.

Next, ordinary kriging is performed to obtain an interpolated image of hydraulic conductivity per depth interval. Values are interpolated in a grid with cells of 0.30 m x 0.30 m x 0.05 m in respectively X-, Y- and Z-direction. The applied search window is an ellipse with a radius of 10 m covering minimum 2 and maximum 12 points.

Figure 20 A and Figure 20 B show the interpolated hydraulic conductivity images respectively in the shallow and deep depth interval. Both show the previously described pattern of high values in the right half and towards the middle of the river upstream and low values along the left bank. In the deep depth interval, low values are also present in the right downstream part of the river. Low values are spatially dominant in the deep depth interval with the highest values upstream, while high K values are dominating in the shallow depth interval. Kriging error variances are given as well (Figure 20 C & D). These are low within the area of interest, in particular within the course of the river. Outside the measurement area, error variances increase.

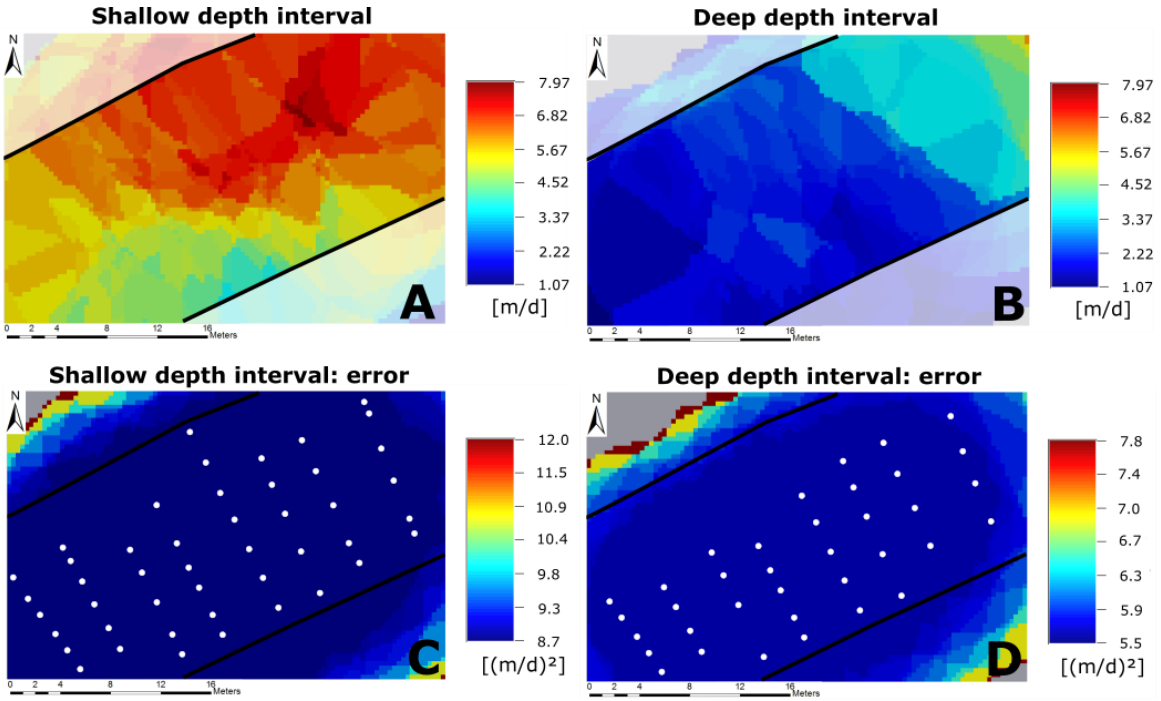

Figure 20 Interpolation with ordinary kriging of hydraulic conductivity measurements (A) in the shallow depth interval (20 – 45 cm), (B) in the deep depth interval (45 – 70 cm). Error variance of ordinary kriging (C) in the shallow depth interval, (D) in the deep depth interval. White dots indicate measured point locations.

3.2. ELECTRICAL RESISTIVITY TOMOGRAPHY (ERT) & INDUCED POLARIZATION (IP)

After ERT and IP data acquisition, data needs to be prepared for inversion. Therefore, the resistivity and chargeability of the water need to be added in the input file. The conductivity of the water is measured in the middle of the river and is 344 µS/cm. This corresponds to a resistivity of 29 Ωm. Chargeability of the water is set at 0 mV/V. In addition, the riverbed topography is required in the inversion of a floating electrodes survey. The water depth is measured at every electrode, which means every 50 cm in each profile. These point measurements are incorporated in the inversion input file. To visualize the bathymetry of the field site, linear interpolation between the electrode locations is performed, shown in Figure 21. The deepest part is situated in the middle of the river, with depths up to 35 cm. From the left bank towards the middle, the slope gradually changes. Closely space contours, indicate a steeper slope along the right bank.

Errors in the measurement survey are assessed based on the stacking error. For each measurement point, two or three stacks are performed. This means that two or three measurements are executed for the same point location and that differences in resistance are immediately and automatically checked in the field. These relative differences in resistance, or stacking errors, should be below 1 % (ABEM Instrument AB, 2012). This is the case for all measurements, except for measurements including electrode 9 in profile 8. This electrode was not well connected with the water and was therefore disabled in the survey of profile 8. Mean stacking errors for each profile vary between 0.06 % and 0.15 % with corresponding standard deviations of 0.05 % and 0.28 %. These errors are negligibly small.

Before the actual inversions, the pseudosection of every profile needs to be evaluated and deviating data points should be removed. In the pseudosections of all measured profiles, fluctuating apparent resistivity is observed at two levels at shallow depth (Figure 22 A). This is not realistic, because adjacent points normally have apparent resistivities of the same order of magnitude (Loke, 2015). This systematic wiggle at the first and third pseudodepth is consequently not realistic and is possibly caused by a problem with the electrode cable. To avoid artificial artefacts in the inversion results, these two levels with wiggly apparent resistivity are removed from the data set in every profile (Figure 22 B & C). One could also suggest removing only high or low apparent resistivities at these levels, but because the cause of the problem is unclear, it is best to remove all data points at these depths.

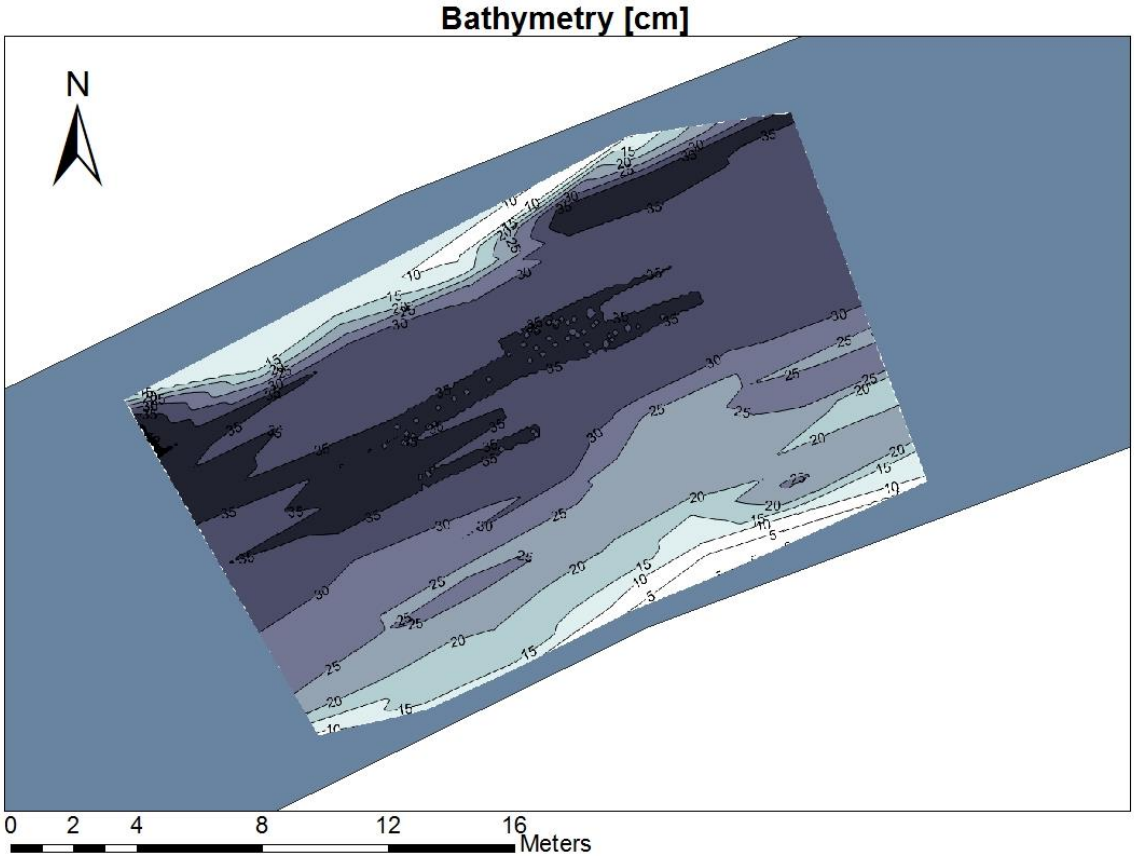

Figure 21 Bathymetry in the field site at the time of the geo-electrical measurements (December 2016), based on linear interpolation between the electrode locations. Contours indicate water depth in cm.

With the complete input files and after extermination of bad data points, the actual inversions are performed. The optimal model is sought by iterative improvement of the model using the RMS error. Inversion stops when the RMS error is smaller than 1 % or when it is not decreasing anymore with more than 5 %. An overview of the resulting number of iterations and RMS values is given in Table 5.

Table 5 Number of iterations for inversion of every profile and RMS of the last iteration for resistivity and chargeability models.

Profile	Number of iterations	RMS for resistivity (%)	RMS for chargeability (%)
2	6	2.1	2.2
3	7	2.1	1.8
4	6	1.6	1.6
5	7	2.0	2.6
6	7	1.8	2.9
7	5	1.7	2.6
8	6	2.1	3.0

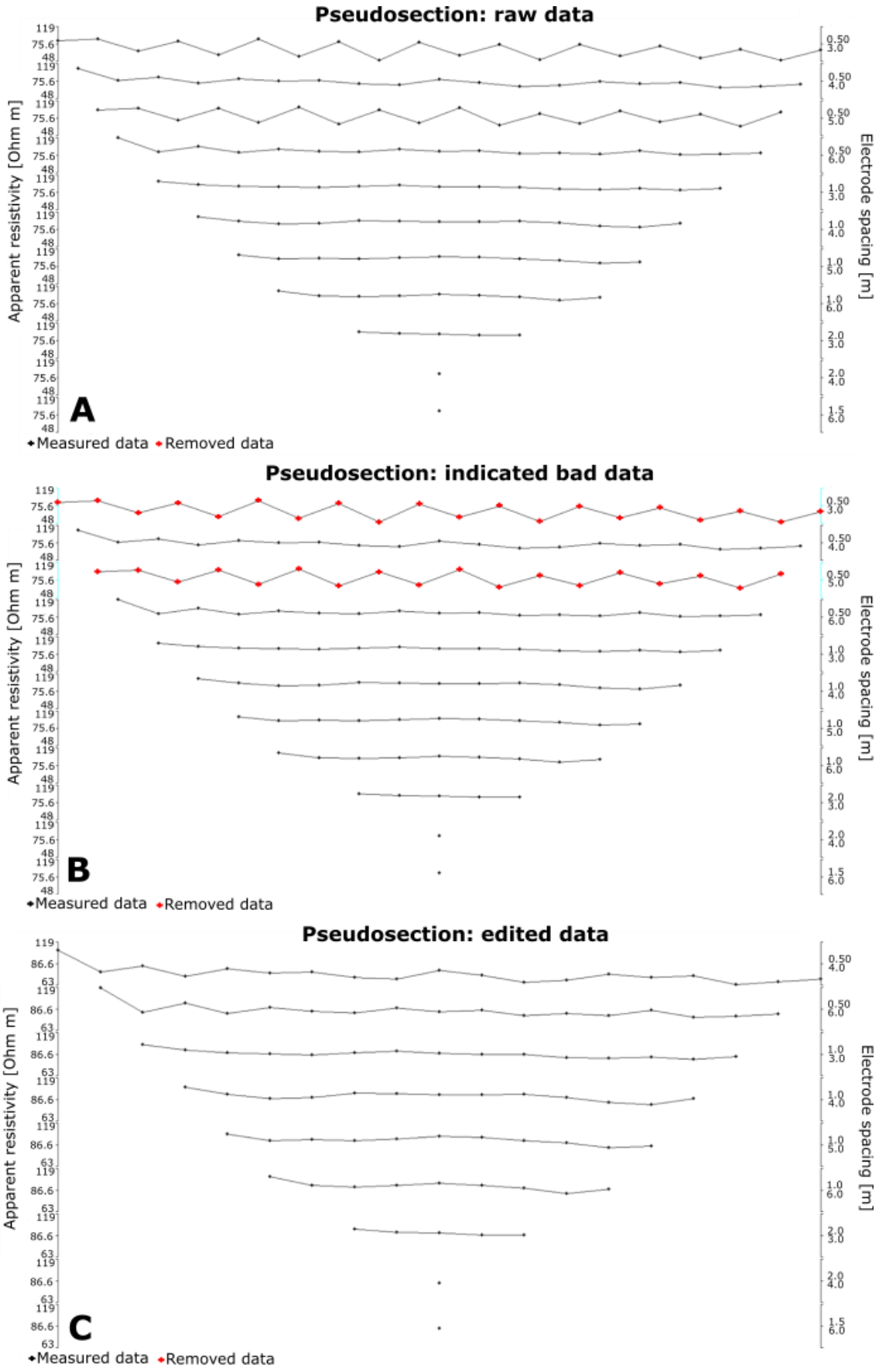

Figure 22 Pseudosections of profile 2. (A) is the pseudosection of raw data. In (B) unreliable data points are indicated to be removed. (C) Bad data points are removed from the pseudosection and data set.

The depth of investigation (DOI) is calculated based on two additional inversions of the data: one with a low reference resistivity and one with a high reference resistivity. Comparison of both determines the depth of investigation. Areas where both models produce equal or similar results, the data constraints the model. Parts where the models deviate from each other indicate that influence of the data is restricted in those areas. Figure 23 shows the inverted reference models (A & B) and the resulting DOI (C) for profile 2. DOIs of the other profiles are shown in Appendix D. The smoothed normalized DOI value is low (DOI < 0.15) for the upper 2.5 m of each profile. Profiles 5, 7 and 8 show some more patchy DOI distributions in the shallow layers, but the DOI value is still small enough to assure reliability of the inversions at shallow depth. From 3 m depth, the DOI rapidly increases horizontally in depth. This means that below 3 m, results of the inversion models are no longer reliable. Hence, interpretation of inverted profiles is acceptable until a depth of 2.5 m. The contrast in resistivity between surface water (29 Ωm) and the riverbed is not markedly high, which causes electrical current being sufficiently dispersed within the riverbed sediments. This results in a DOI larger than the depth of interest in this study, i.e. 1 m deep.

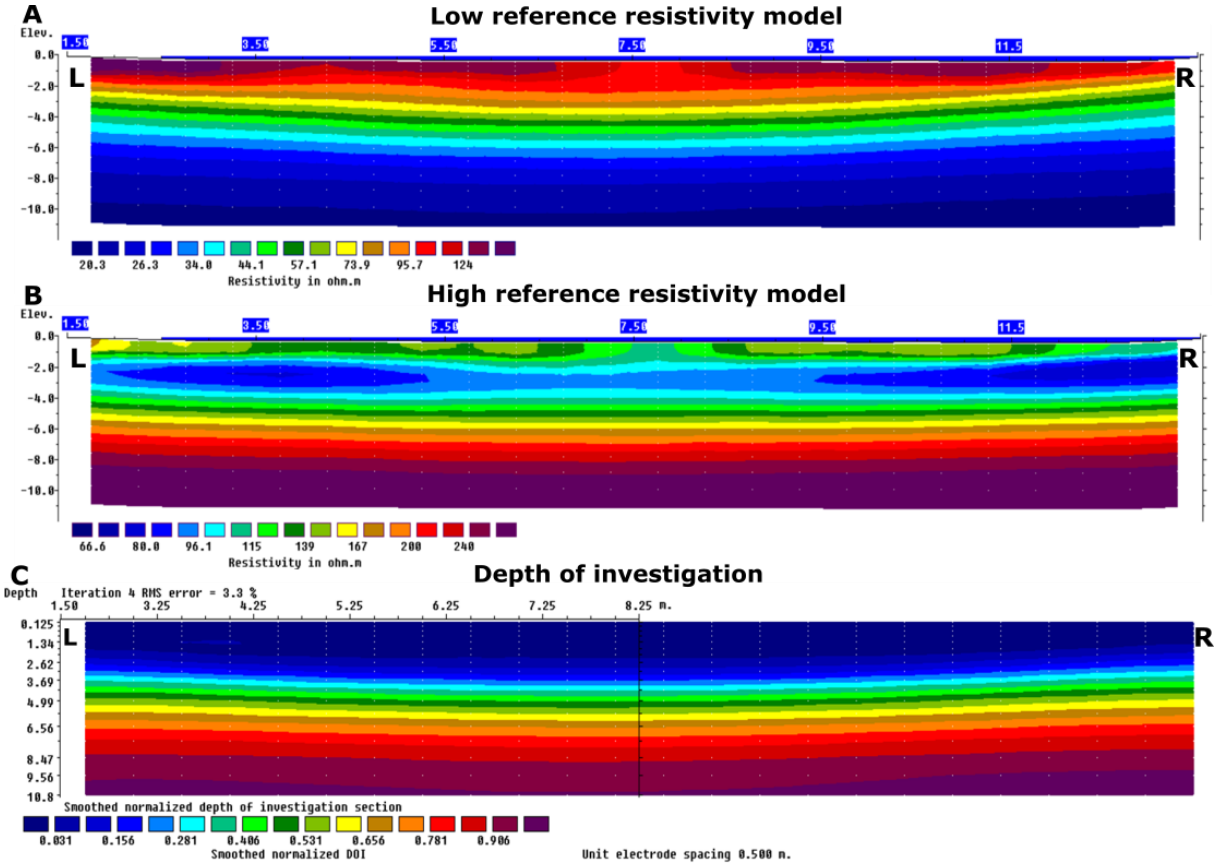

Figure 23 Determination of depth of investigation (DOI) for profile 2. L and R indicate left and right bank respectively. (A) Inverted model based on a low reference resistivity. (B) Inverted model based on a high reference resistivity. (C) Calculated smoothed normalized depth of investigation.

Figure 24 shows true resistivity ρ after inversion of apparent resistivities of profiles 2 to 8. In each profile, resistivity is high (from 90 to 150 Ωm) at the riverbed surface, decreasing with depth in the riverbed (down to 60 Ωm). From 1.5 m depth, horizontal layers of rapidly decreasing ρ occur from which the right part gradually changes to layers dipping from the right bank towards the middle of the riverbed. Resistivity in this deep, inclined structure is low, i.e. < 75 Ωm. In profile 6, this structure extends to the surface. Contour lines are very steep along the right side of this profile, which is presumably not natural. This artificial artefact is possibly caused by submerged electrodes from 12 m in the profile during the field survey. Submerged electrodes are liable to low resistivity of water in all directions, while floating electrodes are only partly affected by the low resistive water layer. Since floating electrodes are assumed in the inversion, this part of profile 6 from 12 m on, is less reliable. In all profiles at shallow depth, local structures of high and intermediate resistivity occur. More specifically, two zones of high ρ

are present at the riverbed surface. First, a zone bordering the left bank up to 1 m into the river occurs with a depth of 0.5 – 1.0 m. Resistivity in this zone is generally higher than 145 Ωm. Second, a zone in the right half of the riverbed is present with ρ between 120 Ωm and 145 Ωm. This zone is 1 to 3 m long in the direction of the profile and 1 m deep. In between these zones of high resistivity in the shallow subsurface of the riverbed, thin patches of intermediate to low resistivity occur. These patches occur in the upper 30 cm of the riverbed and have resistivities between 80 – 110 Ωm. In the middle of the river, at a depth between 0.5 – 1.5 m, a zone of high ρ of 120 – 145 Ωm is present in profiles 2 to 5. From profile 6 to 8 this zone at intermediate depth has gradually lower resistivity. At the right bank, there is a kink in the resistivity layers near the riverbed surface. In profile 2, this is situated at 1 m from the border, in profile 3 at 0.75 m, in profile 4 and 5 at 0.25 m and in profile 7 at 1.5 m. This kink is not visible in profiles 6 and 8. Resistivity is high above the kink (> 120 Ωm) and very rapidly decreases in depth. In general, resistivity is lower upstream and increases downstream in this investigation area.

Figure 25 shows the same profiles but for chargeability M of the riverbed. From a depth of 2 m, M gradually increases from 50 mV/V up to 80 mV/V in more or less horizontal layers. At shallow depth and at the riverbed surface, several structures can be recognized. First, from the right bank, a zone of low chargeability, i.d.10 – 25 mV/V, is present. In profile 6, this zone is more expressed than in the other profiles, which may be due to submersion of electrodes at this location. This low chargeability zone spreads out to intermediate depth (0.5 to 1.5 m deep) below the middle of the river. Chargeability slightly increases to intermediate values in this extension. The result is a large zone of intermediate M at intermediate depth, which is relatively homogeneous. It connects along the left bank with a small zone of low to intermediate chargeability (45 – 55 mV/V), occurring again at the riverbed surface. This small zone at the left bank has a length and depth of 1 m, but does not exist in profiles 4, 5 and 8. There, resistivity keeps increasing from the intermediate zone upwards towards the left bank. Above the intermediate zone in the middle of the river, a thin zone of 20 – 30 cm depth occurs at the surface with chargeability values of 60 mV/V up to > 85 mV/V. This section is rather wide in profile 6, but non-existent in profile 8.

Opposite to the resistivity profiles, there is no changing pattern of chargeability in up- or downstream direction. On the other hand, similar patterns in resistivity and chargeability profiles are horizontal layering in depth, a small zone of 1 m x 1 m at the left bank and a wide zone between 0.5 m and 1.5 m depth in the middle of the river. Although the shapes of the structures are similar, high resistivity values do not correspond with high chargeability values or vice versa. For example, horizontal layers at depth show increasing chargeability but decreasing resistivity in depth. Additionally, the zone at the left bank has a high resistivity but an intermediate chargeability. The kink observed at small distance from the right bank in resistivity profiles is not visible in chargeability profiles. The expected locations of the kinks are incorporated in the low M zone along this bank.

Profiles of normalized chargeability MN are obtained by dividing chargeability by resistivity. They are shown in Figure 26. In this way, bulk conduction of the medium is not integrated in this measure, and only surface polarization properties influence this parameter. From 1.5 m deep, more or less horizontal layers of normalized chargeability occur, with fast increasing values in depth. This increase is more gradual in profiles 1 and 6. At the riverbed surface up to 1 m deep and along the right bank, a zone of low normalized chargeability exists. It has values of < 0.15 mS/m – 0.30 mS/m and extends up to 5 m from the right bank. This zone extends towards intermediate depth in the middle of the river, where values slightly increase to intermediate MN (0.35 – 0.60 mS/m). It spreads out towards the left bank where it reoccurs at the riverbed surface as a low normalized chargeability zone with values between 0.25 mS/m – 0.35 mS/m. This zone of low MN goes to 0.75 m deep and has a length of 1.0 – 1.5 m. Above the extensive zone of intermediate MN, one to three zones of high normalized chargeability occur. These are only 20 – 40 cm thick and occur at the riverbed surface. In profiles 3, 5, 6 and 8, normalized chargeability varies in these surficial riverbed layers between 0.75 mS/m and > 0.95 mS/m, while this is between 0.40 – 0.70 mS/m in profiles 2, 4 and 7. There is no systematically changing pattern in the profiles in up- or downstream direction.

Chargeability and normalized chargeability have corresponding structures. Firstly, they have both increasing values within the horizontal layers in depth. Secondly, for both parameters, low values occur at the riverbed surface at the right bank and intermediate values occur in a small zone at the left bank. Lastly, they have thin zones of high values above a more or less homogeneous zone of intermediate values between 0.5 m – 1.5 m depth, in common. The shape of these two latter structures, as well as the horizontal layering from 2 m depth, are also generally present in resistivity profiles. The kink at the right bank in resistivity profiles is only slightly visible in profile 1 and 5 of normalized chargeability. In profile 6, the inclined structure along the right bank at depth is visible in both the resistivity and normalized chargeability profile, while this is hardly the case in the other profiles. However, as discussed before, this can be strongly influenced by submerged electrodes during the field survey. Hence, caution is required in the interpretation of the last 1.5 m of profile 6. In conclusion, similar general patterns and shapes can be distinguished in profiles of normalized chargeability and chargeability. Factors which could strongly affect resistivity and to some extent chargeability, are thus of limited influence in this case.

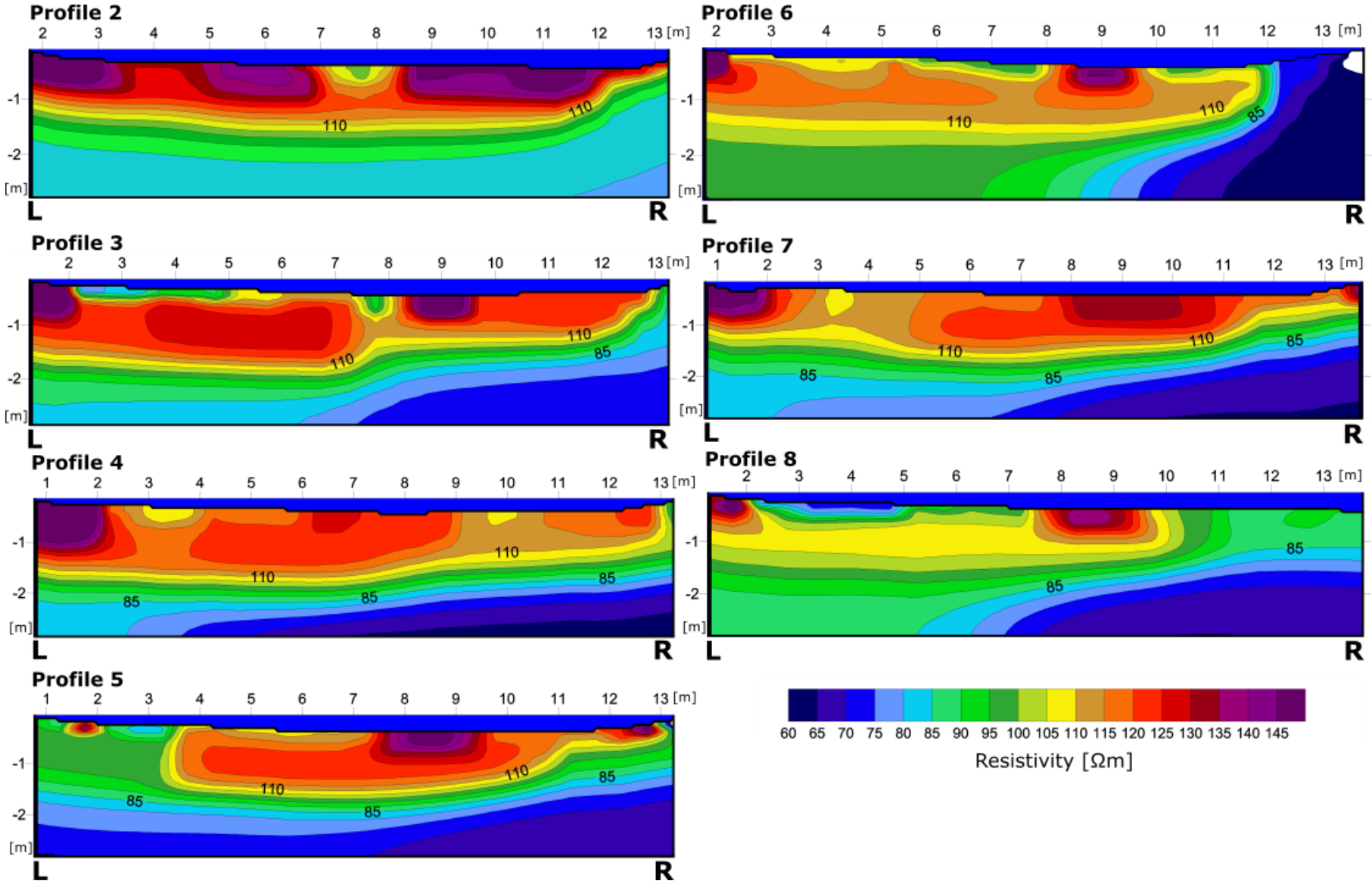

Figure 24 Profiles of true electrical resistivity. L and R indicate left and right bank respectively. Profile 2 is most downstream, profile 8 is most upstream.

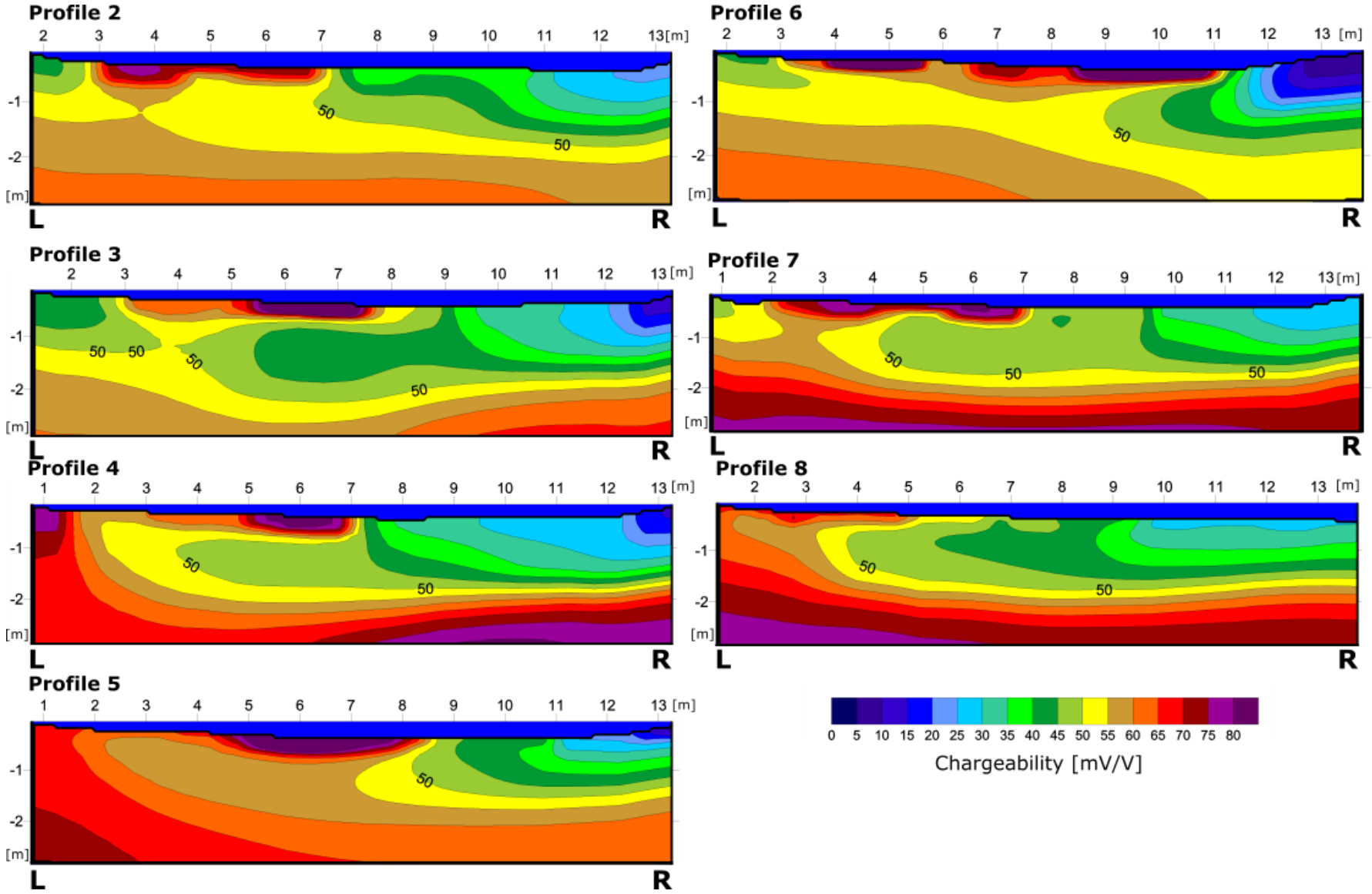

Figure 25 Profiles of true chargeability. L and R indicate left and right bank respectively. Profile 2 is most downstream, profile 8 is most upstream.

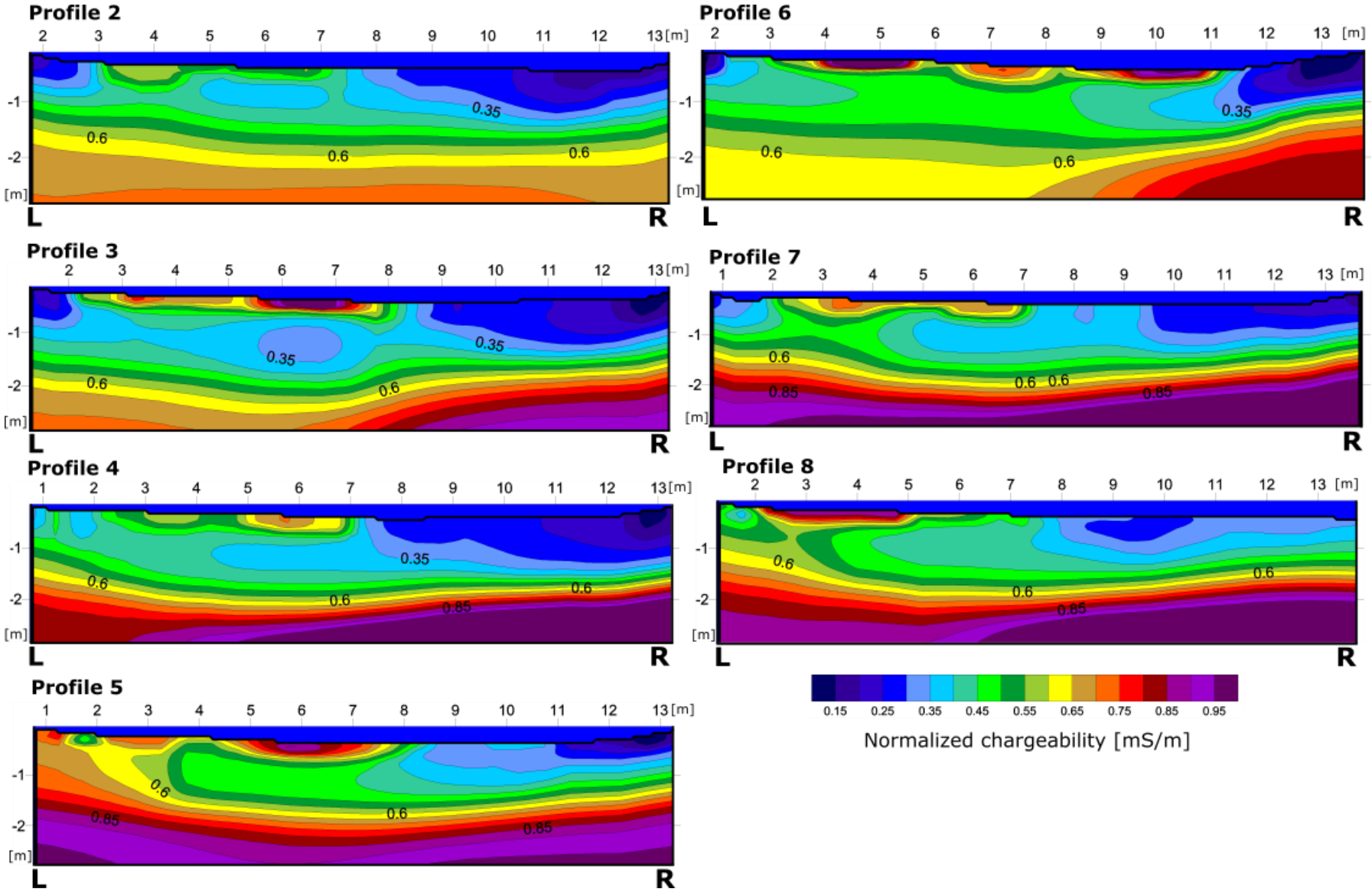

Figure 26 Profiles of normalized chargeability. L and R indicate left and right bank respectively. Profile 2 is most downstream, profile 8 is most upstream.

In order to link hydraulic conductivity data with geo-electrical data, slug test profiles are firstly related to ERT and IP profiles, slug test points are then located within these profiles and lastly, resistivity, chargeability and normalized chargeability data are extracted from their respective profiles. Several methods are tested, described in section 2.6 and results will be discussed in sections 3.4.1 – 3.4.4. Geo-electrical data extracted with method 3, are used for analyses described in the following paragraphs. With this method, resistivity, chargeability and normalized chargeability data at individual point locations are collected by considering a rectangular window with a length of 1.5 m around the corresponding slug test point location (Figure 12 C) and calculating the arithmetic mean of ρ, M and MN within this window. These 'point' data will be compared with corresponding harmonic mean K values in section 3.4.

Descriptive statistics of the resulting data sets of the geo-electrical parameters are given in Table 6. The variation of these parameters is not extreme. Transitions are gradual as shown in the profiles (Figure 24, Figure 25 & Figure 26) and in point maps of the geo-electrical data (Figure 27, Figure 28 & Figure 29). Resistivity and chargeability are normally distributed, while normalized chargeability has a lognormal distribution.

Table 6 Descriptive statistics of datasets of resistivity, chargeability and normalized chargeability, extracted with method 3.

	Resistivity (Ωm)	Chargeability (mV/V)	Normalized chargeability (mS/m)
Mean	114.53	49.85	0.44
Standard deviation	12.86	9.68	0.10
Minimum	85.41	31.17	0.28
Maximum	147.67	66.58	0.68

Figure 27, Figure 28 & Figure 29 show the spatial distribution of extracted data of resistivity, chargeability and normalized chargeability, respectively. Because slug tests are not possible close to the right bank, there is also no corresponding geo-electrical data extracted. Low resistivity is present in the right part of the river section and upstream towards the middle and left bank. High resistivity occurs at the left bank and downstream towards the middle and right half. Overall, there is a more or less diagonal separation between high and low resistivity at the field site. Chargeability and normalized chargeability are low in the right half of the riverbed and high in the left half and middle of the riverbed. This subdivision is more expressed than the subdivision in zones of resistivity.

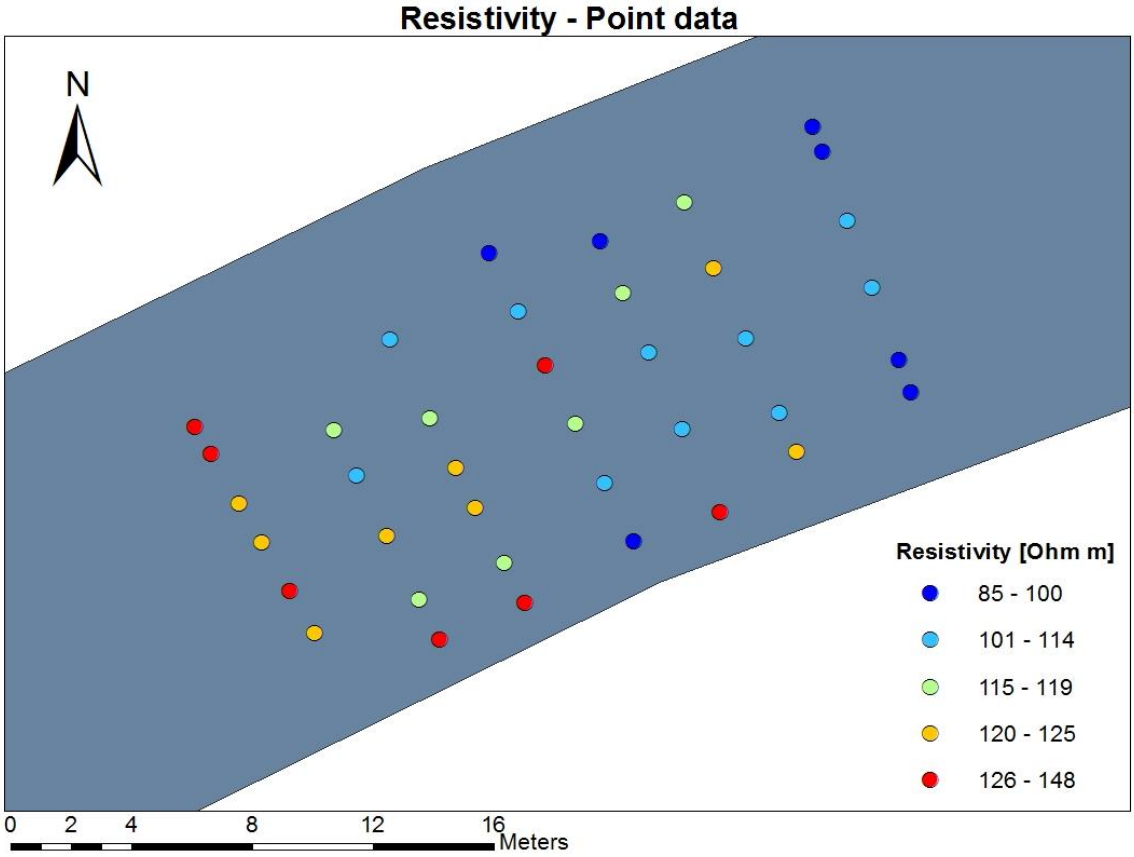

Figure 27 Spatial distribution of extracted point data of resistivity.

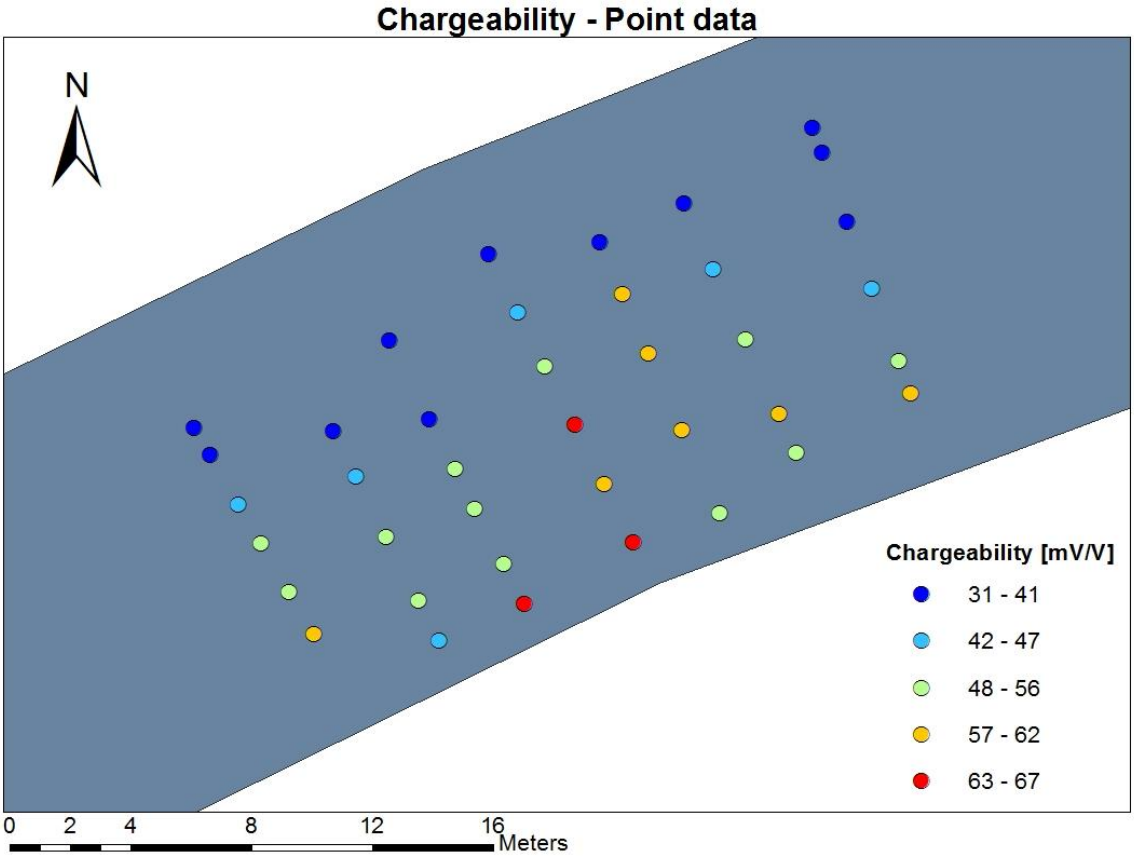

Figure 28 Spatial distribution of extracted point data of chargeability.

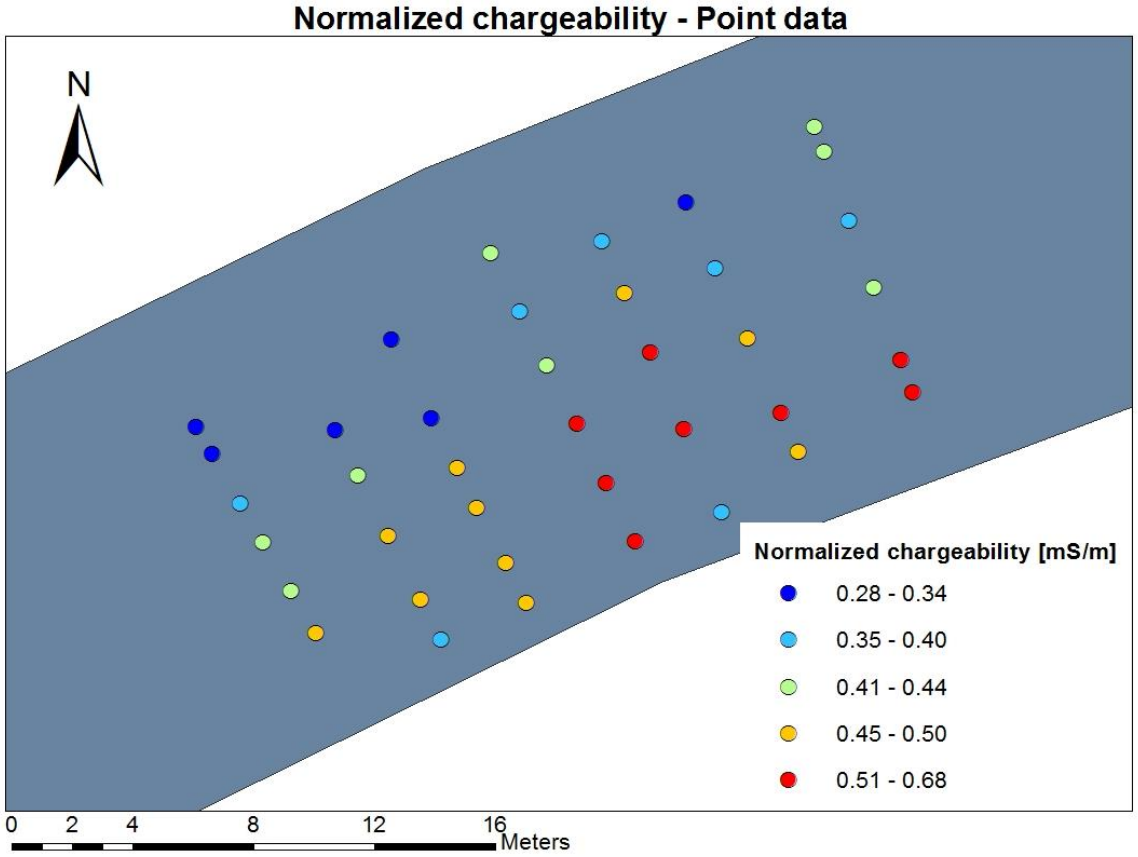

Figure 29 Spatial distribution of extracted point data of normalized chargeability.

Variograms are made with collected point data of the geo-electrical parameters. For each parameter, an omnidirectional variogram is made, as well as two directional variograms: one parallel with the river and one perpendicular to the river. Directional variograms are constructed with a tolerance angle of 45°. The ranges are summarized in Table 7.

Table 7 Ranges, expressed in meter, of different variograms of the geo-electrical parameters.

	Resistivity	Chargeability	Normalized chargeability
Omnidirectional	18.4	11.5	11.0
Parallel with river	11.5	13.6	18.0
Perpendicular to river	20.5	14.1	10.4

Variograms of chargeability are most reliable (Figure 30). The omnidirectional and parallel variograms fit well with a spherical model, while the perpendicular variogram fit well with a Gaussian model. This indicates smoothly varying data in the direction perpendicular to stream flow. The smoothing constraint of inversions may explain this observation. Nuggets are small (Figure 30). Only the variogram in the direction perpendicular to the river has a sill which is much larger than the variance of the dataset. Ranges are of similar magnitude: they are between 11.5 and 14.1 m (Table 7).

For normalized chargeability, variograms are made with logarithmically transformed data because of the lognormal distribution of MN. Spherical models fit to lag points of the omnidirectional and parallel variogram (Figure 31 A & B). The perpendicular variogram fits better to a Gaussian model (Figure 31 C). Ranges are similar as for chargeability (Table 7). The range of the variogram parallel to the river is larger than the range of the perpendicular variogram. However, the sill of this latter variogram is twice as large as the variance of the data. Nuggets of the variograms of normalized chargeability are small.

Variograms of resistivity fit with Gaussian models, indicating data which smoothly vary with distance (Figure 32). Only for the variogram parallel to the river, the sill approximates the variance of the data. Moreover, nuggets have a relatively large contribution to these high sills. Ranges are rather large (Table 7) and outside the short dimension of the study area, except for the parallel variogram. Due to scatter of the variogram data, model fits are more uncertain and ranges are quite variable. The variogram parallel to the river shows the least scatter and the best fit indicating that it is more reliable.

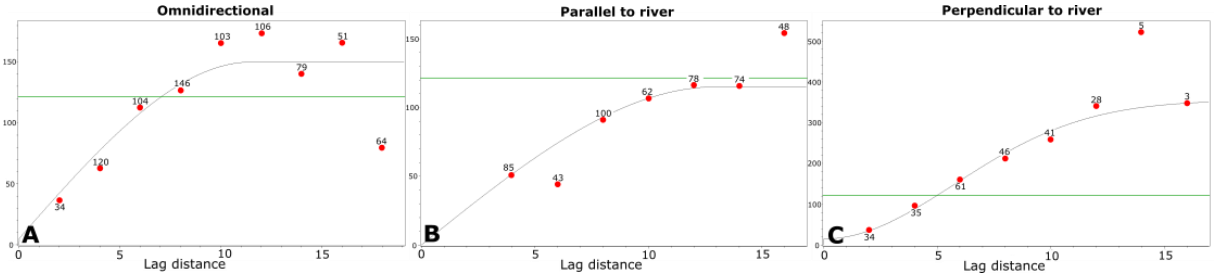

Figure 30 Variograms based on extracted chargeability data (A) omnidirectional, (B) parallel to the river and (C) perpendicular to the river. The vertical axis indicates the semi-variance [(mV/V)²]. The variance of the data is shown with a green line. Numbers at each point indicate the number of pairs for that lag.

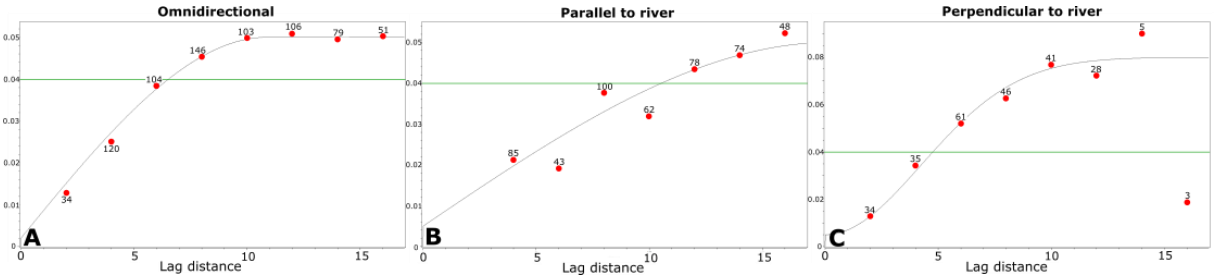

Figure 31 Variograms based on extracted normalized chargeability data (A) omnidirectional, (B) parallel to the river and (C) perpendicular to the river. The vertical axis indicates the semi-variance [(mS/m)²]. The variance of the data is shown with a green line. Numbers at each point indicate the number of pairs for that lag.

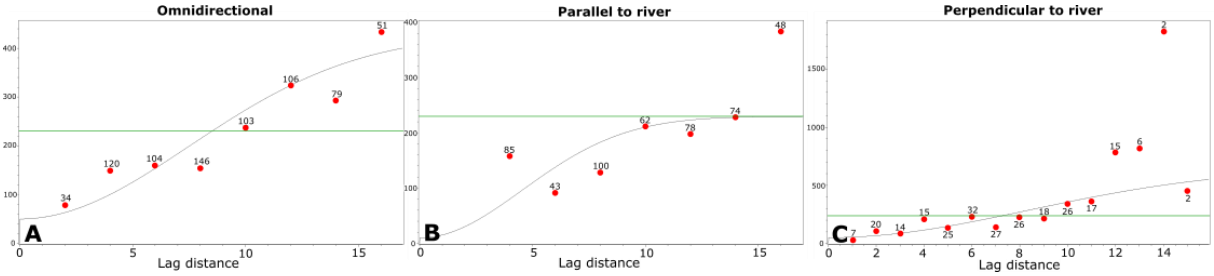

Figure 32 Variograms based on extracted resistivity data (A) omnidirectional, (B) parallel to the river and (C) perpendicular to the river. The vertical axis indicates the semi-variance [(Ωm)²]. The variance of the data is shown with a green line. Numbers at each point indicate the number of pairs for that lag.

Ordinary kriging of geo-electrical point data, using the above described variograms, results in interpolated maps of resistivity, chargeability and normalized chargeability (Figure 33). In correspondence with the point map in Figure 27, a diagonal structure going from the right downstream side to the left upstream side of the river in the study area, separates low and high resistivity zones. These zones gradually fade into each other. Kriging maps of chargeability and normalized chargeability show low values along the right part of the river, which increase towards the middle and left. The diagonal observed in the resistivity map is opposite in the normalized chargeability map: a weak diagonal structure crosses the river from the left downstream corner to the right upstream corner. Distribution of the error variance of the images is the same as for hydraulic conductivity kriging maps, shown in Figure 20 C & D. The variance is low in the study area, but increases in the corner of the grid, which lies outside the river. Unshaded areas in Figure 33, indicating the field site, show reliable interpolation results.

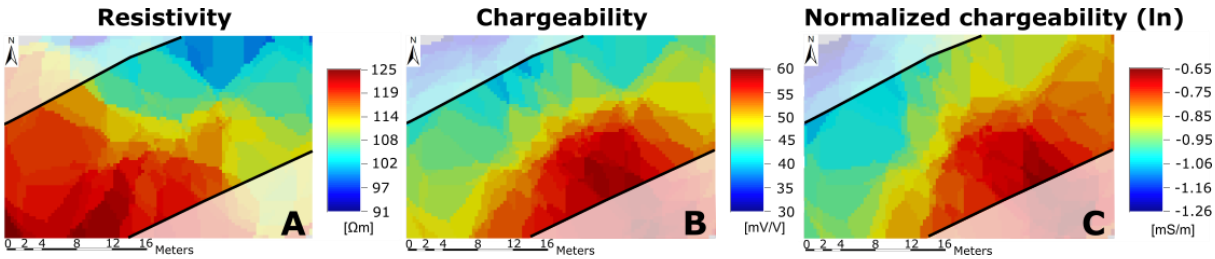

Figure 33 Interpolated maps by ordinary kriging of (A) resistivity, (B) chargeability and (C) logarithmic normalized chargeability.

3.3. RIVERBED DRILLING

At eight locations in the study area (Figure 4), drillings are performed with a riverbed auger (Figure 10). Unfortunately, the auger did not function as it should. The valve at the bottom of the tube did not close when the auger was pulled up and most of the material got lost in this way. Moreover, it was not possible to penetrate deep into the riverbed sediment. Therefore, no long, continuous cores are obtained. However, it was possible to obtain small sediment samples at several locations, and the depth of penetration of the auger can be used as an indication of the type of sediment or amount of compaction.

Generally, two types of sediment are observed: black, sticky, medium- to fine-grained sand with clay, shown in Figure 34 A (type 1), and dark brown to orange sand with a loose texture, shown in Figure 34 B (type 2). This sand is composed of medium-sized, white, transparent, brown, orange and black grains. The clear difference in overall color is visualized in Figure 34 C. The samples taken from the riverbed are intermingled with much, some or no organic material.

Figure 34 Two types of sediment from the riverbed. (A) Type 1: black, sticky sand with clay, taken near the left bank in profile 2. (B) Type 2: brown, loose sand, taken from the middle of profile 2. (C) The same samples next to each other for color comparison.

Three drillings are performed in profile 5. Drilling in the middle of the river, at 6 m from the left bank, is only possible to a depth of 5 – 10 cm. Sediment is composed of dark brown sand with some organic material (type 2). Drillings near the right and left bank, both at 1 m from the bank in the river, deliver

black sand with a lot of organic matter (type 1). It is possible to penetrate the riverbed up to 40 cm along the left side, but only up to 10 cm along the right side.

Also in profile 2, brown sand with little organic matter and no cohesion (type 2) is observed in the middle of the river, at 5.5 m from the left bank. The auger can penetrate to a depth of 40 cm. At the left bank, at 80 cm from the side, drilling is possible to a depth of 40 – 50 cm and black grey sand with a lot of organic material and a sticky texture (type 1) is drilled. Penetration near the right bank, at a distance of 60 cm, is hardly possible (only 10 – 20 cm) and no sediment is retained.

In profile 8, at 1.5 m from the left bank, again black, sticky sand with some organic material (type 1) is observed and the auger could penetrate to a depth of 40 cm. At 3 m from the right bank in profile 8, brown sand with very little organic material (type 2) is drilled from a depth between 0 – 50 cm.

In general, samples near the left bank and right bank are composed of black sand with a sticky texture because of clay and a lot of organic matter. At the left bank, it is easier to penetrate the sediment than at the right bank. At the right border of the river, the riverbed is very hard. Poles at a distance up to 1.5 m from the bank are observed in the water. This proves human interference at this part of the river. In the middle of the river, from a certain distance from the banks, sediments of the riverbed are composed of brown sand with a loose texture. Little organic material is present in these sands and penetration with the riverbed auger is possible to varying depths.

3.4. COMPARISON OF HYDRAULIC CONDUCTIVITY, RESISTIVITY, CHARGEABILITY AND NORMALIZED CHARGEABILITY

Results of hydraulic conductivity and geo-electrical parameters are compared using several methods and on different scales. First of all, measurements of K and ρ, M and MN need to be linked to each other. This is done by coupling the profiles to one another and calculating the corresponding GPS and ERT coordinates. How this is performed and how errors are dealt with is described in section 2.6. Errors in the calculation of GPS coordinates of the geo-electrical profiles are limited: the error is lower than 0.20 m for profiles 4 and 8, and lower than 0.50 m for the other profiles. In a second step, point measurements of K need to be compared to their corresponding ρ, M and MN values. Several methods for data extraction from ERT and IP profiles are considered, explained in section 2.6. Results of comparison of spatial data distributions, scatterplots and linear regressions are described in the following sections. For linear regressions, reported p-values are those of the estimate of the slope of the regression.

3.4.1. HYDRAULIC CONDUCTIVITY AND RESISTIVITY

3.4.1.1. Spatial patterns

Point values and patterns of hydraulic conductivity are spatially compared with point values and patterns of resistivity. This is done for K measurements at shallow depth, deep depth and for mean values of these depth measurements, for each method where applicable.

First, K values and ρ values are compared in the shallow depth interval of 20 – 45 cm. This is only possible with method 1 and 2. In general, it is observed that in this depth interval, K values are significantly higher than those in the deep depth interval of 45 – 70 cm (Figure 16). Although the mean ρ, M and MN are also higher at shallow depth, this difference is not significant, according to an independent samples t-test. The first method, using point comparison, shows some correspondence between K and ρ at shallow depth (Appendix B Figure 1 – Appendix E Figure 8 A): intermediate to high values of K correspond to rather low values in the right and middle of the river, and low values of K at the left bank have high values of resistivity. In the second method, there is limited correspondence observed for this depth interval (Appendix B Figure 1 – Appendix E Figure 9 A). Some values upstream

show an inverse relation, but otherwise only some intermediate K values can be linked to intermediate to low ρ values.

Also, hydraulic conductivity data in the depth interval of 45 – 70 cm are compared to resistivity values at this depth for method 1 and 2. Hydraulic conductivity is generally lower at this depth compared to shallow parts in the riverbed. Both methods show little correspondence between K and ρ (Appendix B Figure 2 – Appendix E Figure 8 B & Figure 9 B). Some low values correspond to intermediate to high (method 1) or intermediate to low (method 2) values, situated in the middle of the riverbed and along the left bank, but generally, similar patterns are not clear.

For all methods, the harmonic mean of depth measurements of hydraulic conductivity is compared to an averaged resistivity value in the riverbed. For method 3, also arithmetic and geometric averages of hydraulic conductivity are compared to resistivity values. The first and second method show limited correspondence between patterns of hydraulic conductivity and resistivity (Figure 17 – Appendix E Figure 8 C & Figure 9 C). Locations where correspondence is present, an inverse relation links the two parameters: high values of K correspond to low values of ρ in the right and upstream part, and low values of K correspond to high values of ρ along the left bank. However, a lot of exceptions are observed. The third and fourth method show generally good correspondence, where high K can be linked with low ρ in space and vice versa (Figure 17, Appendix B Figure 3 & Figure 4 – Appendix E Figure 10 & Figure 11). Overall, a diagonal can be visually drawn from the right downstream corner of the study site to the left upstream corner, separating low and high values of K or ρ (Figure 35). This spatial correspondence between hydraulic conductivity and resistivity is most expressed for comparison between the arithmetic and geometric mean of K with resistivity in method 3.

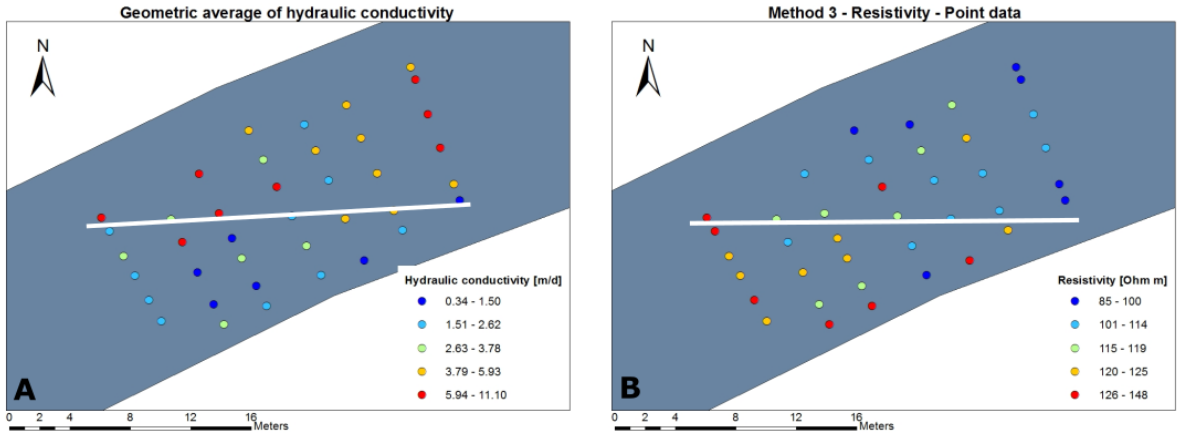

Figure 35 Slight spatial correspondence between geometric mean hydraulic conductivity (A) and resistivity data extracted with method 3 (B). A white diagonal separates zones of high K or ρ and low K or ρ.

3.4.1.2. Scatterplots

Scatterplots of hydraulic conductivity versus resistivity are made to investigate quantitative trends in the data. Plots of untransformed data, log transformed K and/or ρ are analyzed visually. For the different methods, all data, subsets of the data (e.g. separate depth intervals) or mean values of the data are tested. In general, plots show all a lot of scatter, but some trends can be distinguished.

For the first method, considering all data, a more or less decreasing trend is visible in the scatterplots (Appendix E Figure 12). This is especially the case for high values of K. The lower the K values, the wider the range of corresponding resistivities, so the less obvious a trend can be distinguished. These trends are best for plots of hydraulic conductivity versus ln(resistivity) (Figure 36) or untransformed resistivity (Appendix E Figure 12). Plots with ln(hydraulic conductivity) are point clouds without any trend (Appendix E Figure 12). The same is true for the harmonic mean of K data at both depths (Appendix E Figure 15). Log transformed K data also show some correlation, but with most scatter situated at intermediate K values instead of low K values. For data of the shallow depth interval, a decreasing trend is visible, with most scatter situated at intermediate K values (Appendix E Figure 13). Again, trends are

best visible in plots without log transformation of K. In contrast, for the deep depth interval, a decreasing trend is best visible in plots with log transformed hydraulic conductivity data (Appendix E Figure 14). However, the trend is weak and has four clearly deviating points.

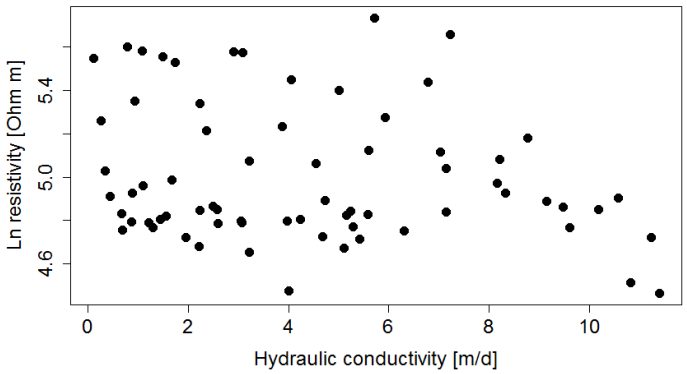

Figure 36 Scatterplot of hydraulic conductivity versus ln(resistivity) for all measured data in method 1.

Extracted resistivity data of the second method are mostly situated between 100 Ωm and 140 Ωm (Figure 37). Therefore, trends are not obvious and can only be distinguished when, visually, more weight is given to extremal points outside this range. Plots with all data (Appendix E Figure 16), data of shallow depth (Appendix E Figure 17) and of deep depth (Appendix E Figure 18) and the harmonic mean of these (Appendix E Figure 19), all show decreasing trends. However, this is only true when the large cloud of data between 100 Ωm and 140 Ωm is less considered. Non-transformed K data is more valuable to observe trends for most data, except for the deep depth interval, where log transformed K data shows better trends with resistivity.

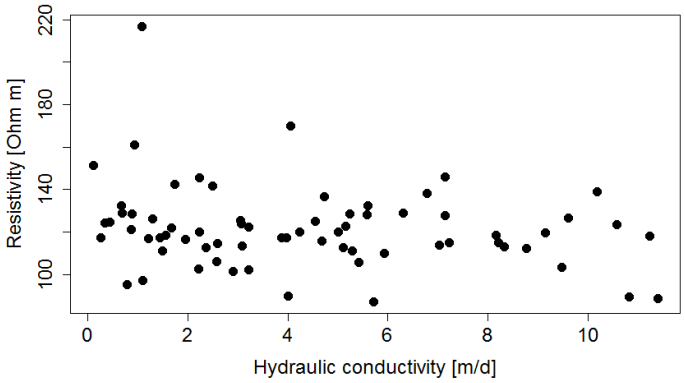

Figure 37 Scatterplot of hydraulic conductivity versus resistivity for all measured data using method 2.

More or less decreasing trends are also visible in plots of hydraulic conductivity and resistivity with method 3. However, the trends show a lot of scatter. The decreasing trend is best visible in plots with harmonic mean values (Appendix E Figure 20), and less in plots with arithmetic (Appendix E Figure 21) and geometric mean values of K (Appendix E Figure 22). Logarithmic transformations of hydraulic conductivity values provide the clearest plots (Figure 38).

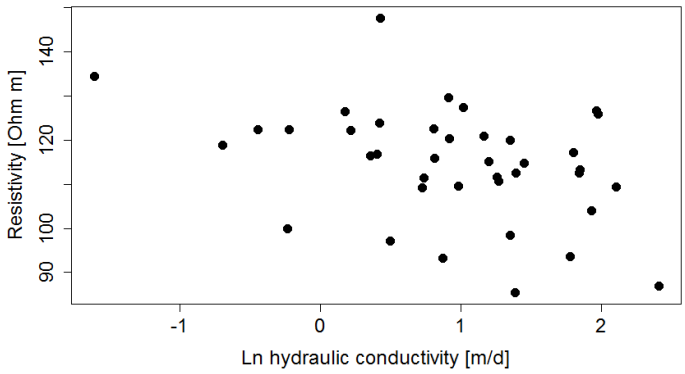

Figure 38 Scatterplot of ln(hydraulic conductivity) versus resistivity for harmonic mean data of method 3.

A slightly decreasing trend is visible for plots of K versus ρ and ln(ρ) in method 4 (Figure 39). This correlation is best seen when a few extremal points are taken into account. In general, correlation is not obvious and for logarithmic transformations of K, scatterplots are composed of a cloud of random points (Appendix E Figure 23).

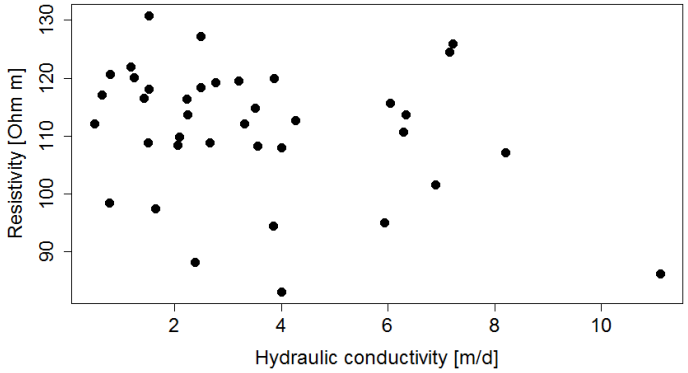

Figure 39 Scatterplot of hydraulic conductivity versus resistivity for harmonic mean data in method 4.

3.4.1.3. Regression analysis

Linear models are fit to scatterplots of hydraulic conductivity versus resistivity, with or without logarithmic transformations. It is investigated which linear regressions are significant and to which degree. All identified significant linear relations are decreasing, but rather weakly: adjusted coefficients of determination do not exceed 0.27.

In the first method, no significant trends between all hydraulic conductivity point data and resistivity point data are found. Linear regressions for data at shallow depth are all significant (Appendix E Figure 24) with the best results for ln(hydraulic conductivity) versus resistivity (Figure 40). The adjusted $R^2 = 0.27$ and $p = 4.43 \times 10^{-4}$ for the model with equation

$$\rho = 248 - 49 * \ln K \tag{3.1}$$

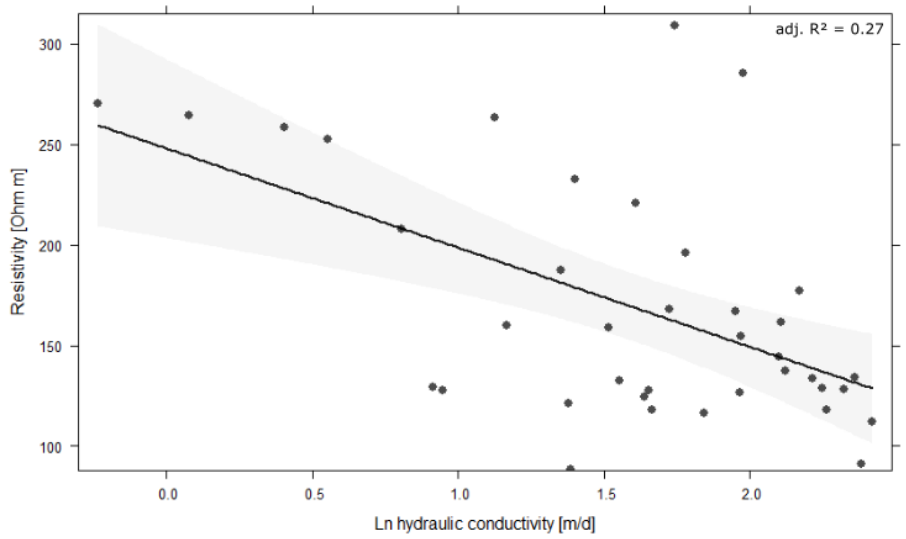

Figure 40 Linear model fit (black line) to ln(hydraulic conductivity) versus resistivity data of the shallow depth interval, extracted by method 1. The grey bands indicate the 95 % confidence interval of the fit.

For point data of deep depth, linear regressions are significant with logarithmically transformed K data (Appendix E Figure 25). The relation between transformed parameters is best, with adjusted $R^2 = 0.14$ and $p = 0.02$:

$$ln\rho = 4.97 - 0.11 * lnK \quad (3.2)$$

Linear models for harmonic mean data of K and resistivity of method 1 are all significant, i.e. with or without transformations (Appendix E Figure 26). The model between ln(resistivity) and ln(hydraulic conductivity) provides the most significant correlation (adjusted $R^2 = 0.20$; $p = 2.26 \times 10^{-3}$):

$$ln\rho = 5.15 - 0.17 * lnK \quad (3.3)$$

With the second method, based on areal averaging of geo-electrical parameter values within a square of 50 cm x 50 cm, some significant relations are found between hydraulic conductivity and resistivity. Logarithmic transformations of K data give better results, with or without transformation of resistivity. When all data is considered, a very weak, but significant linear relation is found with adjusted $R^2 = 0.05$ and $p = 0.04$ (Appendix E Figure 27):

$$\rho = 127 - 4.82 * lnK \quad (3.4)$$

Considering data of method 2 at shallow depth only, no significant correlation between hydraulic conductivity and resistivity is identified. However, for the deep depth interval, linear correlations are found (Appendix E Figure 28) and correlation between logarithmically transformed parameters provides the most significant results (adjusted $R^2 = 0.19$; $p = 0.01$):

$$ln\rho = 4.81 - 0.05 * lnK \quad (3.5)$$

Similarly, correlations between harmonically averaged data are detected in the second method (Appendix E Figure 29). The most significant result is present for the decreasing linear regression between resistivity and ln(hydraulic conductivity) ($R^2 = 0.14$; $p = 0.01$):

$$\rho = 129 - 8.52 * lnK \quad (3.6)$$

In the third method, where data is averaged over a rectangular window of 1.5 m length, resistivity data is correlated to harmonic, arithmetic and geometric mean data of K. For the arithmetic mean of K no significant models can be fit to the data. This is, nevertheless, the case for harmonic and geometric mean data of K, with or without transformations of the parameters (Appendix E Figure 30 & Figure 31).

Correlation between the harmonic mean of hydraulic conductivity and resistivity is strongest if K data is logarithmically transformed (Figure 41). The adjusted R^2 = 0.12 and p = 0.02 and the relation is as follows:

$$\rho = 120 - 5.80 * lnK \tag{3.7}$$

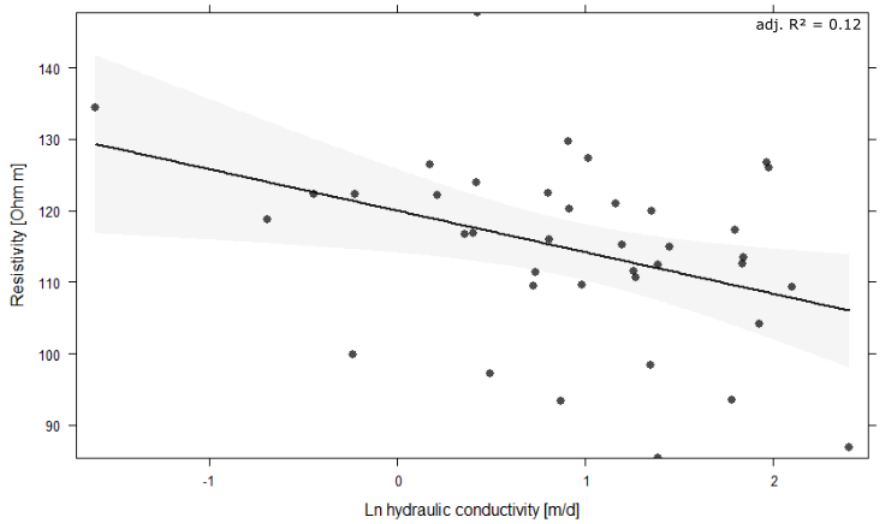

Figure 41 Linear model fit (black line) to ln(hydraulic conductivity) versus resistivity data of harmonic mean data with method 3. The grey bands indicate the 95 % confidence interval of the fit.

Also for geometrically averaged K data, relations are significant (Appendix E Figure 31). Ln(resistivity) and hydraulic conductivity provide the most significant correlation compared to other models, with an adjusted R^2 = 0.10 and p = 0.03:

$$ln\rho = 4.80 - 0.02 * K \tag{3.8}$$

The fourth method is identical to the third method, but based on inversion results after less iterations. No significant linear model can be fit to hydraulic conductivity versus resistivity data, with or without logarithmic transformations.

3.4.1.4. Conclusion

It can be concluded that some weak (adjusted $R^2 \leq 0.27$) linear correlations can be found between hydraulic conductivity and resistivity. The most significant linear regressions mostly appear with logarithmically transformed K data. The fourth method is the least capable in detecting statistically significant correlation between hydraulic conductivity and resistivity. Method 1, 2 and 3 result in linear models, with respectively decreasing correlation coefficients. Visual analysis of scatterplots is not completely in correspondence with the regression analysis. In view of this visual inspection, the first and third method show more correspondence between resistivity and hydraulic conductivity compared to method 2 and 4. When spatial distributions of point data are compared, resistivity in the third and fourth method are visually assessed to show more spatial correlation with hydraulic conductivity than in the first and second method. Considering all this, the first and third method seem to be most useful in detection of correlation between hydraulic conductivity and resistivity at this study site.

3.4.2. HYDRAULIC CONDUCTIVITY AND CHARGEABILITY

3.4.2.1. Spatial patterns

Point maps of hydraulic conductivity and chargeability are compared and similar or differing patterns are distinguished. For the first and second method, point values at the shallow depth interval (20 – 45 cm), deep depth interval (45 – 70 cm) and their harmonic mean are spatially compared. For all situations, a

general pattern is that high hydraulic conductivity values correspond to low to intermediate chargeability values and that low K values correspond to intermediate to high M values (Appendix B Figure 1 & Figure 2, Figure 17 – Appendix F Figure 32 & Figure 33). Generally, low M values occur in the right half of the river, while high M values occur in the left half (Figure 42 B). At the shallow depth interval and for averaged data, a lot of exceptions to these patterns are observed. At the deep depth interval, the spatial correlation seems more obvious and patterns are similar (Figure 42).

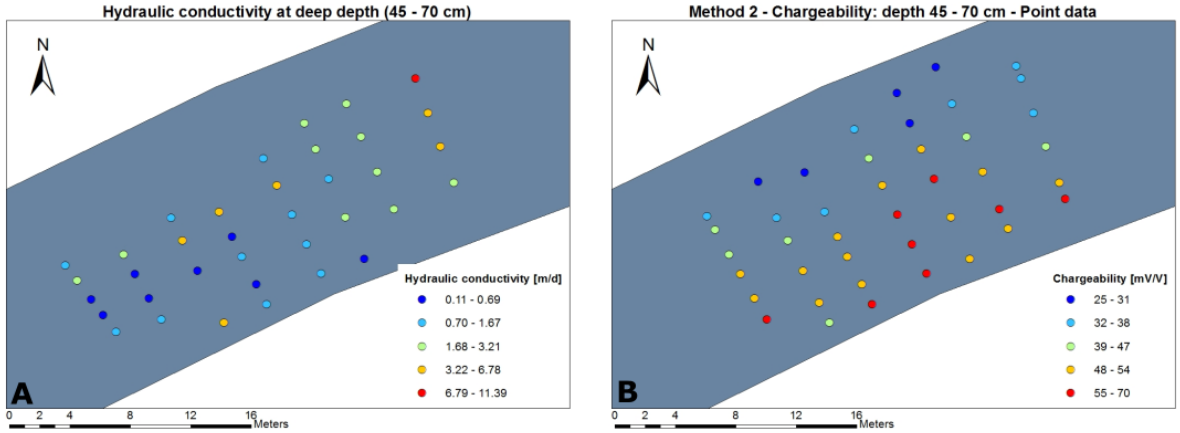

Figure 42 Spatial distribution of (A) hydraulic conductivity and (B) chargeability at deep depth. The data is extracted with method 2. Inverse correlation between both can be observed.

The third method compares the harmonic, arithmetic and geometric mean of depth values of K with average chargeability values. In general, correspondence between K and M. In Figure 43 A & B, the same patterns are observed: points with high K have low M and vice versa. Low values of M and high values of K occur in the right part of the river. High values of M and low values of K occur closely along the left bank and towards the middle in the downstream part of the reach. Correspondence between K and M is most clear when the harmonic mean of K is considered.

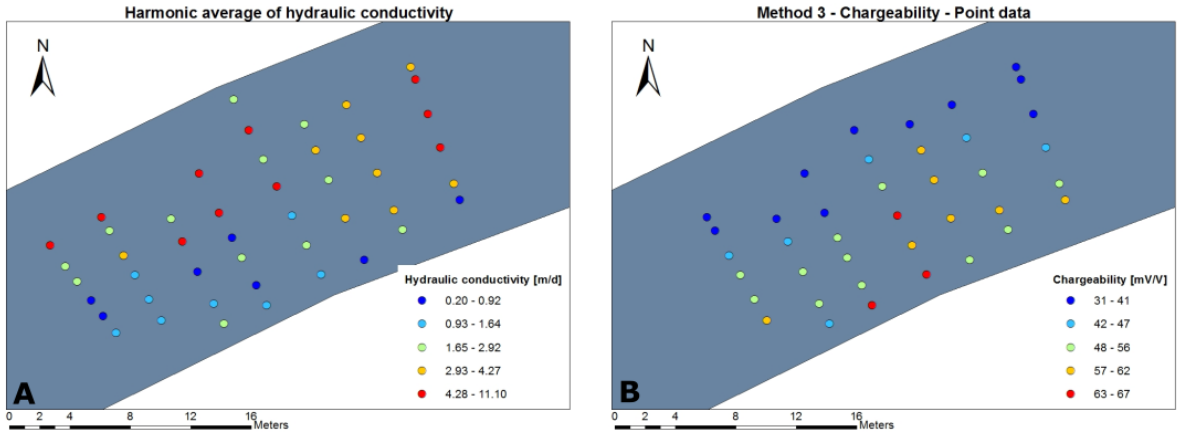

Figure 43 Spatial correlation of (A) hydraulic conductivity (harmonic mean) and (B) chargeability data extracted with method 3.

Spatial patterns of values in the fourth method are almost identical to those of the third method (Appendix F Figure 35). Correspondence is thus good as well. Some little changes in chargeability values show sometimes more and sometimes less correlation.

3.4.2.2. Scatterplots

Scatterplots of hydraulic conductivity versus chargeability are made to visually inspect if there are trends in the data. Logarithmic transformations of data are also investigated if they provide clearer relations than untransformed data.

Considering all hydraulic conductivity and chargeability data in method 1, a more or less decreasing trend is observed (Appendix F Figure 36). However, at low hydraulic conductivity, the range of chargeability is large. In addition, a lot of data is situated between 0 mV/V and 80 mV/V for the whole K range. The visual trend is therefore strongly influenced by extremal points outside this range of M. When hydraulic conductivity is logarithmically transformed, a wide range of M values is situated at high ln(K) values. Logarithmically transformed chargeability data shows hardly any trend with K. Similar scatterplots appear for data from the shallow and deep depth interval, given in Appendix F Figure 37 & Figure 38 respectively. Plots with logarithmically transformed K values and no transformation of M show the clearest trends. A decreasing trend is more expressed when harmonic mean data is considered (Appendix F Figure 39). A relatively clear linear trend is present for ln(hydraulic conductivity) versus chargeability.

Data of the second method do not show any correlation between hydraulic conductivity and chargeability, when considering data of both depths (Figure 44 & Appendix F Figure 40) or for the shallow depth interval (Appendix F Figure 41). A weak decreasing trend with a lot of scatter is, however, observed for data from the deep depth interval (Appendix F Figure 42) and the harmonic mean of the separate depth data (Appendix F Figure 43). Although logarithmic transformation of K provides better visible trends for the deep data, correlation is stronger for harmonic mean data without transformation of K.

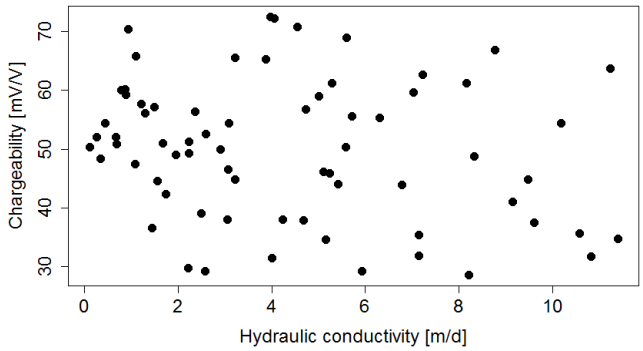

Figure 44 Scatterplot of hydraulic conductivity versus chargeability for all measured data in method 2. There is no pattern in the plot.

Considering the third and fourth method, clearly decreasing trends are visible in scatterplots of hydraulic conductivity versus chargeability (Appendix F Figure 44 – Figure 47). Figure 45 shows the scatterplot of harmonically averaged K versus M for data extracted with method 3. Still, scatter is present, but an inverse correlation is obviously present. The best visible relations are those without transformations of hydraulic conductivity. Based on visual comparison of scatterplots, these two methods cannot be distinguished for which one provides the clearest trend. Nonetheless, using the third method, harmonically averaged K data provide better results than other averages of K.

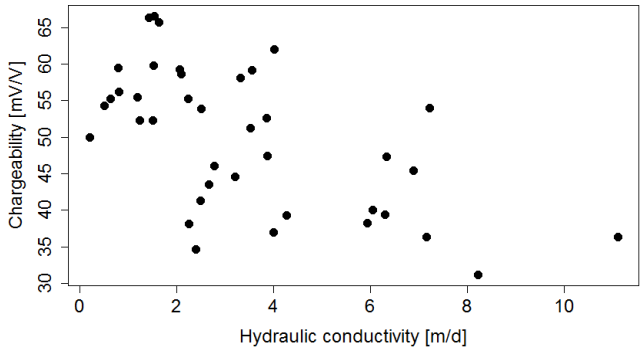

Figure 45 Scatterplot of hydraulic conductivity versus chargeability for harmonically averaged K data and M data extracted with method 3. A decreasing pattern is visible.

3.4.2.3. Regression analysis

Linear trends are observed in scatterplots of hydraulic conductivity versus chargeability and their transformations. For all methods, for datasets and subdatasets, linear models are fit to the scatterplots and their significance is assessed. Linear regressions of K versus M are always decreasing.

For the first method, using point comparison, several significant linear relationships are found, with adjusted coefficients of determination up to 0.36. When all hydraulic conductivity and chargeability data are considered, correlations of K or ln(K) with M are significant (Appendix F Figure 48). The best linear model for this data is found between M and ln(K) with the adjusted $R^2 = 0.08$ and $p = 0.01$:

$$M = 65 - 9.96 * \ln K \tag{3.9}$$

Significant fits between chargeability and hydraulic conductivity are found for shallow depth data of the first method (Appendix F Figure 49), with the most significant one for ln(K) versus M (adjusted $R^2 = 0.36$; $p = 4.56 * 10^{-5}$):

$$M = 111 - 32 * \ln K \tag{3.10}$$

For deep depth data of method 1, the only linear model which is significant, is determined for logarithmically transformed hydraulic conductivity data, without transformation of chargeability data (Appendix F Figure 50). The adjusted $R^2 = 0.18$, $p = 0.01$ and the equation is as follows:

$$M = 53 - 13 * \ln K \tag{3.11}$$

When harmonic mean point data in method 1 is considered, all different relationships between hydraulic conductivity and chargeability, with or without transformation, result in a linear model (Appendix F Figure 51). Again, the combination of untransformed M and transformed K data provides the most significant fit with an adjusted $R^2 = 0.34$ and $p = 5.10 * 10^{-5}$ (Figure 46):

$$M = 70 - 21 * \ln K \tag{3.12}$$

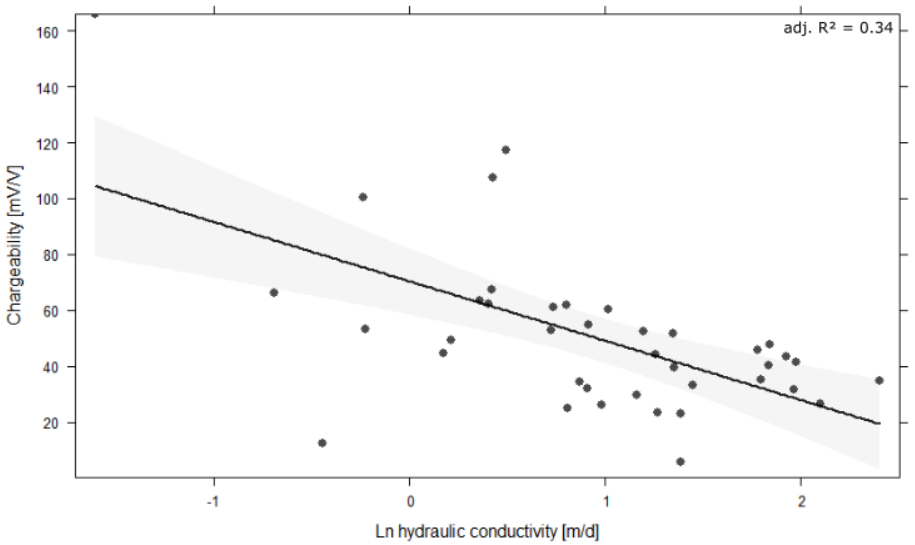

Figure 46 Linear model fit (black line) to ln(hydraulic conductivity) versus chargeability data, harmonically averaged and extracted with method 1. The grey bands indicate the 95 % confidence interval of the fit.

When data extracted by the second method is considered, less significant correlations are identified. Neither all data nor data at shallow depth in the riverbed provide significant linear relations between hydraulic conductivity and chargeability, with or without transformations. However, deep depth data and harmonically averaged data do show significant correlations (Appendix F Figure 52 & Figure 53). Clear

correlation is present between untransformed M and K data for data measured in the deep depth interval. The adjusted $R^2 = 0.25$, $p = 2.39 * 10^{-3}$ and the equation is expressed as:

$$M = 54 - 1.96 * K \tag{3.13}$$

The most significant linear model for harmonic mean data of K and M, extracted by method 2, is recovered for K versus ln(M) with an adjusted $R^2 = 0.35$ and $p = 5 * 10^{-5}$. The linear model is shown in Figure 47 and has the following equation:

$$lnM = 4.06 - 0.06 * K \tag{3.14}$$

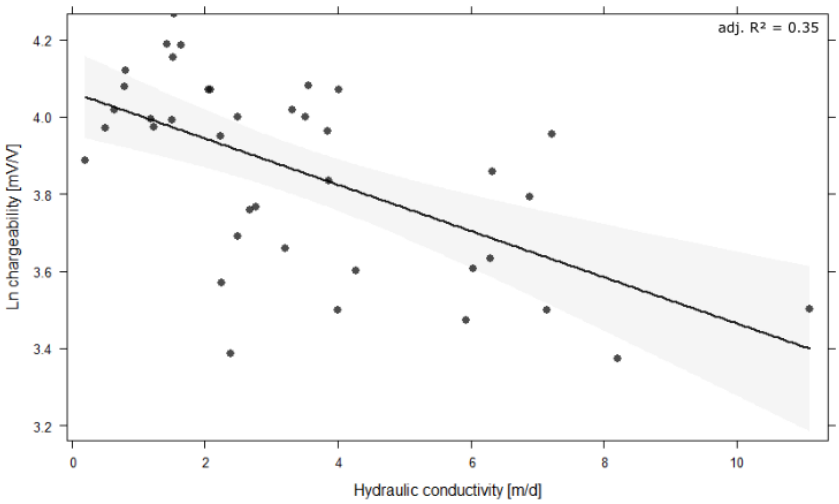

Figure 47 Linear model fit (black line) to hydraulic conductivity versus ln(chargeability) data, harmonically averaged and extracted with method 2. The grey bands indicate the 95 % confidence interval of the fit.

The third method seeks for relationships between differently averaged data of hydraulic conductivity and chargeability averaged in a window. Linear relations between both are all significant for harmonic (Appendix F Figure 54), arithmetic (Appendix F Figure 55) and geometric mean of K (Appendix F Figure 56). The most significant linear model is found for harmonic mean K versus logarithmically transformed chargeability and is shown in Figure 48. The adjusted R^2 for this model = 0.35 and $p = 4.46 * 10^{-5}$. The equation is written as:

$$lnM = 4.06 - 0.05 * K \tag{3.15}$$

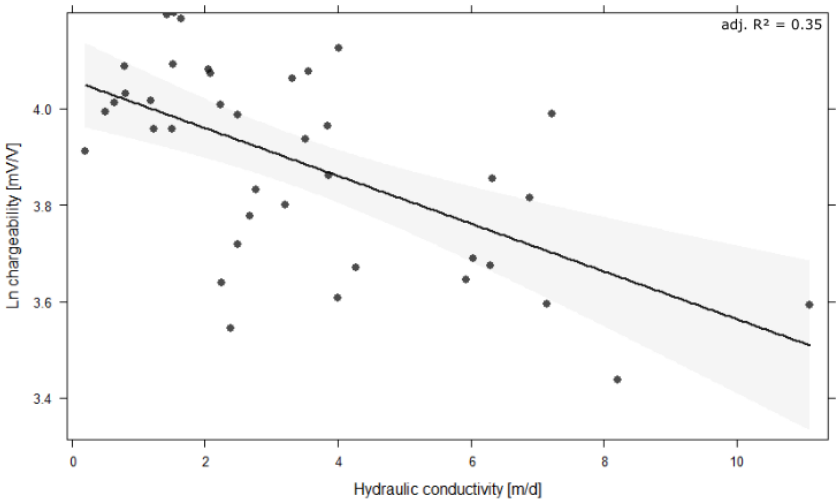

Figure 48 Linear model fit (black line) to harmonically averaged hydraulic conductivity versus ln(chargeability) data, extracted with method 3. The grey bands indicate the 95 % confidence interval of the fit.

Also for the arithmetic and geometric mean of K, logarithmic data of chargeability and no transformation of hydraulic conductivity provide the best correlations. The equations are very similar as equation (3.14). For arithmetically averaged K data, the adjusted $R^2 = 0.22$, $p = 1.57 * 10^{-3}$ and the equation is:

$$lnM = 4.07 - 0.04 * K \tag{3.16}$$

For the geometrically averaged K data, the adjusted $R^2 = 0.30$, $p = 1.84 * 10^{-4}$ and the equation is very similarly written as:

$$lnM = 4.07 - 0.05 * K \tag{3.17}$$

The same can be stated for the fourth method (Appendix F Figure 57), where the equation of the most significant model is almost equal to those above (equations (3.14) – (3.17)), with adjusted $R^2 = 0.33$ and $p = 1.03 * 10^{-4}$ (Figure 49):

$$lnM = 4.05 - 0.05 * K \tag{3.18}$$

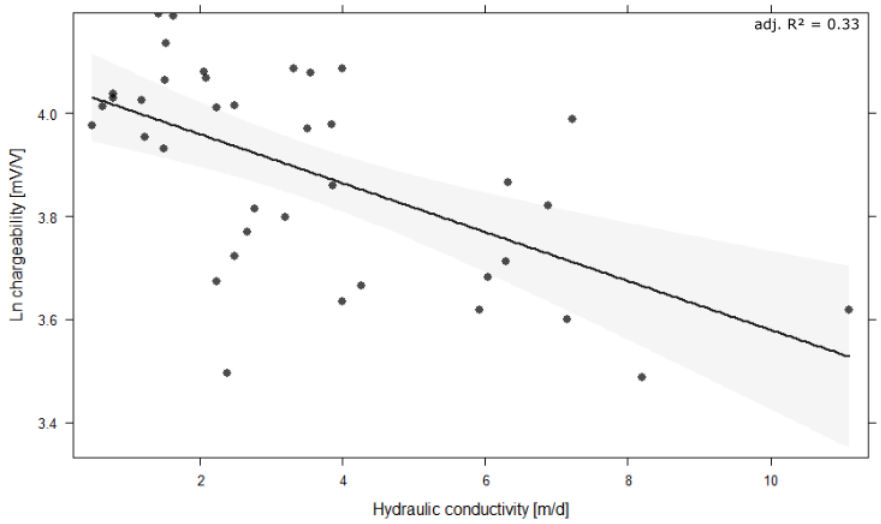

Figure 49 Linear model fit (black line) to harmonically averaged hydraulic conductivity versus ln(chargeability) data, extracted with method 4. The grey bands indicate the 95 % confidence interval of the fit.

3.4.2.4. Conclusion

The third and fourth method provide the clearest results in terms of correlation between chargeability and hydraulic conductivity. Relatively obvious trends are observed visually from comparison of spatial patterns and from scatterplots, and quantitatively from linear regression analyses. The latter show that, for all methods, logarithmic transformation of one of the variables provide more significant relations than double-logarithmic or no transformations. Correlation between M and K is limited with data collected with method 2. Method 1 results in some visual and quantitative relationships, especially for subdatasets such as separate depth data. However, general correspondence is less expressed as for method 3 and 4. It can be remarked that visual inspection and quantitative correlation are not always in correspondence. For example, with method 3 and 4, the most significant linear correlation is expected with logarithmic transformation of K after visual inspection of scatterplots, while linear model fits have higher adjusted R^2 and lower p-values without transformation of K. On the other hand, for method 1 and 2, visually expected relations between M and ln(K) are also translated in significant linear model fits.

3.4.3. HYDRAULIC CONDUCTIVITY AND NORMALIZED CHARGEABILITY

3.4.3.1. Spatial patterns

Spatial distributions of hydraulic conductivity and normalized chargeability are analyzed and correspondence in patterns is sought. Point data of the shallow depth interval, deep depth interval and of data averaged over the depths are considered.

First, data extracted from the shallow depth interval of 20 – 45 cm are compared. Hydraulic conductivity is generally high at this depth with the highest values to the right and in the upstream half of the river section and lower values of K along the left bank (Appendix B Figure 1). Normalized chargeability is low in the right half and high dominantly in the left half for data of the first and second method (Appendix G Figure 58 A & Figure 59 A). The first method also has some points of high MN in the left half. Inverse correspondence between both is therefore present generally for the first method (Figure 50), but a lot of exceptions in point data occur. The pattern of normalized chargeability can be visually split in two halves with the second method, but this is not the case for hydraulic conductivity data. Correspondence is thus limited for the shallow depth data of method 2.

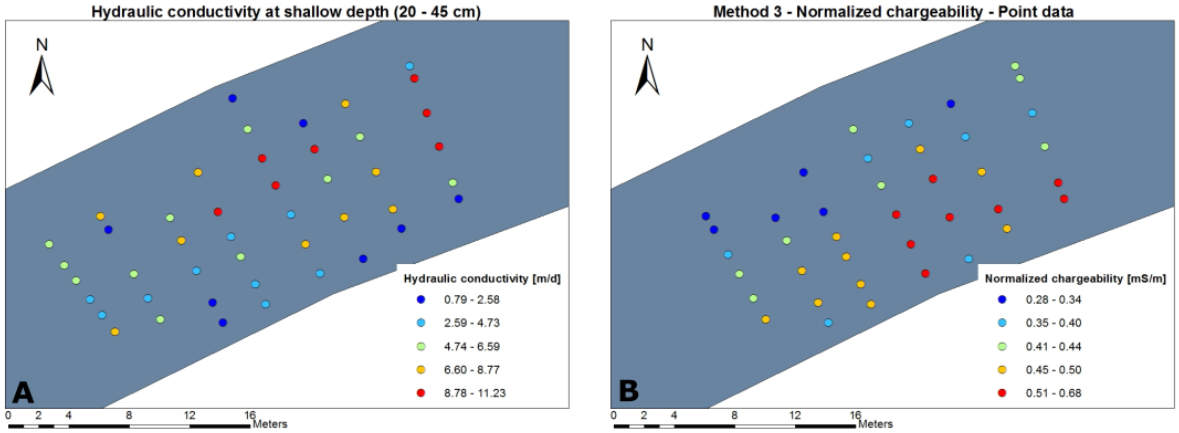

Figure 50 Spatial distribution of (A) hydraulic conductivity and (B) normalized chargeability at deep depth. The data is extracted with method 1. Inverse correlation between both can slightly be observed.

Hydraulic conductivity data in the deep depth interval of 45 – 70 cm is low compared to K data of the shallow interval. The lowest K values are situated in the left half downstream and closely along the whole left bank (Appendix B Figure 2). Higher values of K, relatively for this depth, occur in the right half and upstream also further towards the middle and left part of the river. This corresponds with low to intermediate MN values for the first and second method (Appendix G Figure 58 B & Figure 59 B). The lowest K values correspond to low to intermediate values of MN for the second method, although for the first method, only those values situated along the left bank correspond to low MN values. The low K values in the downstream left half correspond to intermediate to high values of MN. There is thus some general correspondence between hydraulic conductivity and normalized chargeability in the first method, but some parts are also deviating from the inverse relation. For the second method, there is no straightforward correspondence between K and MN because, for example, some parts of high K correspond to low, intermediate or high MN.

When the depth data is averaged for every point location, high K values are situated in the right half and upstream also towards the middle and left of the river (Figure 17). Low K values occur closely along the left bank and in the left downstream quarter of the river section. Correspondence with normalized chargeability in the first method is not completely straightforward. High K values correspond to low or intermediate values of MN, but low K values correspond along the left bank to high MN values and in the left downstream half to rather low MN values (Appendix G Figure 58 C). Also, the second method results in data which shows an ambiguous relation between hydraulic conductivity and normalized

chargeability. The inverse relation of high K corresponding to low MN and vice versa is not valid for the upstream half of the reach and points along the left bank (Appendix G Figure 59 C).

Harmonic mean, arithmetic mean and geometric mean of K of the two depths are very similar (Figure 17, Appendix B Figure 3 & Figure 4). Point maps of normalized chargeability for the third and fourth method are more or less separated in a right and left part with respectively low and high values of MN (Figure 29 & Appendix G Figure 61). The left half is more extended, but two exceptions of low MN occur in this part. Figure 51 shows how, visually, different regions can be delineated, showing an inverse relation between hydraulic conductivity and normalized chargeability. This is observed for the left downstream quarter (low K, high MN), the right downstream quarter (high K, low MN), the right upstream quarter (high K, low MN) and points closely along the left bank (low K, high MN). This qualitative inverse relationship is not seen for the left upstream quarter of the river section, where both high K and high MN values occur. More in-depth cluster analyses will be discussed in section 3.4.7. Overall, correspondence between K and MN for the third and fourth method is good, with the harmonic mean of K showing the strongest correlation with MN.

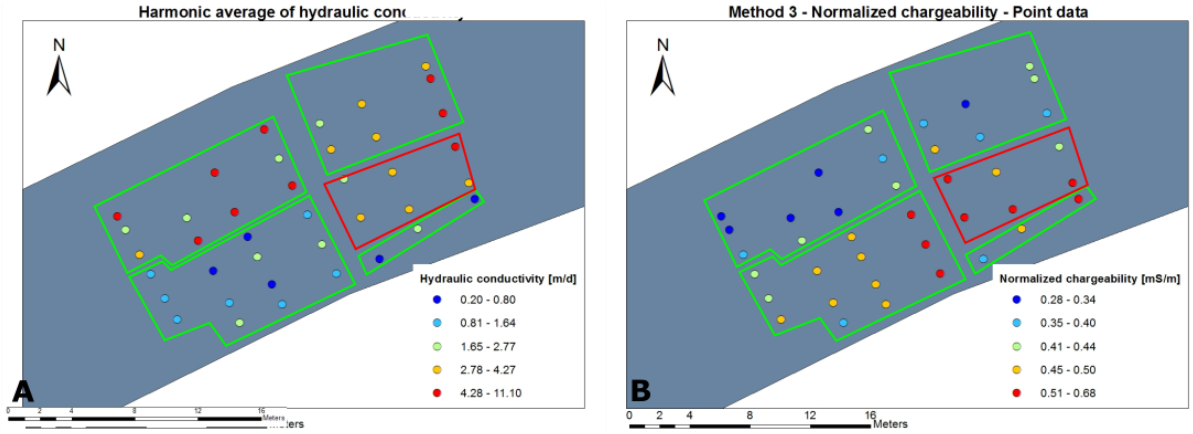

Figure 51 Spatial correlation of (A) hydraulic conductivity (harmonic mean) and (B) normalized chargeability data extracted with method 3. Green frames indicate corresponding correlations and the red frame shows an area deviating from the trend.

3.4.3.2. Scatterplots

Scatterplots with hydraulic conductivity and normalized chargeability are made with every method, described in Table 2. Some weak trends are observed using the first method. A very slightly decreasing trend is found for all data of the first method if K is logarithmically transformed (Figure 52 & Appendix G Figure 62). This is observed because of a few points at low ln(K) values and high MN values. However, most MN data are situated between 0.20 mS/m and 0.50 mS/m. This creates visually a horizontal point cloud in this range and makes it difficult to distinguish a relation between K and MN. When the separate depths are considered, a decreasing relation is slightly better visible, but plots are very scattered (Appendix G Figure 63 & Figure 64). Logarithmic transformations of hydraulic conductivity enhance visibility of a trend, but there is a lot of scatter at high values of ln(K). A decreasing trend is best visible for harmonically averaged data of the depth measurements in method 1 (Appendix G Figure 65). Again, transformed K data provide scatterplots with a clearer correlation, but the scatter at high ln(K) values hampers the trend.

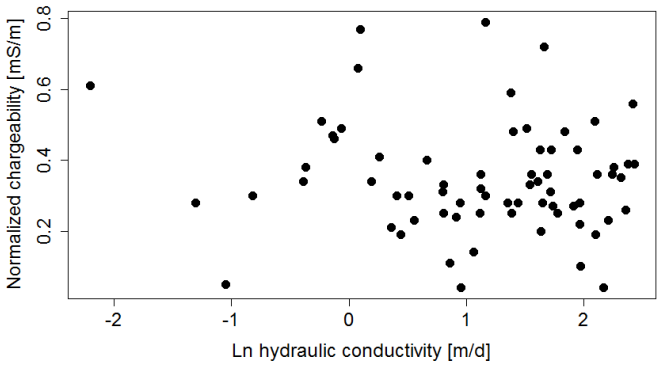

Figure 52 Scatterplot of ln(hydraulic conductivity) versus normalized chargeability for all measured data of method 1. A few extremal points make a weak pattern visible.

Trends are difficult to detect with use of data of the second method. Considering all data (Appendix G Figure 66) or data at the shallow depth interval (Appendix G Figure 67), scatterplots show point clouds of data without any pattern or relation. For data of the deep depth interval, a weakly decreasing relation is found, which is best observed in plots with logarithmically transformed hydraulic conductivity data (Appendix G Figure 68). Scatter is however strongly present. Harmonic mean data of K and MN show a linearly decreasing trend with a wide range of points around the expected line of correlation (Appendix G Figure 69).

Data extracted with the third and fourth method clearly show decreasing trends between hydraulic conductivity and normalized chargeability (Appendix G Figure 70 – Figure 73). However, there is still a considerable amount of scatter around the supposed linear trend line. A similar trend is observed for harmonic, arithmetic and geometric mean data of K (Figure 53 A, B & C), but with a slightly better result, more specifically less scatter, for harmonic mean K data (Figure 53 A) and for the fourth method (Figure 53 D).

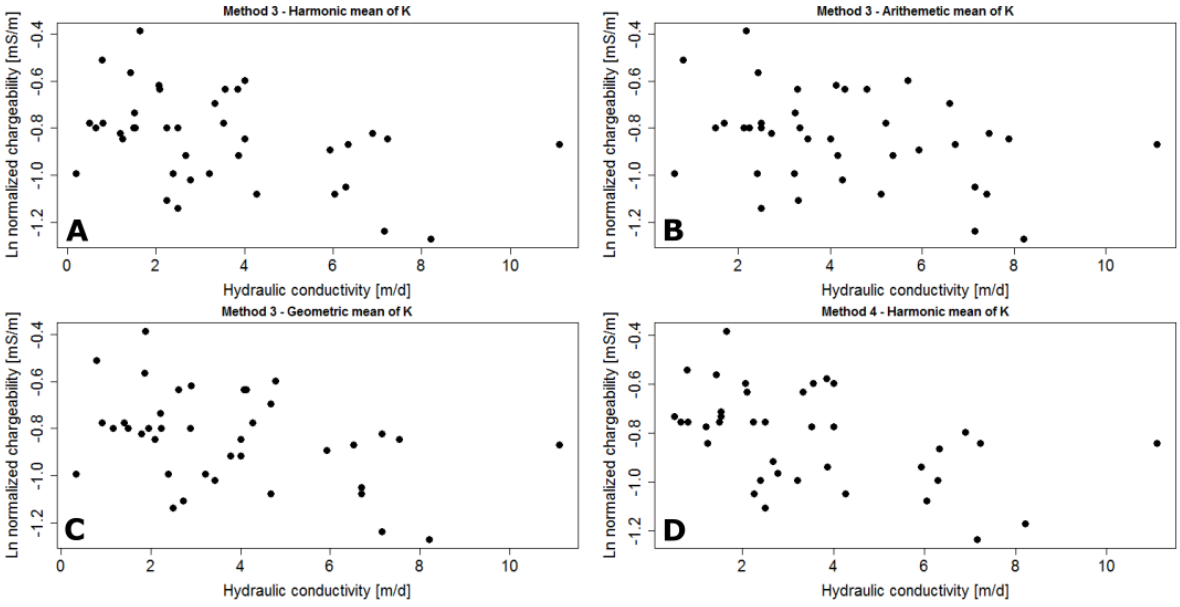

Figure 53 Scatterplots of hydraulic conductivity versus ln(normalized chargeability) for data extracted with method 3 (A, B, C) and method 4 (D). (A) and (D) are plots with harmonically averaged K data, (B) with arithmetically averaged K data and (C) with geometrically averaged K data.

3.4.3.3. Regression analysis

Linear trends are observed in scatterplots and therefore, linear regression models are fit to data of hydraulic conductivity versus normalized chargeability. For the first method, no significant linear relations

are identified when all data, data at shallow depth or data at deep depth are considered. Data harmonically averaged over the two depths show a weak significant correlation between MN and logarithmically transformed K data (adjusted R^2 = 0.09 and p = 0.03). The linear model fit is shown in Figure 54 and the equation is as follows:

$$MN = 0.38 - 0.06 * \ln K \tag{3.19}$$

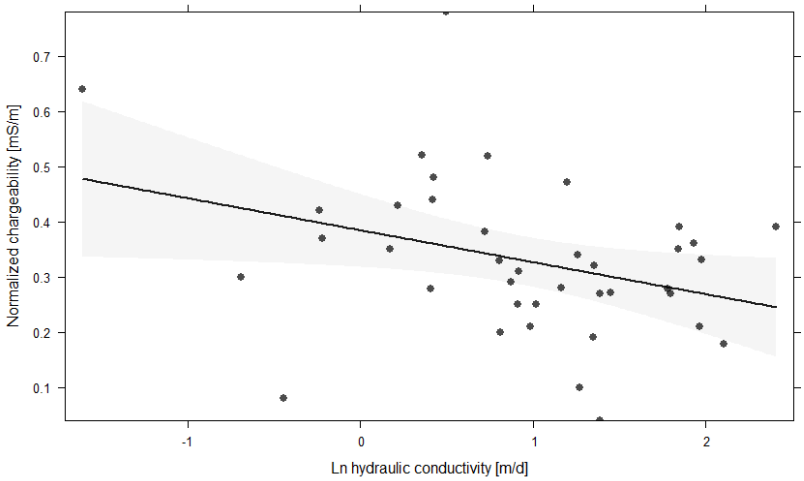

Figure 54 Linear model fit (black line) to ln(hydraulic conductivity) versus normalized chargeability data, harmonically averaged and extracted with method 1. The grey bands indicate the 95 % confidence interval of the fit.

Also for the second method, no significant linear trends are found, except for harmonic mean data, without transformation of hydraulic conductivity (Appendix G Figure 74). The most significant correlation is found for both untransformed K and MN data with the adjusted R^2 = 0.12 and p = 0.02 (Figure 55):

$$MN = 0.46 - 0.02 * K \tag{3.20}$$

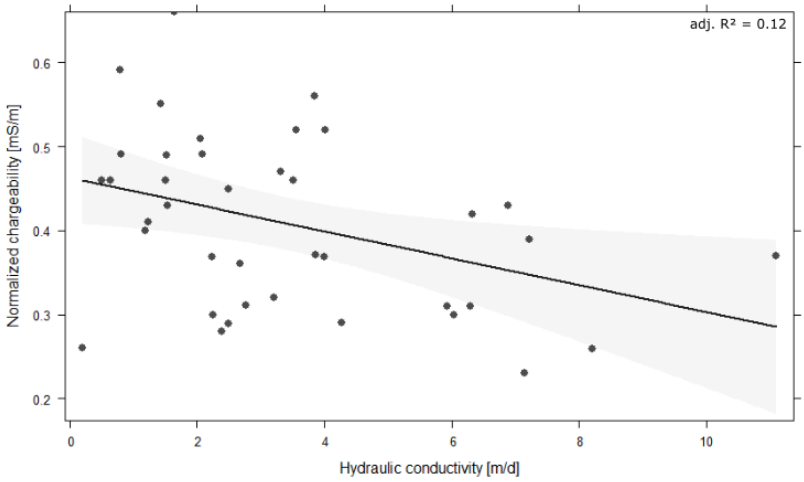

Figure 55 Linear model fit (black line) to hydraulic conductivity versus normalized chargeability data, harmonically averaged and extracted with method 2. The grey bands indicate the 95 % confidence interval of the fit.

The third method results in significantly decreasing trends between normalized chargeability and hydraulic conductivity data (Appendix G Figure 76, Figure 77 & Figure 78). This is only valid if K data is not transformed. For harmonically, arithmetically and geometrically averaged hydraulic conductivity data, the same, best fit results:

$$lnMN = -0.73 - 0.03 * K \tag{3.21}$$

However, adjusted R^2 values and p values are different. For harmonic, arithmetic and geometric mean K data, adjusted R^2 values are respectively 0.14, 0.08 and 0.12 and p values are respectively 0.01, 0.04 and 0.02. Their linear model fits are shown graphically in Figure 56 A, B and C, respectively.

Linear models fitted to the scatterplots of the fourth method are all significant (Appendix G Figure 79) with the most significant result for both log transformed MN and K data (Figure 56 D). The adjusted $R^2 = 0.19$, $p = 3.75 * 10^{-3}$ and the equation is as follows:

$$lnMN = -0.70 - 0.12 * lnK \tag{3.22}$$

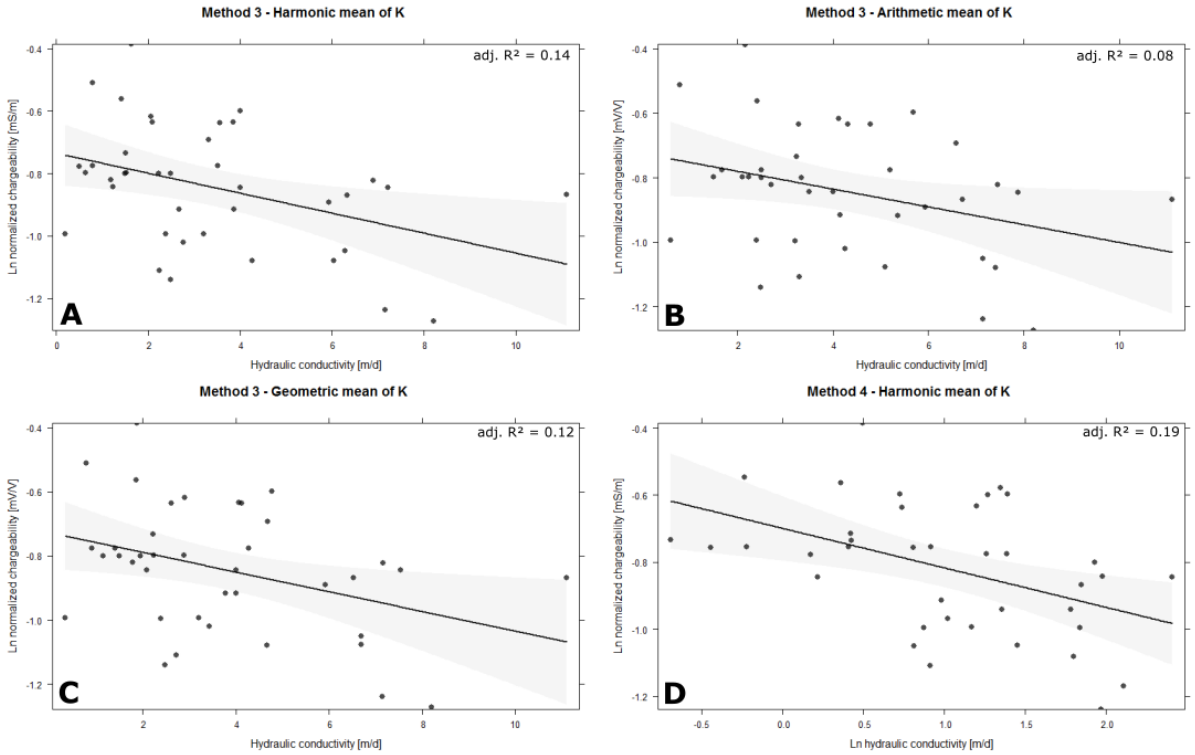

Figure 56 Linear model fit (black line) to hydraulic conductivity versus ln(normalized chargeability) data, extracted with method 3 (A, B & C) and method 4, with log transformed K data (D). (A) and (D) are plots with harmonically averaged K data, (B) with arithmetically averaged K data and (C) with geometrically averaged K data. The grey bands indicate the 95 % confidence interval of the fit.

3.4.3.4. Conclusion

The fourth method delivers the strongest correlation between hydraulic conductivity and normalized chargeability. The linear regression is most significant in comparison with others and scatterplots show the clearest trends. Also, visual spatial patterns are, together with the third method, corresponding best. The third method provides equivalent results. The second method is less indicative for correlation between K and MN. Scatterplots hardly show any correlation and also spatially, little correspondence is observed. The first method shows some correlation between K and MN, if their spatial distribution or scatterplots are observed visually. Furthermore, quantitative and qualitative visual observations are closely related for normalized chargeability and hydraulic conductivity: trends that are expected from scatterplots for transformed or untransformed variables are quantitatively confirmed in significant linear regressions.

3.4.4. INTERMEZZO: BEST DATA EXTRACTION METHOD

Four methods to extract geo-electrical data from ERT & IP cross sections are compared and their efficiency in comparability with hydraulic conductivity is assessed. This is done for hydraulic conductivity versus resistivity in section 3.4.1, versus chargeability in section 3.4.2 and versus normalized

chargeability in section 3.4.3. First, for all methods, similar spatial patterns in the distribution of hydraulic conductivity and geo-electrical parameters are investigated. The third method provides the clearest results, although patterns are very similar to the fourth method. Next, the first method gives comparable patterns, followed by results of the second method. Second, scatterplots and regression analyses show similar outcomes in terms of optimal method application. The third and fourth method result in clearly decreasing trends, which are significant for all geo-electrical parameters. Also the first method provides interesting correlation between hydraulic conductivity and geo-electrical parameters, which is most expressed for electrical resistivity. The second method is least effective in correlating hydraulic conductivity and any of the geo-electrical parameters. Both in spatial distribution of point data as in scatterplots, little correlation is observed.

Overall, the third method provides the most effective data extraction method for correlation of hydraulic conductivity and geo-electrical parameters, especially for chargeability and normalized chargeability. Extracting geo-electrical data from a depth profile using a rectangular window of 1.50 m length, and the width shortened at the water surface (Figure 12 C), results in averaged geo-electrical data which is comparable to averaged hydraulic conductivity data over similar dimensions. Moreover, results discussed in sections 3.4.1, 3.4.2 & 3.4.3 show that depth measurements of K which are averaged harmonically, are most approaching the real hydraulic conductivity value for the assumed dimensions. The amount of iterations in geo-electrical inversions, when RMS is at a small level, changes the results slightly, and more iterations seems to increase correlation with K subtly.

Therefore, data extracted with the third method will be used in further analyses, where harmonically averaged hydraulic conductivity results are compared with geo-electrical results. Variograms will be compared to assess the spatial range of influence of the parameters. Afterwards, kriging images will be investigated. In addition, PCA and CA will be performed to identify structures and patterns quantitatively in the investigated river section. Visually observed clusters will be analyzed and compared as well.

3.4.5. VARIOGRAMS

Variograms of hydraulic conductivity and of geophysical parameters are compared. More specifically, ranges, which indicate the distance of influence of a parameter in the subsurface, are used to find similarities or differences between hydrogeological and geophysical properties. Variograms of hydraulic conductivity are discussed in section 3.1 and those of the geo-electrical parameters are evaluated in section 3.2. To summarize, an overview of the ranges of all variograms is given in Table 8. The magnitude of ranges will be compared, but one must be aware that the more scatter in a variogram, the more uncertain and thus the more ranges can vary from the given value.

Table 8 Ranges of variograms of all hydraulic conductivity data, harmonically averaged hydraulic conductivity data, resistivity, chargeability and normalized chargeability data. Ranges are expressed in meter.

	Hydraulic conductivity (all)	Hydraulic conductivity (harmonic mean)	Resistivity	Chargeability	Ln(Normalized chargeability)
Omnidirectional	8.1	12	18.4	11.5	11
Parallel to river	8.8	12	11.5	13.6	18
Perpendicular to river	5.1	11	20.5	14.1	10.4

A first finding is that ranges of hydraulic conductivity variograms are smaller when all data are considered than when data are harmonically averaged over the two depths. Averaging leads to 36 – 116 % larger ranges than when data is not averaged over the depth intervals. This shows how averaging of spatial data leads to homogenization of the variable. In addition, the difference in ranges between omnidirectional and directional variograms is hardly present for harmonically averaged K data. Also, the ranges of the variograms show that heterogeneity of the parameters is larger in the perpendicular

direction for normalized chargeability and all hydraulic conductivity data, but larger in the direction parallel to the river for resistivity and chargeability. Further, because the scale of geo-electrical data is more similar to the scale of averaged hydraulic conductivity data, variograms of the latter are compared with those of resistivity, chargeability and normalized chargeability.

Firstly, resistivity shows a similar range as K for variograms parallel to the river. Ranges of the omnidirectional variogram and perpendicular variogram of ρ are much larger, i.e. almost up to the double of those of hydraulic conductivity. This means that resistivity has a larger spatial influence than hydraulic conductivity in the river sediment.

Secondly, the ranges of the variograms of chargeability in omnidirectional and parallel direction are very analogous to those of hydraulic conductivity. The spatial effect of chargeability in the direction perpendicular to the river, which is also the direction of the IP profiles, is somewhat higher than that of hydraulic conductivity, but the uncertainty involved in variograms might dissolve this difference.

Lastly, normalized chargeability has similar ranges as hydraulic conductivity for the omnidirectional and perpendicular variograms. In contrast to resistivity and chargeability, the range of the variogram across the river is not outside the dimension of the study area and is comparable to the range of K in this direction. However, in the direction parallel to the river, the range of MN is higher than the range of K.

3.4.6. KRIGING

Maps of point data interpolated with ordinary kriging are given in Figure 57. Because resistivity, chargeability and normalized chargeability data are extracted by averaging over a window, it is recommended to compare their spatial patterns with those of K data averaged over a similar scale. First, patterns of geophysical parameters will thus be compared with those of hydraulic conductivity harmonically averaged over the separate depth intervals. In a later stage, interpolated maps of the separate depth intervals can be considered.

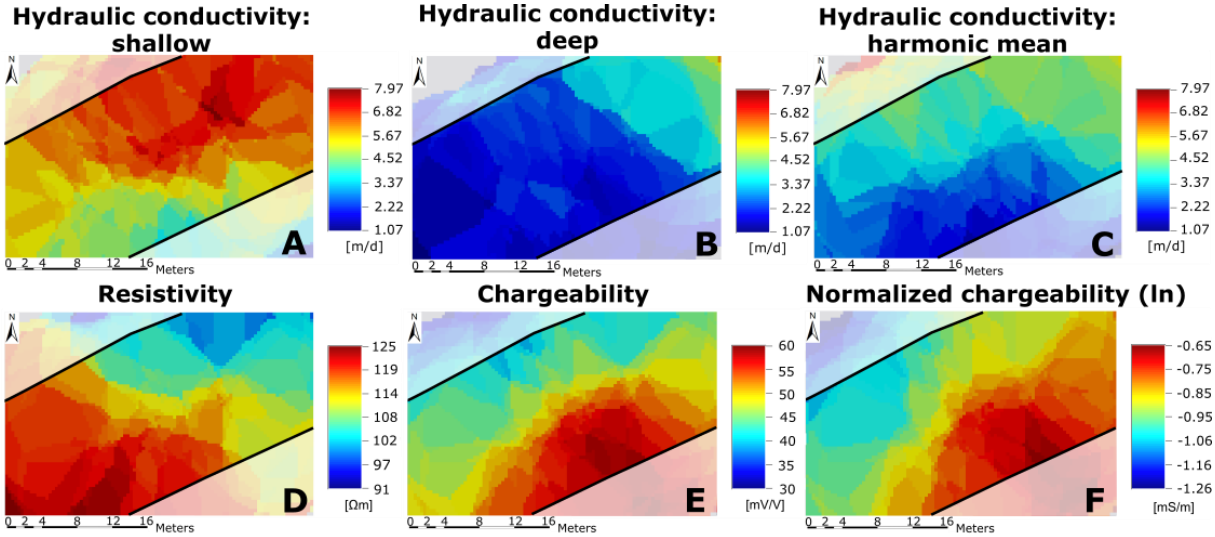

Figure 57 Maps based on ordinary kriging of hydraulic conductivity (A) at shallow depth, (B) at deep depth, (C) harmonically averaged over the depths and of (D) resistivity, (E) chargeability and (F) normalized chargeability.

Spatially interpolated mean hydraulic conductivity data shows a distribution very similar to that of chargeability data (Figure 57 C & E). Areas where one parameter is high, the other is low and vice versa. A semicircle of low K along the left bank is present as a semicircle of high M. It smoothly and symmetrically spreads to higher K values and lower M values towards the middle and right part of the river. This semi-circular zone is also present in the kriging map of normalized chargeability as a high MN zone (Figure 57 F). Opposed to chargeability, it spreads less similar as in the hydraulic conductivity

map. The map of normalized chargeability evolves in a diagonally (from right upstream to left downstream) dominated image, which cannot be recognized in the hydraulic conductivity map.

The semi-circular shape of low K values along the left bank is not delineated in the resistivity map (Figure 57 D), although high values of ρ correspond to the area. Actually, resistivity is high in the left downstream corner of the river section and it spreads to lower values towards the right upstream corner, showing a diagonal structure across the rectangular reach. Hydraulic conductivity is low along the left side but a faint diagonal band of intermediately low K values is comparable to a diagonal band of intermediate ρ values.

Patterns of resistivity can be more clearly recognized in the hydraulic conductivity map of shallow depth measurements (Figure 57 A). The same diagonal structure is present from left upstream to right downstream, but with inverted color scales. The semi-circular shape at the left bank, observed in Figure 57 C, E & F, is weakly present in the shallow depth map of K as a somewhat lower K zone, but it is less expressed as for the harmonic mean of K, M and MN. There is thus some, but less clear, correspondence between the shallow depth K map and kriging maps of M and MN. Hydraulic conductivity data of deep depth (Figure 57 B) results in a map which shows few or no correspondence to maps of resistivity, chargeability and normalized chargeability.

3.4.7. CLUSTERING

Point maps of hydraulic conductivity and geophysical parameters are compared and corresponding patterns or zones are delineated. Several methods of clustering are suggested. First, clusters are visually determined based on comparison between point maps of hydraulic conductivity and one or more geophysical parameters. Here, two ways of visual clustering are suggested. The first one is based on visual correspondence between hydraulic conductivity and chargeability and/or normalized chargeability. The second way is based on spatial correlation between hydraulic conductivity and resistivity. Second, clusters are quantitatively delineated based on a Principal Component Analysis (PCA) and Cluster Analysis (CA). With all cluster methods, scatterplots of the data within the clusters are made and it is evaluated if a clearer or less clear relationship between K and ρ, M or MN is found than when all data is used for comparison, as discussed in the previous sections. Scatterplots are made with or without transformation of data, according to the most significant linear regression for method 3, stated in sections 3.4.1.3 for resistivity, 3.4.2.3 for chargeability, and 3.4.3.3 for normalized chargeability. Next, variability of hydraulic conductivity within the clusters is analyzed.

3.4.7.1. Visual clustering based on K – M/MN correlation

Figure 58 shows clusters which are detected from visual comparison of the spatial distribution of patterns of hydraulic conductivity and both chargeability and normalized chargeability. Four clusters are distinguished, each containing 7 to 13 points. Visual comparison is based on observed inverted correlation between K and geo-electrical parameters. Table 9 qualitatively indicates the magnitude of the parameters in the clusters. Cluster 1 and cluster 2 are easily and clearly outlined and it is expected that these zones do not show a lot of variability of K within their cluster. Cluster 3 and 4 contain more points which are interchangeable between clusters and are therefore more dependent on the choice of the researcher. The four clusters approximately correspond to the subdivision in quarters, described in section 3.4.3.1.

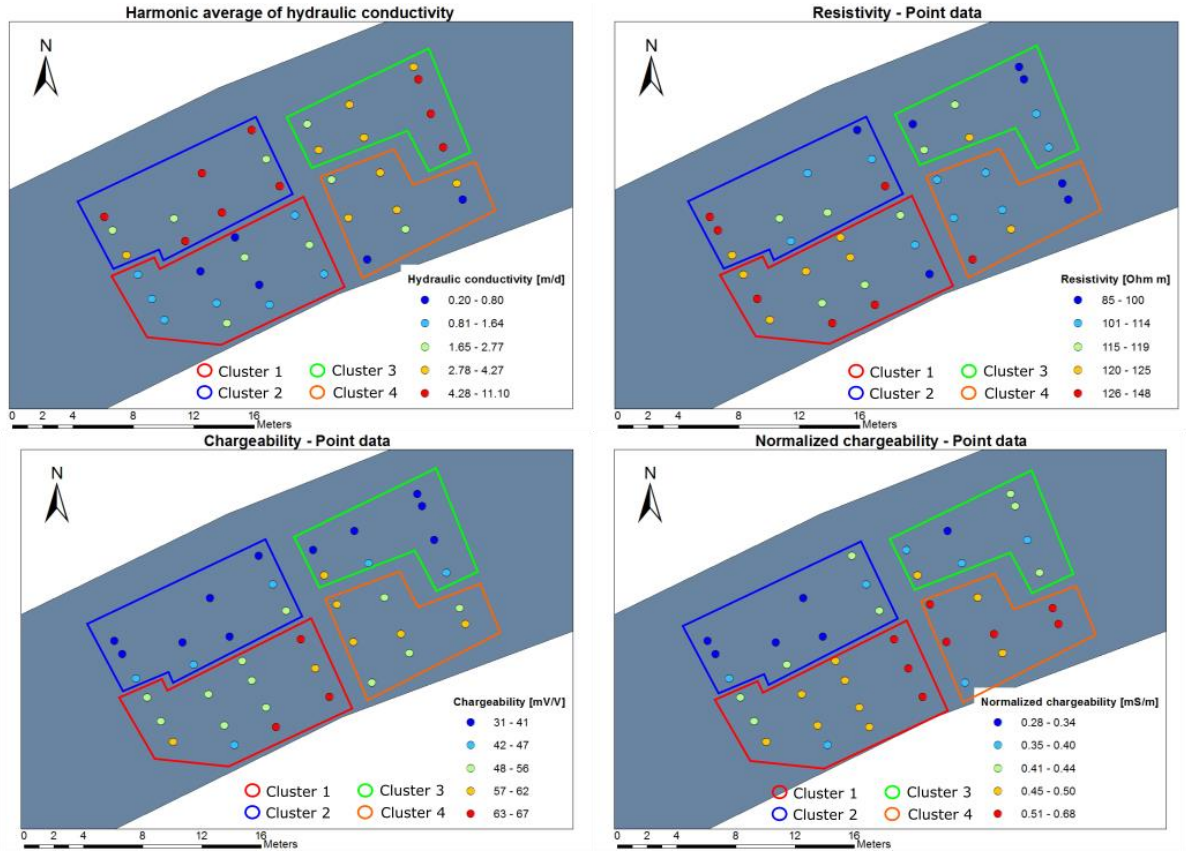

Figure 58 Clustering based on visual correlation between hydraulic conductivity and (normalized) chargeability.

Table 9 Qualitative description of the parameters in the clusters and number of points per cluster, for visual clustering based on K – M/MN correlation.

Cluster	Number of points	Hydraulic conductivity	Chargeability	Normalized chargeability	Resistivity
1	13	Low	Intermediate to high	High	Intermediate to high
2	10	High	Low	Low	Low to high
3	7	Intermediate to high	Low	Low to intermediate	Low to intermediate
4	9	Low to intermediate	Intermediate	High	Low

Scatterplots of hydraulic conductivity versus geo-electrical parameters are made for data within the clusters. Ln(hydraulic conductivity) versus resistivity shows a decreasing trend within clusters 3 and 4 (Appendix H Figure 80). For hydraulic conductivity versus ln(chargeability) or ln(normalized chargeability), this is only the case for cluster 1 (Appendix H Figure 81 & Figure 82). In general, plots of data within the clusters are rather scattered and clear patterns or correlation within clusters are absent. Scatterplots of data averaged over each cluster show clearly decreasing trends for all three parameters (Figure 59). Linear trends are present for chargeability and resistivity, with one deviating point for this latter. However, one must be careful with interpretation of these scatterplots because they only contain four points, i.e. the averages of the four clusters. It shows that low K zones correspond to high ρ, M or MN zones or the other way around, but there are too few points to fit a meaningful linear model to these plots.

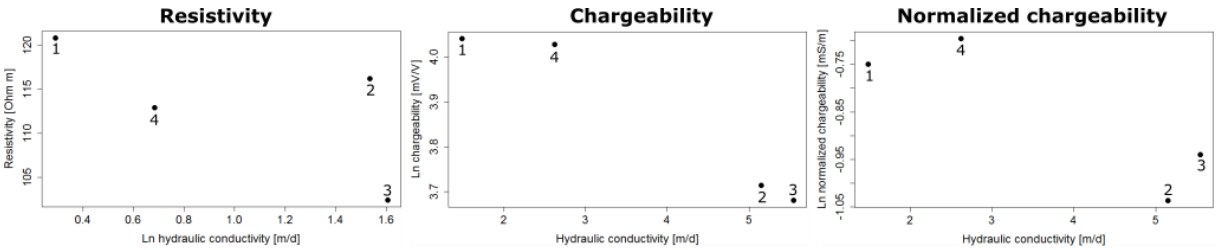

Figure 59 Scatterplots of the mean values of the parameters in the clusters based on visual correlation between K and M/MN. The numbers indicate the number of the cluster.

Table 10 gives the variability of hydraulic conductivity within the zones. This is very low in clusters 1 and 4 and relatively high in cluster 3. Although cluster 1 and 2 are clear to delineate at first sight, variability in cluster 2 is still higher than expected.

Table 10 Descriptive statistics showing variability of hydraulic conductivity within the clusters based on K – M/MN correlation.

	Mean (m/d)	Variance (m/d)²	Minimum (m/d)	Maximum (m/d)
Cluster 1	1.49	0.45	0.50	2.77
Cluster 2	5.15	5.09	2.25	8.21
Cluster 3	5.54	8.33	2.39	11.10
Cluster 4	2.62	1.91	0.20	4.01

3.4.7.2. Visual clustering based on K – ρ correlation

Figure 60 shows another way to cluster data based on visual detection of patterns. Based on comparison between hydraulic conductivity and resistivity, four clusters are delineated and their qualitative basis is given in Table 11. The first and second cluster can be clearly separated. The third and fourth cluster consist of left-over points, for which the inverse relation between K and ρ is not entirely valid. For those clusters, a lot of variation is expected.

Table 11 Qualitative description of the parameters in the clusters and number of points per cluster, for visual clustering based on K – ρ correlation.

Cluster	Number of points	Hydraulic conductivity	Resistivity	Chargeability	Normalized chargeability
1	10	Low	High	Intermediate	Intermediate
2	20	High	Low	Low to intermediate	Low to high
3	6	Low	Low to high	High	High
4	3	High	High	Low	Low

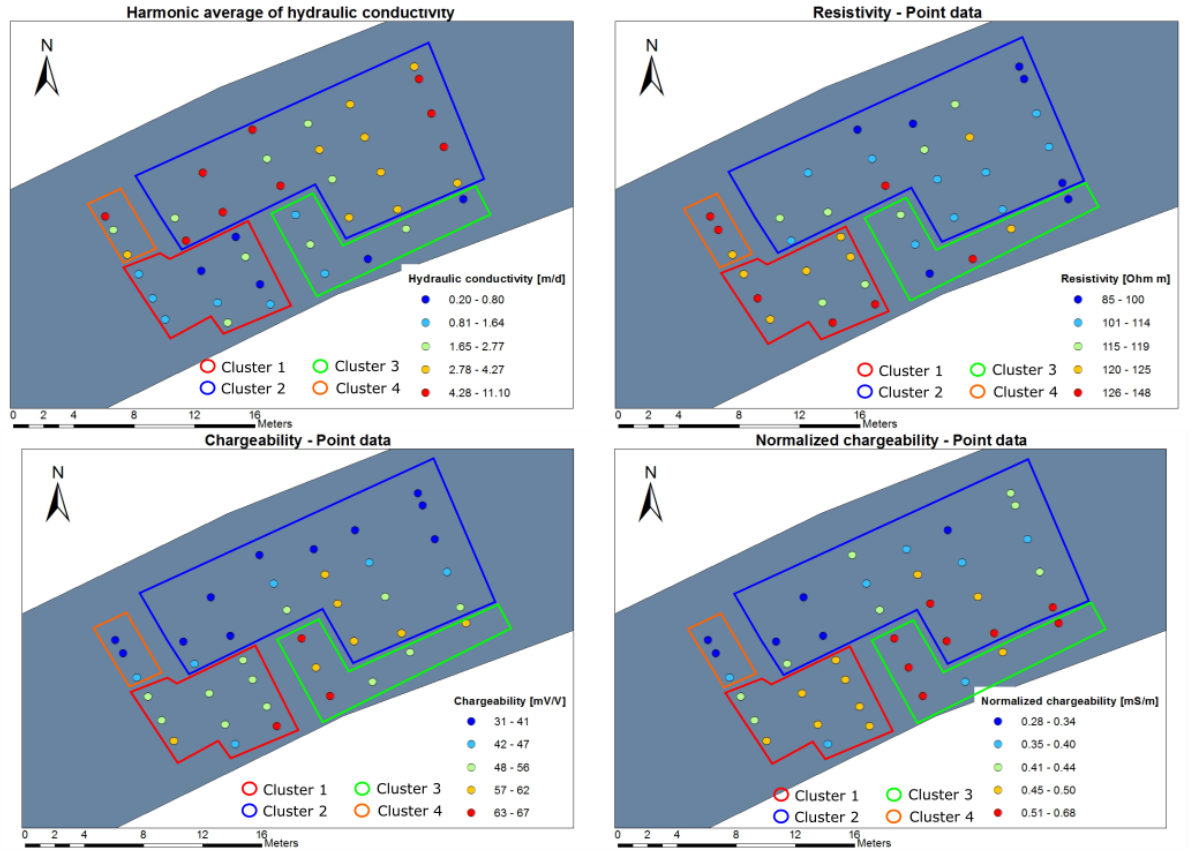

Figure 60 Clustering based on visual correlation between hydraulic conductivity and resistivity.

When scatterplots are made for hydraulic conductivity versus geo-electrical parameters, a few trends can be distinguished. In the ρ – ln(K) plot, no pattern or trend can be observed for any cluster (Appendix H Figure 84). For the plots with chargeability and normalized chargeability, decreasing trends are present for cluster 1 and 2 (Appendix H Figure 85 & Figure 86). Scatterplots of mean values of the clusters weakly show decreasing trends (Appendix H Figure 87). There is, however, scatter and not clearly one linear trend. A linear trend can be seen for cluster 1 and 2 for K versus ρ, but cluster 3 and 4 are randomly situated in the plot. This is expected since cluster 3 and 4 are composed of left-over points. It indicates that cluster 1 and 2 satisfy the qualitative, inverse relation, while cluster 3 and 4 contain points which do not fulfil this correlation. Still, scatterplots of only mean values of the clusters are not reliable because of too few points.

Variability of hydraulic conductivity within the clusters is given in Table 12. Hydraulic conductivity has a low variance in clusters 1 and 3 and higher variances in clusters 2 and 4. Variances are in the same order of magnitude as visual clustering discussed in section 3.4.7.1.

Table 12 Descriptive statistics showing the variability of hydraulic conductivity within the clusters, based on K – ρ correlation.

	Mean (m/d)	Variance (m/d)²	Minimum (m/d)	Maximum (m/d)
Cluster 1	1.42	0.55	0.50	2.77
Cluster 2	4.77	5.33	2.09	11.10
Cluster 3	1.39	0.60	0.20	2.24
Cluster 4	4.28	6.29	2.49	7.15

3.4.7.3. Clustering based on Principal Component Analysis (PCA) and Cluster Analysis (CA)

Principal Component Analysis (PCA)

A Principal Component Analysis (PCA) is performed with data of harmonically averaged hydraulic conductivity, resistivity, chargeability and normalized chargeability. This is done based on a correlation matrix. The first two principal components PC 1 and PC 2 explain most of the variance, i.e. 57 % and 31 % respectively. PC 3 and PC 4 explain respectively 11 % and 0.1 %. The first principal component corresponds most to chargeability, normalized chargeability (logarithmically transformed) and hydraulic conductivity. The loading of M to the first component is -0.64, of MN this is -0.54 and the loading of K is 0.52 (Table 13). Resistivity contributes more to the second component with a loading of - 0.82. The other variables have loadings smaller than 0.51 for PC 2 (Table 13).

Table 13 Loadings of the variables to the four principle components.

	PC 1	PC 2	PC 3	PC 4
K	0.52	0.27	0.81	-0.01
Rho	-0.20	-0.82	0.39	-0.37
M	-0.64	0.05	0.40	0.66
ln(MN)	-0.54	0.51	0.16	-0.65

These relations between variables and principle components are visualized in a correlation biplot, shown in Figure 61. Angles between variables and points reflect mutual correlations. The angle between chargeability and normalized chargeability is the smallest and in the same direction, indicating that they are most strongly correlated. Next, the biplot shows that chargeability and hydraulic conductivity are strongly inversely correlated. The angle between both vectors is approximately 160°. Consequently, the angle between the prolongation of the M vector to higher loadings, and the vector of K, is thus only ca. 20°. Also normalized chargeability shows such an inverse relation with K, but their correlation angle is larger than for M (ca. 55°). Resistivity and hydraulic conductivity show a similar inverse correlation as normalized chargeability and K (ca. 50°), but in another direction with respect to the principal components. The resistivity vector is more aligned to PC 2, while the other variables contribute more to PC 1. Especially chargeability is dominantly explained by PC 1 in comparison with PC 2.

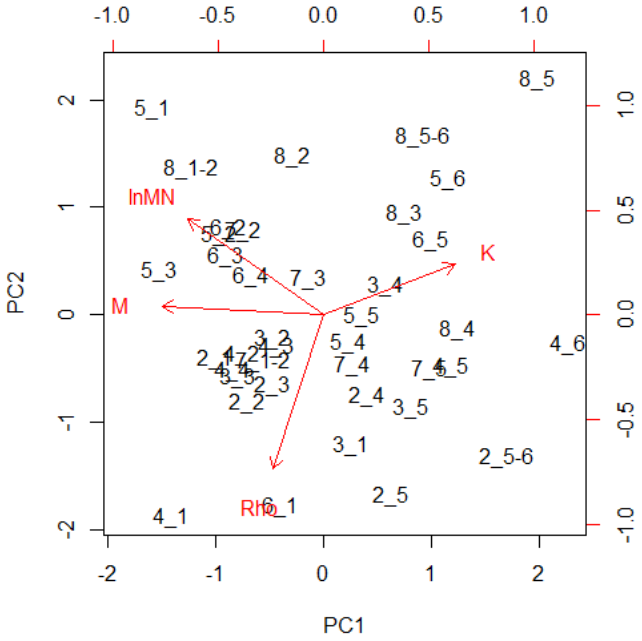

Figure 61 Correlation biplot of the PCA. The numbers indicate the point locations as 'profile _ point in profile' (point 1 in a profile is at the left bank) and are indicated in Figure 62. The left and bottom axis represent the scores of the objects. The top and right axis represent the loadings of the variables.

The correlation biplot (Figure 61) also shows correlation between points, so that roughly clusters in the data can be distinguished. First, points with low K values and situated between the M and ρ vector, i.e. in the prolongation of the K vector to low scores on the PC 1 axis, are strongly correlated. These are points of the left downstream part of the river (Figure 62, cluster 1). Next, points in the middle of the river section are related to each other especially by their high MN and high M values (Figure 62, cluster 2). Lastly, points situated in the right part of the river are also correlated to each other, although less strongly as the two clusters described above. They are related by their low M and MN values, and their high ρ and high K values (Figure 62, cluster 3).

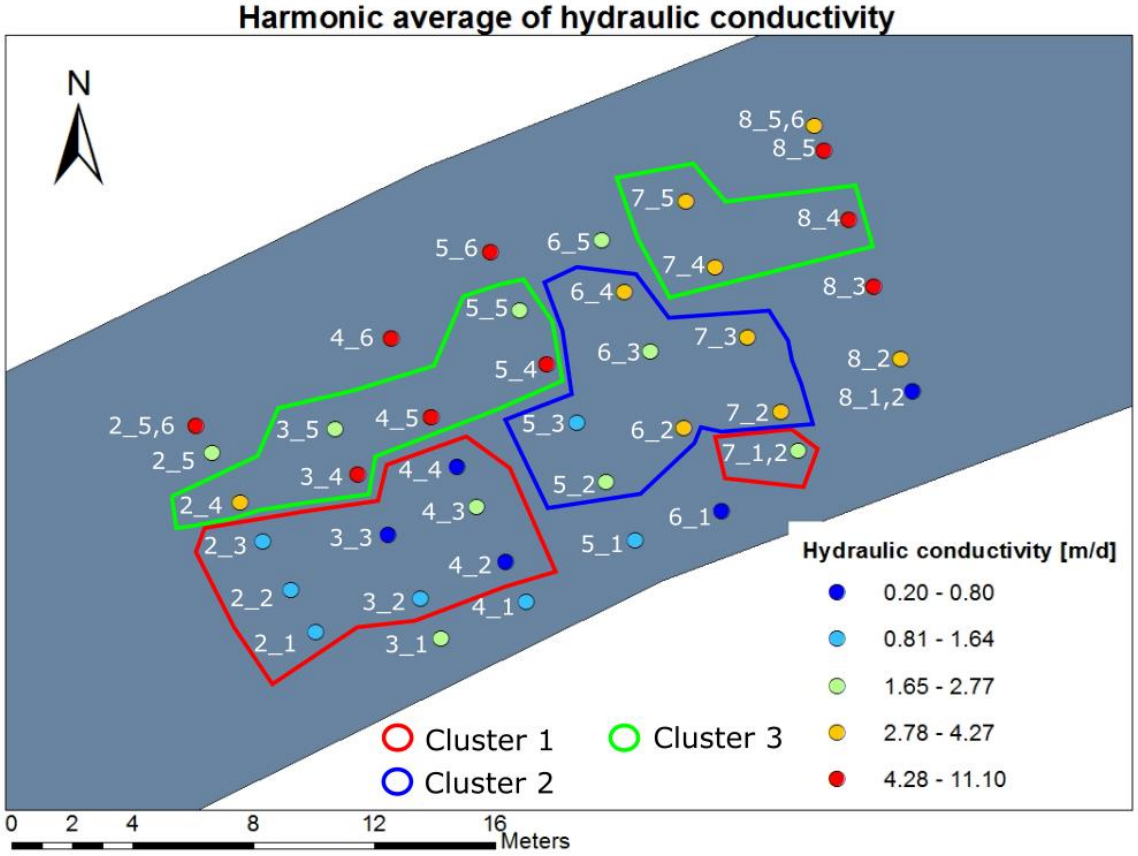

Figure 62 Clusters based on correlation of point locations in the correlation biplot of the PCA analysis. Numbers indicate the names of point locations (indicated as 'profile _ point in profile' with point 1 in a profile is at the left bank).

Cluster Analysis (CA)

Four hierarchical clustering methods are applied to quantitatively analyze clusters in the total dataset of hydraulic conductivity, resistivity, chargeability and normalized chargeability. Differences between these methods are described in section 2.7.4. Single linkage agglomerative clustering is performed resulting in four clusters and four points, which are at a further distance from points incorporated in the clusters (Appendix H Figure 88). Complete linkage agglomerative clustering results in five clusters with one separate point, most closely related to the cluster with points of the middle part of the river and left upstream part (Appendix H Figure 89). Almost identical clusters are determined with the Ward's minimum variance method (Appendix H Figure 91). Nonetheless, with this method, all points are included in a cluster. The unweighted average linkage agglomerative clustering method (UPGMA) results in four clusters (Figure 63), which are almost identical to those of the single linkage agglomerative clustering method. Only one point (2_1) is shifted from one cluster to another. The best clustering method is determined based on cophenetic correlation and the Gower distance. Cophenetic correlation is the highest for the UPGMA method and the Gower distance is the lowest also for this method.

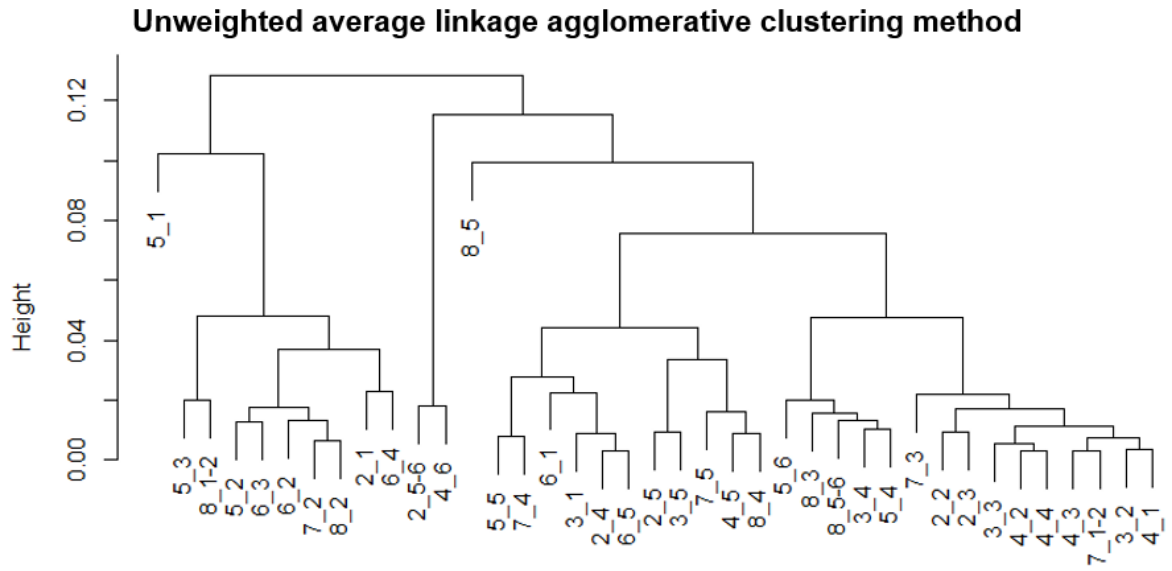

Figure 63 Dendrogram of the UPGMA clustering method. The point numbers are indicated as 'profile _ point in profile' (point 1 in a profile is at the left bank). These numbers are indicated in Figure 62.

Figure 64 shows the points grouped in the clusters according to the UPGMA clustering method on point maps of the parameters. More or less the same points are grouped in a cluster as was derived from the PCA biplot (Figure 61). Further analysis of clustered data is based on clusters shown in Figure 64. Points which do not belong to any cluster are treated as a separate group, which is also included in the analysis.

Table 14 qualitatively describes the magnitude of the parameters in the clusters. In general, an inverse relation between hydraulic conductivity and geo-electrical parameters is expressed in the clusters, which can also be observed in Figure 64. Inverse correlation is present for resistivity in clusters 1 and 4 (except for one point) and for the individual points. For chargeability, this is the case in clusters 2, 3 and 4 and for the individual points. A clear inverse relation between hydraulic conductivity and normalized chargeability is present for clusters 2 and 3 and a weak inverse relation occurs for clusters 1 and 4, and the left-over points.

Table 14 Qualitative description of the parameters in the clusters and number of points per cluster, for the UPGMA clustering method.

Cluster	Number of points	Hydraulic conductivity	Resistivity	Chargeability	Normalized chargeability
1	10	Low	High	Intermediate	Intermediate to high
2	9	Low to intermediate	Low	High	High
3	11	Intermediate to high	Low – intermediate – high	Low	Low
4	5	High	Low	Low	Intermediate
Individual points	4	3 high, 1 low	3 low, 1 high	3 low, 1 high	2 low, 1 intermediate, 1 high

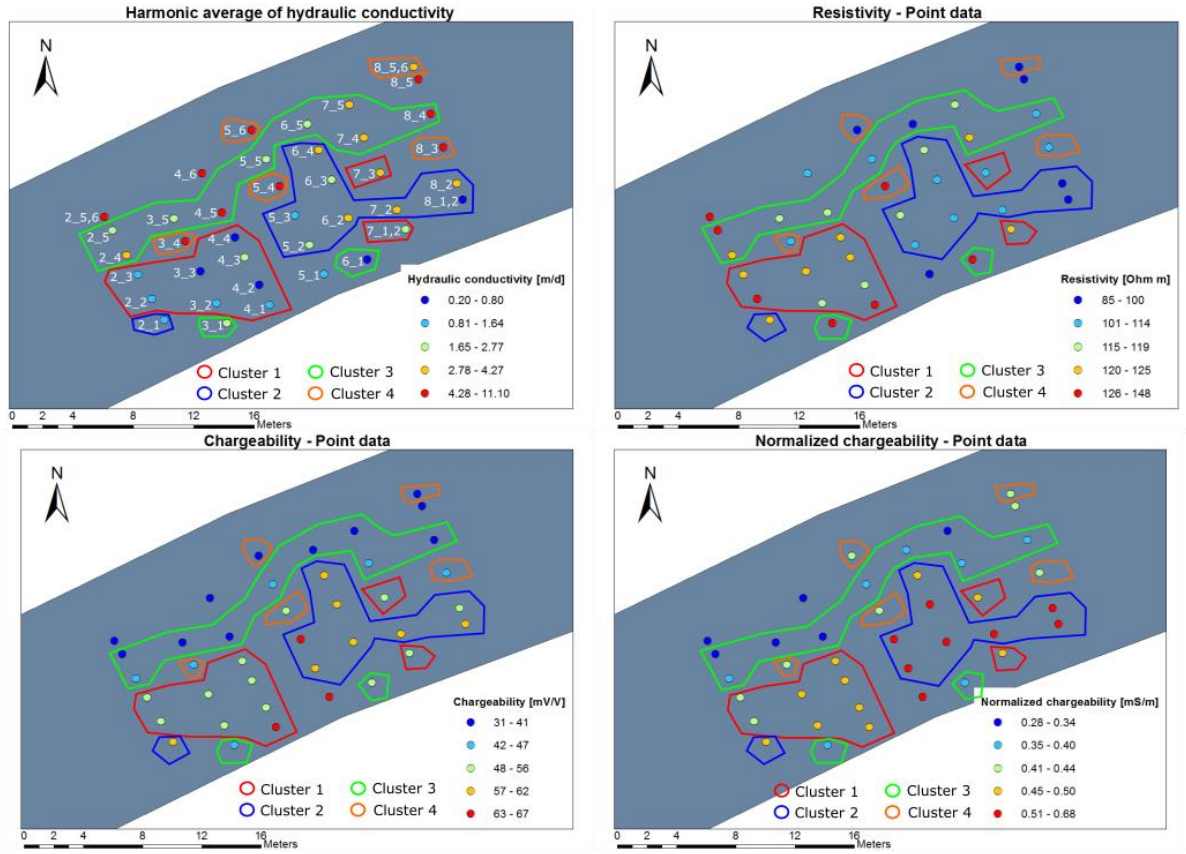

Figure 64 Clusters determined by the UPGMA clustering method. Numbers indicate the names of point locations (indicated as 'profile _ point in profile' with point 1 in a profile is at the left bank).

Decreasing trends in scatterplots of hydraulic conductivity versus resistivity within the clusters are observed for clusters 1, 2 and 3, while cluster 4 shows an increasing trend and the left-over points show no trend at all (Appendix H Figure 92). The same is valid for scatterplots of hydraulic conductivity versus chargeability, except that individual points do show a decreasing trend (Appendix H Figure 93). In plots of K versus normalized chargeability, there is only a decreasing trend for cluster 2 and individual points (Appendix H Figure 94). Clusters 1, 3 and 4 do not show any trend. Scatterplots with only the mean values of the cluster data show decreasing trends for resistivity, chargeability and normalized chargeability (Appendix H Figure 95). These are, however, not reliable because of too little points.

Variability of hydraulic conductivity within the clusters is in all clusters low to very low, as shown in Table 15. Points which are not contained in a cluster have a very high variance of K. This type of clustering results thus in much less variability of hydraulic conductivity – and other variables – than with visual clustering. This is a consequence of the statistical cluster analysis, which aims at minimizing the variance in the dataset, considering all variables. This quantitative method is useful to minimize variability of parameters, but results in less continuous clusters in space than with visual clustering.

Table 15 Descriptive statistics showing the variability of hydraulic conductivity within the clusters, based on UPGMA clustering.

	Mean (m/d)	Variance (m/d)²	Minimum (m/d)	Maximum (m/d)
Cluster 1	1.57	0.89	0.50	3.52
Cluster 2	2.51	1.41	0.79	4.01
Cluster 3	3.31	3.06	0.20	6.29
Cluster 4	6.07	1.59	4.00	7.22
Cluster 5	7.02	15.67	1.64	11.10

4. Discussion

In this section, results will be discussed and interpreted. First, spatial patterns and variability of hydraulic conductivity, resistivity, chargeability and normalized chargeability will be explained separately. Next, comparisons between K and the geophysical parameters will be clarified. Possible causes for similarities or differences will be given and specific statistical or geostatistical correlations will be discussed. In the end, recommendations will be suggested for similar studies or future research.

4.1. HYDRAULIC CONDUCTIVITY

Results of the slug test analysis show that hydraulic conductivity in the riverbed of the Aa varies over two orders of magnitude in a study area of only 25 m x 15 m (Figure 16). The total range of K values of 0.11 m/d to 11.39 m/d, is completely in the range typical for riverbed materials, stated by Calver (2001). Also Sebok et al. (2014) found such a local heterogeneity in streambed sediments. They assigned this to very local differences in the sediment and morphology. Results obtained from the slug tests give very detailed information on heterogeneity of K in the riverbed on a small scale. However, in areas between measurement point locations, hydraulic conductivity is unknown and could have very different values than neighboring points. Nonetheless, Landon et al. (2001) stated that local spatial variability of K is negligible within 3 m distance from a point.

The range of hydraulic conductivities observed in the study area correspond to lithologies of medium to very fine sand and silt according to Hartmann et al. (1988) (Table 16). Ranges given in Table 16 are however general indications and intermingling of different classes is not considered. From field observations, it is known that some clay and organic matter is intermixed with sand sediments in the study area.

Table 16 Hydraulic conductivity ranges per grain size class according to Hartmann et al. (1988).

Lithology	Grain size [µm]	Hydraulic conductivity [m/d]
Very coarse and coarse sand	500 - 2000	20 - 100
Medium, fine and very fine sand	63 - 500	1 - 20
Silt	2 - 63	0.01 - 1
Clay	< 2	0.001 - 0.01

A significant difference in hydraulic conductivity between the two depth intervals is observed. Hydraulic conductivity in the shallow depth interval of 20 – 45 cm below the riverbed is significantly higher than hydraulic conductivity in the depth interval of 45 – 70 cm (Figure 15 & Figure 16). According to K – lithology correlation of Hartmann et al. (1988) (Table 16), sediments in the shallow depth interval are mostly composed of medium to very fine sands. Indeed, drillings in this depth interval revealed similar observations: medium to fine grained sands with variation in clay and organic matter content are present at this depth. In contrast, sediments in the deeper depth interval are interpreted to consist of more clay and less sand, according to their significantly lower K values. This can also explain why the slug test piezometer could not penetrate the sediments, or yield results at this depth at some locations, especially close to the right and left border of the river. Hence, based on hydraulic conductivity data, two layers can be distinguished within the upper 70 cm of the riverbed, at the field site under investigation. The deeper layer of the two forms a low K barrier, which can inhibit fast river – aquifer interaction.

As shortly mentioned above, riverbed drillings in the shallow depth interval confirm the stated interpretations: sand or clayey sand is observed up to a depth of 50 cm. Along the left bank, black, sticky sand with clay and organic material occurs. This clay and organic deposition inhibit flow of water through the fine sandy material. Consequently, hydraulic conductivity is low along this bank (Appendix B Figure

1). In the middle of the river, sediment is composed of brown, loose sand with hardly any clay or organic material. This makes water flow through the sediment fluent with few obstacles, and results in higher values of hydraulic conductivity (Appendix B Figure 1). Close to the right bank, almost no slug test measurements could be performed because the piezometer could not penetrate the sediment. Also penetration of the riverbed auger was not or hardly possible. In addition, poles at a distance up to 1.5 m from the right border make it likely that the area between the poles and the right bank is part of a particular structure, possibly made by man. Based on few observations of black, sticky sand with a lot of organic matter, low hydraulic conductivity is expected along the right border. This is confirmed by the only obtained measured point at a close distance from the right border, made in profile 5 (Appendix B Figure 1).

When values at the two depths are averaged at every location, a pattern of a high and low K zone is visible at the field site in the Aa river (Figure 17). The high K zone is present in the middle and to the right of the river. The low K zone is present along the left bank, and is expected closely to the right bank, where only one slug test measurement could be performed. Because measurements in the deep depth interval are not possible at all locations, especially towards the right bank, only K values at shallow depth are considered in harmonically averaged values at those points. Since hydraulic conductivity in the shallow depth interval is significantly higher than in the deep depth interval, this visually enlarges the zone of high K slightly towards the right part of the river. The high K zone corresponds to a zone of brown, loosely packed, fine – medium sand, while the low K zone can be linked to a zone of fine sand with a lot of organic matter and clay. This zonation exists because the flow velocity of water is higher in the middle of the river than near the borders. Consequently, larger grains are deposited in the middle of the river and deposition of smaller grains occurs near the borders. Moreover, plants on the banks, hanging over the river or present in the river water, slow down water current and can trap small particles. In addition, plants are producers of organic material, which is abundantly present in sediments near the banks. This organic matter results in the black color and sticky texture of sediments along the left and right bank. Zones where black sediments occur are even visible on an aerial photograph of the river (Figure 65). Also Wharton et al. (2006) and Boulton et al. (1998) stated that, besides sedimentation and erosion processes, also siltation around macrophytes or bacterial growth and biofilms can affect hydraulic conductivity in riverbed sediments.

The reason for a wider low K zone along the left bank than along the right bank, can be the occurrence of the field site in a slightly meandering part of the Aa river. Flow velocities are slightly higher in the outer bend, which is along the right bank, than in the inner bend or left bank. Consequently, there will be little more deposition of fine particles in the left part of the river, while erosional processes are more operating on the right bank. Evidence for incision of the river along the right bank is found from wooden poles which are presumed to be planted next to the right bank as fortification after straightening of the river in the 1960's. At the field site, where the bend occurs, these poles do not longer occur directly along the bank, but are situated at distances up to 1 or 2 m from the bank. In a straighter part of the river, outside the field site, poles still touch the right border of the river. The bathymetry of the field site (Figure 21) also shows a steeper right part and weaker sloping left part of the river. Similar observations and processes have been described in the study of Binley et al. (2013). In addition, fluctuations of the water level in the river are common (Figure 66). This is due to weirs up- and downstream (Figure 2), which are opened or closed for random periods. Discharges can be variable and sudden changes can also influence the morphology and sedimentation processes in the river section. Moreover, other human interactions such as sand dumping from construction sites, agricultural waste, etc. may affect the river sediment and morphology.

Figure 65 Aerial photograph with the study site indicated by the red rectangle. Zones with black sediments along the borders are delineated with black lines. (modified from Geopunt, 2017).

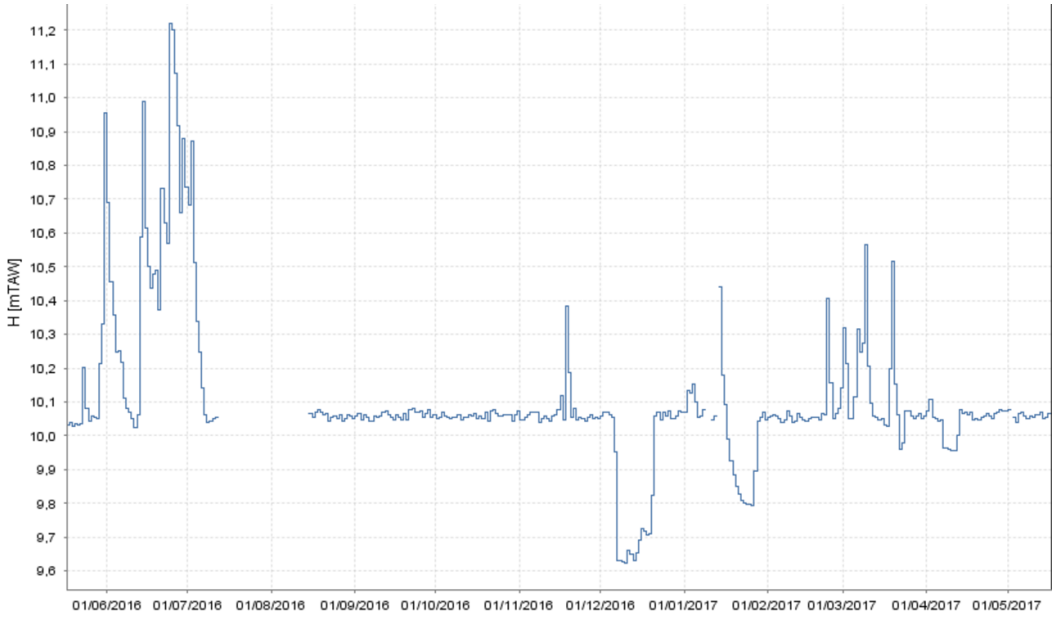

Figure 66 Changes in the water level at the field site from June 2016 until May 2017 (Waterinfo, 2017).

Consequently, this zonation in the spatial distribution of harmonic mean of hydraulic conductivity is an indication of areas of the river where fast or slow vertical flow through sediments can occur. In the middle to right half of the river section, groundwater and river water exchange can be interpreted easier and faster than in the left part of the river, at this location. Moreover, large spatial heterogeneity of riverbed conductivity increases the proportion of high groundwater – surface water fluxes (Kalbus et al., 2009).

Variograms of hydraulic conductivity data, i.e. of all K data and of the separate depths, show that ranges of variograms perpendicular to the river are 30 % to 50 % smaller than those of variograms parallel to the river. Spatial dependence of hydraulic conductivity is therefore larger in the direction of the stream. This is because flow influences sediments and their properties. It shapes the riverbed and elongates structures in the direction of flow. Spatial sediment distribution perpendicular to flow is more determined by the overall morphology of the river. The scale of influence of hydraulic conductivity is 8.1 m – 10.5 m

in parallel direction, while it is 4.7 m – 5.1 m in perpendicular direction, when K is considered in small volumes such as for slug test measurements. In a larger volume, when K is averaged over the measurement depths, the scale of influence is 11 – 12 m in parallel and perpendicular direction. Hence, this shows that a smaller measurement scale leads to more heterogeneity of hydraulic conductivity. Further, high nuggets are an indication of heterogeneity below the scale of measurement and/or of errors in the measurements. In addition, ranges of directional variograms at shallow depth are somewhat higher than those in the deep depth interval. Possibly, there is more directional heterogeneity in the deep interval than in the shallow interval, although uncertainty in the variograms should also be considered. Nevertheless, this changing nature of variograms with depth was also described in the study of Cardenas & Zlotnikz (2003).

It is important to be aware of the time dimension of the results. Measurements of hydraulic conductivity are performed in the summer of 2016 and are representative for this period. Sedimentation and erosion processes continuously affect the upper sediments in the riverbed. This is mainly the case when sudden changes in discharges or peak flows occur. Consequently, also values and patterns of hydraulic conductivity can change throughout the year. Moreover, also human interaction can have a strong influence. Therefore, studies using this data should be completed within a certain time frame.

4.2. RESISTIVITY, CHARGEABILITY AND NORMALIZED CHARGEABILITY

Spatial distribution of resistivity, chargeability and normalized chargeability can be understood when their main influencing factors are considered. These dependencies are described in section 2.9. Pore volume is the main influence for bulk resistivity in sandy environments. Clay content is also important for two reasons. On the one hand, it can decrease the pore volume, increasing resistivity (Table 3). On the other hand, it can decrease resistivity due to its electrical double layer (Table 3). In contrast, clay content is the most important factor determining normalized chargeability and chargeability. For chargeability, porosity is also influential (Table 3).

Qualitatively, profiles and spatial patterns of chargeability and normalized chargeability are very similar (Figure 25 & Figure 26; Figure 28 & Figure 29). A close relation between chargeability and normalized chargeability is also shown in the biplot of the PCA analysis (Figure 61), where the angle between M and MN is small. Influence of resistivity on normalization of chargeability is thus limited, which can be interpreted as little presence of large salinity or temperature contrasts in the reach. These are bulk conduction properties, which have an influence on both M and ρ, but which are removed by normalization. Few differences between M and MN indicate few influence of these bulk conduction properties. Therefore, mainly clay/OM content and porosity differences are causes of changes in geo-electrical profiles.

Several structures and patterns are observed in profiles of resistivity ρ, chargeability M and normalized chargeability MN (Figure 24, Figure 25 & Figure 26). Firstly, from ca. 1.5 m depth, resistivity decreases in horizontal layers with depth, while chargeability and normalized chargeability increase. This can be explained by an increase in clay content and organic matter with depth. Influence of pore volume is restricted here, as this would not correspond with the contrasting patterns of ρ, M and MN (Table 3). A dipping structure from the right bank towards the middle of the river at 1.75 m – 3 m depth is possibly a zone with an increased clay content because resistivity is very low (< 80 Ωm) and normalized chargeability has values > 80 mS/m.

Secondly, thin zones of 20 cm – 40 cm deep with high chargeability and normalized chargeability are visible at the riverbed surface. MN values are up to > 0.95 mS/m, which could indicate clay and organic rich zones (Table 4). Corresponding areas cannot be delineated in the resistivity profiles. This could be explained by the compensating effect of clay in a sandy environment. However, riverbed drillings reveal

few organic matter or clay at a distance from the banks, where these zones occur. This means that another factor has a stronger influence. Possibly, these thin zones are areas with well compacted sand. In this case, porosity would be relatively lower than locations where sand is not that compacted, so few water is present in the pores. This can explain why chargeability and normalized chargeability are high and resistivity is rather high as well near the riverbed surface. A drilling in such a zone in profile 5 confirms this hypothesis: penetration with the riverbed auger was hardly possible, probably indicating closely packed sand.

Along the right bank, there is a shallow, elongated zone of approximately 3 – 4 m long, with low chargeability and low normalized chargeability values. There is no clearly delineated corresponding zone of resistivity, because in this part of the river, resistivity decreases very rapidly in depth. In addition, a kink is present in resistivity profiles, where this low M and MN zone occurs. These low (normalized) chargeability values can indicate a low clay content along this right border. Another explanation could be loosely packed sand with, accordingly, a high porosity. Rapidly decreasing resistivity can indicate a sharp contrast between highly resistive sands, due to pore volume reduction, at the riverbed surface and increasing clay or more loosely packed sand below it. These suggested explanations are however not well in correspondence with what is observed from drilled riverbed material. Sediment near the right bank is composed of sticky sand with quite some organic matter and clay. Penetration with the riverbed auger is also difficult, which would indicate closely packed sand, in contrast to the earlier suggested loose sands. Possibly, the kink in the resistivity profiles indicates an artificial structure made at this border on top of the original riverbed. Another explanation could be seepage of groundwater to the river, through the riverbed. Relatively higher salinity and temperature of groundwater with respect to river water, lowers M and MN and can possibly compensate for the increasing effect of the presence of clay. Upward migration of groundwater could also explain increasing resistivity towards the riverbed surface. The effect of groundwater seeps to riverbed resistivity is also discussed by Nyquist et al. (2008).

A zone of approximately 1 m x 1 m at the left bank has high resistivity (> 145 Ωm), but low to intermediate chargeability (45 – 55 mV/V) and low normalized chargeability values (0.25 – 0.35 mS/m). This contrast in resistivity and normalized chargeability could again be an indication of differences in clay content with the surrounding areas. However, this is not in correspondence with riverbed drillings, from which black, sticky sands with a lot of OM and clay are recovered in this part of the river. Therefore, another factor should be considered. Possibly, organic material and clay decrease the pore volume between sediments. Consequently, less water is present and resistivity is higher. But also higher values for chargeability and normalized chargeability would be expected in this case. An additional explanation for low to intermediate chargeability could be the upward flux of groundwater towards the river. Higher salinity and temperature of groundwater with respect to river water in winter can yield lower chargeability at these locations. On the other hand, this factor would also decrease resistivity. Probably, several factors compensate or interact, not leading to one straightforward explanation.

Also other zones with high resistivities occur at the riverbed surface until a depth of approximately 1 m. These zones are situated in the middle part of the river and show some correspondence with zones of relatively lower MN, but do not show correspondence with M. A low clay content, typically observed in the middle of the river, can explain high resistivity and low normalized chargeability. In addition, more sandy material could allow surface water infiltration in this upper part of the riverbed. Because surface water has a lower salinity and temperature than groundwater in winter, resistivity of pore water in these zones will be higher than in zones with no river water infiltration and a lot of clay or organic matter. This confirms observations of strikingly high resistivity values in zones at the riverbed surface. Because these distinct factors (i.e. low clay content and low pore water salinity and temperature) have contrasting effects on chargeability, their influences are possibly compensated, making these zones not distinguishable in chargeability profiles (Figure 25).

Patches of high resistivity at the riverbed surface continue in a large zone between 0.5 m – 1.5 m depth with relatively high ρ values (120 – 145 Ωm) and intermediate M (35 – 55 mV/V) and MN values (0.35 – 0.60 mS/m). These zones are rather homogeneous and connect superficial structures at intermediate

depth. Clay decreasing the pore volume can explain high resistivity values. The amount is not supposed to be large, because values of chargeability and normalized chargeability are not strikingly high. In addition, compacted sand could explain high resistivity. In this case, intermediate chargeability and normalized chargeability values are only possible if clay content is limited. This is because small pore volume would increase M, so few clay should decrease its value again. Therefore, this zone at intermediate depth is possibly a sand layer with some or few clay content on top of more and more clayey material.

Moreover, one must be aware that sediments in the direction perpendicular to ERT & IP profiles may also influence resistivity, chargeability and normalized chargeability. However, as described by Gommers (2017), comparison of 2D and 3D inversions in this river section show that influence of the third direction is limited.

Overall, considering extracted data in the upper 1 m of the riverbed, spatial distributions of M and MN (Figure 28 & Figure 29) show that the right part of the river section has low M and MN values, corresponding to somewhat more sandy material than in the left and middle part of the river, where values are higher, representing slightly more clay and OM. Possibly, the morphology of the river at the location of the field site can explain this pattern. The right part is situated in the outer bend of a weak meander and therefore, higher flow velocities can occur at this side of the river, depositing coarser particles than in the inner bend. Consequently, fine particles accumulate at the left side of this river section, where flow velocities are relatively lower. However, spatial distribution of resistivity (Figure 27) is not completely in correspondence with patterns of chargeability and normalized chargeability. This could be explained by the double effect of clay on resistivity. Locations which are similar to M and MN are mainly affected by the effect of decreasing pore volume due to infill of fine particles. On the other hand, deviating locations, for example where resistivity is low, while M and MN are high, indicate that the effect of the EDL of clay is more dominant. Another suggested explanation for low resistivity in large part of the right half and high resistivity in large part of the left half of the river, is the effect of river and groundwater interaction in the riverbed. Areas where low resistivity is present, pores are filled with more conductive water, more specifically groundwater. Groundwater generally has a higher temperature and salinity, resulting in a higher conductivity of this fluid. In contrast, areas where high resistivity is present, surface water has an important contribution in the pore fluid. Because flow velocity is slower at the left side of the river than at the right side, river water has more time to infiltrate in the riverbed and can be more dominating in river – groundwater interaction within this part of the riverbed, while the opposite is true at the right side of the river.

Variograms of chargeability and resistivity (Figure 30 & Figure 32) show that ranges of variograms perpendicular to the river are larger than ranges of variograms parallel to the river. In addition, for all variograms of the geo-electrical parameters, Gaussian models fit better to variograms in perpendicular direction than spherical models. This indicates data smoothly varying with distance. This is a consequence of smoothing within ERT and IP profiles. The smoothing constraint in inversions avoids large contrasts of geo-electrical values in a specific profile. Points perpendicular to the river originate from points within the same ERT or IP profile and are thus inherently related to each other. Separate profiles, by contrast, are not directly related to each other and are therefore more independent. Still, one must be aware of uncertainty in variograms. Variograms of resistivity are for example rather ambiguous and their high nuggets could indicate heterogeneity at a smaller scale than the measurement scale. Variograms with obvious model fits can be considered reliable and acceptable for comparison.

Directional variograms of normalized chargeability have larger ranges in the direction parallel to the river than perpendicular to the river. This is because sedimentological processes operate in the direction of the stream, resulting in a longitudinal organization of sediments. For example, clay and organic matter accumulation along the borders is much longer in the direction of the stream than its width perpendicular to the borders (Figure 65).

4.3. COMPARISON OF HYDRAULIC CONDUCTIVITY, RESISTIVITY, CHARGEABILITY AND NORMALIZED CHARGEABILITY

4.3.1. COMPARISON OF DATA EXTRACTION METHODS

Different methods of data extraction from ERT and IP profiles are compared in sections 3.4.1 – 3.4.4. The methods are explained in section 2.6 and visualized in Figure 12. With method 1, individual points are extracted without averaging any of the values. This results in a simplification of the slug test depth intervals and in a simplification of ERT and IP model results. One point value in an ERT or IP profile cannot be considered as the real, exact value at that location. It is the model that provides an approximation of reality showing how geo-electrical properties are distributed in the riverbed. In addition, smoothing in the inversion weakens sharp contrasts. Furthermore, such local point locations are very sensitive to errors in GPS coordinates or calculated ERT coordinates. On the other hand, two depth intervals can be considered and compared, resulting in more data points. But in general, method 1 results in data which is very localized and therefore not in agreement with the scale of the measurements.

Method 2 uses five points to average values of resistivity, chargeability and normalized chargeability. These points are separated at a distance which is comparable to the influential area of slug tests. However, the area over which values are averaged are still not in the scale of ERT & IP measurements. In addition, little points are used to average values, which make resulting ρ, M and MN values still not representative. Although two separate depth intervals are considered, the ρ, M or MN value of the central point in the shallow depth interval is also used in the calculation of the value in the deep depth interval and vice versa (Figure 12 B). There is consequently interference of values of the two depth intervals.

Averaging in a window with a length of 1.50 m around the central point takes the influential area of ERT and IP measurements into account. This is the case for method 3 and 4. Because the length and height of the influential area varies with distance between the electrodes, these dimensions can be too small, or for the height it can also be too large. Because the height of the window incorporates completely the two depth intervals of slug tests, hydraulic conductivity is averaged over these intervals.

Results of less iterations in the inversions are used in method 4, with the same data extraction method as method 3. This has as an advantage that artificial artefacts are not enlarged. On the other hand, natural contrasts are smoothed exaggeratedly.

The method providing the most expressed correlations was found to be the third method, with use of the harmonic average of K. This is because smoothed resistivity, chargeability or normalized chargeability are averaged over a wide range which corresponds to the influential area of their measurement. If too few points are considered, such as in method 1 and 2, point data are less representative for the true value. In addition, more iterations provide more detail and more correspondence between the model based apparent resistivity and the measured apparent resistivity and is consequently closer to reality. The reason why the harmonic average of K, and not the geometric or arithmetic average, is most in correspondence with geo-electrical parameters is because low hydraulic conductivity values strongly influence vertical flow through the riverbed. The harmonic average is therefore most representative on the larger scale of the combined depth intervals. An extra reason why the second method is less effective than the other methods is the overlapping of values for calculation of geo-electrical parameter values between the two depth intervals. A suggested improvement is to average K values in combination with this dimension of the square window, instead of considering the two separate depths. This can be interesting as a better test of correlation on the scale of slug tests.

4.3.2. CORRELATION BETWEEN HYDRAULIC CONDUCTIVITY, RESISTIVITY, CHARGEABILITY AND NORMALIZED CHARGEABILITY

A link between hydraulic conductivity and geo-electrical parameters is investigated and a general trend is identified. An inverse correlation exists between hydraulic conductivity and chargeability, normalized chargeability and resistivity. This means that, where high values of K occur, values of M, MN or ρ are low and where K is low, geo-electrical parameters show high values. This tendency is observed in the spatial distribution of point data, as well as in continuous maps, obtained with kriging. Scatterplots show decreasing trends and linear models fitted to these, have significant negative slopes. However, linear regressions, given in sections 3.4.1.3, 3.4.2.3 and 3.4.3.3, cannot serve as predictive models. There is too much scatter for that purpose.

Factors influencing the different parameters are important in the understanding of mutual relations. These factors and theoretically expected correlations are described in section 2.9. Moreover, observed sediment lithologies in the riverbed are crucial indicators for these correlations. Overall, the dominant lithology in the riverbed is medium to fine grained sand. Near the borders at the riverbed surface, sand is intermingled with organic matter and clay, resulting in black and sticky sands. To explain the theory of expected correlations (section 2.9) with results in this study, patterns observed in clusters identified with visual comparison between K and M/MN (section 3.4.7.1) are explained. Data points and clusters are visualized in Figure 58.

In the first cluster in the left downstream quarter of the river section, hydraulic conductivity is low. This can be explained by the increased clay and organic matter content along this border, both because of proximity of plants from the border and because of deposition of fine particles in the inner bend of a weak meander. In addition, the higher the clay content, the more chargeable the sediment. Chargeability and normalized chargeability are consequently high in this cluster. Resistivity is also mostly high, with few exceptions. Decreased pore volume because of fine particles filling the pores, leads to a lower water content and thus higher resistivities. In contrast, the effect of the EDL, associated with clay and OM, is of minor influence on resistivity in this cluster.

The second cluster is situated in the right downstream quarter of the reach. Loose, medium grained sand with few, but variable organic matter and clay content result in high values of hydraulic conductivity. Lower OM and clay content in comparison with the sections close to the border, result in low values for chargeability and normalized chargeability. Values of resistivity are variable: both low and high values occur in cluster 2. Low values can be explained by increased porosity in more uniform sands. Points with high resistivity possibly indicate zones which are relatively more compacted, or where there is influence of river water. River water has a lower salinity and temperature than ground water in winter, and a deviation of the dominant water type in sediments can result in changing resistivities. This effect is also discussed by Nyquist et al. (2008). They stated that surface water infiltration increases resistivity in the top layer of the riverbed. The third cluster, situated in the right upstream part, shows the same correlations as the second cluster.

Correlations observed in the fourth cluster are the same as the first cluster, for points along the left bank. In the middle of the cluster, situated in the left upstream part of the river, intermediate K values correspond to intermediate M values, high MN and low ρ values. No drillings have been performed in this section of the river, but based on intermediate K and M values, some clay and organic matter are supposed to be intermingled with sand. High values of normalized chargeability and low values of resistivity reveal that clay indeed has an increased influence in this part of the river. Possibly, compaction is limited, resulting in an increased pore volume and clay particles less blocking pore connections.

The same inverse correlations are present between clusters obtained by the other clustering methods described in sections 3.4.7.2 and 3.4.7.3. The inverse relation between hydraulic conductivity and chargeability, normalized chargeability and resistivity can serve as a tool to identify or define zones of expected low or high hydraulic conductivity where no measurements of K are present, but geophysical methods can be performed (Slater, 2007; Weller et al., 2015). However, prediction of values or ranges

of values is not possible, although relative changes in patterns can be detected, when other factors such as lithology are considered. Therefore, drilling in the riverbed is important. A perfect relation between hydraulic conductivity and geo-electrical parameters is not realistic because of approximations in inversions: ERT and IP inversions are smoothed, there is influence of the third direction in 2D profiles and values of thick layers can influence values and thicknesses of thin layers in the model. Also other factors, which are not discussed can affect K, ρ, M and MN (Slater, 2007), e.g. roughness of the internal surface (Weller et al., 2015), pore throat diameters (Titov et al., 2010), etc.

A curious observation along the right bank is hard sediment between wooden poles at 1 or 2 m from the bank and the bank itself. Slug test measurements are not possible in this part of the river, except for one measurement in profile 5. Even measurements in the deep interval at point locations at a few meters away from the poles, are sometimes impossible. From drillings and an aerial photograph in Figure 65, black sands with some organic matter and a lot of clay are expected along this bank, leading to low hydraulic conductivity values. In addition, profiles of resistivity (Figure 24) show a kink structure with high values, fast decreasing to low values in depth. This kink structure is not visible in profiles of chargeability (Figure 25) and normalized chargeability (Figure 26). In these profiles, an elongated zone with low values of M and MN is present. Low M and MN values are not in correspondence with the observed and expected clayey sands. Possibly, there is an artificial influence in this part of the river, such as a wooden platform, installed on the riverbed sediment. This could possibly explain observed high, and rapidly decreasing, resistivity and low chargeability and normalized chargeability values, as well as impossible penetration of the piezometer in this part of the river section.

4.3.3. COMPARISON OF VARIOGRAMS AND CLUSTERING METHODS

Comparison of variograms of hydraulic conductivity and geo-electrical parameters reveal that most similarities in ranges exist between hydraulic conductivity and chargeability and normalized chargeability. Ranges of resistivity are mostly larger and Gaussian models, instead of spherical models, fit to the data. This can be explained again by the influencing factors of the parameters. Resistivity is dependent on pore volume and electrical surface properties, while the other parameters are strongly dependent on only interconnected pore surface area. Different determining factors for resistivity can possibly compensate for one another, resulting in larger influencing distances and more smoothly varying data. Next, it is found that most ranges of geo-electrical properties are larger than those of hydraulic conductivity. This could be because of less obstacles for electrical current or charge accumulation in the medium than for water flow through the pores. In addition, smoothing in the inversion of ERT and IP profiles spreads out heterogeneity.

Visual and quantitative clustering methods are applied on the dataset of hydraulic conductivity, resistivity, chargeability and normalized chargeability and are described in section 3.4.7. Visual clustering is based on spatial correspondence between parameters. Different types of clustering are possible, dependent on the focus of the researcher. Therefore, it is a subjective method. On the other hand, clusters are constructed as continuous zones in space and it gives a first idea of patterns that exist in the dataset. Although visual clustering is subjective, variability of hydraulic conductivity is low in two of the four clusters of both visual clustering methods.

A quantitative way of clustering is made with cluster analysis. This method groups points which are most closely related based on their value, without consideration of their location in space. Advantages are the fact that this method is objective and that variability of all variables in the dataset is minimized. This results in a low variance of K in all clusters delineated with CA. On the other hand, clusters are less continuous in space. Cluster 4 of the CA is, for example, composed of individual points which are not neighboring at all (Figure 64). Moreover, some points are not closely related to a cluster. Nevertheless, cluster 1, 2 and 3 are spatially continuous, except for a few points. Two of these clusters are longitudinally oriented, which can be explained by sedimentological processes which dominantly operate in the direction of flow. This directional preference of cluster orientation is also the case for clusters 2 and 3 of the visual clustering method based on K – ρ correlation. In addition, this stronger

spatial dependence in the direction parallel to the stream in comparison with the perpendicular direction is confirmed in variograms of hydraulic conductivity and normalized chargeability.

4.4 RECOMMENDATIONS

When similar surveys or studies will be performed, it is important to consider some points of particular attention. In this section, recommendations and remarks are suggested based on experiences in this study, in order to improve the setup, analyses and comparison methods of analogous research projects.

First, different measurement surveys (here slug tests, ERT, IP and drilling) are recommended to be performed in the same period. If there is time in between measurements, several processes or interventions can occur, which influence the river. For example, incisive and sedimentation processes can result in changes in the spatial grain size distribution and consequently, hydraulic conductivity distribution of the river section, as well as riverbed topography (Sebok et al., 2014). Changes in landscape conditions or human interventions can also have an impact on the river and its characteristics. Examples of human interaction are dumping of sediment from construction sites, changes in the water level and discharge of the river due to opening or closing of the weirs, up- and downstream (Figure 66). This latter can strongly influence sedimentological processes. In addition, changes in water level between two measurement periods of different surveys, make connection of profiles more troublesome afterwards. It changes the width of the river and, consequently, the length of the profiles. If the site of investigation is not in a straight section of the river, these changes in profile lengths are asymmetric.

Second, it is important to measure GPS coordinates in every survey. This makes linkages of profiles and data, and the error on coordinates more accurate. Certainly, for studies on a very local scale, this is an essential criterium.

Next, drilling at several locations of the study site is necessary and if possible, to the depth of influence of the applied methods. This is important to have lithological references for ERT and IP, to make their interpretation meaningful. In addition, laboratory tests can enhance knowledge on lithologies in the study site.

Further, it is important to compare data at the same scale. Therefore, averages have been considered to obtain data which are representative with respect to the influential area of the measurement methods. This is, however, not straightforward because slug tests and ERT or IP setups have different scales of influence, which are moreover not accurately known, and depend on the specific locality. On the one hand, the slug test radius is dependent on the sediment: clay leads to a small influential radius, while sand allows influence from a further distance. On the other hand, the influential zone of ERT and IP is dependent on the distance between electrodes, operational in each measurement. This is, nonetheless, different for most measurements in one profile, so a trade off for averaging should be taken for data extraction. Another issue is smoothing involved in ERT and IP inversions. This fades heterogeneity, while slug tests are very local measurements with the purpose of showing heterogeneity in the riverbed.

Another problem that was encountered in this study, is that the two depth intervals of the slug test measurements are not resolvable within the influential area of one ERT or IP measurement. If correlations at different depths want to be investigated or imaged, another method for K determination is recommended, to reach depths of more than 1 m, or the spacing between electrodes can be reduced.

It is important to keep in mind that comparisons between hydraulic conductivity and electrical properties of the subsurface are local and dependent on circumstances in the study site itself. Correlations that are made in this study are indicative, but not predictive. In combination with other complementary data, they can serve as input for further, more complex research projects. For example, characterization of zones based on similarities in patterns of K, ρ, M and MN can be used as training images in multiple point statistics. Other applications could be the integration of hydraulic conductivity as a constraint in the inversion process of ERT and IP profiles.

5. Conclusion

Characterization of spatial heterogeneity of hydraulic conductivity (K) in a riverbed is investigated with use of electrical resistivity tomography (ERT) an induced polarization (IP). These two geophysical methods use electrical current to map electrical properties of the subsurface. ERT provides resistivity (ρ) profiles, IP provides chargeability (M) profiles and both methods combined result in profiles of normalized chargeability (MN). Heterogeneity of hydraulic conductivity in riverbeds is currently of special interest in hydrogeological research, because it determines river – groundwater interaction. It is therefore important to improve our understanding in this phenomenon and to increase accuracy of groundwater models. Because resistivity, chargeability and normalized chargeability are determined by similar factors which influence hydraulic conductivity, the hypothesis of correlation between these parameters is investigated. Previous research on a link between hydraulic conductivity and geo-electrical properties has been performed, but with different focusses than in this study. For example, a link was sought on the scale of an aquifer and on land (Attwa & Günther, 2013; Slater, 2007), while this research project focused on a local scale of a riverbed. Spectral IP or ERT have been used separately in studies to find correlation with K (Attwa & Günther, 2013; Salako & Adepelumi, 2016), but combined interpretation of resistivity, chargeability and normalized chargeability in relation with hydraulic conductivity is not yet performed.

Therefore, the aim of this dissertation was to investigate correlation between hydraulic conductivity and resistivity, chargeability and normalized chargeability. Trends or patterns were explored in collected data, as well as spatial correspondence or similarities between hydraulic conductivity and geo-electrical parameters. If correlation was detected, it was investigated if predictive relations exist. In other words, the possibility to replace and/or complement conventional methods of K determination by ERT and/or IP, was examined.

The study site to investigate these objectives, is a section of 25 m x 15 m in the Aa river in Belgium. This river is a typical lowland river, which flows through the province of Antwerp. The water level fluctuates between 20 – 70 cm high above the riverbed. Measurements of hydraulic conductivity are performed with slug tests and analysis is based on the Bouwer and Rice (1976) method. Slug tests are performed at two depth intervals in the riverbed: between 20 – 45 cm and between 45 – 70 cm depth. ERT and IP measurements on the same profiles result, after inversions, in profiles of resistivity, chargeability and normalized chargeability (i.e. M/ρ), up to 2.5 m deep. Riverbed drillings are performed to obtain information on the lithology of the riverbed up to a depth of 50 cm. Comparison of the parameters under consideration is based on visual inspection to find intuitive patterns, on statistics and geostatistics.

Results of the different methods should be compared on a similar scale to make their interpretation meaningful. The influential area of ERT and IP is determined by the electrode configuration. Because a spacing of 0.5 m between the electrodes is applied, the length of the influential area, which is perpendicular to the flow direction, is at least 1.5 m. The height of influence is not exactly known and is variable. Also the third direction, parallel to the stream has an influence, but is assumed to be constant in the inversions. On the other hand, slug tests are measured at two depth intervals of each 25 cm, but to match scales, these separate depth measurements are harmonically averaged. The height of the influential area of slug tests is, in this way, enlarged to 50 cm, but the slug test radius is unknown. A suggested estimate is 1.5 m, according to Ramey et al. (1975). Averaging of ρ, M and MN in a window of 1.5 m long and < 1.5 m high, overlain on the profiles, delivers values which can be compared to harmonically averaged K values in a relevant way.

Data of hydraulic conductivity, resistivity, chargeability and normalized chargeability are compared at several levels. First, spatial patterns are investigated using point maps and maps interpolated by ordinary kriging. Next, trends in scatterplots are examined and their significance is assessed by linear regressions. Further, variograms are used to explore the distance of spatial influence of all parameters. In addition, clusters in the data of the studied river section are determined based on visual comparison

or PCA and CA. The latter minimizes variability of K (and the other parameters) within clusters, but clusters are less spatially continuous than visually delineated clusters.

Overall, it is found that the strongest correlation is present between hydraulic conductivity and chargeability. There is also clear correlation between hydraulic conductivity and normalized chargeability. Significant correlation between K and resistivity also exists, although it is less expressed than for M and MN. Correlation between hydraulic conductivity and geo-electrical parameters in the riverbed is inverse. This means that high values of K correspond to low values of M, MN or ρ and vice versa. For resistivity, some areas in a few, particular clusters show a positive correlation with K. However, these detected relationships are indicative, and not predictive. Linear regressions between K and M, K and MN or K and ρ are significant, but too much scatter inhibits their predictive function.

The reason why chargeability and normalized chargeability are more closely related to hydraulic conductivity than resistivity is, is because chargeability and normalized chargeability are determined by similar factors which determine hydraulic conductivity. M, MN and K are determined by interconnected pore surface area. Concretely, this means that M and MN are determined by surface conductivity and specific surface area of minerals in the medium. The electrical double layer (EDL) of clay minerals is the most important area to store electrical energy, in other words to charge sediments. The higher the amount of clay or organic matter (OM) in the riverbed, the higher chargeability or normalized chargeability. Also porosity can play a role. The higher the porosity, the more water can be present in the pores, the lower M because water is not chargeable. Resistivity, on the other hand, is also dependent on clay content. The EDL of clay minerals provide easy pathways for electrical current, which decrease resistivity. However, porosity and properties of pore water also have an important influence on resistivity. The higher the porosity, the more water is present in the medium, the higher conductivity and lower resistivity. In addition, salinity and temperature of pore water can influence resistivity, as well as chargeability. Nonetheless, fine particles of clay or OM can decrease pore volume, leading to higher resistivity. This contrasts with the effect of the EDL which decreases resistivity. Therefore, the effect of the EDL of clay is the dominant effect in clay or silt environments, while the effect of porosity is dominant in sandy environments (Purvance & Andricevic, 2000). For hydraulic conductivity, clay content and fine organic material are major factors determining the value of K. These materials can block pore connections and in this way, hamper water flow through pores. Altogether, a high clay or OM content, results in low K values, high M or MN values and low ρ, if clay is very dominant, or high ρ, if the pore volume decrease is dominating. Moreover, compaction of sandy material leads to decreased porosity and therefore, decreased K, increased M and MN, as well as increased ρ. Because resistivity has other dependencies than M, MN and K, compensation of their influences can occur, resulting in a relation with K which is not straightforward.

Patterns in the river section of all considered parameters, i.e. K, ρ, M and MN, are mainly determined by the presence of clay and organic material near the borders of the sandy riverbed and by the absence of these fine particles in the middle of the river. This is explained by the difference in flow velocity between the middle and sides of the river, influenced by plants at the borders. A broader area of low hydraulic conductivity in the left part of the river section in comparison with the right part, can be explained by the situation of the study site in a weak bend. The right bank is situated in the outer bend, where incision occurs, evidenced by wooden poles at a distance from the bank. Deposition of finer particles occurs more in the left half of the river, because of typically lower flow velocities in the inner bend. This pattern of incision and deposition is also visible in riverbed topography, which shows steep sides at the right side of the reach and flatter sides at the left side. Moreover, the Aa river is strongly influenced by human intervention. For example, the river was straightened in the 1960's, wooden poles are planted along the right bank, the water level and discharges of the river are regulated by weirs up- and downstream, etc. Therefore, it is recommended to execute surveys in the same period of time. This avoids changes in the river, either natural or artificial. It is also important to obtain the same representative volume when several methods are applied.

A suggestion for further work is to compare resistivity, chargeability and normalized chargeability from ERT and IP measurements with vertical hydraulic conductivity. In this study, comparison only focused on horizontal hydraulic conductivity. With use of standpipe tests, vertical hydraulic conductivity can be obtained and serve as an input for comparative analyses with ERT and IP parameters. In addition, other geophysical methods are suggested to be tested in their correlation with hydraulic conductivity. For example, electromagnetic induction can provide mapped surfaces of conductivity at shallow levels in the riverbed. Since conductivity is the inverse of resistivity, positive correlation with hydraulic conductivity is expected, to a similar extent as the obtained correlation of hydraulic conductivity and resistivity.

It can be concluded that chargeability, normalized chargeability and resistivity can help in characterization of hydraulic conductivity in riverbeds, but ERT and IP cannot replace conventional methods of K determination, such as slug tests. This is because correlation is shown not to be predictive and is only locally applicable for this study area. However, detected relations are interesting to incorporate in more complex, geostatistical analyses and models, in addition to other input data, to improve insight in spatial heterogeneity in a specific area.

6. References

ABEM Instrument AB (2012). Instruction Manual Terrameter LS. Sundbyberg, Sweden. 122p.

al Hagrey, S. A., & Michaelsen, J. (1999). Resistivity and percolation study of preferential flow in vadose zone at Bokhorst, Germany. *Geophysics, 64* (3), 746–753, doi:10.1190/1.1444584.

Alyamani, M.S., & Sen, Z. (1993). Determination of hydraulic conductivity from complete grain-size distribution curves. *Ground water, 31* (4), 551-555.

Amaya, A. G., Dahlin, T., Barmen, G. & Rosberg, J-E (2016). Electrical Resistivity Tomography and Induced Polarization for Mapping of the Subsurface of Alluvial Fans: A Case Study in Punata (Bolivia). *Geosciences, 6*, 51.

Anibas, C., Buis, K., Verhoeven, R., Meire, P., & Batelaan, O. (2011). A simple thermal mapping method for seasonal spatial patterns of groundwater – surface water interaction. *Journal of Hydrology*, *397*(1–2), 93–104. https://doi.org/10.1016/j.jhydrol.2010.11.036

Anibas, C., Fleckenstein, J. H., Volze, N., Buis, K., Verhoeven, R., Meire, P., & Batelaan, O. (2009). Transient or steady-state ? Using vertical temperature profiles to quantify groundwater – surface water exchange, *2177*, 2165–2177. https://doi.org/10.1002/hyp

Anibas, C., Schneidewind, U., Vandersteen, G., & Joris, I. (2016). From streambed temperature measurements to spatial- temporal flux quanti fi cation : using the LPML method to study groundwater – surface water interaction, *216*, 203–216. https://doi.org/10.1002/hyp.10588

Archie, G.E. (1942). The electrical resistivity log as an aid in determining some reservoir characteristics. *Trans Am. Inst. Min. Metal. and Petr. Eng*., *146*, 54-62.

Attwa, M., & Günther, T. (2013). Spectral induced polarization measurements for predicting the hydraulic conductivity in sandy aquifers. *Hydrology and Earth System Sciences*, *17*(10), 4079–4094. https://doi.org/10.5194/hess-17-4079-2013

Bal, K. & Meire, P. (2009). The influence of macrophyte cutting on the hydraulic resistance of Lowland Rivers. *Journal of Aquatic Plant Management, 47*, 65–68.

Barker, J.A. & Black, J.H. (1983). Slug tests in fissured aquifers. *Water Resources Research 19 (6),* 1558-1564.

Beyer, W. (1964). Zur Bestimmung der Wasserdurchlässigkeit von Kiesen und Sanden aus der Kornverteilungskurve. *Wasserwirtschaft Wassertechnik 14* (6), 165–168.

Binley, A., Slater, L., Fukes, M., and Cassiani, G. (2005). Relationship between spectral induced polarization and hydraulic properties of saturated and unsaturated sandstone. *Water Resour. Res., 41*, W12417, doi:10.1029/2005WR004202.

Binley, A., Winship, P., West, L. J., Pokar, M. & Middleton, R. (2002). Seasonal variation of moisture content in unsaturated sandstone inferred from borehole radar and resistivity profiles. *J. Hydrol., 267*, 160– 172, doi:10.1016/S0022-1694(02)00147-6.

Binley, A., Ullah, S., Heathwaite, A. L., Heppell, C., Byrne, P., Lansdown, K., … Zhang, H. (2013). Revealing the spatial variability of water fluxes at the groundwater-surface water interface, *49*, 3978–3992. https://doi.org/10.1002/wrcr.20214

Börner, F. D., Schopper, W., and Weller, A. (1996). Evaluation of transport and storage properties in the soils and groundwater zone from induced polarization measurements. *Geophys. Prosp., 44,* 583–601, doi:10.1111/j.1365-2478.1996.tb00167.x.

Boulton, A., Findlay, S., Marmonier, P., Stanley, E., & Valett, H. (1998). The functional significance of the hyporheic zone in streams and rivers. *Annu. Rev. Ecol. Syst., 29*, 59–81.

Bouwer, H. & Rice, R.C. (1976). A slug test for determining hydraulic conductivity of unconfined aquifers with completely or partially penetrating wells*. Water Resources Research, 12*, 423-428.

Butler, J. J. (1996). Slug Tests in Site Characterization: Some Practical Considerations. *Environmental Geosciences*, *3*(3), 154–163.

Butler, J. J. (1998). The design, performance, and analysis of slug tests. *Lewis Publishers*, New York, 252 p.

Butler Jr., J.J., Zlotnik, V.A. & Tsou, M.S. (2001). Drawdown and stream depletion produced by pumping in the vicinity of a finite width stream of shallow penetration. *Ground Water, 39* (5), 651 – 659.

Calver, A. (2001). Riverbed Permeabilities: Information from Pooled Data. *Ground water, 39* (4), 546 – 553.

Cardenas, M. B., & Zlotnik, V. A. (2003). Three-dimensional model of modern channel bend deposits, *39*(6), 1–13. https://doi.org/10.1029/2002WR001383

Cardenas, M. B., Zlotnikz, V., & A. (2003). Three-dimensional model of modern channel bend deposits. *Water Resources Research*, *39*(6), 1–13. https://doi.org/10.1029/2002WR001383

Chambers, J. M. (1992). Chapter 4: Linear models. In: Chambers, J.M. & Hastie, T.J. Statistical Models in S, Wadsworth & Brooks/Cole.

Chen, X. (2005). Statistical and geostatistical features of streambed hydraulic conductivities in the Platte River , Nebraska, (7), 693–701. https://doi.org/10.1007/s00254-005-0007-1

Chen, X., Burbach, M., & Cheng, C. (2008). Electrical and hydraulic vertical variability in channel sediments and its effects on streamflow depletion due to groundwater extraction, 250–266. https://doi.org/10.1016/j.jhydrol.2008.01.004

Chen, X., & Chen, X. (2003). Stream water infiltration , bank storage , and storage zone changes due to stream-stage fluctuations, *280*, 246–264. https://doi.org/10.1016/S0022-1694(03)00232-4

Chou, T.-K., Chouteau, M., & Dubé, J.-S. (2016). Estimation of Saturated Hydraulic Conductivity during Infiltration Test with the Aid of ERT and Level-Set Method. *Vadose Zone Journal*, *15*(7), 0. https://doi.org/10.2136/vzj2015.05.0082

Christensen, N.B. (2000). The electrical resistivity of geological formations. *Aarhus University,* Aarhus, 20p.

Christensen, N.B. & Christiansen, A.V. (2015). Environmental applications of geoelectrical methods. *Aarhus University,* Aarhus, 74p.

Clifford, J., & Binley, A. (2010). Geophysical characterization of riverbed hydrostratigraphy using electrical resistance tomography, 493–501. https://doi.org/10.3997/1873-0604.2010035

Crestani, E., Camporese, M., & Salandin, P. (2015). Assessment of hydraulic conductivity distributions through assimilation of travel time data from ERT-monitored tracer tests. *Advances in Water Resources*, *84*(January 2016), 23–36. https://doi.org/10.1016/j.advwatres.2015.07.022

Crook, N., Binley, A., Knight, R., Robinson, D. A., Zarnetske, J., & Haggerty, R. (2008). Electrical resistivity imaging of the architecture of substream sediments, *44*(December), 1–11. https://doi.org/10.1029/2008WR006968

Dahlin, T. (1996). 2D resistivity surveying for environmental and engineering applications. *First Break, 14,* 275-284.

Daily, W., Ramirez, A., LaBrecque, D. & Nitao, J. (1992). Electrical resistivity tomography of vadose water movement. *Water Resour. Res., 28*, 1429– 1442, doi:10.1029/91WR03087.

deGroot-Hedlin, C. & Constable, S. (1990). Occam's inversion to generate smooth, two-dimensional models form magnetotelluric data. Geophysics, *55*, 1613-1624.

Di Maio, R., Piegari, E., Todero, G., & Fabbrocino, S. (2014). A combined use of Archie and van Genuchten models for predicting hydraulic conductivity of unsaturated pyroclastic soils. *Journal of Applied Geophysics*, *112*, 249–255. https://doi.org/10.1016/j.jappgeo.2014.12.002

Doetsch, J. (2016). Electrical Resistivity Tomography (ERT): Measurement Principles. *Exploration and Environmental Geophysics, ETH Zurich*, 8p.

DOV (2010). Databank Ondergrond Vlaanderen. Database Subsurface of Flanders. https://dov.vlaanderen.be/.

DOV (2016). Databank Ondergrond Vlaanderen. Database Subsurface of Flanders. https://dov.vlaanderen.be/.

Edwards, L. (1977). A modified pseudosection for resistivity and IP. *Geophysics, 42*, 1020–1036. doi:10.1190/1.1440762

Elliott, A. H. & Brooks, N. H. (1997). Transfer of nonsorbing solutes to a streambed with bed forms: Theory. *Water Resour. Res., 33* (1), 123–136.

Everitt, B. (1974). Cluster Analysis. *Heinemann Educ. Books.*, London.

Fadl, A.E. (1979). A modified permeameter for measuring hydraulic conductivity of soils. *Soil Science, 128* (2), 126-128.

Farzamian, M., Monteiro Santos, F. A., & Khalil, M. A. (2015a). Application of EM38 and ERT methods in estimation of saturated hydraulic conductivity in unsaturated soil. *Journal of Applied Geophysics*, *112*, 175–189. https://doi.org/10.1016/j.jappgeo.2014.11.016

Farzamian, M., Monteiro Santos, F. A., & Khalil, M. A. (2015b). Estimation of unsaturated hydraulic parameters in sandstone using electrical resistivity tomography under a water injection test. *Journal of Applied Geophysics*, *121*, 71–83. https://doi.org/10.1016/j.jappgeo.2015.07.014

Finsterle S. & Kowalsky, M.B. (2008). Joint hydrological-geophysical inversion for soil structure identification. *Water Resour Res, 7*:287–93. http://dx.doi.org/10.2136/ vzj2006.0078.

Gelhar, L. W. (1993). Stochastic Subsurface Hydrology. *Prentice-Hall, Old Tappan, N. J.,* 390p.

Genereux, D. P., Leahy, S., Mitasova, H., Kennedy, C. D., & Corbett, D. R. (2008). Spatial and temporal variability of streambed hydraulic conductivity in West Bear Creek, North Carolina, USA. *Journal of Hydrology*, *358*(3–4), 332–353. https://doi.org/10.1016/j.jhydrol.2008.06.017

Geopunt (2017). Luchtfoto Vlaanderen, winter 2013 – 2015 – kleur, www.geopunt.be

Ghysels, G., Anibas, C., Mutua, S., Huysmans, M. (2016). Modeling the influence of riverbed heterogeneity on river-aquifer exchange fluxes using multiple-point statistics. *GeoENV, Lisbon*.

Gommers, K. (2017). Design and assessment of ERT and IP setup in rivers: numerical and field experiments. *Not published Master's thesis,* KU Leuven, 70p.

Groetsch, C.W. (1999). Inverse Problems: Activities for Undergraduates. *Cambridge University Press*. 234 p.

Hartmann, R., Michiels, P., Gabriëls, D. & De Stooper, E. (1988). Field monitoring of surface and subsurface runoff on a slope in a loamy region. *Soil Technology, 1 (2),* 175-180.

Hayley, K., Bentley, L.R., Gharibi, M., Nightingale, M., (2007). Low temperature dependence of electrical resistivity: implications for near surface geophysical monitoring. *J. Geophys. Res. Lett. 34* L18402.

Hazen, A. (1893). Some physical properties of sands and gravels. *Massachusetts State Board of Health, 24th Annual Report.*

Hördt, A., Blaschek, R., Kemna, A., and Zisser, N. (2007). Hydraulic conductivity estimation from induced polarisation data at the field scale—the Krauthausen case history. *J. Appl. Geophys., 62*, 33–46.

Hunt, B. (1999). Unsteady stream depletion from ground water pumping. *Ground Water, 37* (1), 98–102.

Hutchinson, P. A. & Webster, I. T. (1998). Solute Uptake in Aquatic Sediments due to Current-Obstacle Interactions. *J. Environ. Eng., 124* (5), 419–426.

Hvorslev, M.J. (1951). Time lag and soil permeability in ground-water observations. *U.S. Army Waterways Experiment Station Bulletin, 36*, Vicksburg, Mississippi.

Jadoon K.Z., Slob E., Vanclooster M. & Vereecken H. (2008). Uniqueness and stability analysis of hydrogeophysical inversion for time-lapse ground-penetrating radar esti- mates of shallow soil hydraulic properties. *Water Resour Res, 44*:W09421. http://dx.doi.org/10.1029/2007WR006639.

Kalbus, E., Reinstorf, F., & Schirmer, M. (2006). Measuring methods for groundwater – surface water interactions : a review, 873–887.

Kalbus, E., Schmidt, C., Molson, J. W., Reinstorf, F., & Schirmer, M. (2009). Influence of aquifer and streambed heterogeneity on the distribution of groundwater discharge, 69–77.

Kazakis, N., Vargemezis, G., & Voudouris, K. S. (2016a). Estimation of hydraulic parameters in a complex porous aquifer system using geoelectrical methods. *Science of the Total Environment*, *550*, 742–750. https://doi.org/10.1016/j.scitotenv.2016.01.133

Kazakis, N., Vargemezis, G., & Voudouris, K. S. (2016b). Estimation of hydraulic parameters in a complex porous aquifer system using geoelectrical methods. *Science of the Total Environment*, *550*, 742–750. https://doi.org/10.1016/j.scitotenv.2016.01.133

Kelly, W.E. (1977). Geoelectric sounding for estimation aquifer hydraulic conductivity. *Ground Water 15 (6),* 420–425.

Kennedy C.D., Genereux D.P., Mitasova H., Corbett D.R. & Leahy S. (2008). Effect of sampling density on estimation of streambed attributes. *Journal of Hydrology, 355*, 164–180. DOI: 10.1016/j.jhydrol.2008.03.018.

Kruschwitz, S., Binley, A., Lesmes, D., and Elshenawy, A. (2010). Textural controls on low-frequency spectra of porous media. *Geophysics, 75*, 113–123, doi:10.1190/1.3479835.

Landon, M. K., Rus, D. L. & Harvey, F. E. (2001). Comparison of Instream Methods for Measuring Hydraulic Conductivity in Sandy Streambeds. *Ground Water, 39* (6), 870 – 885.

Loke, M.H. (2015). RES2DINVx64 ver. 4.05 with multi-core and 64-bit support. *Geotomosoft, Malaysia*, 138p.

Loke, M.H., Acworth, I. and Dahlin, T. (2003). A comparison of smooth and blocky inversion methods in 2D electrical imaging surveys. *Exploration Geophysics, 34*, 182-187.

Loke, M. H., Chambers, J. E., Rucker, D. F., Kuras, O., & Wilkinson, P. B. (2013). Recent developments in the direct-current geoelectrical imaging method. *Journal of Applied Geophysics*, *95*, 135–156. https://doi.org/10.1016/j.jappgeo.2013.02.017

Looms M.C., Binley A., Jensen K.H., Nielsen L. & Hansen T.M. (2008). Identifying unsaturated hydraulic parameters using an integrated data fusion approach on cross-borehole geophysical data. *Vadose Zone J, 7* (1), 227–37. http://dx.doi.org/10.2136/vzj2007.0087.

Mardia, K. V., Kent, J.T. and Bibby, J.M. (1979). Multivariate Analysis. *Academic Press*, London.

McDonald, M.G. & Harbaugh, A.W. (1988). MODFLOW, A Modular three dimensional finite-difference groundwater flow model. *U.S. Geological Survey Techniques of Water-Resources Investigation, Book 6* (Chapter A1), 586 pp.

Myers, D. E. (1992). Kriging, cokriging, radial basis functions and the role of positive definiteness. *Computers and Mathematics with Applications*, *24*(12), 139–148. https://doi.org/10.1016/0898-1221(92)90176-I

Nyquist, J. E., Freyer, P. A., & Toran, L. (2008). Stream Bottom Resistivity Tomography to Map Ground Water Discharge, *46*(4), 561–569. https://doi.org/10.1111/j.1745-6584.2008.00432.x

Oldenburg, D.W. & Li, Y. (1999). Estimating depth of investigation in dc resistivity and IP surveys. *Geophysics, 64*, 403-416.

Oliver, M.A. & Webster, R. (1990). Kriging: a method of interpolation for geographical information systems. *International Journal of Geographical Information Science, 4*: 313-332.

Purvance, D.T., Andricevic, R. (2000). On the electrical-hydraulic conductivity correlation in aquifers. *Water Resour Res 36*, 2905–2913.

Ramey Jr., J.J., Agarwal, R.G., Martin, I. (1975). Analysis of 'Slug Test' or DST flow period data. *J. Can. Pet. Technol. 14 (3),* 37–47. http://dx.doi.org/10.2118/ 75-03-04.

Remy, N. (2004). S-GeMS: The Stanford Geostatistical Modeling Software: A Tool for New Algorithms Development. *Geostatistics Ban*, 865-871.

Revil, A. & Florsch, N. (2010). Determination of permeability from spectral induced polarization in granular media. Geophys. J. Int*., 181*, 1480–1498, doi:10.1111/j.1365-246X.2010.04573.x.

Revil, A., Cathles, L.M.I. (1999). Permeability of shaly sands. *Water Resour Res 35(3)*, 651–662.

RStudio Team (2015). RStudio: Integrated Development for R. *RStudio, Inc., Boston*, MA URL http://www.rstudio.com/.

Salako, A. O., & Adepelumi, A. A. (2016). Evaluation of hydraulic conductivity of subsoil using electrical resistivity and ground penetrating radar data: example from Southwestern Nigeria. *International Journal of Geo-Engineering*, *7*(1), 5. https://doi.org/10.1186/s40703-016-0018-7

Sanchez-León, E., Leven, C., Haslauer, C. P., & Cirpka, O. A. (2016). Combining 3D Hydraulic Tomography with Tracer Tests for Improved Transport Characterization. *Groundwater*, *54*(4), 498–507. https://doi.org/10.1111/gwat.12381

Schlichter, C. S. (1905). Field Measurements of the Rate of Movement of Underground Waters. *U.S. Geol. Surv. Water Supply, Paper 140*.

Schön, J.H. (1996). Physical properties of rocks – fundamentals and principles of petrophysics. *Handbook of geophysical exploration: seismic exploration, 18. Pergamon Press*, 583 pp.

Scott, J.B.T., Barker, R.D. (2003). Determining throat size in Permo-Triassic sandstones from low frequency electrical spectroscopy. *Geophys Res Lett GL012951*:30.

Sebok, E., Duque, C., Engesgaard, P., & Boegh, E. (2014). Spatial variability in streambed hydraulic conductivity of contrasting stream morphologies : channel bend and straight channel. https://doi.org/10.1002/hyp.10170

Shepherd, R. G. (1989). Correlations of Permeability and Grain-Size. *Ground Water, 27* (5), 633–638.

Sillanpäa, M. (1956). Studies on the hydraulic conductivity of soils and its measurement. *Acta Agr: Fenlz., 87*, 1- 109.

Slater, L. (2007). Near surface electrical characterization of hydraulic conductivity: From petrophysical properties to aquifer geometries - A review. *Surveys in Geophysics*, *28*(2–3), 169–197.

https://doi.org/10.1007/s10712-007-9022-y

Slater, L. D., & Lesmes, D. (2002). IP interpretation in environmental investigations. *Geophysics*, *67*(1), 77. https://doi.org/10.1190/1.1451353

Sophocleous, M. A., Koussis, A. D., Martin, J. L., & Perkins, S. P. (1995). Evaluation of simplified stream-aquifer depletion models for water rights administration. *Ground Water, 33*, 579–588.

Spitzer, K. (1998). The three-dimensional DC sensitivity for surface and subsurface sources. *Geophysical Journal International, 134*, 736–746. doi:10.1046/j.1365-246x.1998.00592.x

Sun, D. & Zhan, H. (2007). Pumping induced depletion from two streams. *Advances in Water Resources, 30*, 1016–1026.

Telford, W.M., Sheriff, R.E., Geldert, L.P. (1990). Resistivity methods. *Applied geophysics. Cambridge University Press*, Cambridge, pp 523–524.

Terzaghi, K. (1925). Erdbaumechanik auf bodenphysikalischer Grundlage. *Deuticke*, Wien.

Thibodeaux, L. J. & Boyle, J. D. (1987): Bedform-generated convective transport in bottom sediments. *Nature, 325*, 341–343.

Titov, K., Tarasov, A., Ilyin, Y., Seleznev, N., & Boyd, A. (2010). Relationships between induced polarization relaxation time and hydraulic properties of sandstone. *Geophysical Journal International*, *180*(3), 1095–1106. https://doi.org/10.1111/j.1365-246X.2009.04465.x

Waterinfo (2017). Waterinfo Vlaanderen. Water information Flanders. https://www.waterinfo.be/

Weller, A., Slater, L., Binley, A., Nordsiek, S., & Xu, S. (2015). Permeability prediction based on induced polarization: Insights from measurements on sandstone and unconsolidated samples spanning a wide permeability range. *Geophysics*, *80*(2), D161–D173. https://doi.org/10.1190/geo2014-0368.1

Wharton, G., Cotton, J. A., Wotton, R. S., Bass, J. A. B., Heppell, C. M., Trimmer, M., Sanders, I. A., & Warren, L. L. (2006). Macrophytes and suspension-feeding invertebrates modify flows and fine sediments in the Frome and Piddle catchments, Dorset (UK). *J. Hydrol., 330*, 171–184.

Woldeamlak, S. (2007). Spatio-temporal Impacts of Climate and Land-use Changes on the Groundwater and Surface Water Resources of a Lowland Catchment. *PhD Thesis, Vrije Universiteit Brussel*, Brussels, Belgium.

Yadav, G.S., Abolfazli, H. (1998). Geoelectrical soundings and their relationship to hydraulic parameters in semiarid regions of Jalore, Northwestern India. *J. Appl. Geophys. 39*, 35–51.

Zlotnik, V. (1994). Interpretation of slug and packer tests in anisotropic aquifers. *Ground Water 32 (5)*: 761-766.

Appendices

1 APPENDIX A: LINK GEO-ELECTRICAL PARAMETERS - LITHOLOGY

Table 1 Overview of ranges of resistivity and normalized chargeability from case studies in literature.

Material	Variable	Range	Description	Reference
Sand	Resistivity [Ωm]	160 – 250	Gravel and sand	Amaya et al., 2016
	Resistivity [Ωm]	50 – 170	Fluvial sand and gravel	Christensen, 2000
	Resistivity [Ωm]	40 – 150	Late- or fluvioglacial sand with fresh water	Christensen, 2000
	Resistivity [Ωm]	120 – 200	Glacial deposits, mainly sands	Christensen, 2000
	Resistivity [Ωm]	60 – 200	Sand under the groundwater table	Christensen, 2000
	Resistivity [Ωm]	40 – 1200	Sand and gravel	Doetsch, 2016
	Resistivity [Ωm]	20 – 50	Sand	Kazakis et al., 2016
	Resistivity [Ωm]	100 – 400	Coarse alluvial sediments	Nyquist et al., 2008
	Normalized chargeability [mS/m]	0.01 – 0.025	Gravel and sand	Amaya et al., 2016
	Normalized chargeability [mS/m]	< 0.25	Clear sand	Slater & Lesmes, 2002
Clay	Resistivity [Ωm]	10 – 25	Clay	Amaya et al., 2016
	Resistivity [Ωm]	1 – 20	Interglacial clay	Christensen, 2000
	Resistivity [Ωm]	4 – 10	Postglacial clay	Christensen, 2000
	Resistivity [Ωm]	30 – 50	Glacial deposits, mainly clay	Christensen, 2000
	Resistivity [Ωm]	10 – 30	Lacustrine clay	Christensen, 2000
	Resistivity [Ωm]	2 – 70	Postglacial clay, silt	Christensen, 2000
	Resistivity [Ωm]	20 – 50	Clay	Christensen, 2000
	Resistivity [Ωm]	5 – 30	Clay	Doetsch, 2016
	Resistivity [Ωm]	1 – 10	Clay	Kazakis et al., 2016
	Resistivity [Ωm]	20 – 100	Residual clay sediments	Nyquist et al., 2008
	Resistivity [Ωm]	1 – 100	Clays	Telford et al., 1990
	Resistivity [Ωm]	8 – 33	Soil (20 – 40 % clay)	Telford et al., 1990
	Resistivity [Ωm]	4 – 20	London clay	Telford et al., 1990
	Resistivity [Ωm]	10 – 15	Lias clay	Telford et al., 1990
	Normalized chargeability [mS/m]	> 0.50	Clay	Amaya et al., 2016
Sand & clay	Resistivity [Ωm]	100 – 160	Sand and clay	Amaya et al., 2016
	Resistivity [Ωm]	20 – 100	Sand and clay, glacial	Christensen, 2000
	Resistivity [Ωm]	10 – 800	Alluvium and sand	Telford et al., 1990
	Resistivity [Ωm]	30 – 215	Sand clay/ clayey sand	Telford et al., 1990
	Normalized chargeability [mS/m]	0.10 – 0.25	Sand and clay	Amaya et al., 2016
Peat, organic matter	Resistivity [Ωm]	10 – 25	Peat/mud	Christensen, 2000
	Resistivity [Ωm]	30 – 70	Peat	Christensen, 2000
Fresh water	Resistivity [Ωm]	3 – 120	Fresh water	Doetsch, 2016
	Resistivity [Ωm]	20 – 100	Rainfall runoff	Telford et al., 1990
Groundwater	Resistivity [Ωm]	10 – 40	Groundwater	Christensen, 2000

2 APPENDIX B: SPATIAL DISTRIBUTIONS OF K

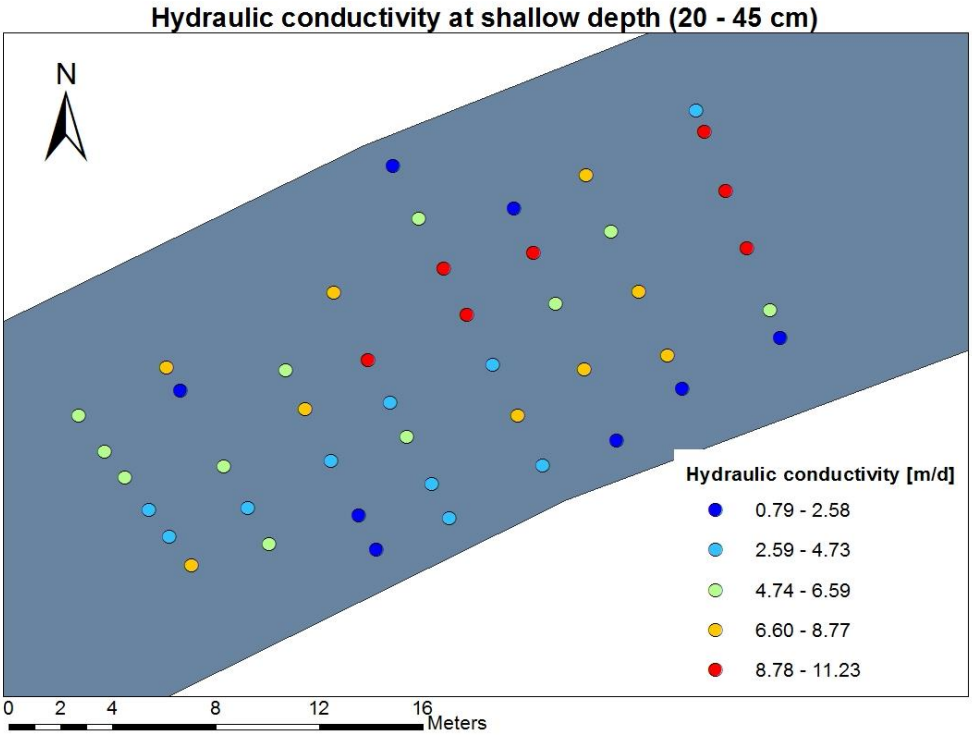

Figure 1 Spatial distribution of hydraulic conductivity values measured in the depth interval of 20 – 45 cm.

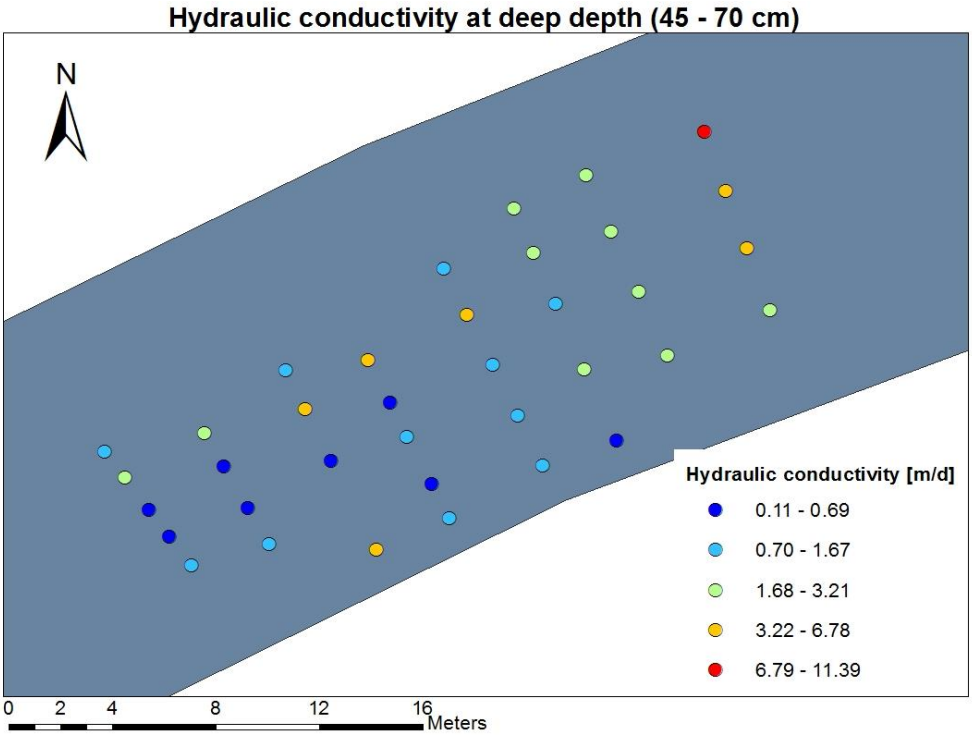

Figure 2 Spatial distribution of hydraulic conductivity values measured in the depth interval of 45 – 70 cm.

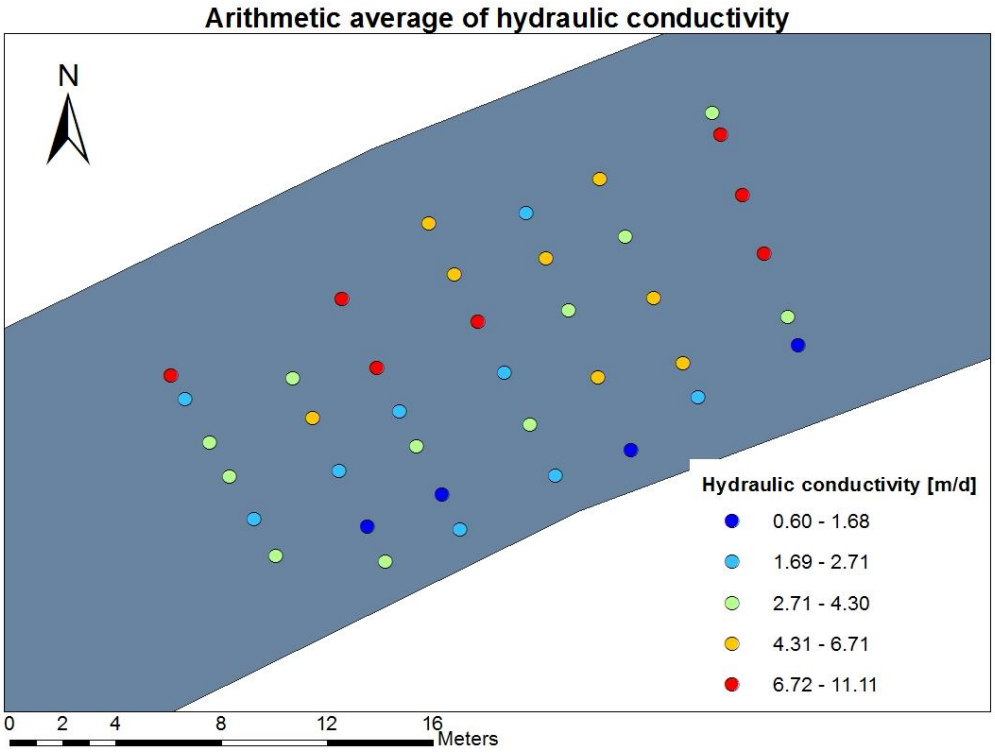

Figure 3 Spatial distribution of hydraulic conductivity data arithmetically averaged over the two depth intervals.

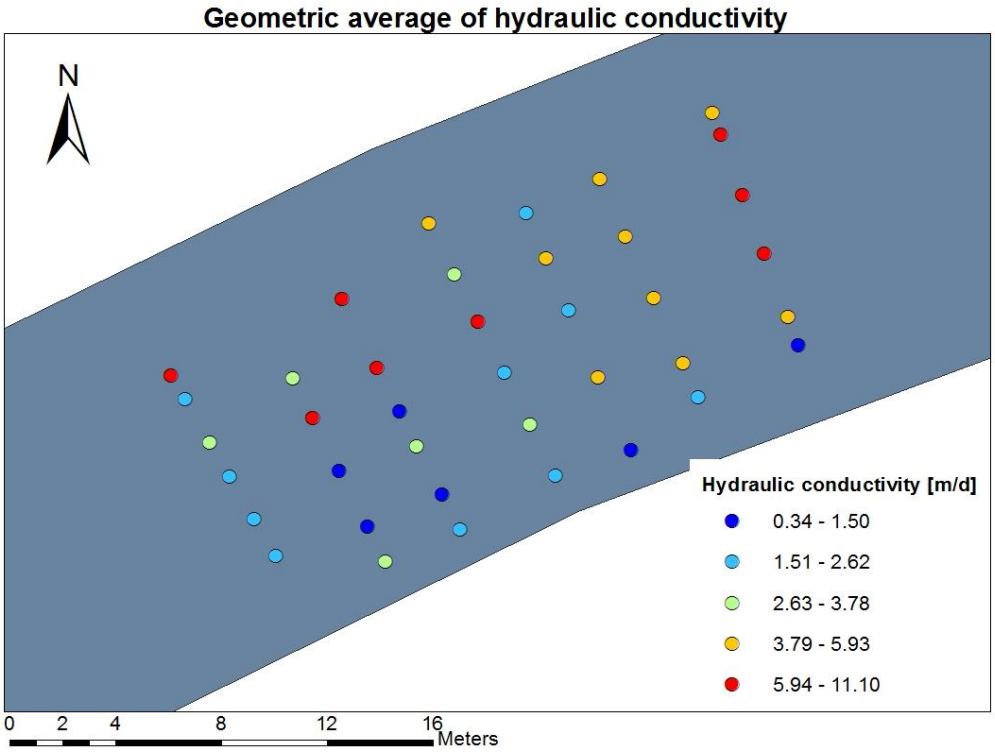

Figure 4 Spatial distribution of hydraulic conductivity data geometrically averaged over the two depth intervals.

3 APPENDIX C: VARIOGRAMS OF K IN DEPTH INTERVALS

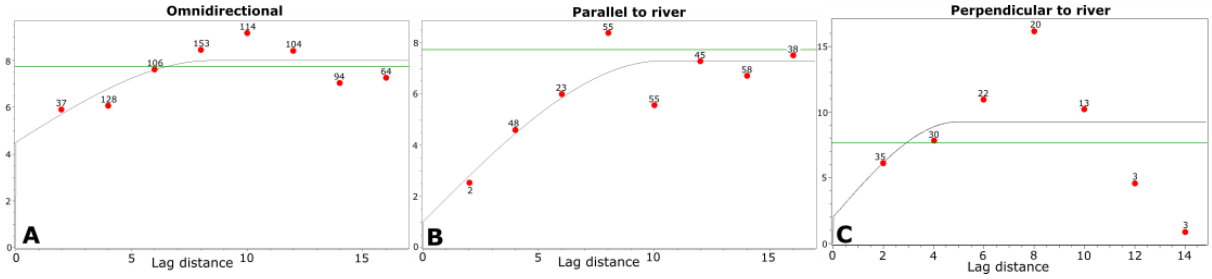

Figure 5 Variograms based on hydraulic conductivity data at shallow depth (A) omnidirectional, (B) parallel to the river and (C) perpendicular to the river. The vertical axis indicates the semi-variance ((m/d)²). The variance of the data is shown with a green line. Numbers at each point indicate the number of pairs for that lag.

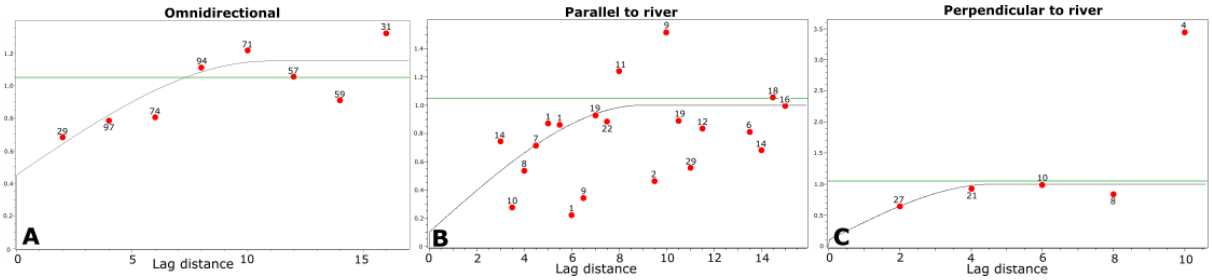

Figure 6 Variograms based on logarithmic hydraulic conductivity data at deep depth (A) omnidirectional, (B) parallel to the river and (C) perpendicular to the river. The vertical axis is the semi-variance ((m/d)²). The variance of the data is shown with a green line. Numbers at each point indicate the number of pairs for that lag.

4 APPENDIX D: DEPTH OF INVESTIGATION (DOI)

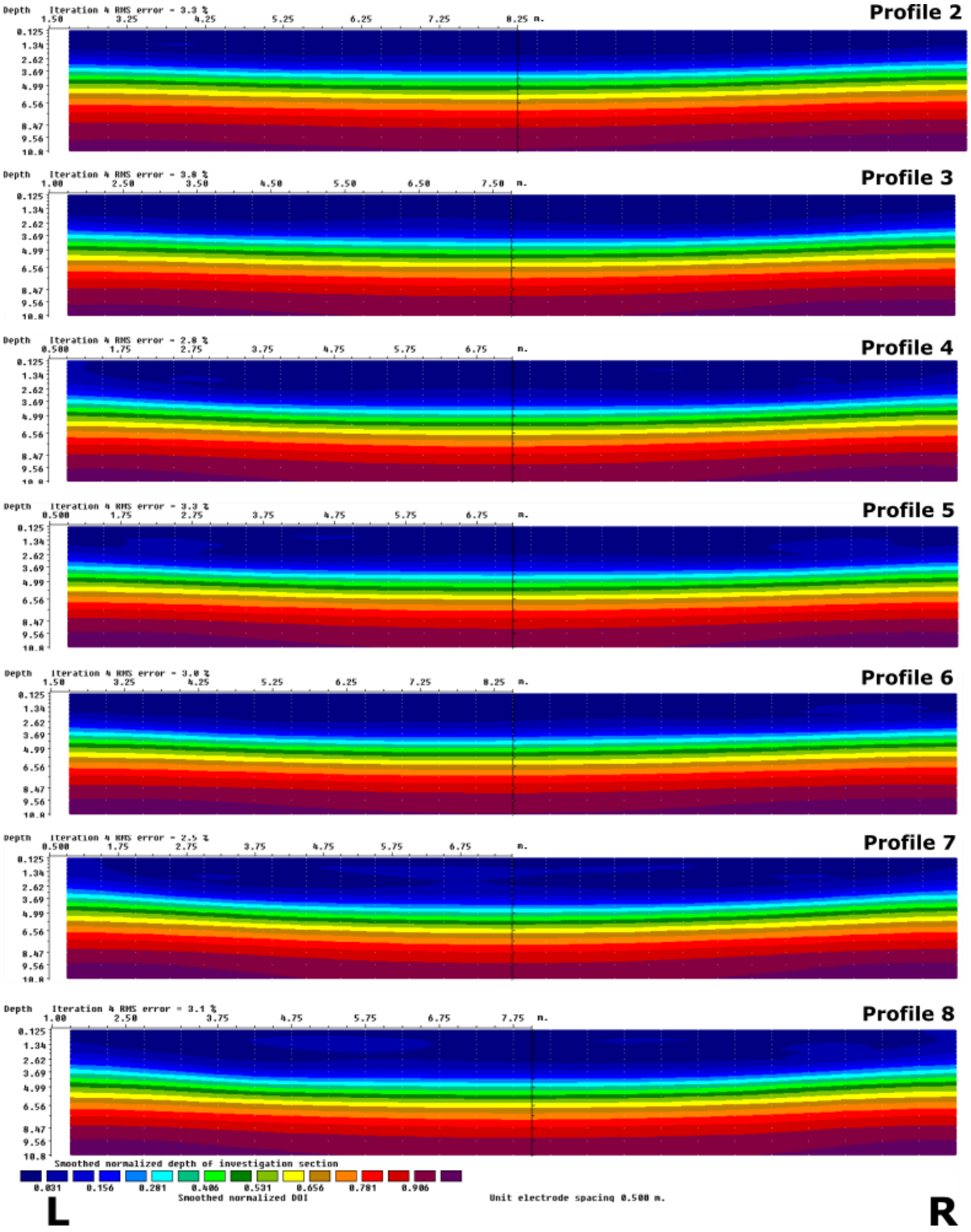

Figure 7 Depth of investigation of the ERT and IP survey for every profile. L and R indicate left and right bank respectively. Profile 2 is most downstream, profile 8 is most upstream.

5 APPENDIX E: HYDRAULIC CONDUCTIVITY & RESISTIVITY

a. SPATIAL DISTRIBUTIONS

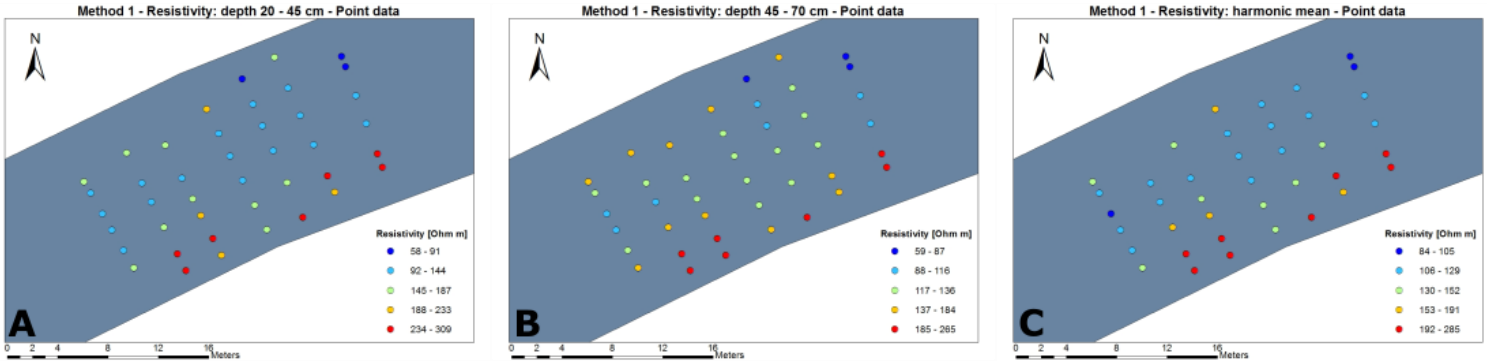

Figure 8 Point maps of resistivity data extracted with method 1. Point data (A) at shallow depth, (B) at deep depth, (C) harmonically averaged over the two depth intervals.

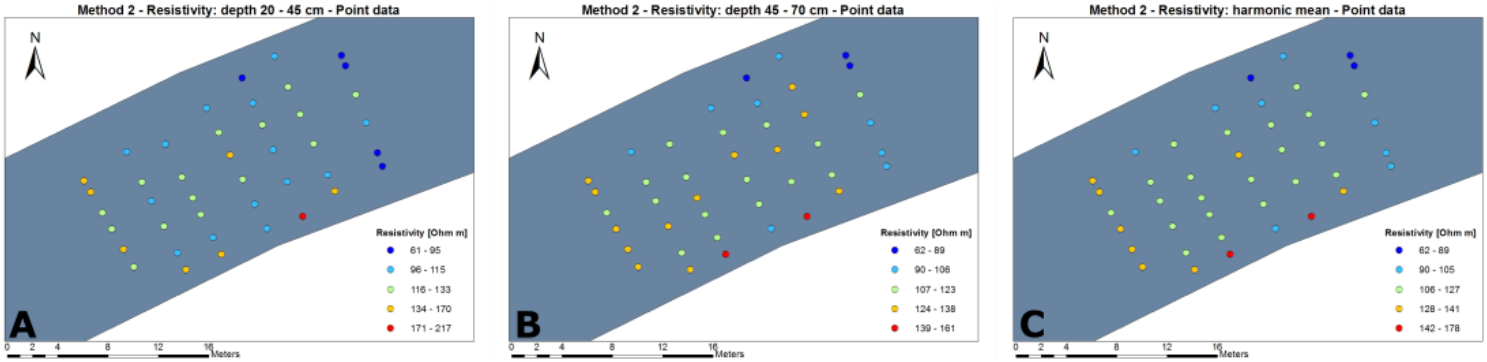

Figure 9 Point maps of resistivity data extracted with method 2. Point data (A) at shallow depth, (B) at deep depth, (C) harmonically averaged over the two depth intervals.

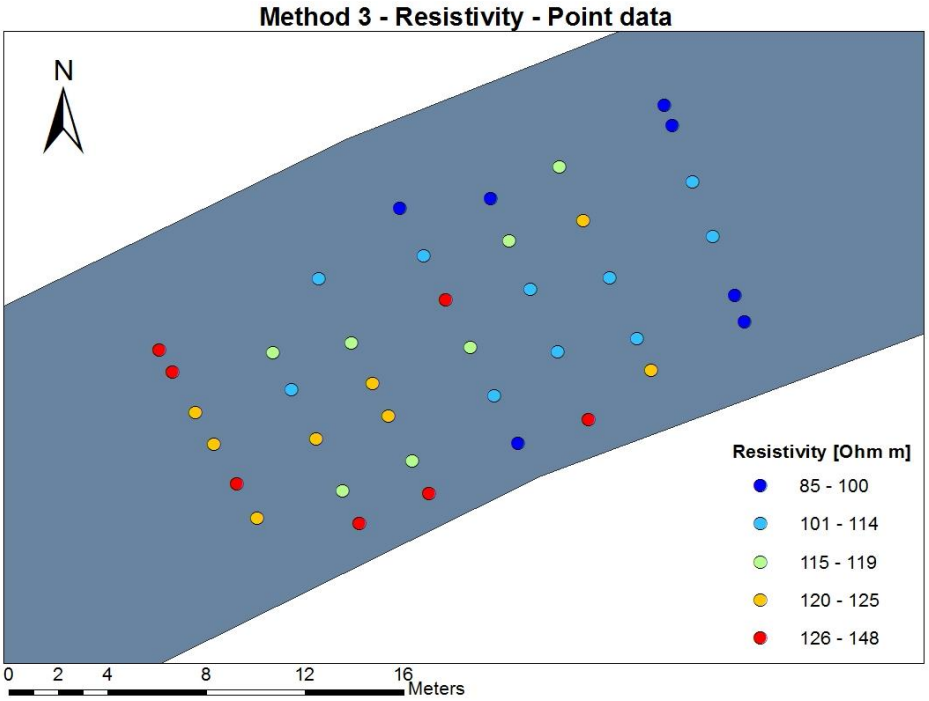

Figure 10 Point map of resistivity data extracted with method 3.

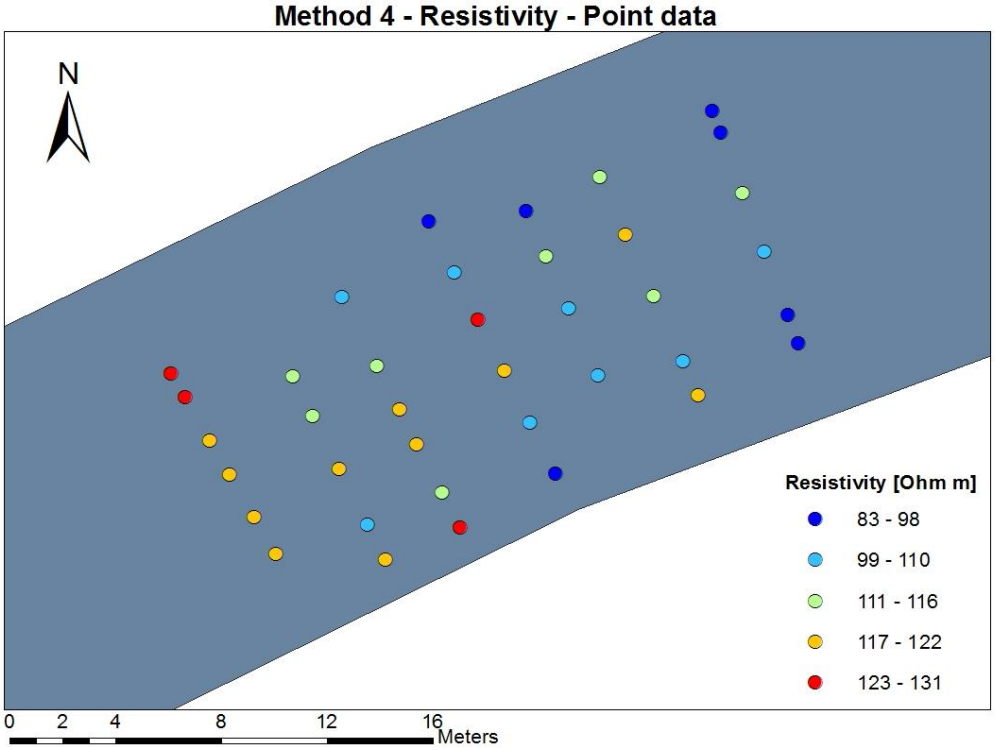

Figure 11 Point map of resistivity data extracted with method 4.

b. SCATTERPLOTS

i. Method 1

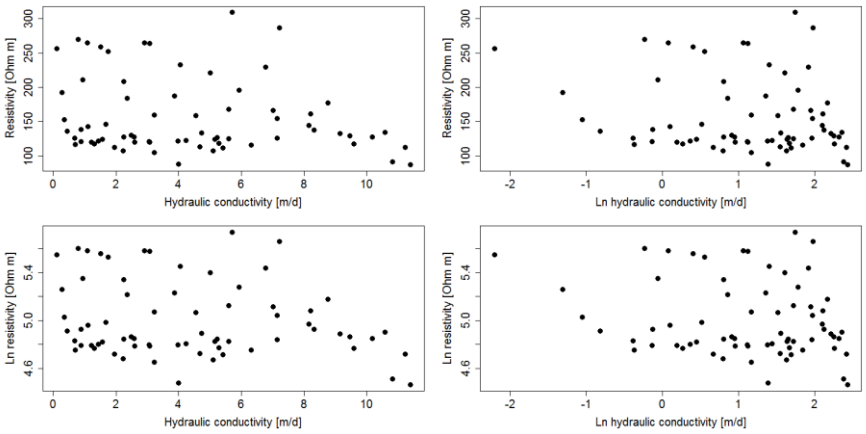

Figure 12 Scatterplots of hydraulic conductivity versus resistivity for all data extracted with the first method, with and/or without logarithmic transformations of the parameters.

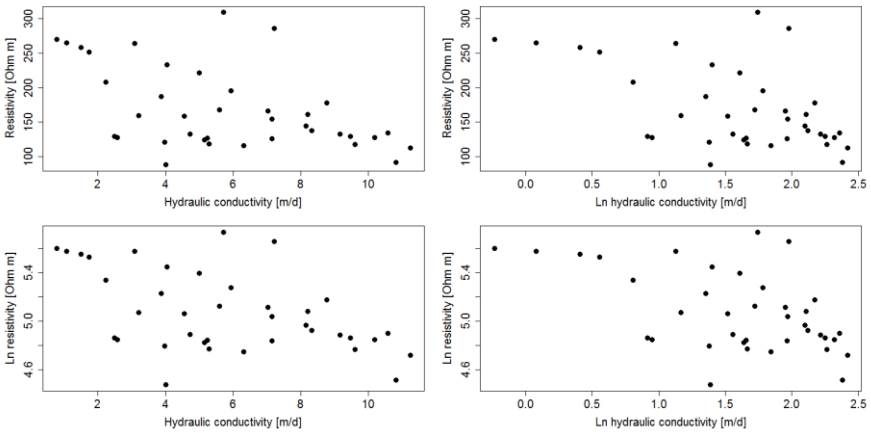

Figure 13 Scatterplots of hydraulic conductivity versus resistivity for shallow depth data extracted with the first method, with and/or without logarithmic transformations of the parameters.

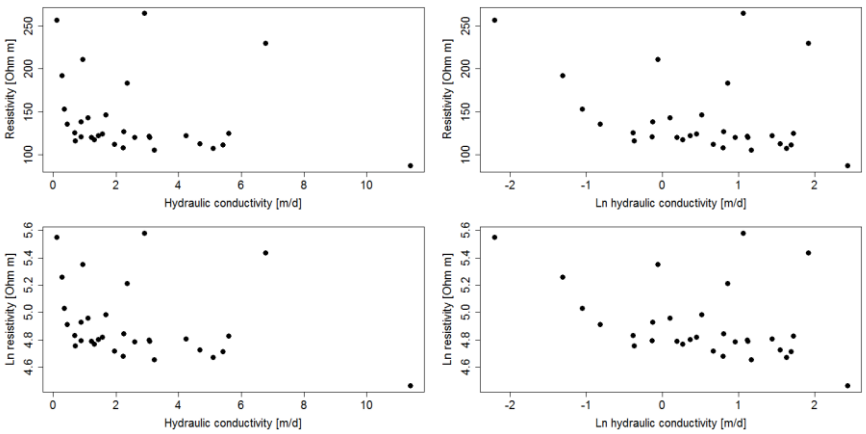

Figure 14 Scatterplots of hydraulic conductivity versus resistivity for deep depth data extracted with the first method, with and/or without logarithmic transformations of the parameters.

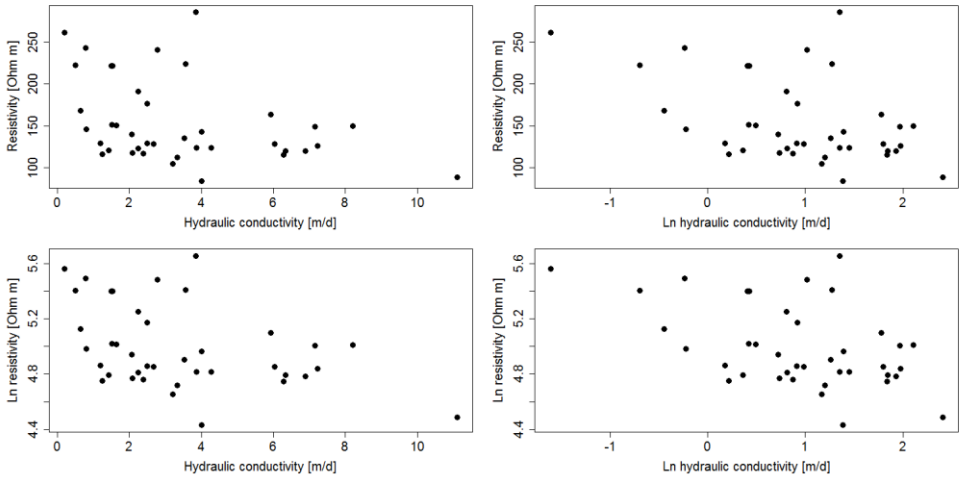

Figure 15 Scatterplots of hydraulic conductivity versus resistivity for harmonically averaged data extracted with the first method, with and/or without logarithmic transformations of the parameters.

ii. Method 2

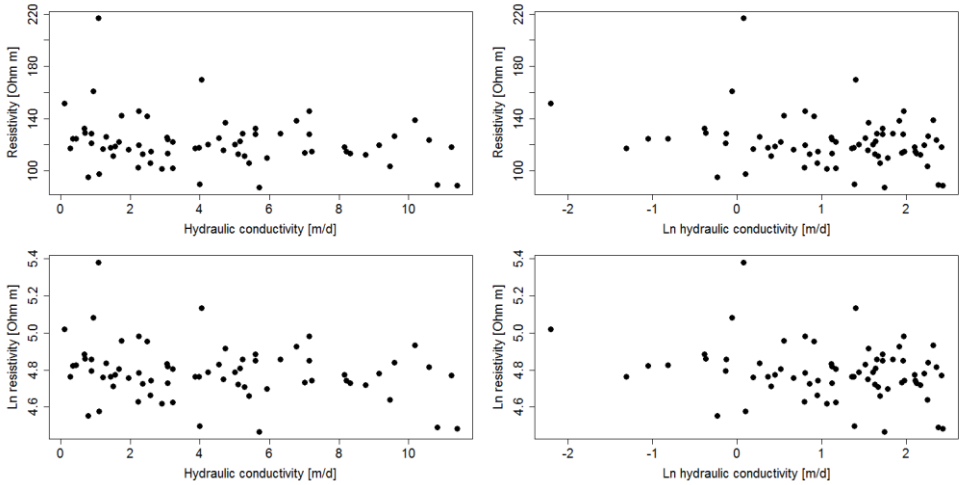

Figure 16 Scatterplots of hydraulic conductivity versus resistivity for all data extracted with the second method, with and/or without logarithmic transformations of the parameters.

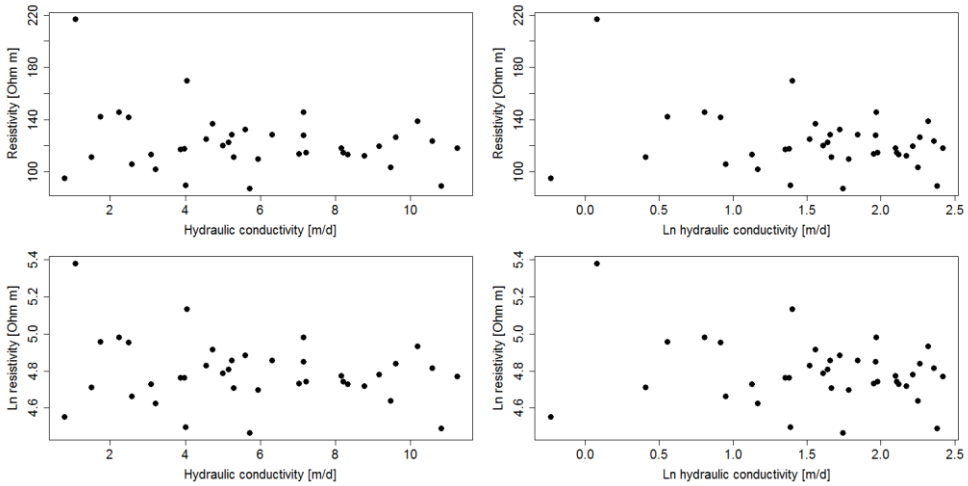

Figure 17 Scatterplots of hydraulic conductivity versus resistivity for shallow depth data extracted with the second method, with and/or without logarithmic transformations of the parameters.

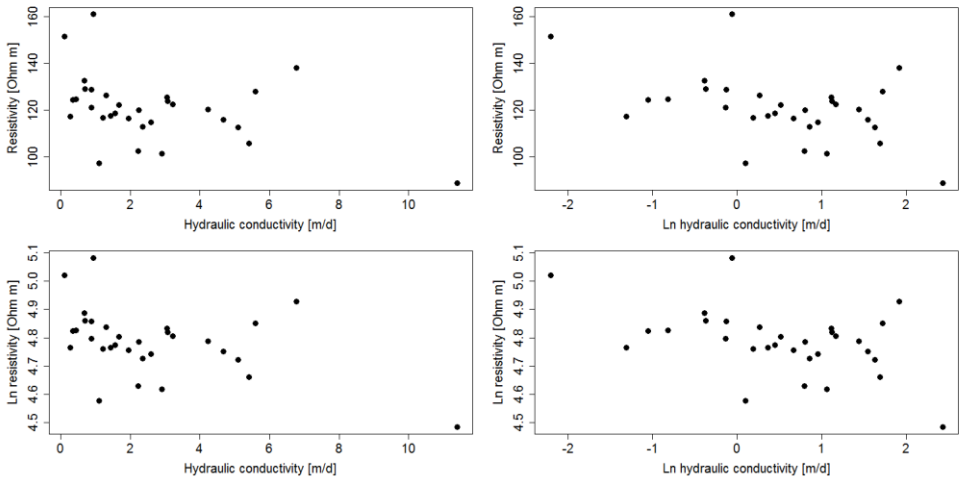

Figure 18 Scatterplots of hydraulic conductivity versus resistivity for deep depth data extracted with the second method, with and/or without logarithmic transformations of the parameters.

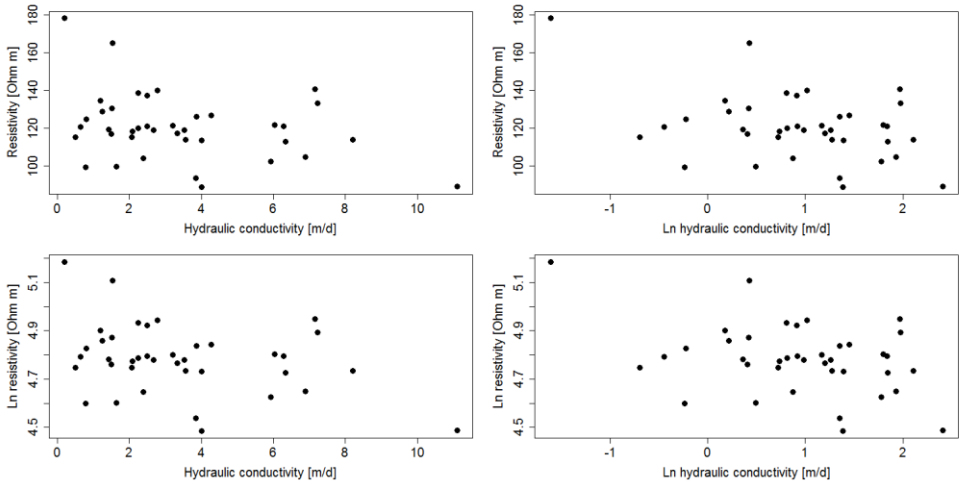

Figure 19 Scatterplots of hydraulic conductivity versus resistivity for harmonically averaged data extracted with the second method, with and/or without logarithmic transformations of the parameters.

iii. Method 3

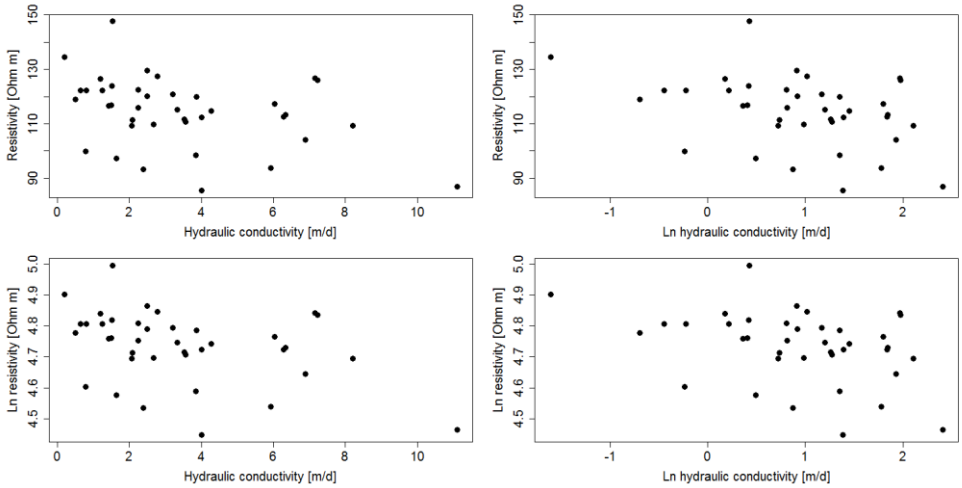

Figure 20 Scatterplots of harmonically averaged hydraulic conductivity versus resistivity for data extracted with the third method, with and/or without logarithmic transformations of the parameters.

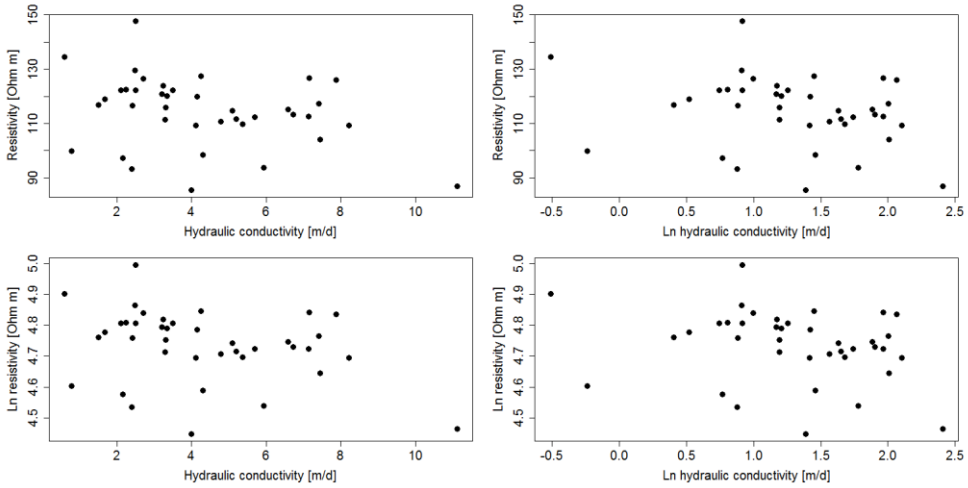

Figure 21 Scatterplots of arithmetically averaged hydraulic conductivity versus resistivity for data extracted with the third method, with and/or without logarithmic transformations of the parameters.

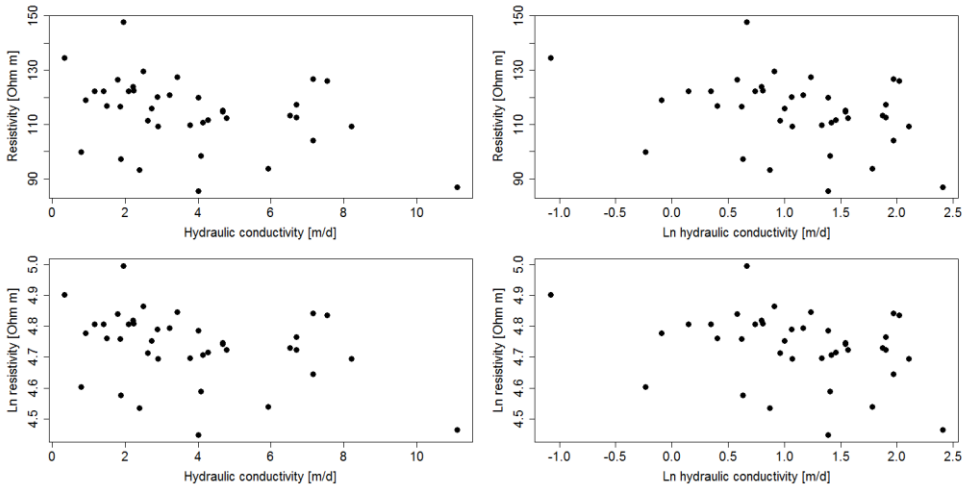

Figure 22 Scatterplots of geometrically averaged hydraulic conductivity versus resistivity for data extracted with the third method, with and/or without logarithmic transformations of the parameters.

iv. Method 4

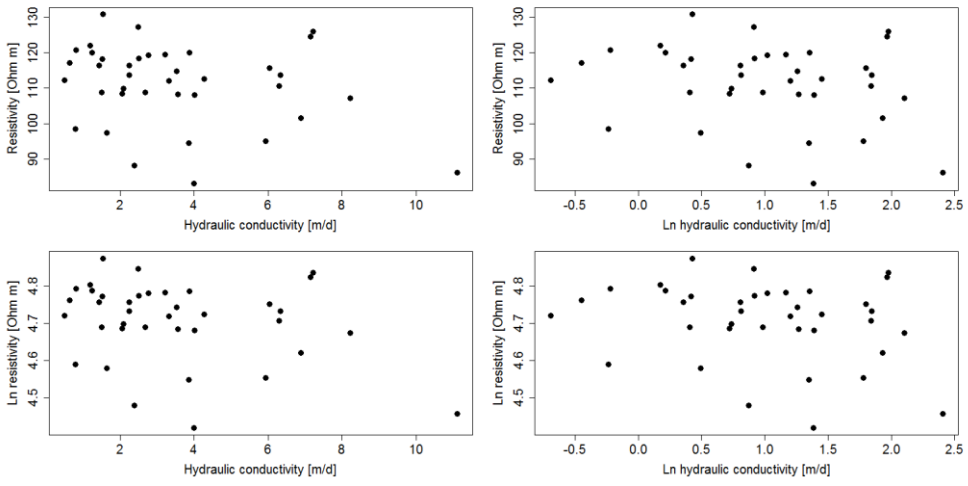

Figure 23 Scatterplots of harmonically averaged hydraulic conductivity versus resistivity for data extracted with the fourth method, with and/or without logarithmic transformations of the parameters.

C. SIGNIFICANT LINEAR REGRESSIONS

i. Method 1

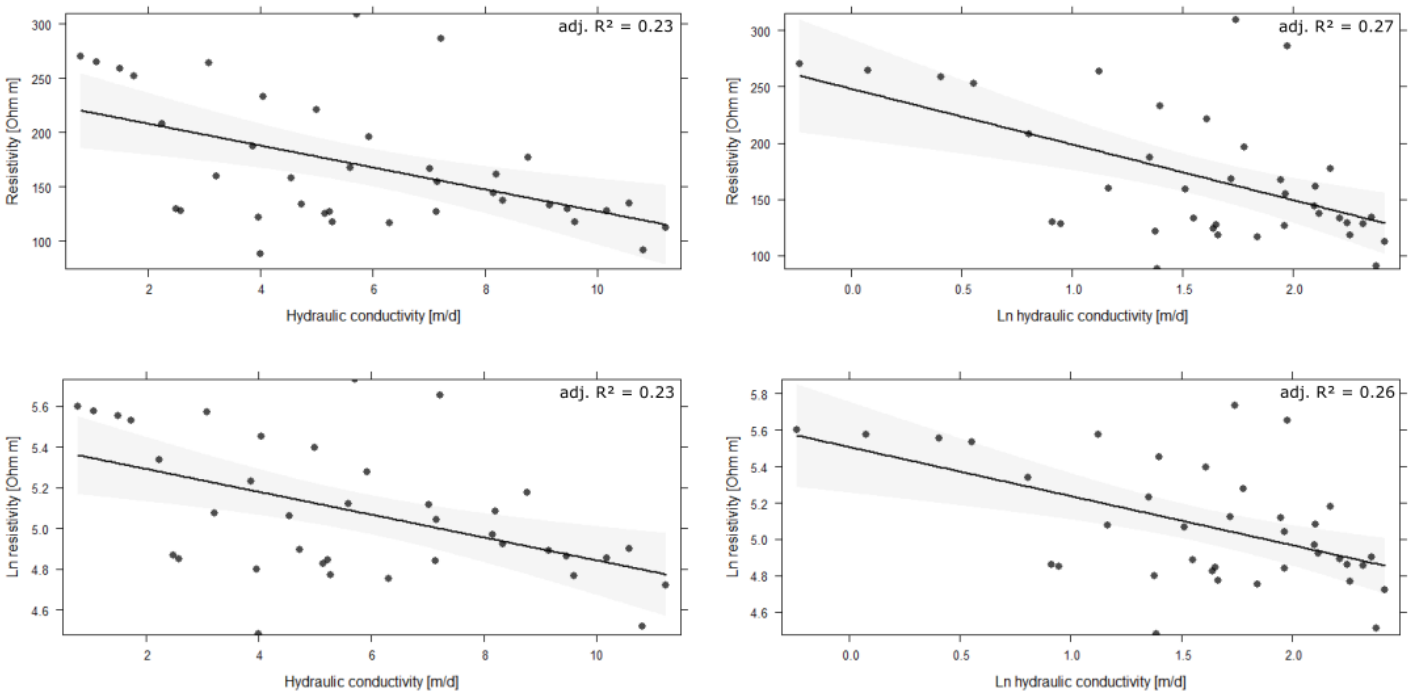

Figure 24 Significant linear models fitted to the scatterplots of hydraulic conductivity versus resistivity of shallow depth data extracted with method 1, with and/or without logarithmic transformations of the parameters. The grey bands indicate the 95 % confidence interval of the fits.

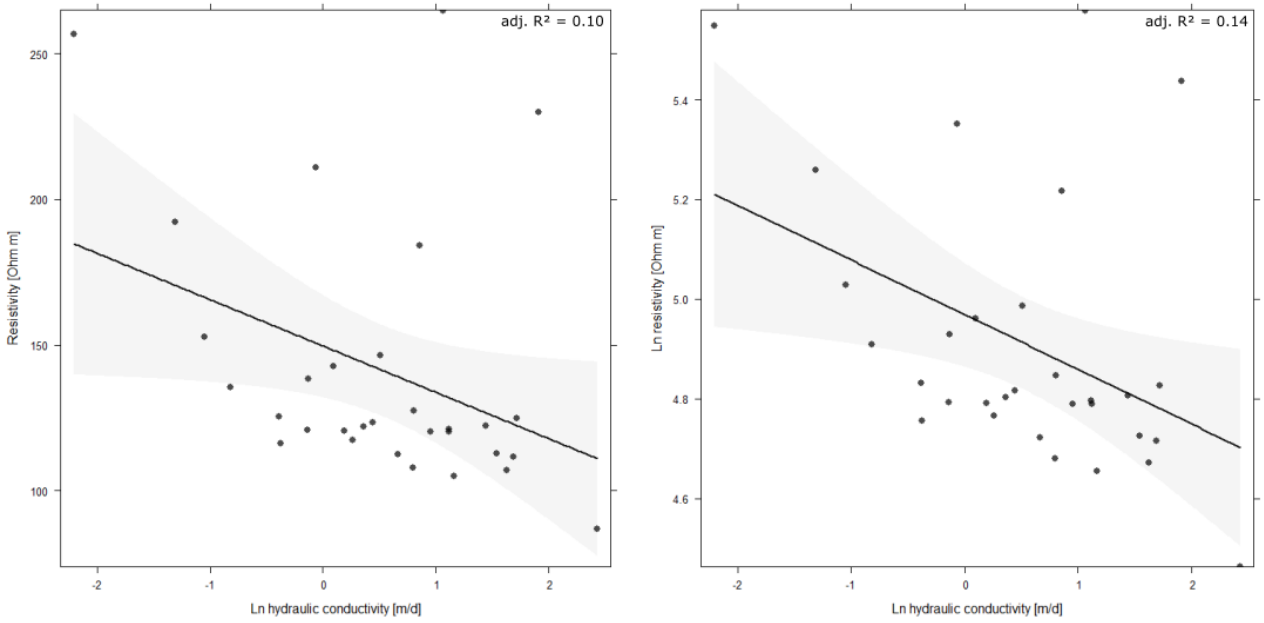

Figure 25 Significant linear models fitted to the scatterplots of hydraulic conductivity versus resistivity of deep depth data extracted with method 1, with logarithmic transformation of hydraulic conductivity. The grey bands indicate the 95 % confidence interval of the fits

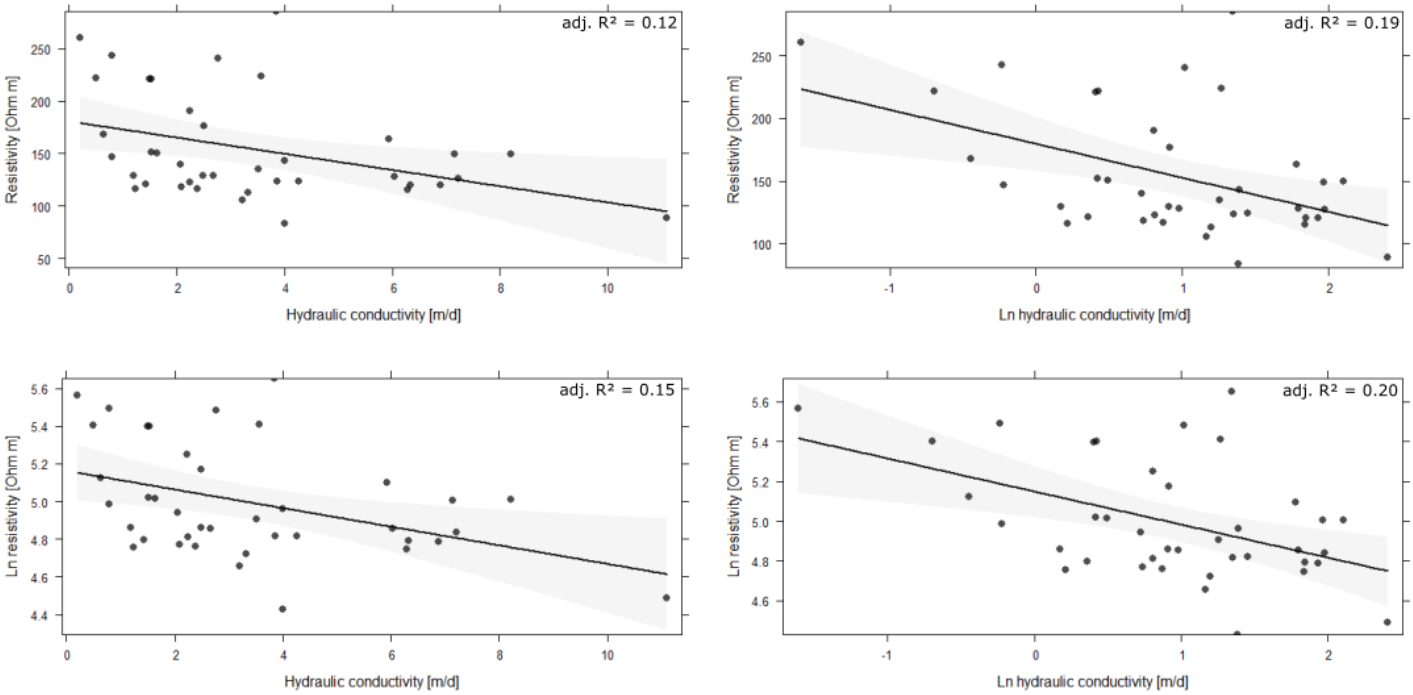

Figure 26 Significant linear models fitted to the scatterplots of hydraulic conductivity versus resistivity of harmonically averaged data extracted with method 1, with and/or without logarithmic transformations of the parameters. The grey bands indicate the 95 % confidence interval of the fits.

ii. Method 2

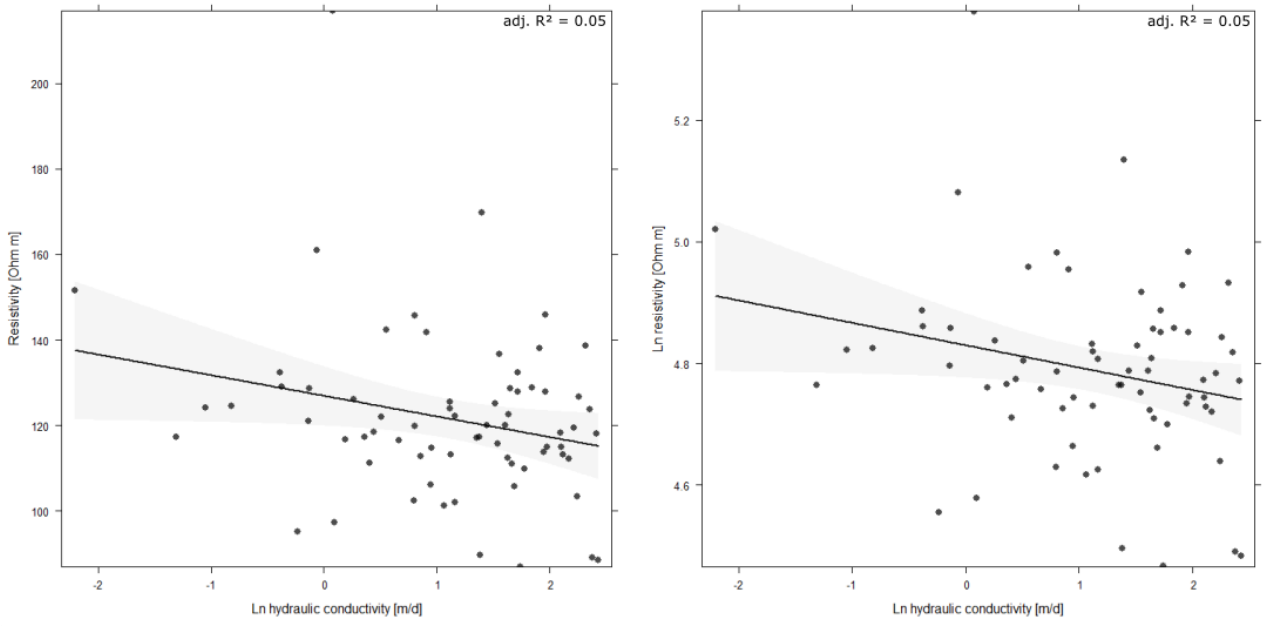

Figure 27 Significant linear models fitted to the scatterplots of hydraulic conductivity versus resistivity of all data extracted with method 2, with logarithmic transformation of hydraulic conductivity. The grey bands indicate the 95 % confidence interval of the fits.

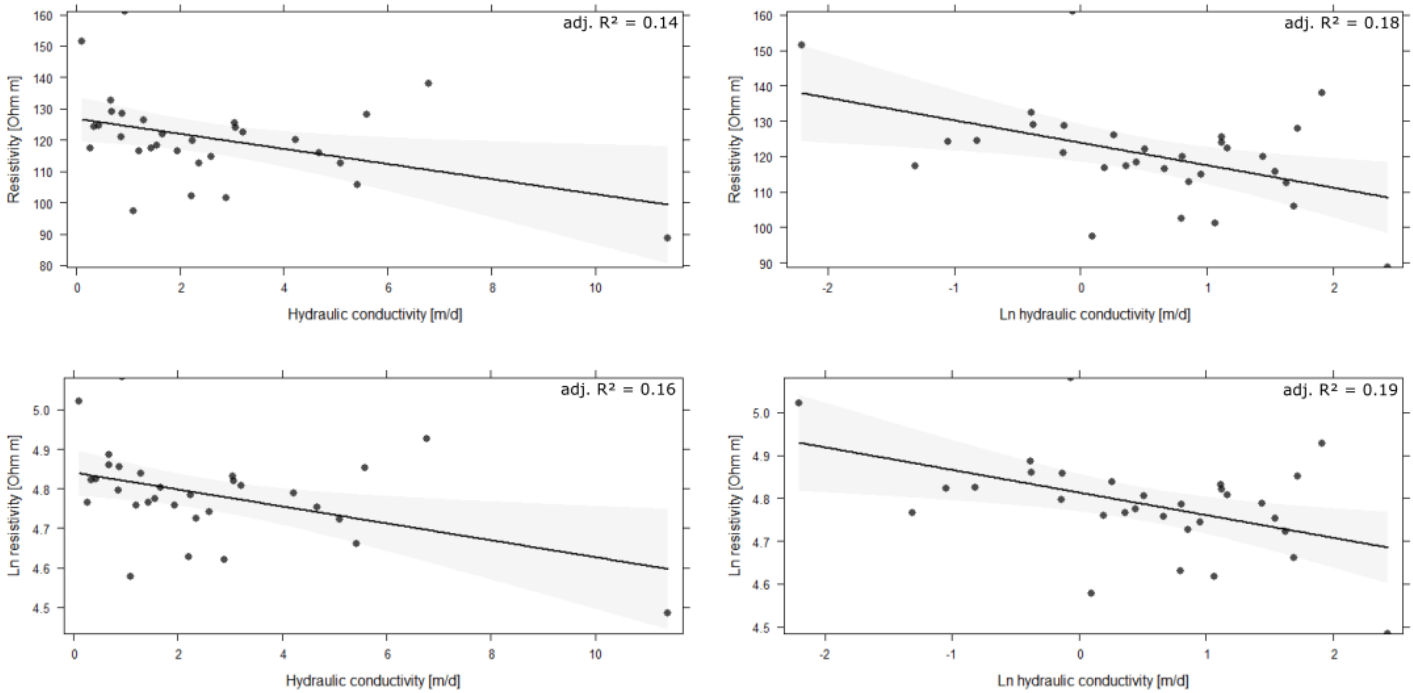

Figure 28 Significant linear models fitted to the scatterplots of hydraulic conductivity versus resistivity of deep depth data extracted with method 2, with and/or without logarithmic transformations of the parameters. The grey bands indicate the 95 % confidence interval of the fits.

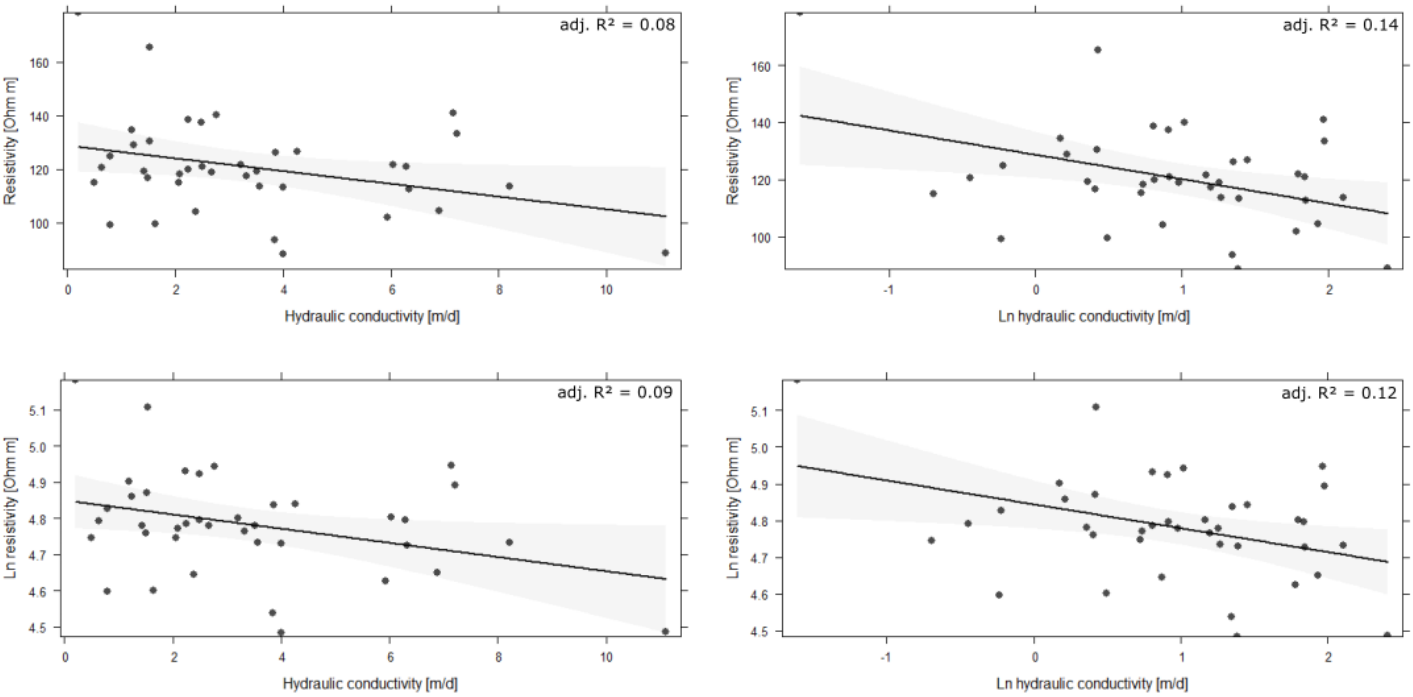

Figure 29 Significant linear models fitted to the scatterplots of hydraulic conductivity versus resistivity of harmonically averaged data extracted with method 2, with and/or without logarithmic transformations of the parameters. The grey bands indicate the 95 % confidence interval of the fits.

iii. Method 3

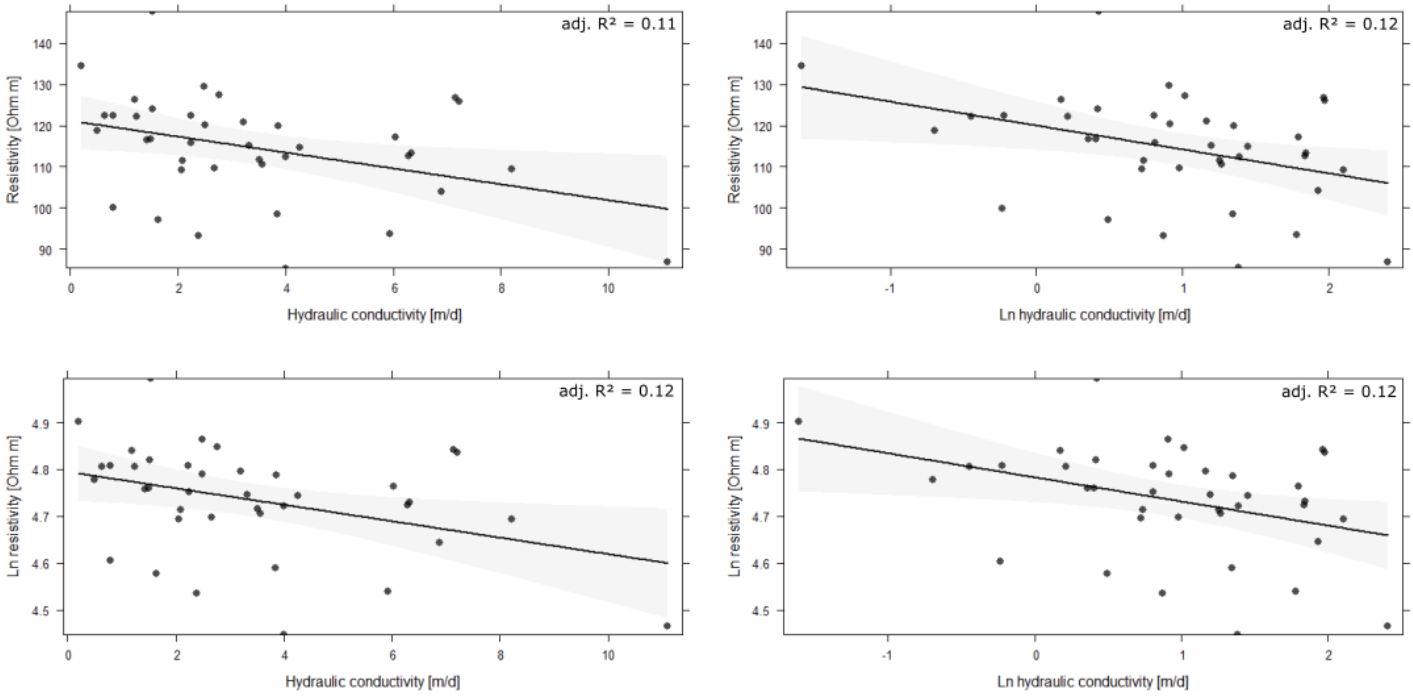

Figure 30 Significant linear models fitted to the scatterplots of harmonically averaged hydraulic conductivity versus resistivity of data extracted with method 3, with and/or without logarithmic transformations of the parameters. The grey bands indicate the 95 % confidence interval of the fits.

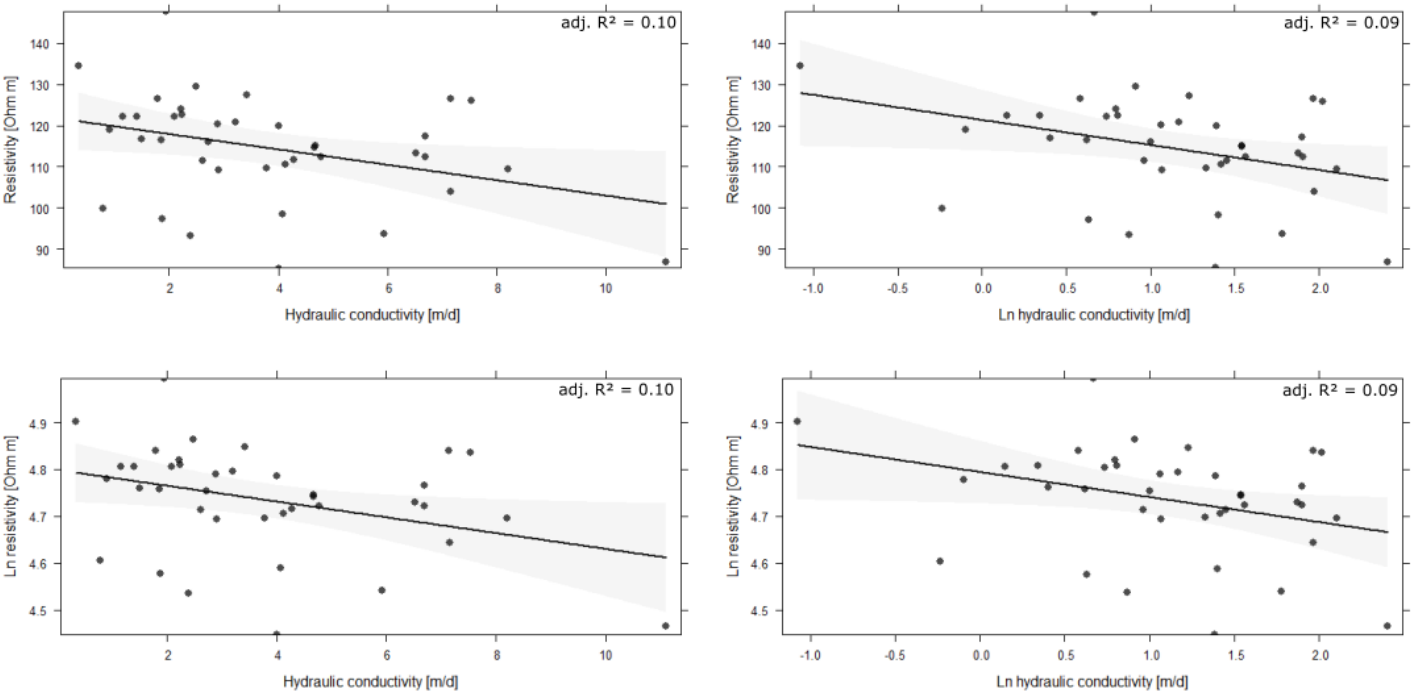

Figure 31 Significant linear models fitted to the scatterplots of geometrically averaged hydraulic conductivity versus resistivity of data extracted with method 3, with and/or without logarithmic transformations of the parameters. The grey bands indicate the 95 % confidence interval of the fits.

6 APPENDIX F: HYDRAULIC CONDUCTIVITY & CHARGEABILITY

a. SPATIAL DISTRIBUTIONS

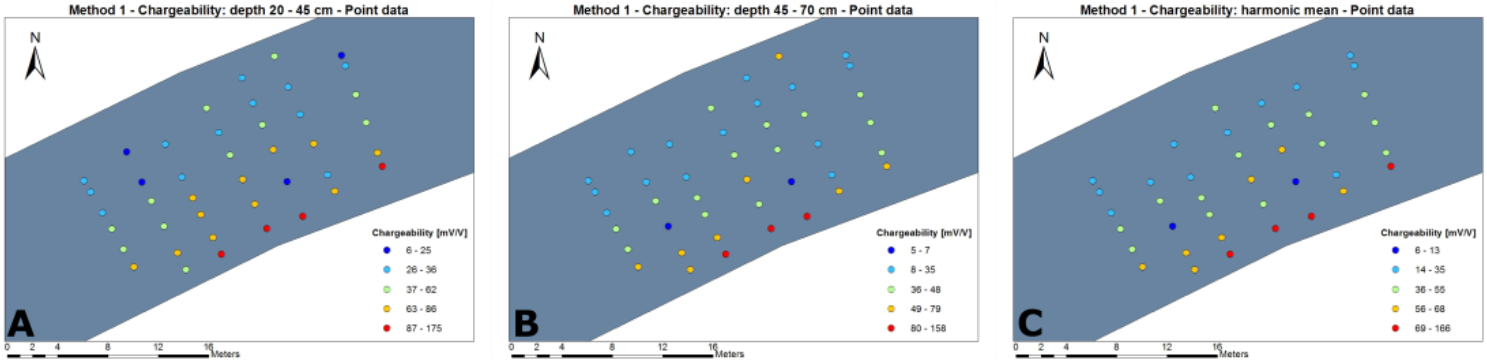

Figure 32 Point maps of chargeability data extracted with method 1. Point data (A) at shallow depth, (B) at deep depth, (C) harmonically averaged over the two depth intervals.

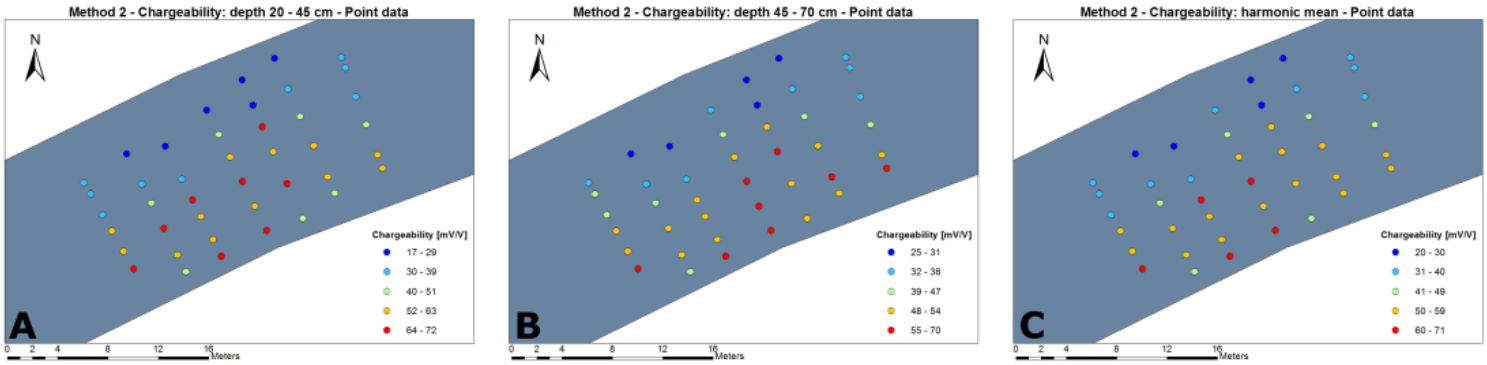

Figure 33 Point maps of chargeability data extracted with method 2. Point data (A) at shallow depth, (B) at deep depth, (C) harmonically averaged over the two depth intervals.

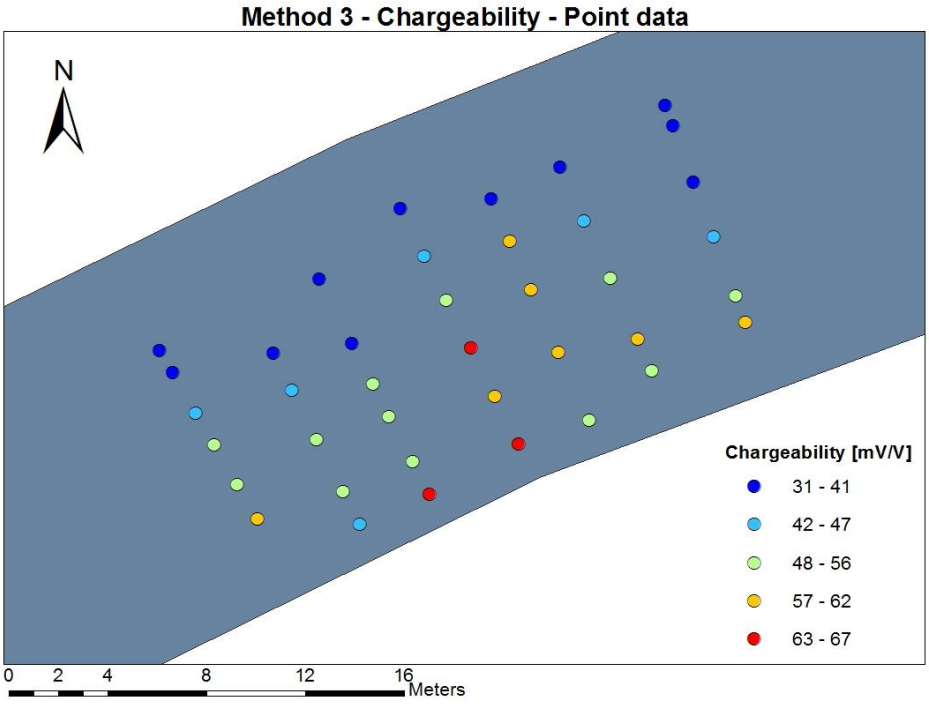

Figure 34 Point map of chargeability data extracted with method 3.

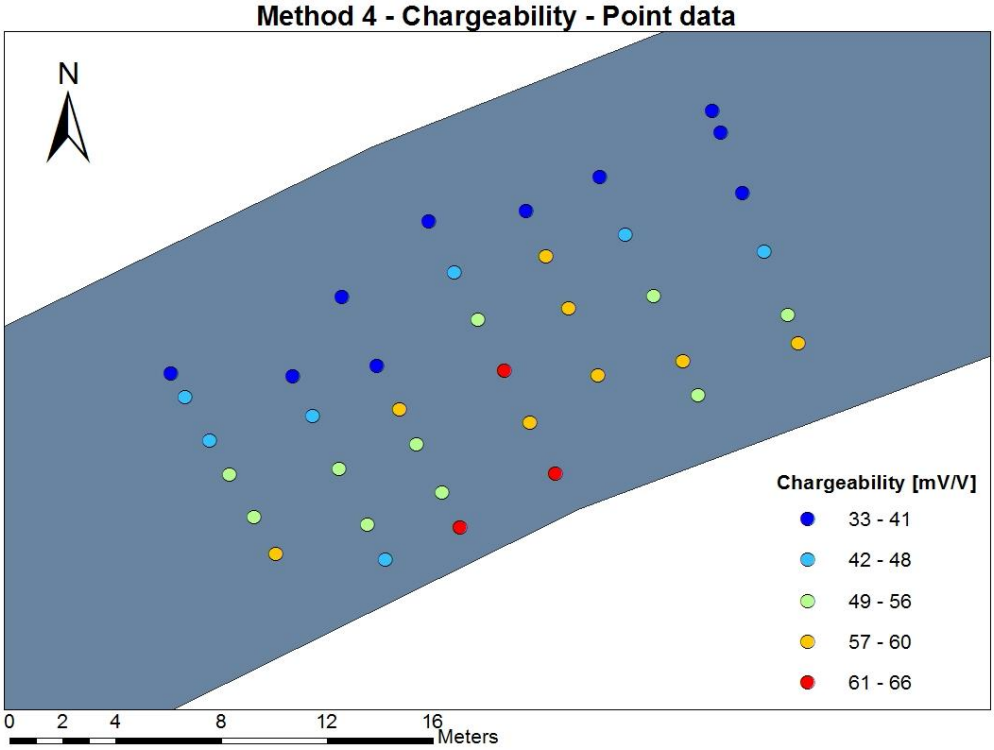

Figure 35 Point map of chargeability data extracted with method 4.

b. SCATTERPLOTS

i. Method 1

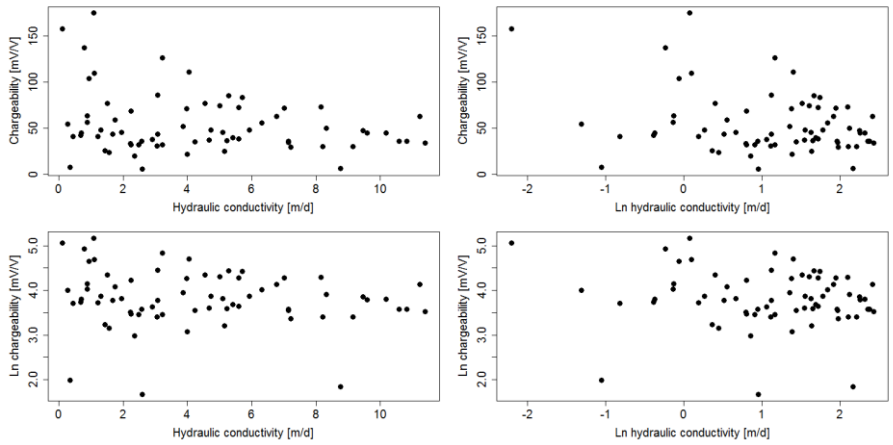

Figure 36 Scatterplots of hydraulic conductivity versus chargeability for all data extracted with the first method, with and/or without logarithmic transformations of the parameters.

5

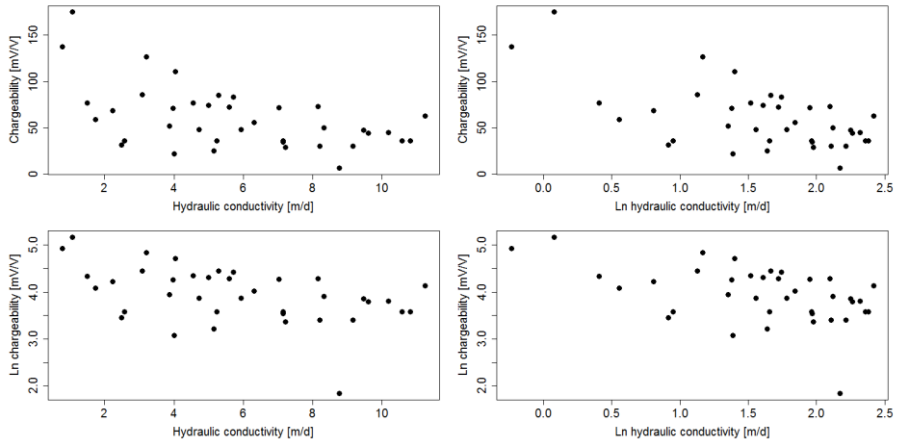

Figure 37 Scatterplots of hydraulic conductivity versus chargeability for shallow depth data extracted with the first method, with and/or without logarithmic transformations of the parameters.

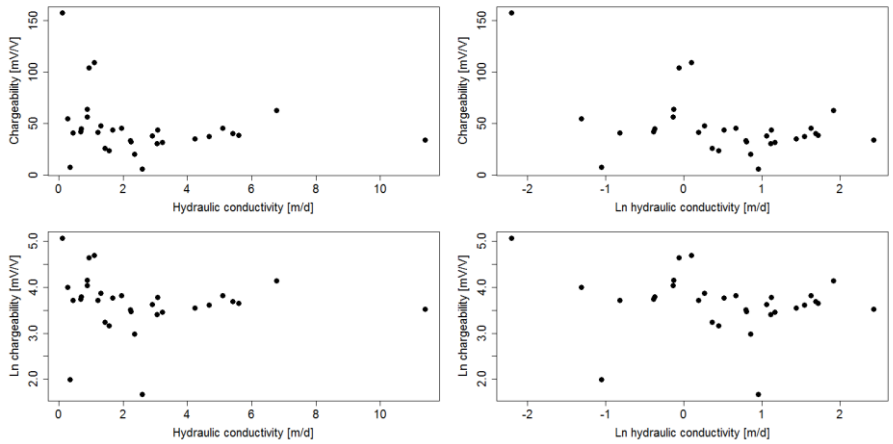

Figure 38 Scatterplots of hydraulic conductivity versus chargeability for deep depth data extracted with the first method, with and/or without logarithmic transformations of the parameters.

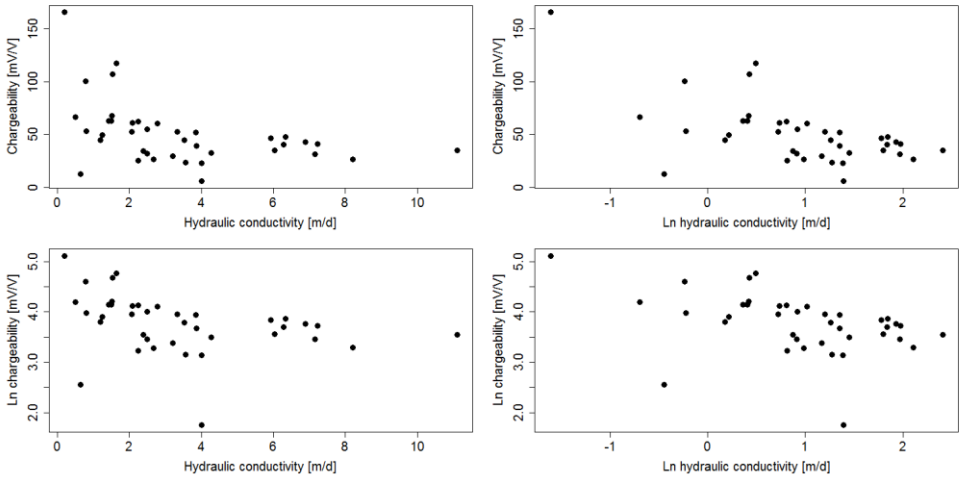

Figure 39 Scatterplots of hydraulic conductivity versus chargeability for harmonically averaged data extracted with the first method, with and/or without logarithmic transformations of the parameters.

ii. Method 2

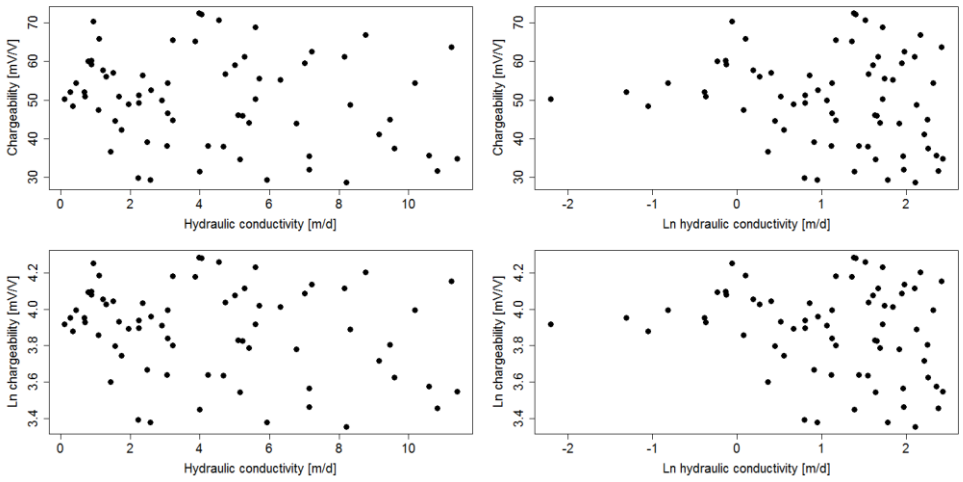

Figure 40 Scatterplots of hydraulic conductivity versus chargeability for all data extracted with the second method, with and/or without logarithmic transformations of the parameters.

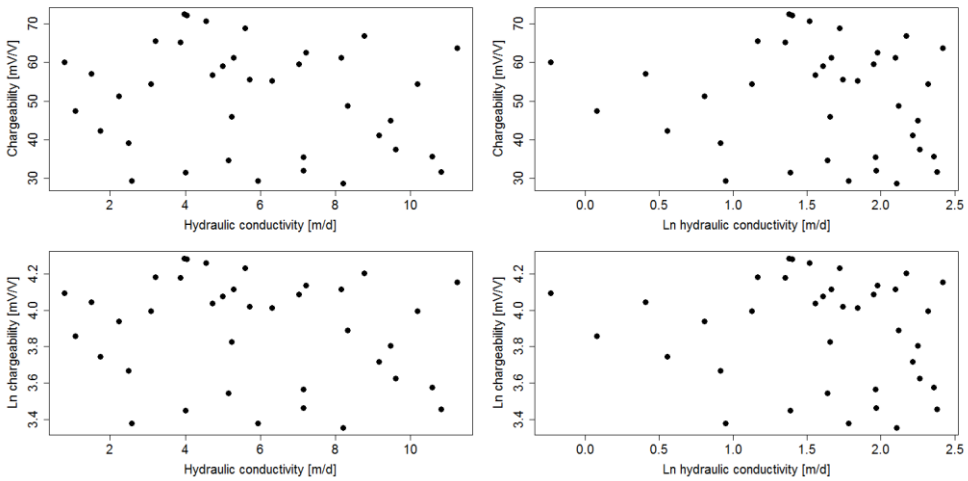

Figure 41 Scatterplots of hydraulic conductivity versus chargeability for shallow depth data extracted with the second method, with and/or without logarithmic transformations of the parameters.

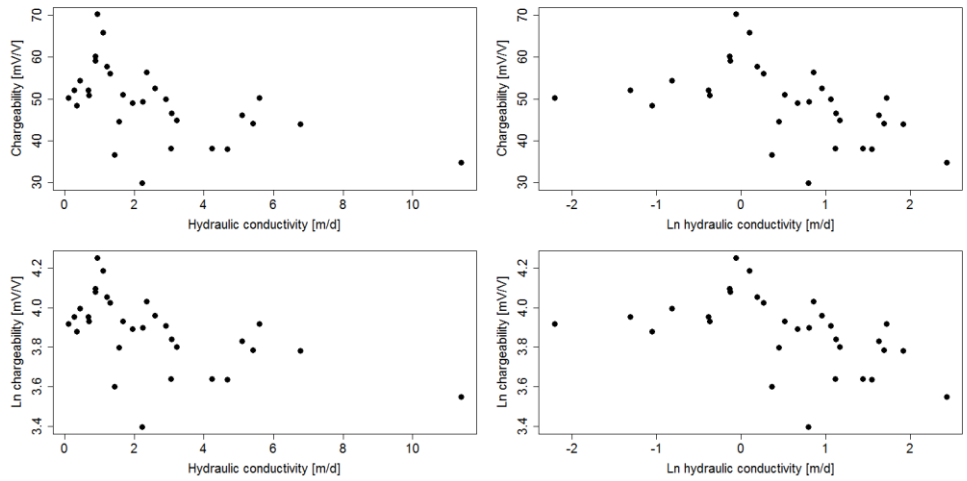

Figure 42 Scatterplots of hydraulic conductivity versus chargeability for deep depth data extracted with the second method, with and/or without logarithmic transformations of the parameters.

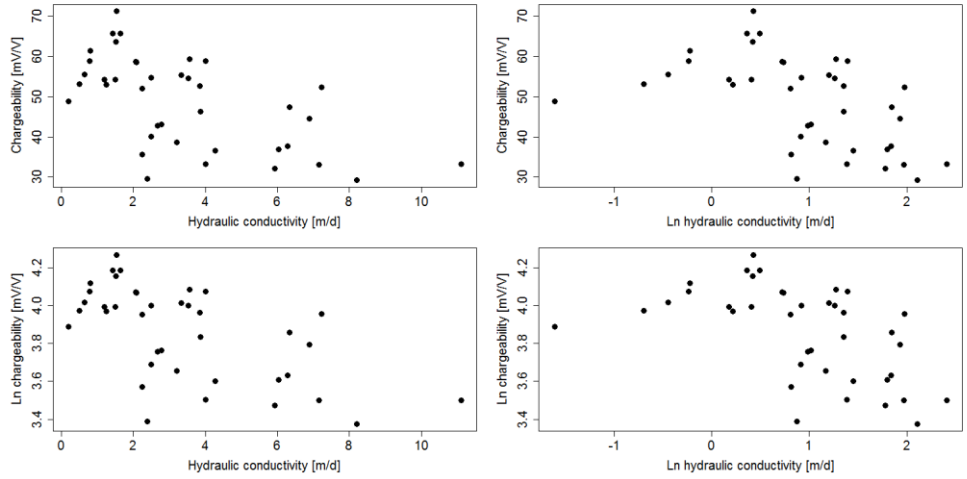

Figure 43 Scatterplots of hydraulic conductivity versus chargeability for harmonically averaged data extracted with the second method, with and/or without logarithmic transformations of the parameters.

iii. Method 3

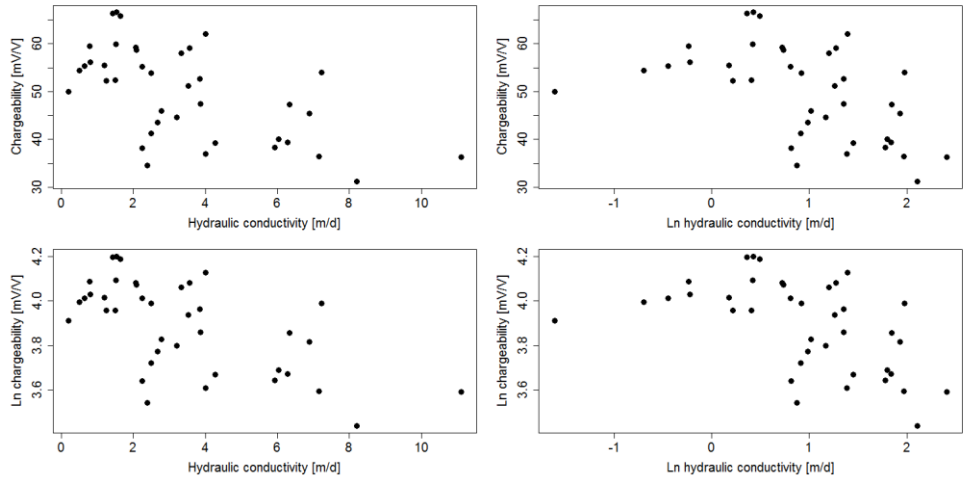

Figure 44 Scatterplots of harmonically averaged hydraulic conductivity versus chargeability for data extracted with the third method, with and/or without logarithmic transformations of the parameters.

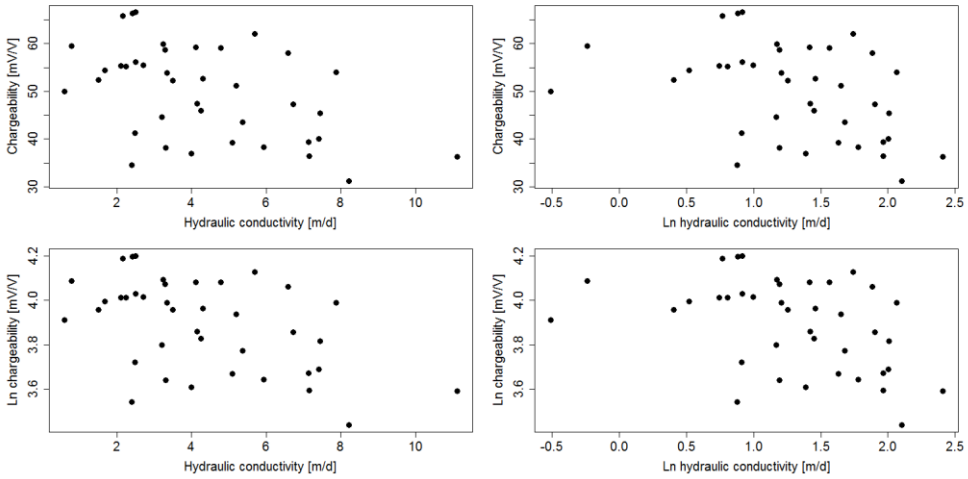

Figure 45 Scatterplots of arithmetically averaged hydraulic conductivity versus chargeability for data extracted with the third method, with and/or without logarithmic transformations of the parameters.

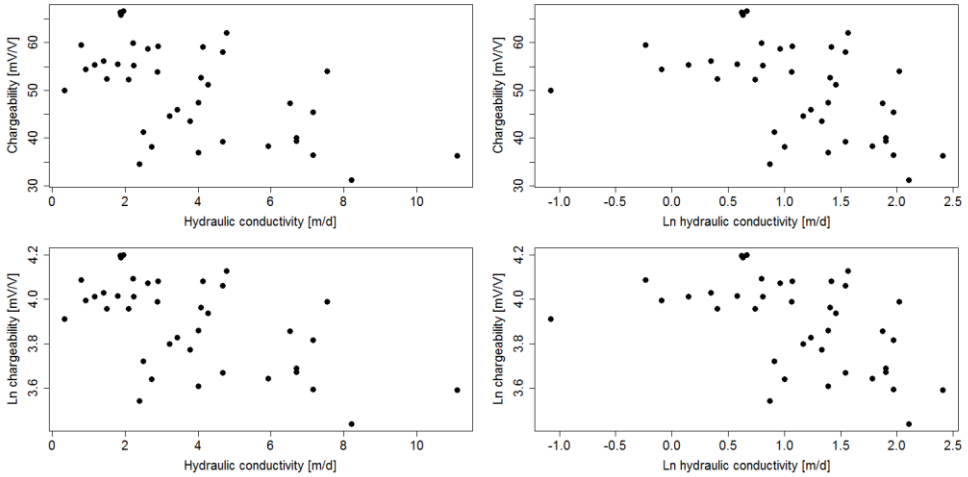

Figure 46 Scatterplots of geometrically averaged hydraulic conductivity versus chargeability for data extracted with the third method, with and/or without logarithmic transformations of the parameters.

iv. Method 4

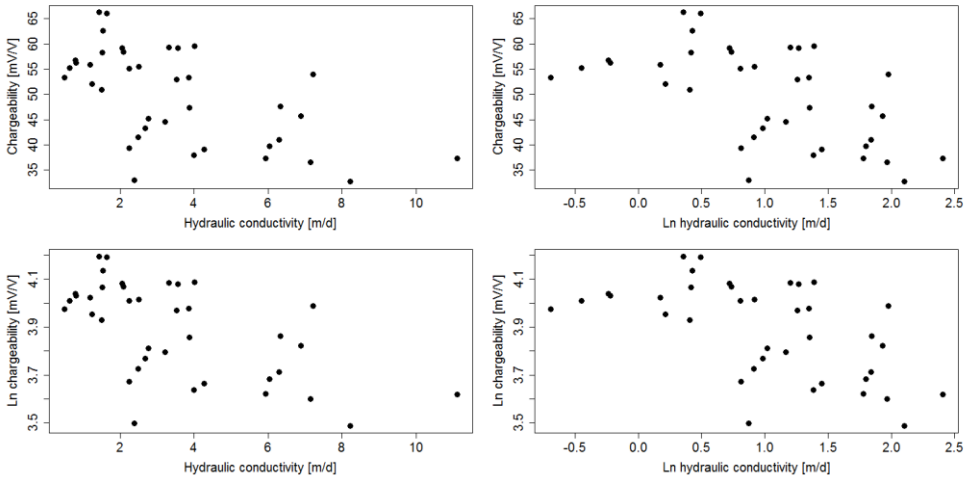

Figure 47 Scatterplots of harmonically averaged hydraulic conductivity versus chargeability for data extracted with the fourth method, with and/or without logarithmic transformations of the parameters.

C. SIGNIFICANT LINEAR REGRESSIONS

i. Method 1

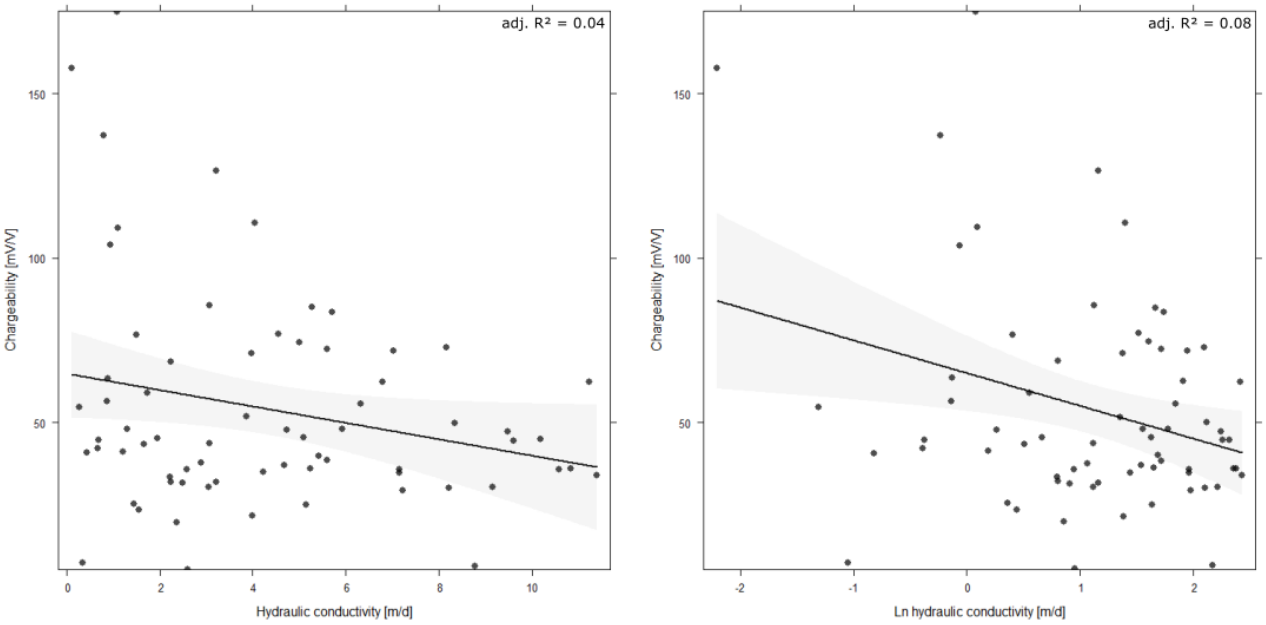

Figure 48 Significant linear models fitted to the scatterplots of hydraulic conductivity versus chargeability of all data extracted with method 1, without logarithmic transformation of chargeability. The grey bands indicate the 95 % confidence interval of the fits.

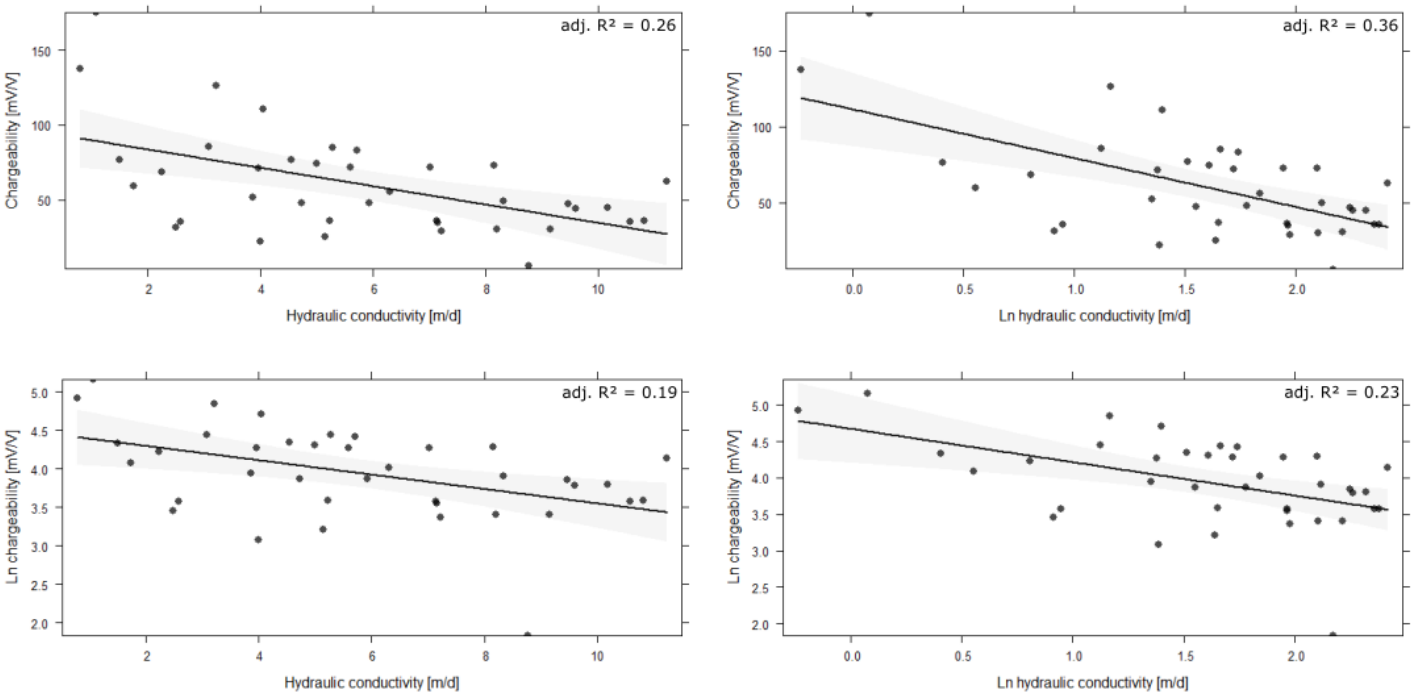

Figure 49 Significant linear models fitted to the scatterplots of hydraulic conductivity versus chargeability of shallow depth data extracted with method 1, with and/or without logarithmic transformations of the parameters. The grey bands indicate the 95 % confidence interval of the fits.

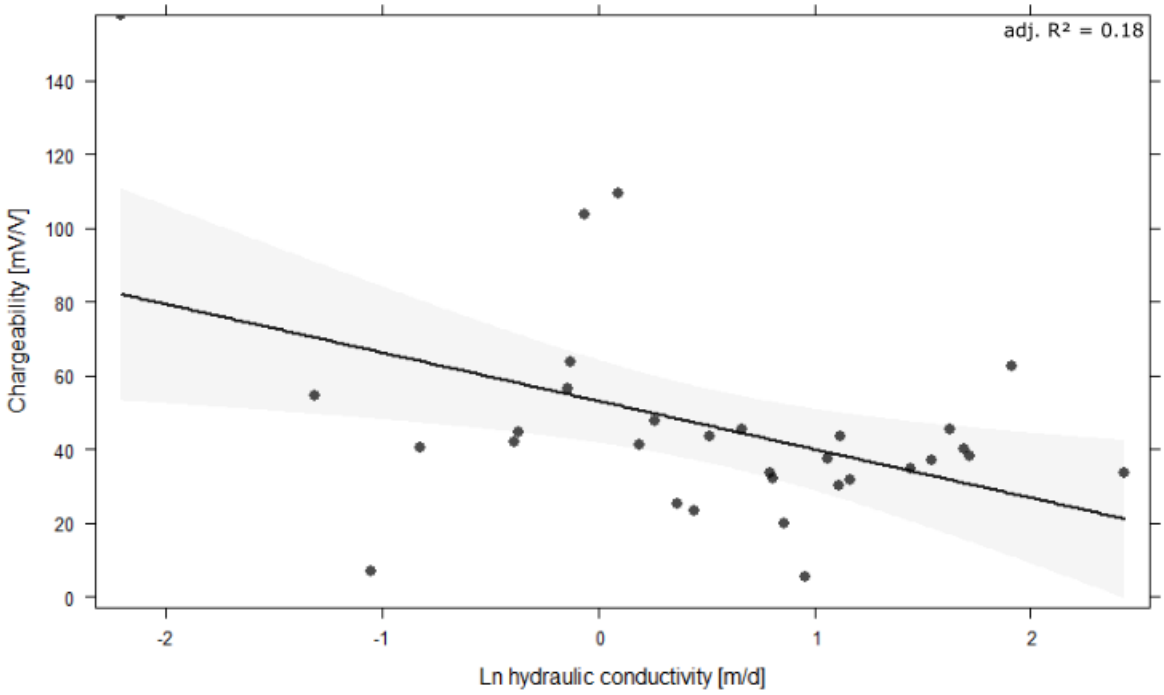

Figure 50 Significant linear models fitted to the scatterplots of hydraulic conductivity versus chargeability of deep depth data extracted with method 1, with transformation of hydraulic conductivity and untransformed chargeability. The grey bands indicate the 95 % confidence interval of the fit.

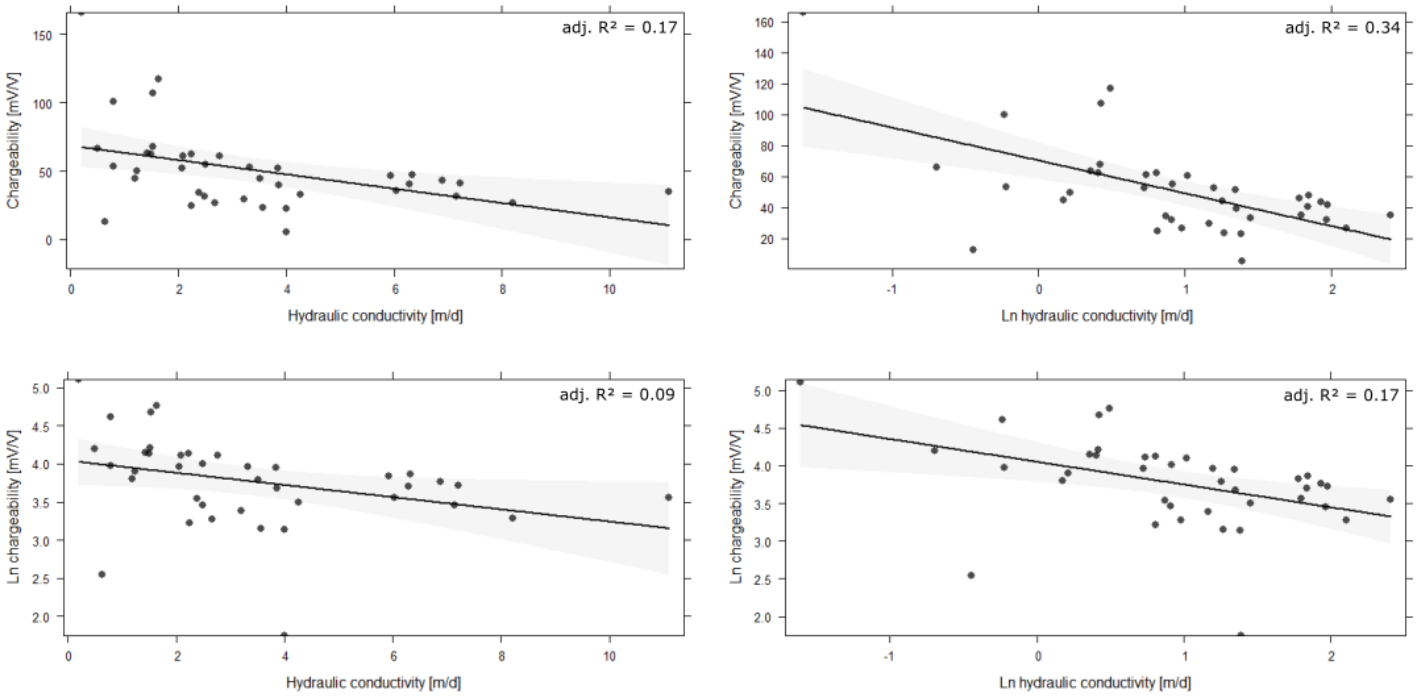

Figure 51 Significant linear models fitted to the scatterplots of hydraulic conductivity versus chargeability of harmonically averaged data extracted with method 1, with and/or without logarithmic transformations of the parameters. The grey bands indicate the 95 % confidence interval of the fits.

ii. Method 2

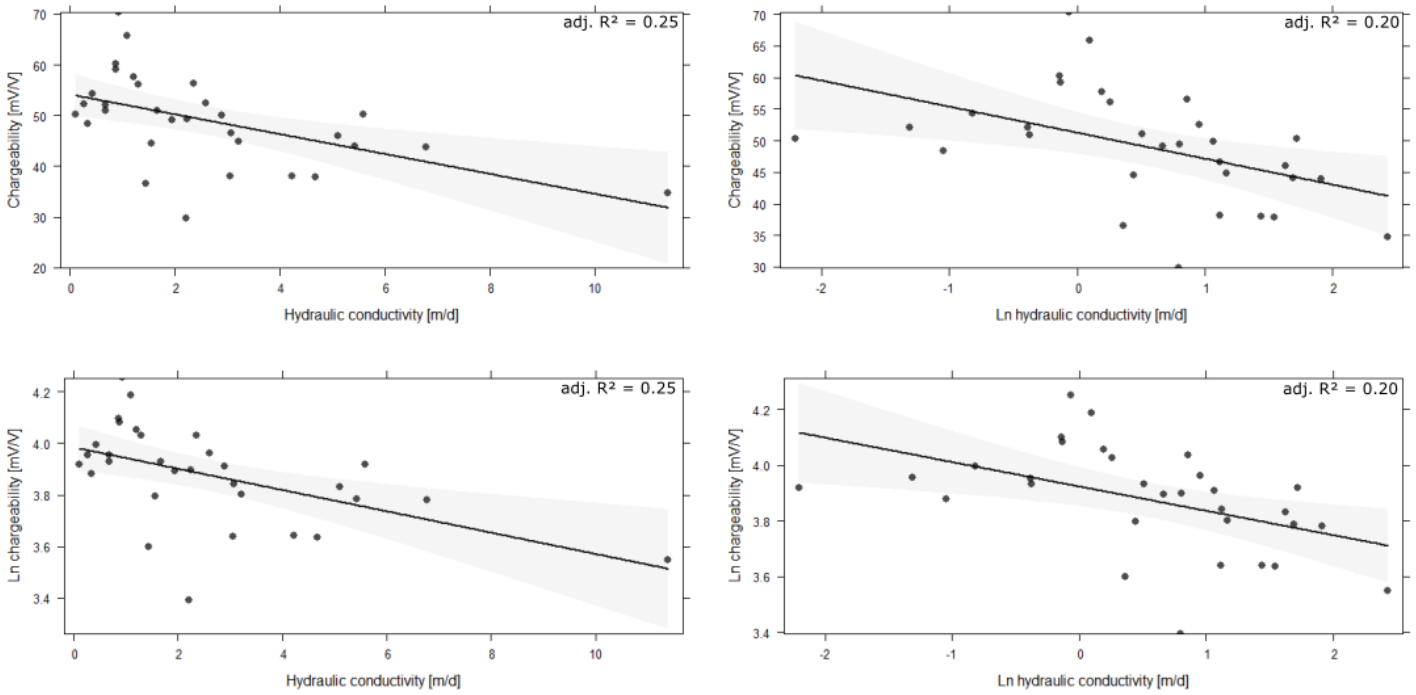

Figure 52 Significant linear models fitted to the scatterplots of hydraulic conductivity versus chargeability of deep depth data extracted with method 2, with and/or without logarithmic transformations of the parameters. The grey bands indicate the 95 % confidence interval of the fits.

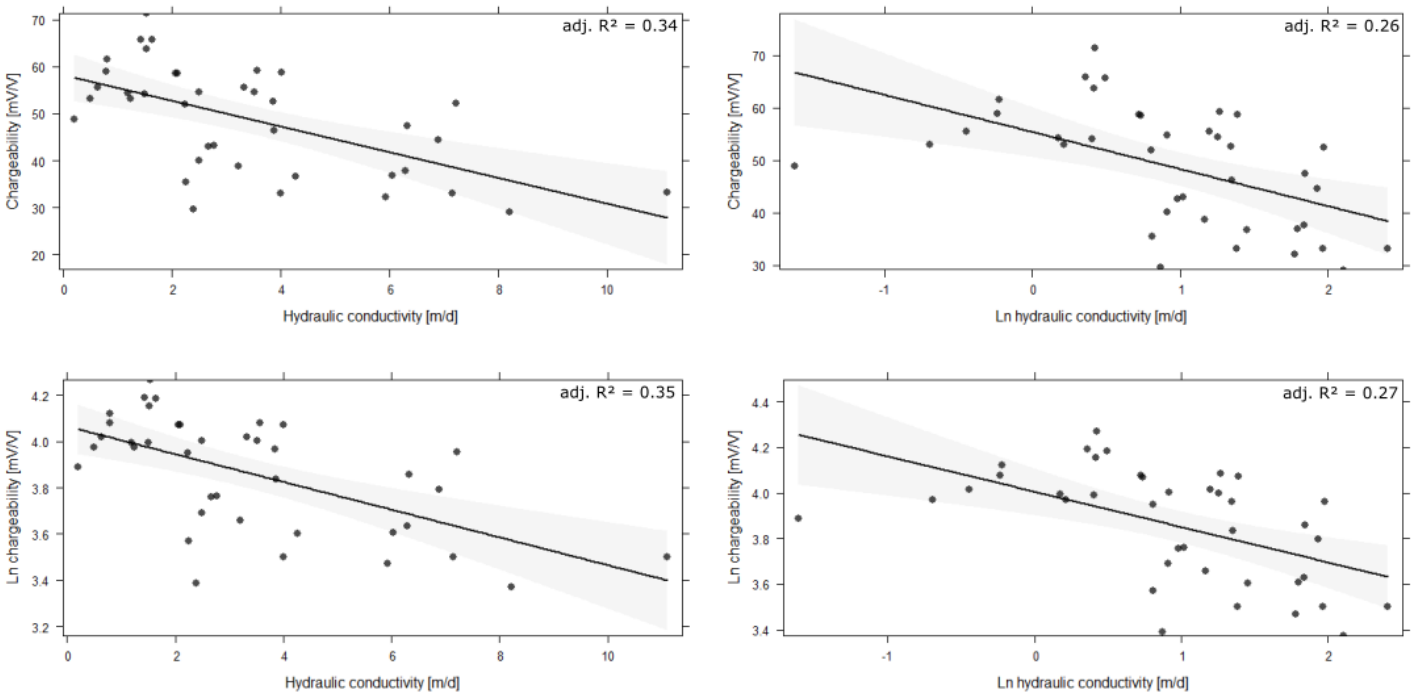

Figure 53 Significant linear models fitted to the scatterplots of hydraulic conductivity versus chargeability of harmonically averaged data extracted with method 2, with and/or without logarithmic transformations of the parameters. The grey bands indicate the 95 % confidence interval of the fits.

iii. Method 3

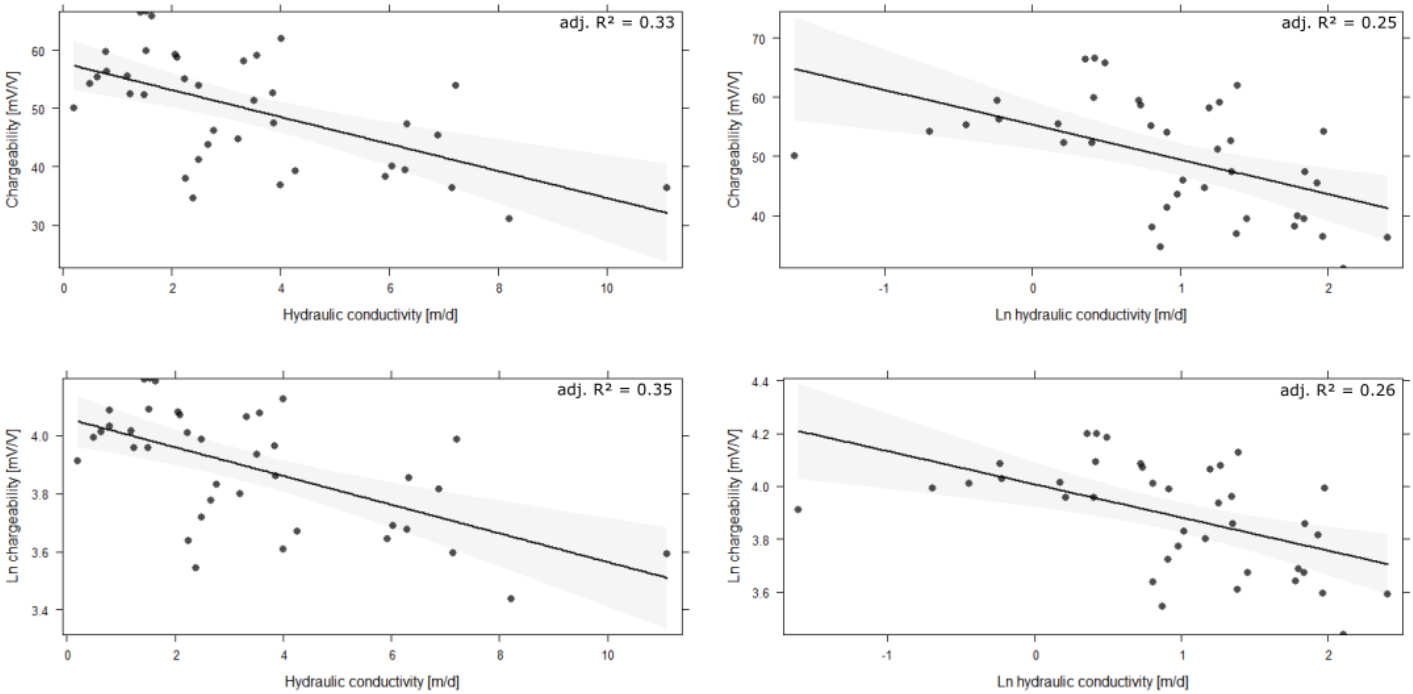

Figure 54 Significant linear models fitted to the scatterplots of harmonically averaged hydraulic conductivity versus chargeability of data extracted with method 3, with and/or without logarithmic transformations of the parameters. The grey bands indicate the 95 % confidence interval of the fits.

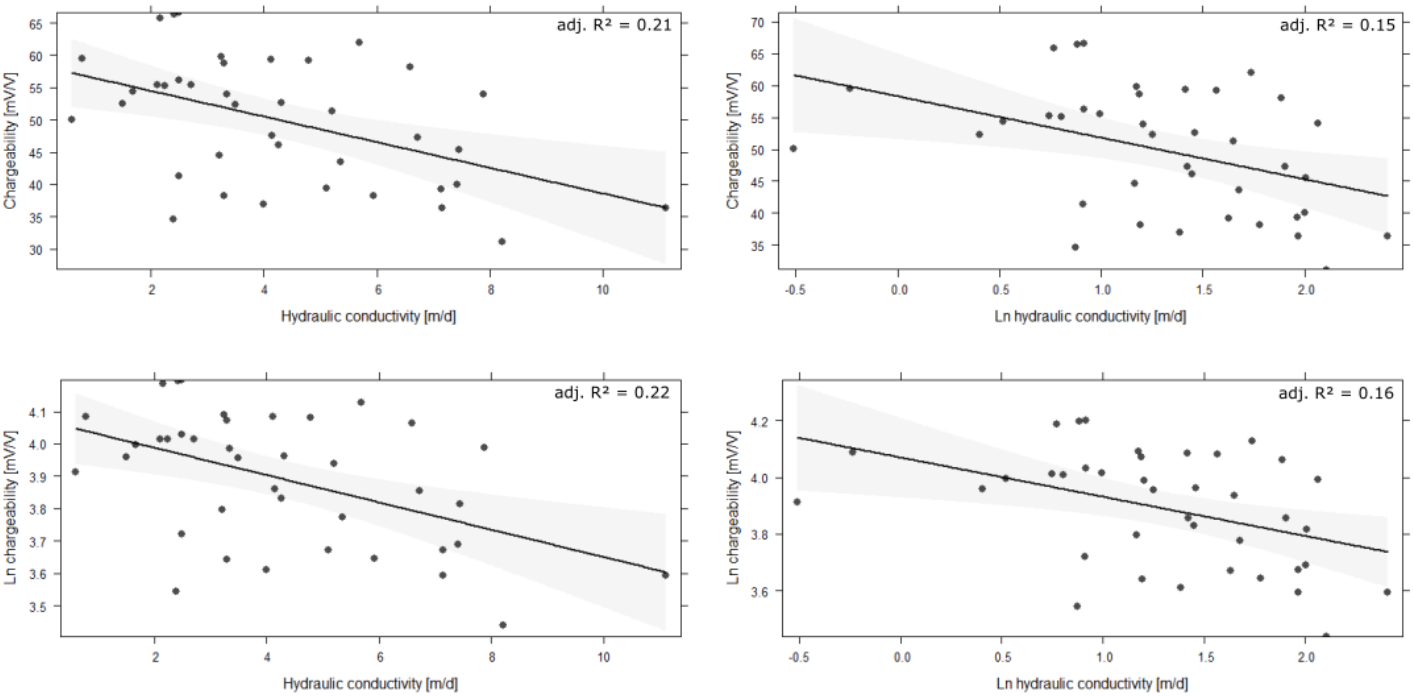

Figure 55 Significant linear models fitted to the scatterplots of arithmetically averaged hydraulic conductivity versus chargeability of data extracted with method 3, with and/or without logarithmic transformations of the parameters. The grey bands indicate the 95 % confidence interval of the fits.

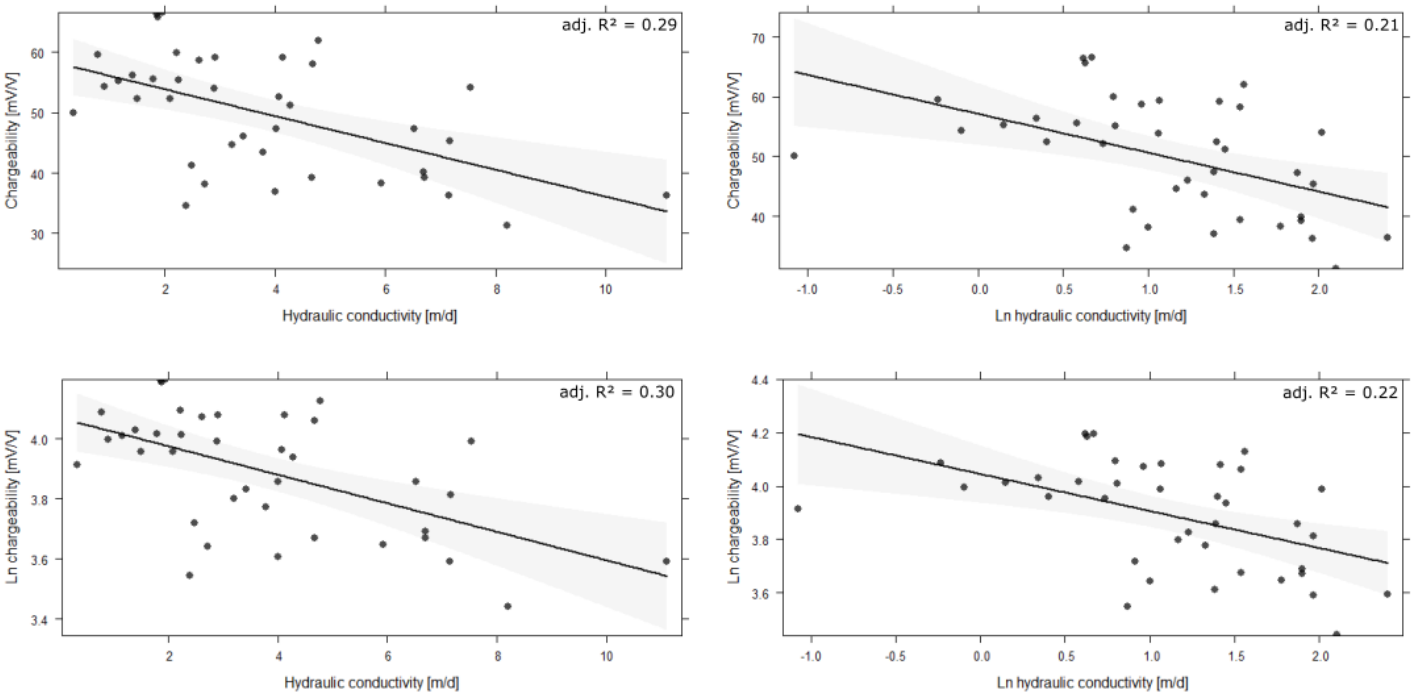

Figure 56 Significant linear models fitted to the scatterplots of geometrically averaged hydraulic conductivity versus chargeability of data extracted with method 3, with and/or without logarithmic transformations of the parameters. The grey bands indicate the 95 % confidence interval of the fits.

iv. Method 4

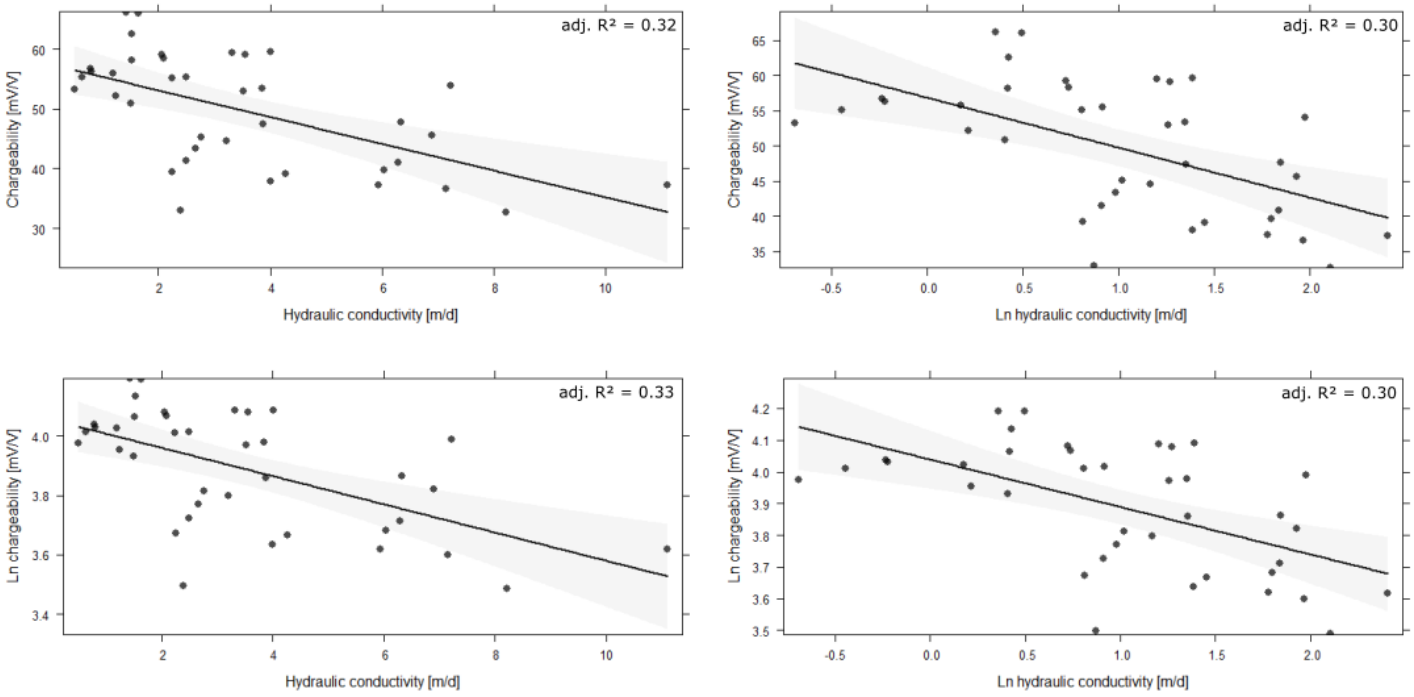

Figure 57 Significant linear models fitted to the scatterplots of harmonically averaged hydraulic conductivity versus chargeability of data extracted with method 4, with and/or without logarithmic transformations of the parameters. The grey bands indicate the 95 % confidence interval of the fits.

7 APPENDIX G: HYDRAULIC CONDUCTIVITY & NORMALIZED CHARGEABILITY

a. SPATIAL DISTRIBUTIONS

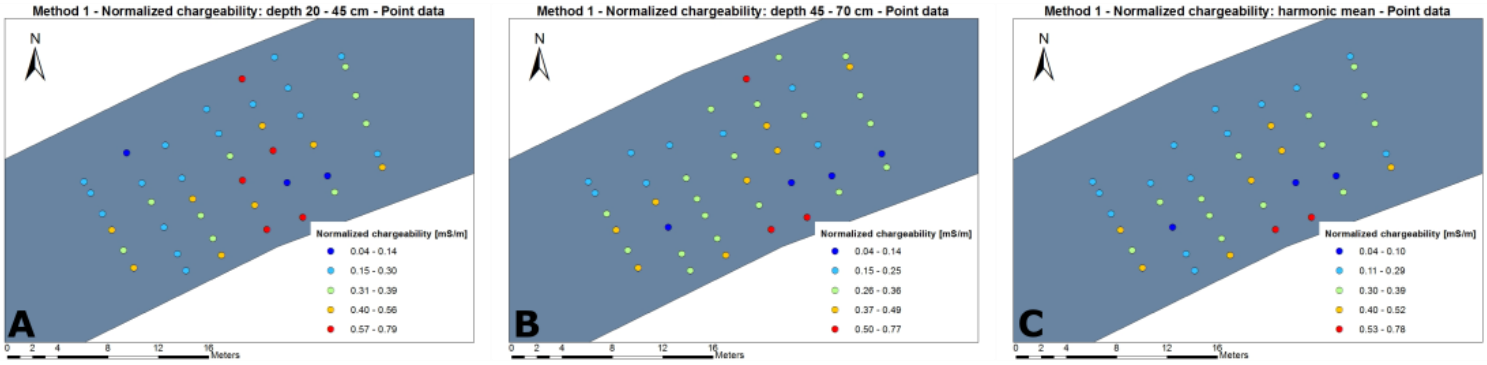

Figure 58 Point maps of normalized chargeability data extracted with method 1. Point data (A) at shallow depth, (B) at deep depth, (C) harmonically averaged over the two depth intervals.

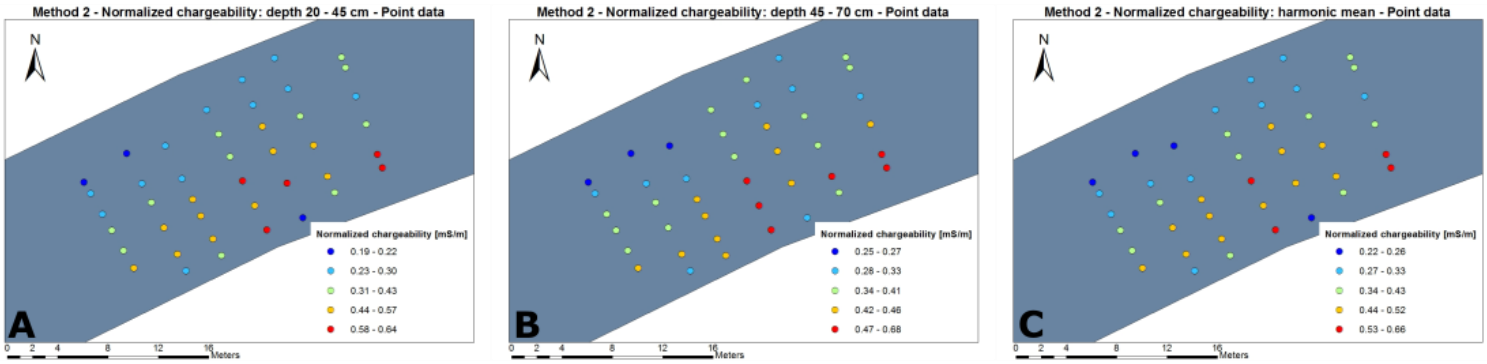

Figure 59 Point maps of normalized chargeability data extracted with method 2. Point data (A) at shallow depth, (B) at deep depth, (C) harmonically averaged over the two depth intervals.

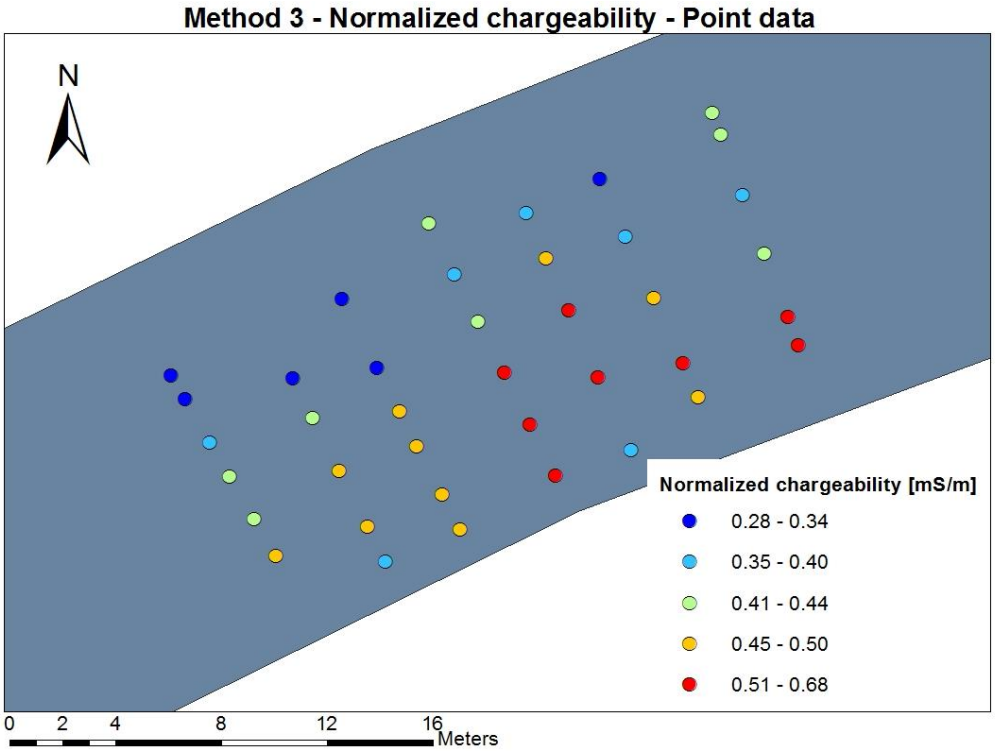

Figure 60 Point map of normalized chargeability data extracted with method 3.

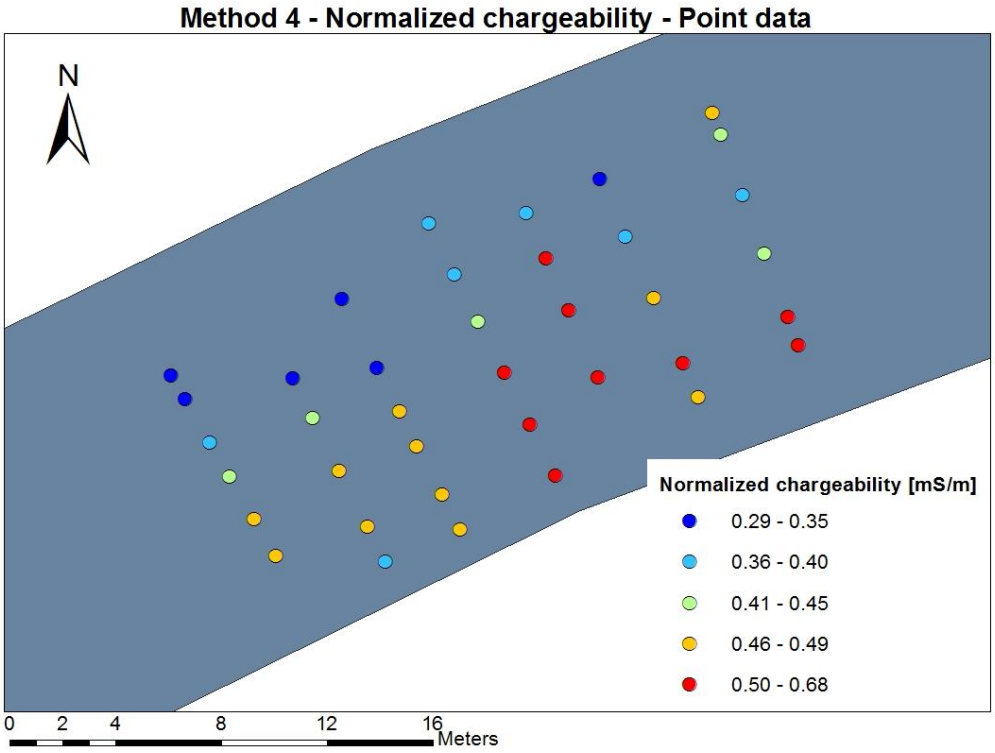

Figure 61 Point map of normalized chargeability data extracted with method 4.

b. SCATTERPLOTS

i. Method 1

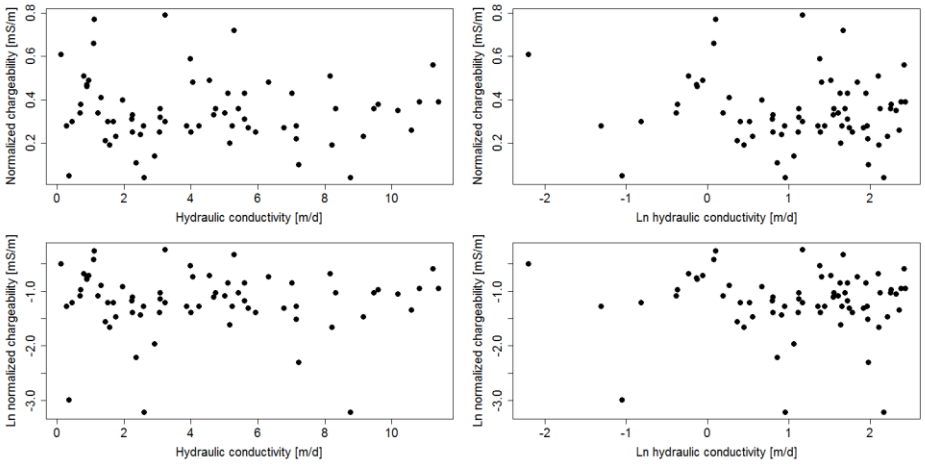

Figure 62 Scatterplots of hydraulic conductivity versus normalized chargeability for all data extracted with the first method, with and/or without logarithmic transformations of the parameters.

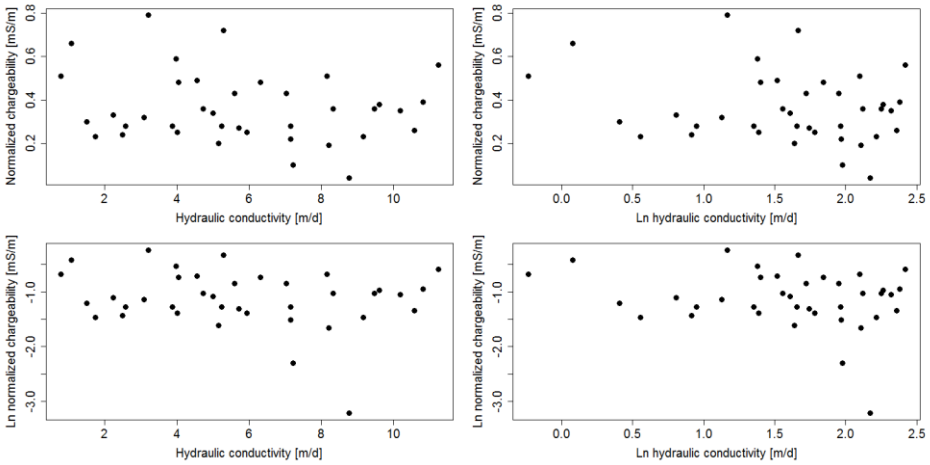

Figure 63 Scatterplots of hydraulic conductivity versus normalized chargeability for shallow depth data extracted with the first method, with and/or without logarithmic transformations of the parameters.

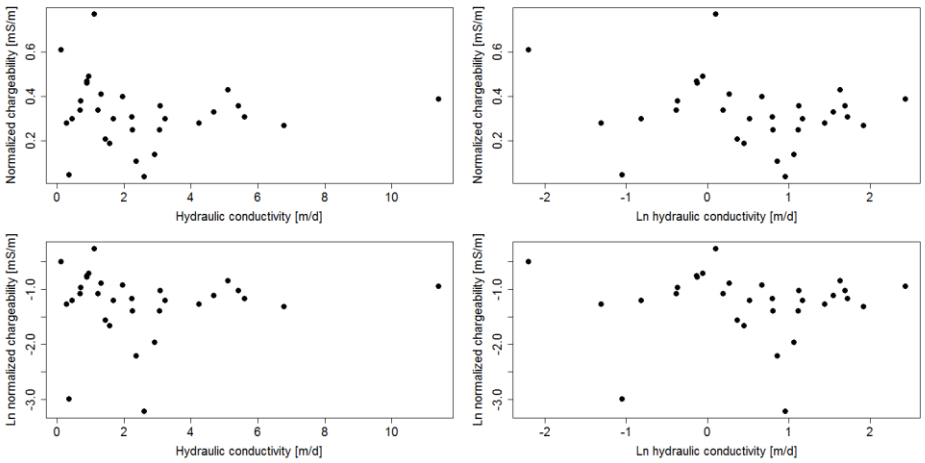

Figure 64 Scatterplots of hydraulic conductivity versus normalized chargeability for deep depth data extracted with the first method, with and/or without logarithmic transformations of the parameters.

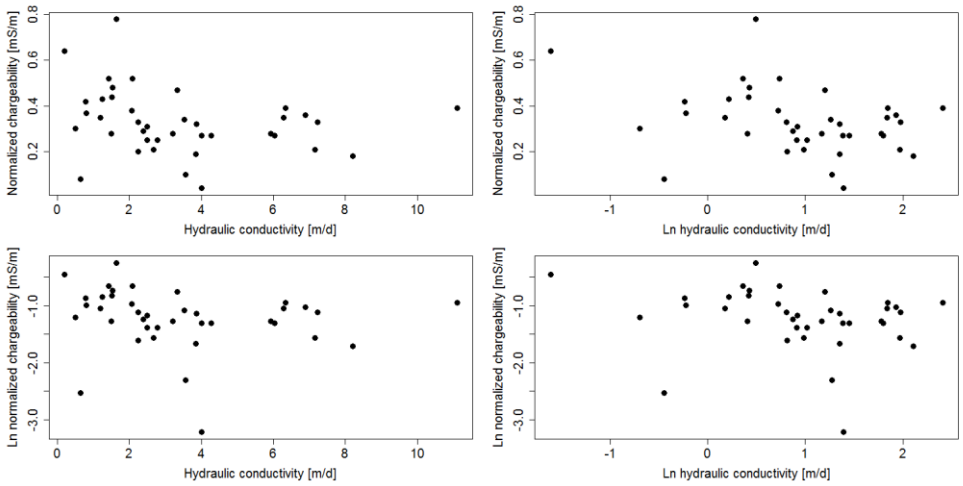

Figure 65 Scatterplots of hydraulic conductivity versus normalized chargeability for harmonically averaged data extracted with the first method, with and/or without logarithmic transformations of the parameters.

ii. Method 2

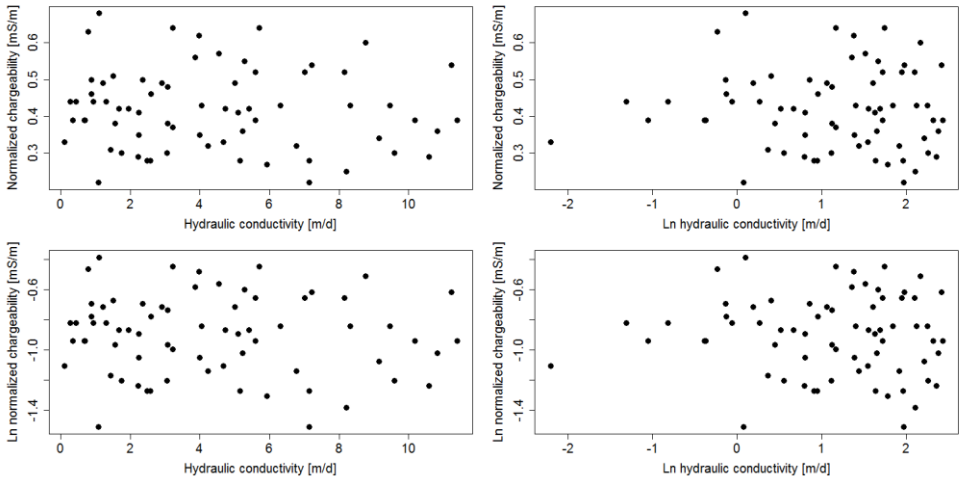

Figure 66 Scatterplots of hydraulic conductivity versus normalized chargeability for all data extracted with the second method, with and/or without logarithmic transformations of the parameters.

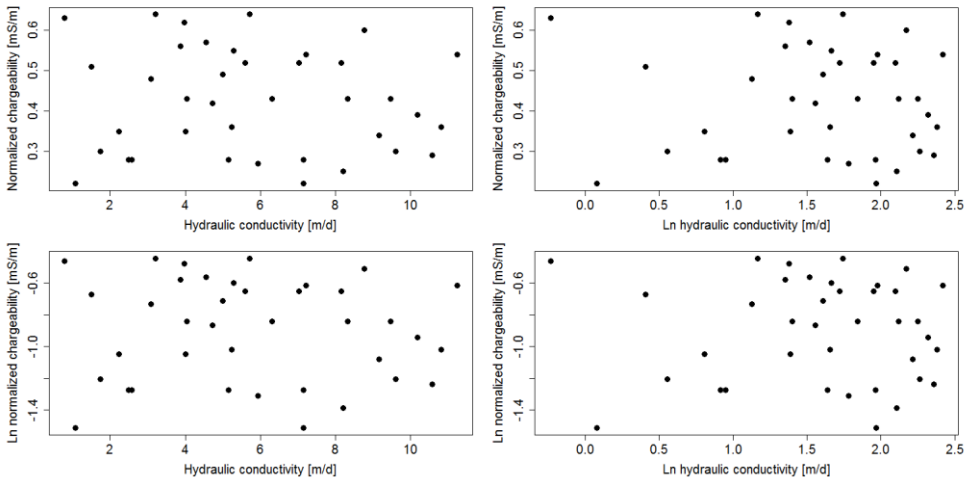

Figure 67 Scatterplots of hydraulic conductivity versus normalized chargeability for shallow depth data extracted with the second method, with and/or without logarithmic transformations of the parameters.

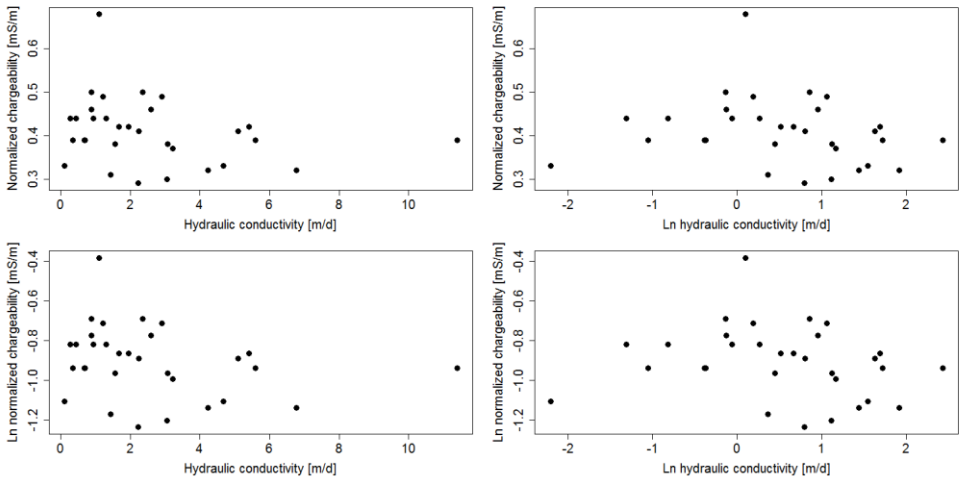

Figure 68 Scatterplots of hydraulic conductivity versus normalized chargeability for deep depth data extracted with the second method, with and/or without logarithmic transformations of the parameters.

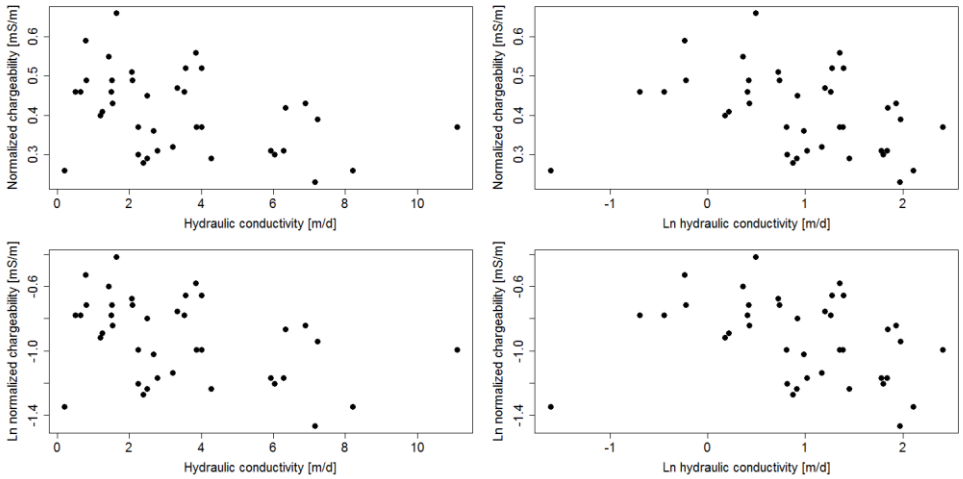

Figure 69 Scatterplots of hydraulic conductivity versus normalized chargeability for harmonically averaged data extracted with the second method, with and/or without logarithmic transformations of the parameters.

iii. Method 3

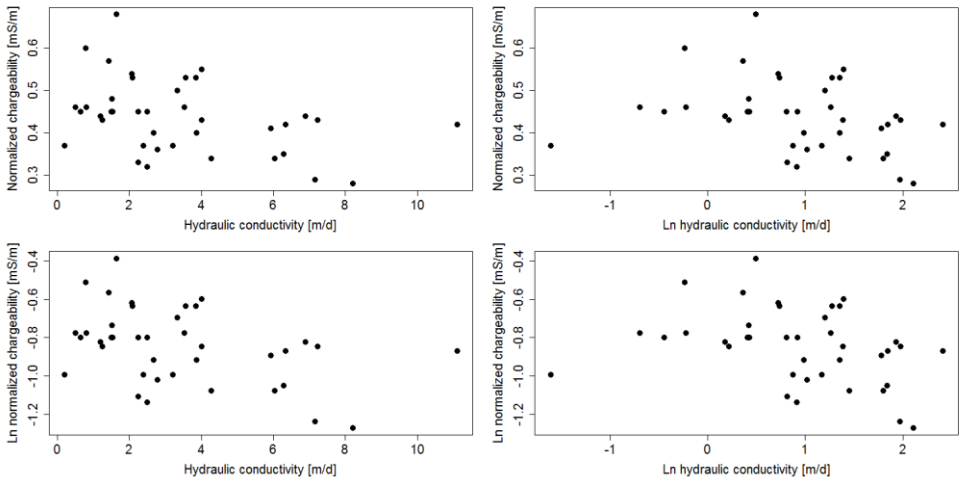

Figure 70 Scatterplots of harmonically averaged hydraulic conductivity versus normalized chargeability for data extracted with the third method, with and/or without logarithmic transformations of the parameters.

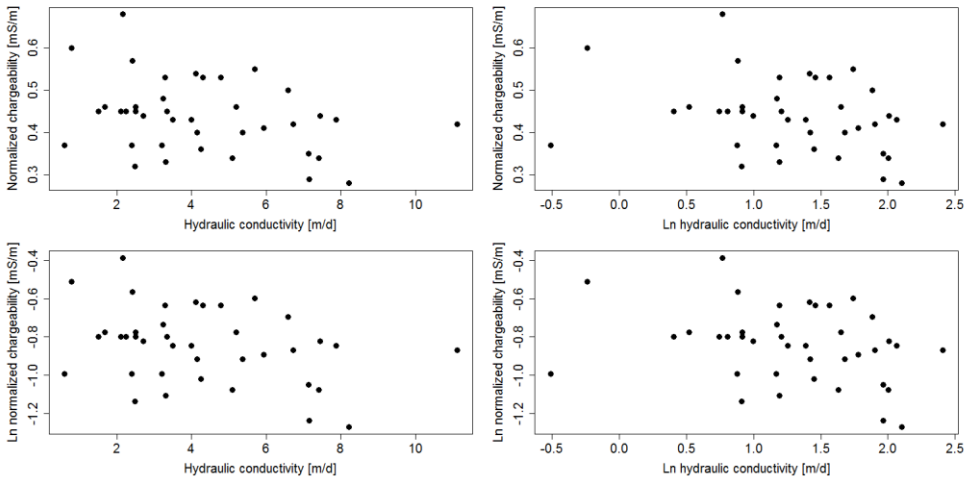

Figure 71 Scatterplots of arithmetically averaged hydraulic conductivity versus normalized chargeability for data extracted with the third method, with and/or without logarithmic transformations of the parameters.

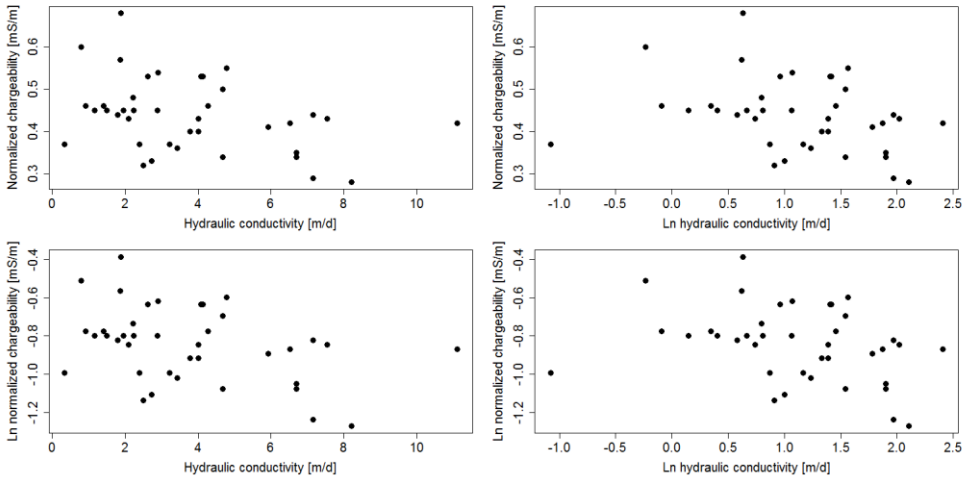

Figure 72 Scatterplots of geometrically averaged hydraulic conductivity versus normalized chargeability for data extracted with the third method, with and/or without logarithmic transformations of the parameters.

iv. Method 4

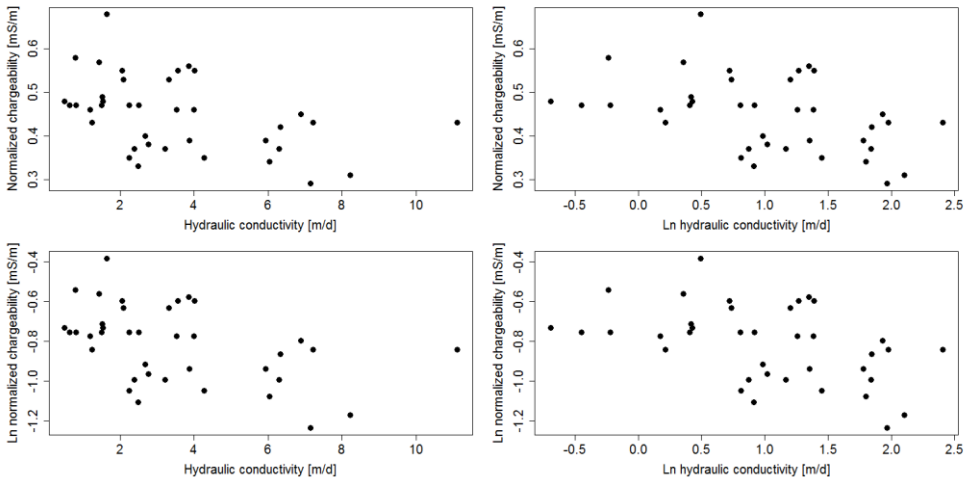

Figure 73 Scatterplots of harmonically averaged hydraulic conductivity versus normalized chargeability for data extracted with the fourth method, with and/or without logarithmic transformations of the parameters.

C. SIGNIFICANT LINEAR REGRESSIONS

i. Method 1

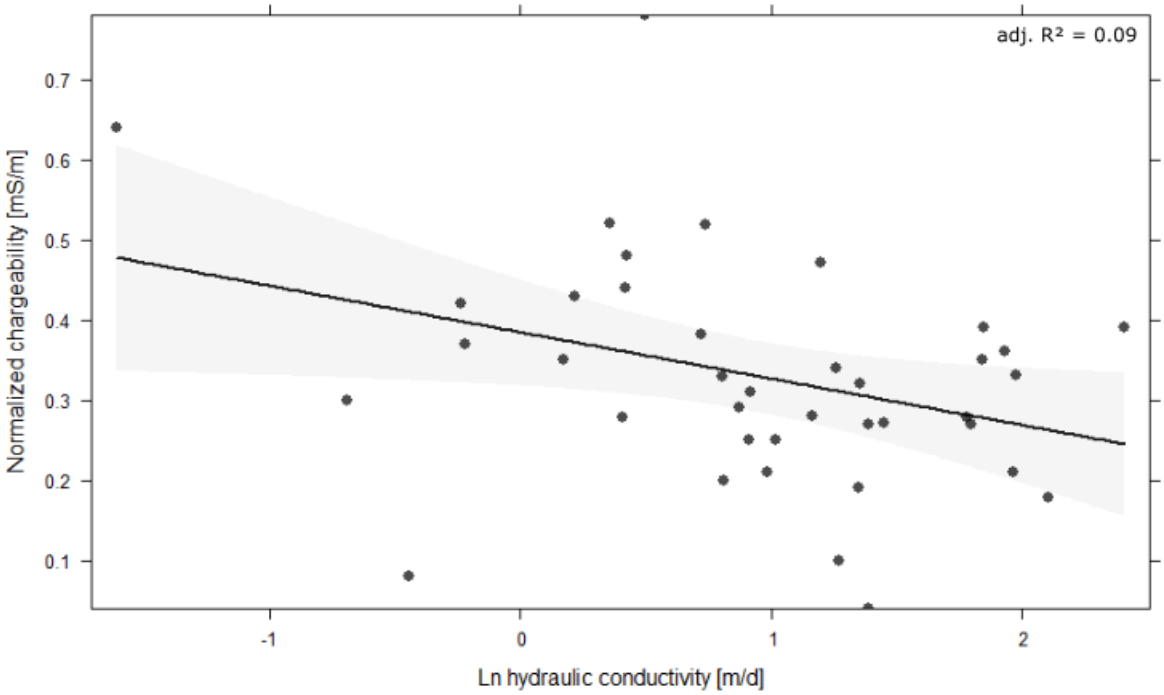

Figure 74 Significant linear models fitted to the scatterplots of hydraulic conductivity versus normalized chargeability of harmonically averaged data extracted with method 1, with logarithmic transformation of hydraulic conductivity and untransformed normalized chargeability. The grey bands indicate the 95 % confidence interval of the fit.

ii. Method 2

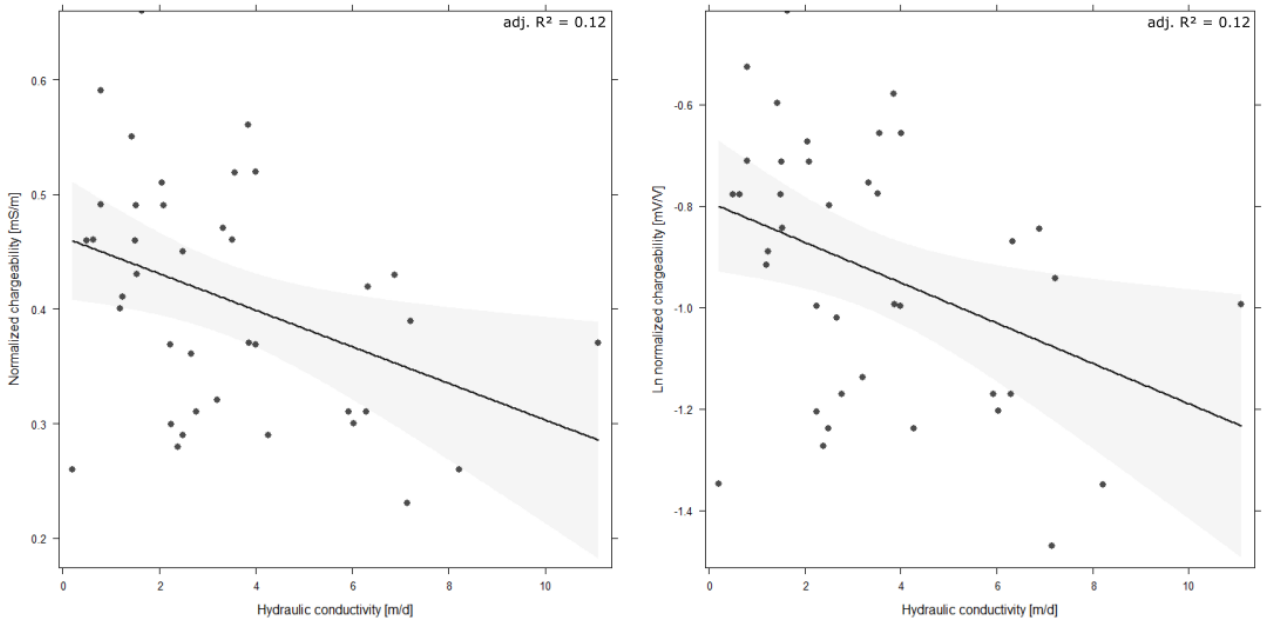

Figure 75 Significant linear models fitted to the scatterplots of hydraulic conductivity versus normalized chargeability of harmonically averaged data extracted with method 2, without logarithmic transformation of hydraulic conductivity. The grey bands indicate the 95 % confidence interval of the fits.

iii. Method 3

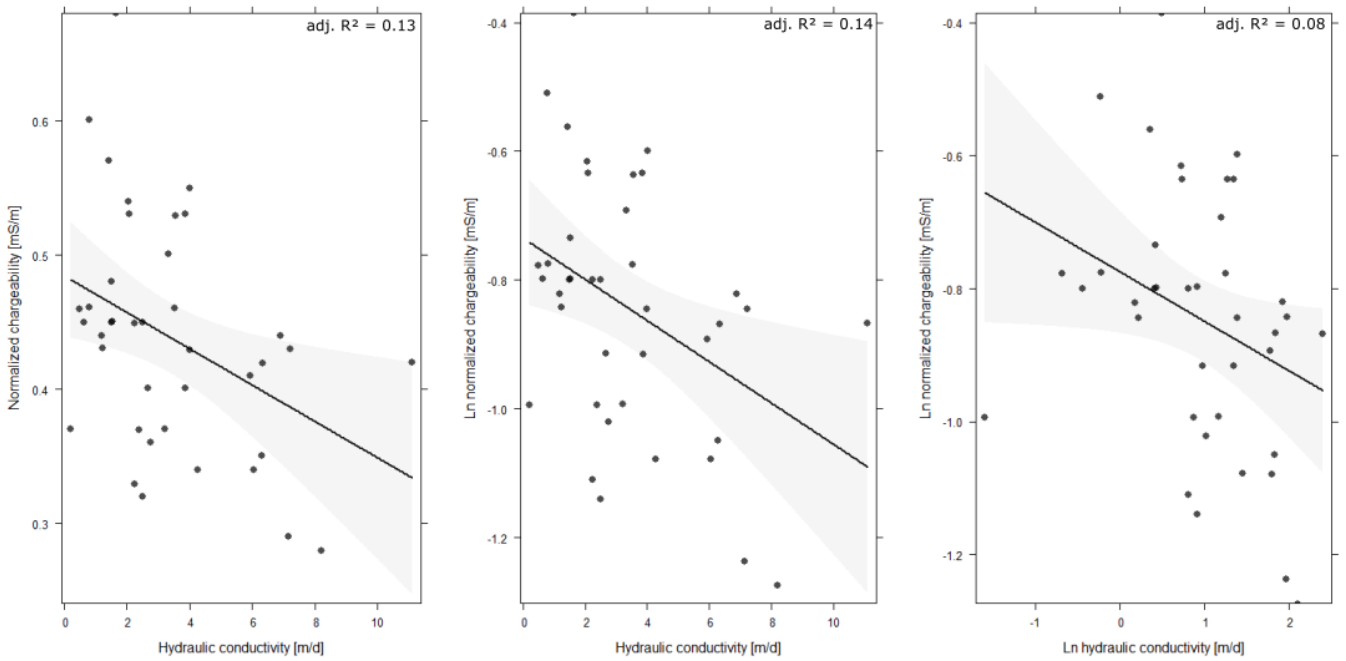

Figure 76 Significant linear models fitted to the scatterplots of harmonically averaged hydraulic conductivity versus normalized chargeability of data extracted with method 3, with and/or without logarithmic transformations of the parameters. The grey bands indicate the 95 % confidence interval of the fits.

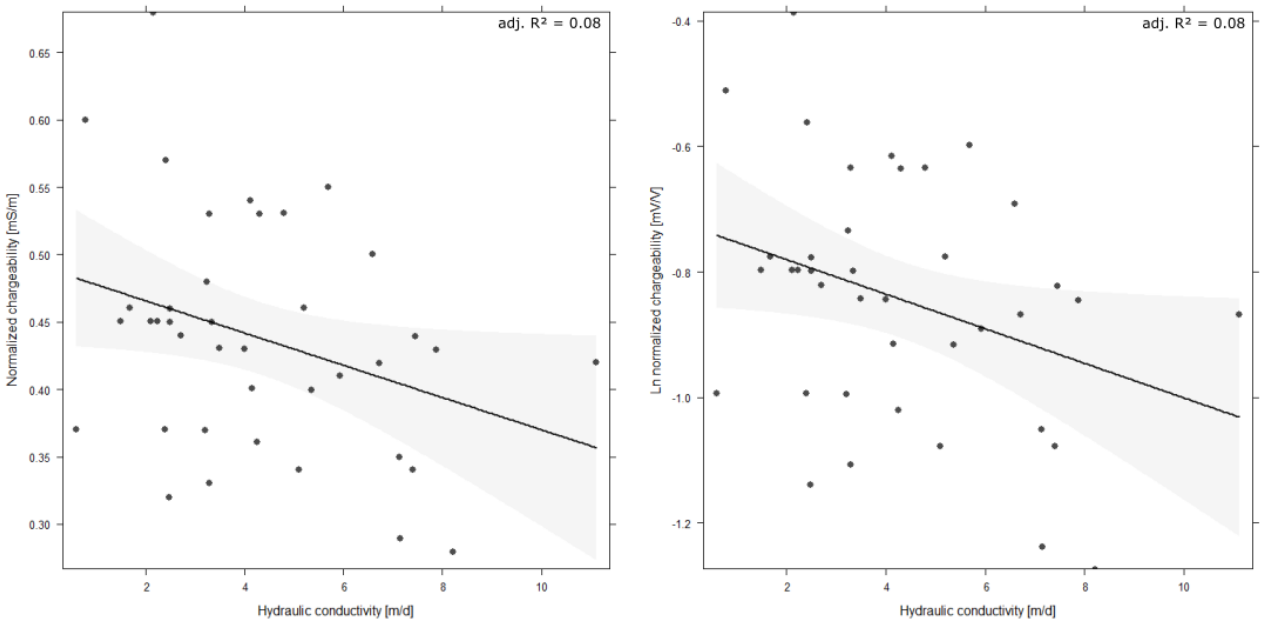

Figure 77 Significant linear models fitted to the scatterplots of arithmetically averaged hydraulic conductivity versus normalized chargeability of data extracted with method 3, without logarithmic transformation of hydraulic conductivity. The grey bands indicate the 95 % confidence interval of the fits.

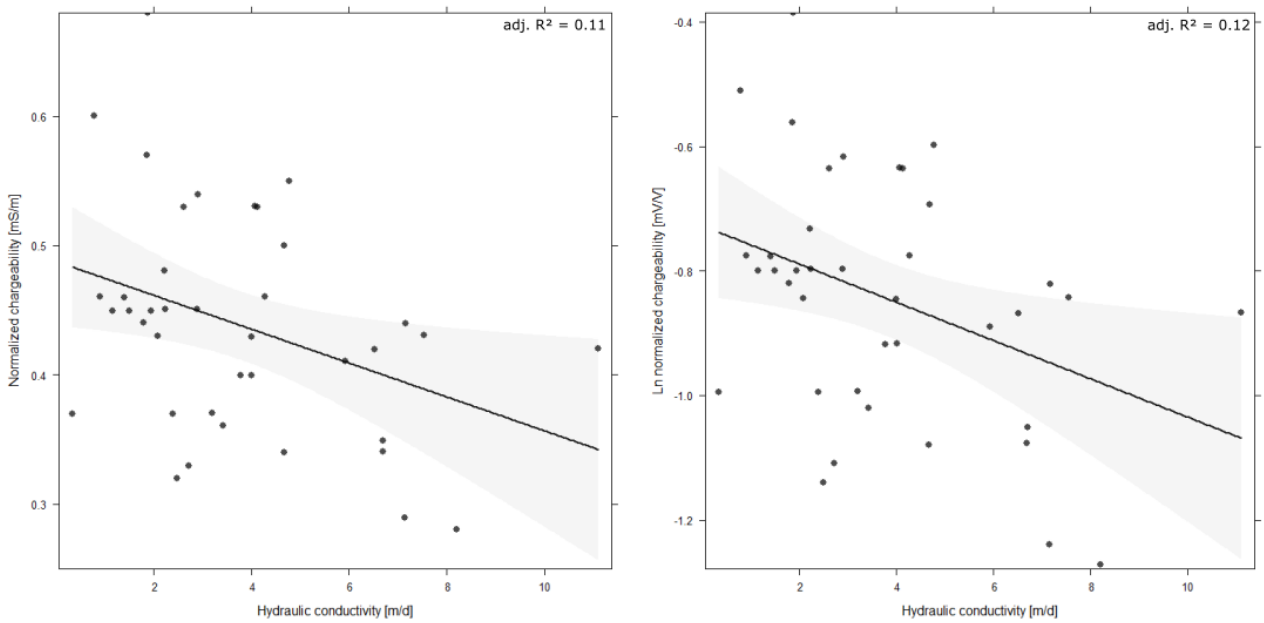

Figure 78 Significant linear models fitted to the scatterplots of geometrically averaged hydraulic conductivity versus normalized chargeability of data extracted with method 3, without logarithmic transformation of hydraulic conductivity. The grey bands indicate the 95 % confidence interval of the fits.

iv. Method 4

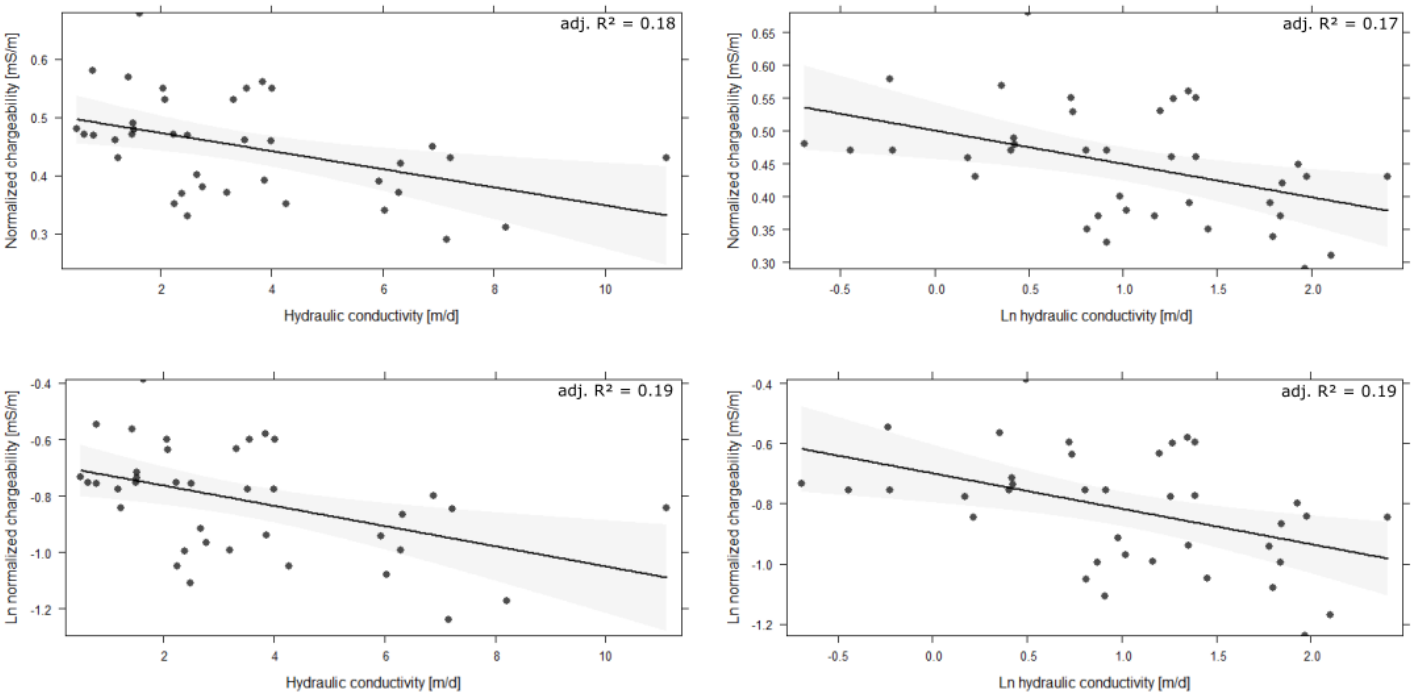

Figure 79 Significant linear models fitted to the scatterplots of harmonically averaged hydraulic conductivity versus normalized chargeability of data extracted with method 4, with and/or without logarithmic transformations of the parameters. The grey bands indicate the 95 % confidence interval of the fits.

8 APPENDIX H: CLUSTERING

a. SCATTERPLOTS OF VISUAL CLUSTERING BASED ON K – M/MN CORRELATION

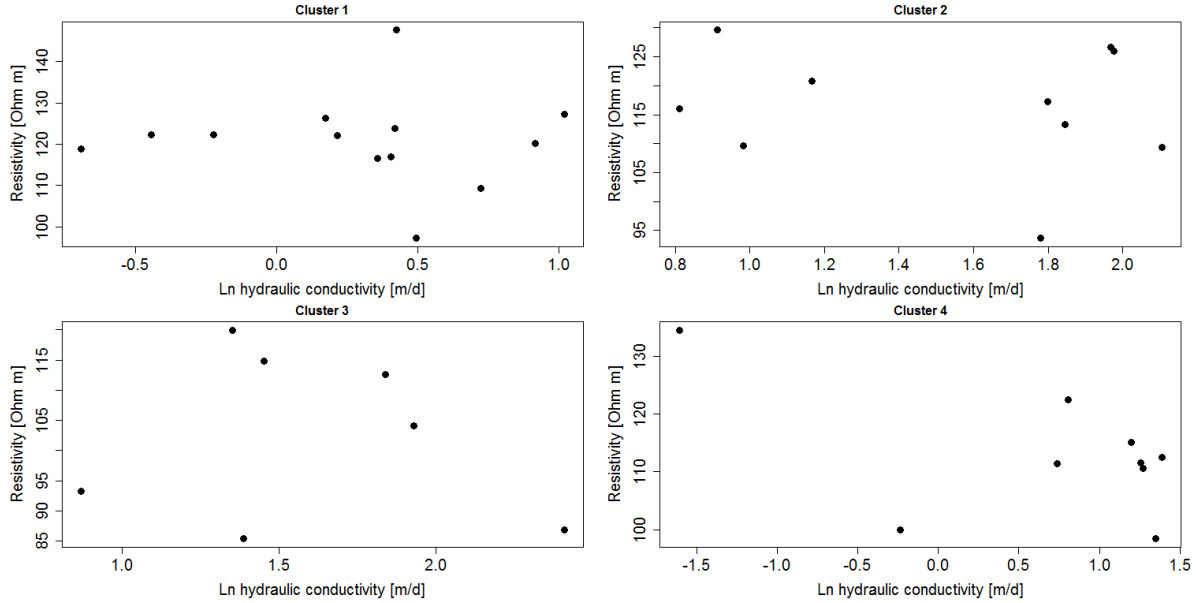

Figure 80 Scatterplots of ln(hydraulic conductivity) versus resistivity for data within the clusters, based on visual correlation between K and M/MN.

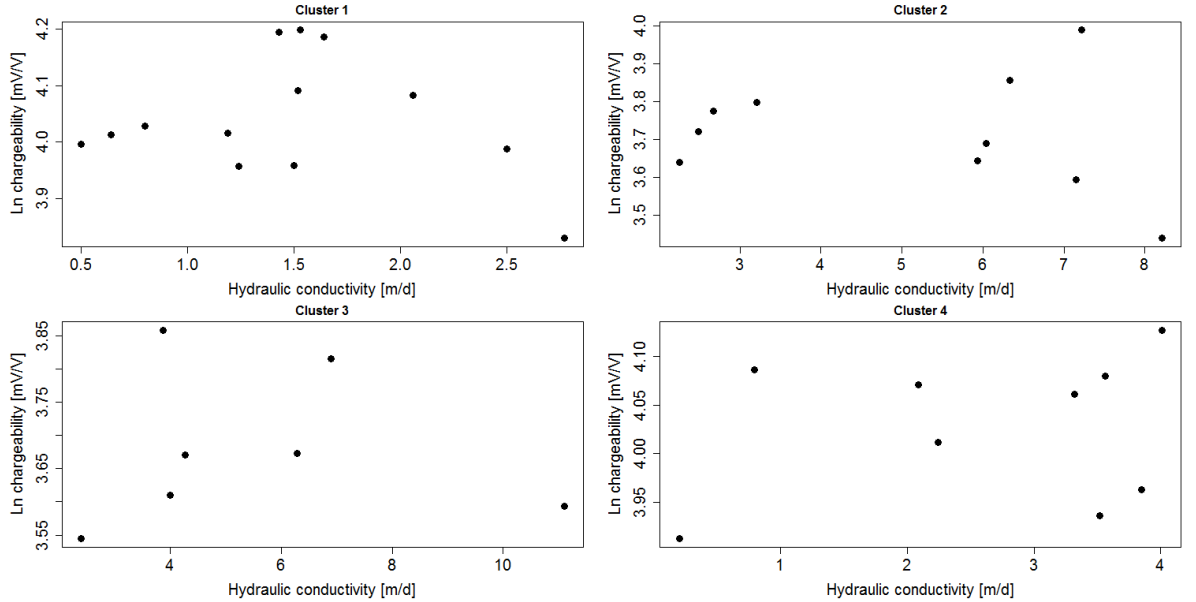

Figure 81 Scatterplots of hydraulic conductivity versus ln(chargeability) for data within the clusters, based on visual correlation between K and M/MN.

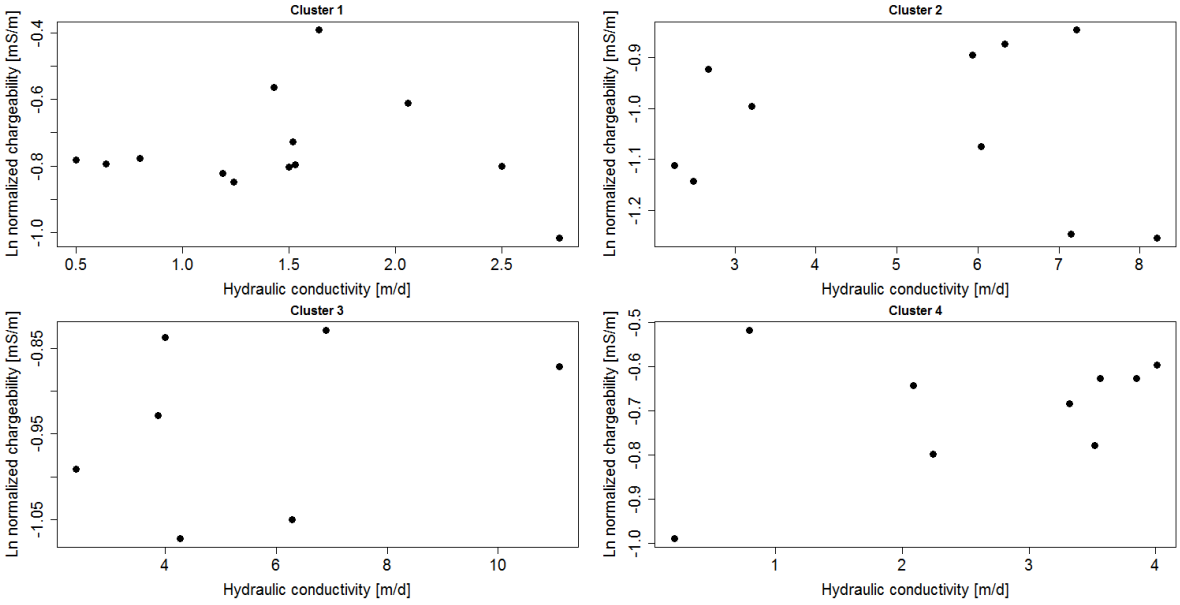

Figure 82 Scatterplots of hydraulic conductivity versus ln(normalized chargeability) for data within the clusters, based on visual correlation between K and M/MN.

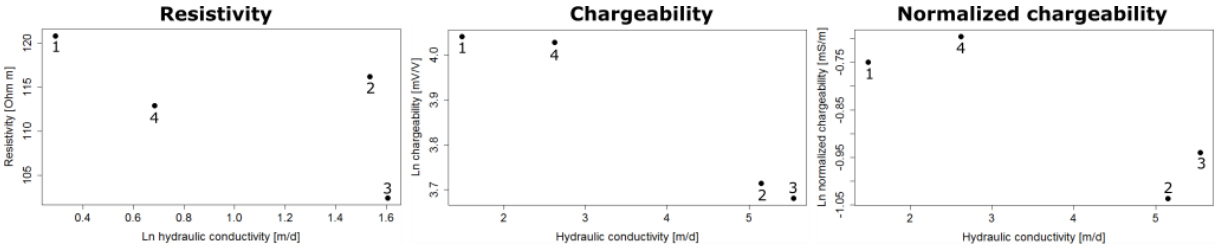

Figure 83 Scatterplots of the mean values of the parameters in the clusters, based on visual correlation between K and M/MN. The numbers indicate the number of the cluster.

b. SCATTERPLOTS OF VISUAL CLUSTERING BASED ON K – P CORRELATION

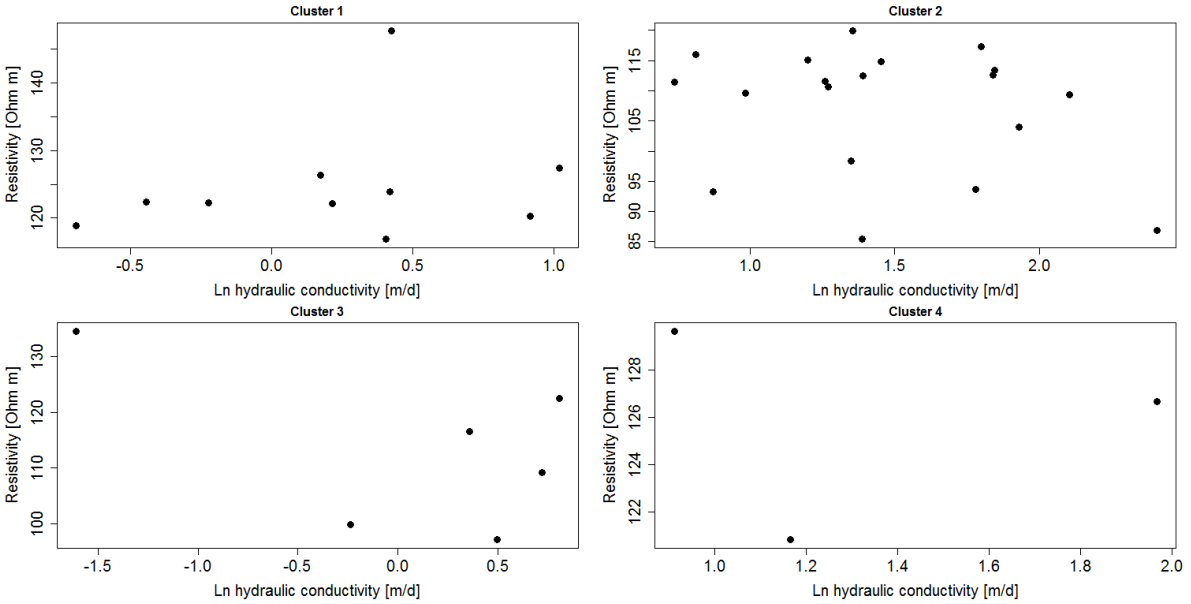

Figure 84 Scatterplots of ln(hydraulic conductivity) versus resistivity for data within the clusters, based on visual correlation between K and ρ.

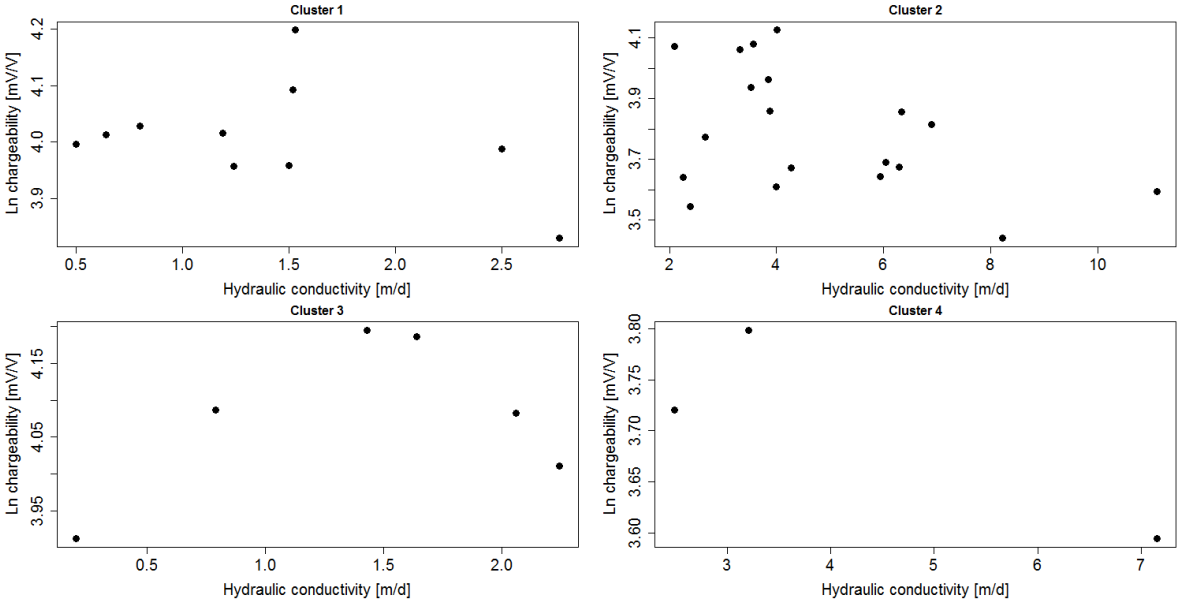

Figure 85 Scatterplots of hydraulic conductivity versus ln(chargeability) for data within the clusters, based on visual correlation between K and ρ.

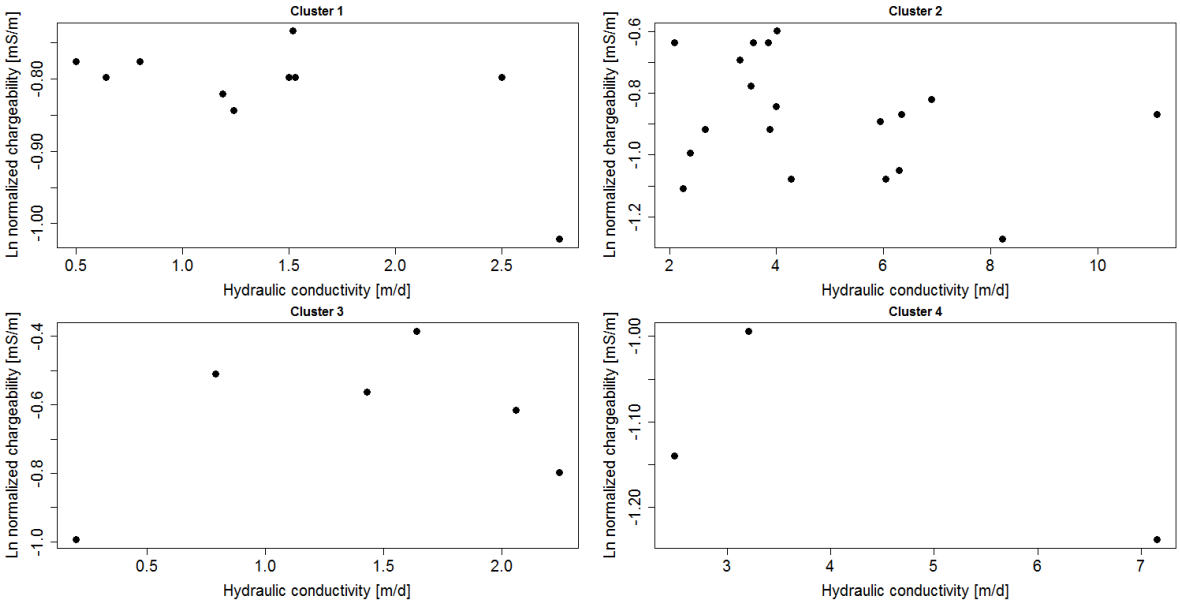

Figure 86 Scatterplots of hydraulic conductivity versus ln(normalized chargeability) for data within the clusters, based on visual correlation between K and ρ.

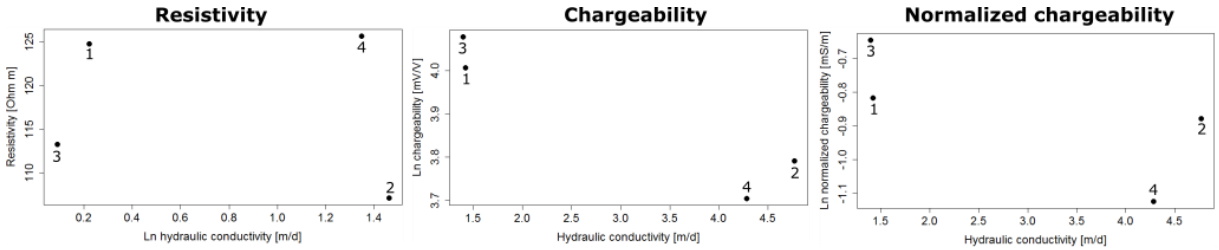

Figure 87 Scatterplots of the mean values of the parameters in the clusters, based on visual correlation between K and ρ. The numbers indicate the number of the cluster.

C. DENDROGRAMS OF CLUSTER ANALYSES

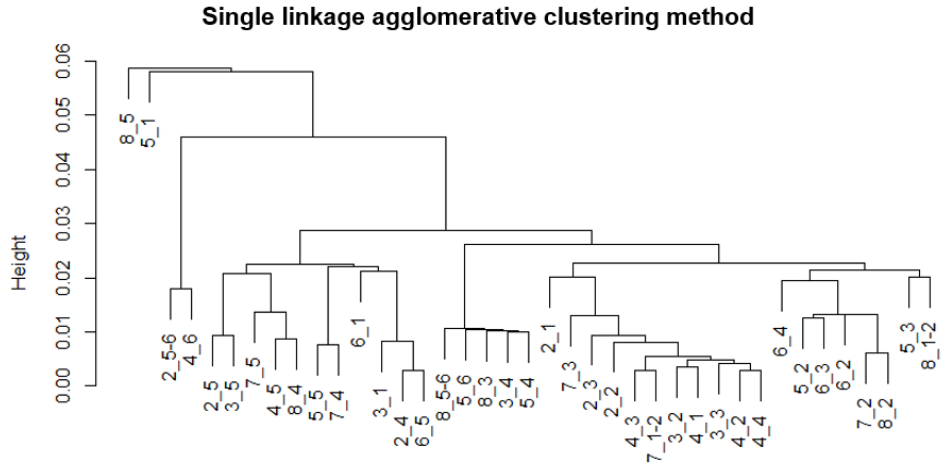

Figure 88 Dendrogram of the single linkage agglomerative clustering method. The point numbers are indicated as 'profile _ point in profile' (point 1 in a profile is at the left bank). These numbers are indicated on the point maps of the Cluster Analysis in the main text.

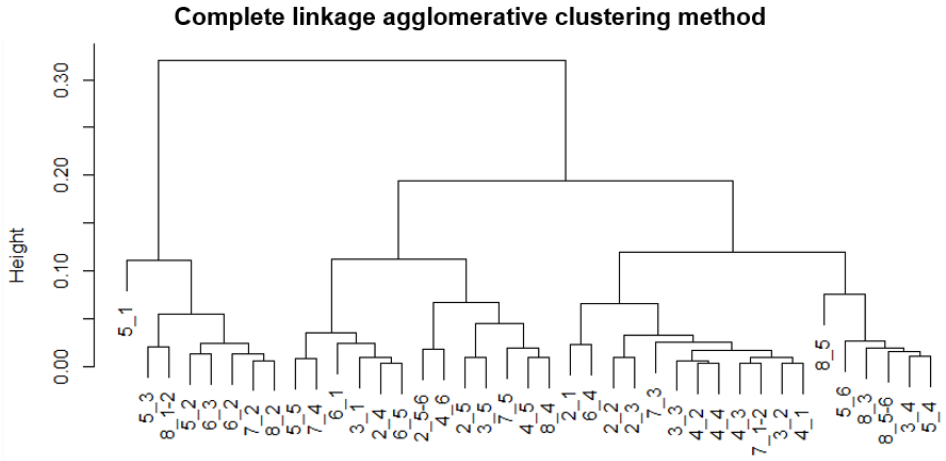

Figure 89 Dendrogram of the complete linkage agglomerative clustering method. The point numbers are indicated as 'profile _ point in profile' (point 1 in a profile is at the left bank). These numbers are indicated on the point maps of the Cluster Analysis in the main text.

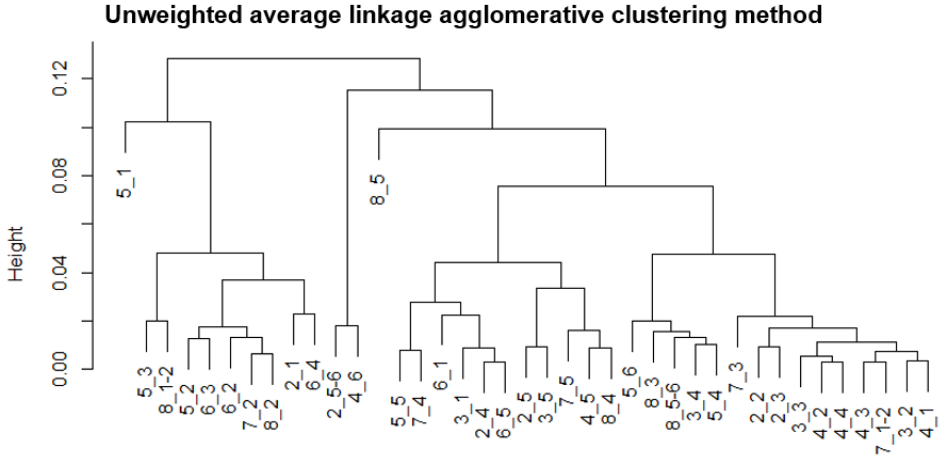

Figure 90 Dendrogram of the UPGMA cluster method. The point numbers are indicated as 'profile _ point in profile' (point 1 in a profile is at the left bank). These numbers are indicated on the point maps of the Cluster Analysis in the main text.

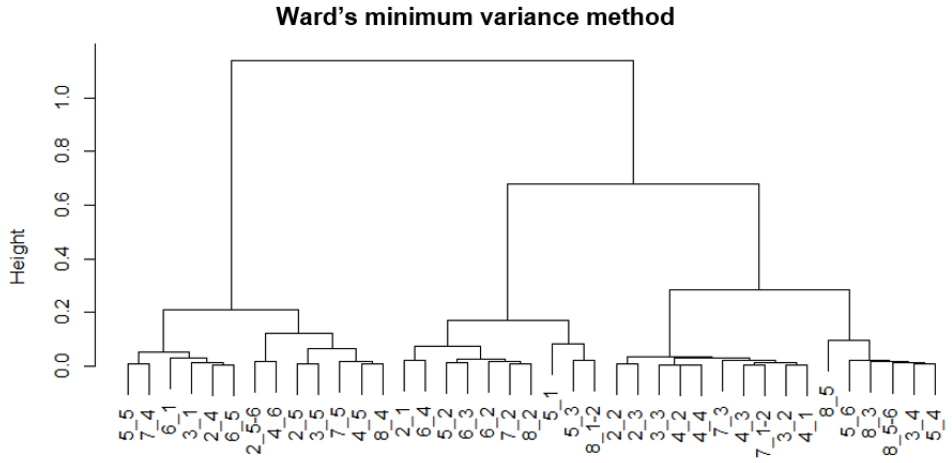

Figure 91 Dendrogram of Ward's minimum variance method. The point numbers are indicated as 'profile _ point in profile' (point 1 in a profile is at the left bank). These numbers are indicated on the point maps of the Cluster Analysis in the main text.

d. SCATTERPLOTS OF CLUSTERING BASED ON CLUSTER ANALYSIS

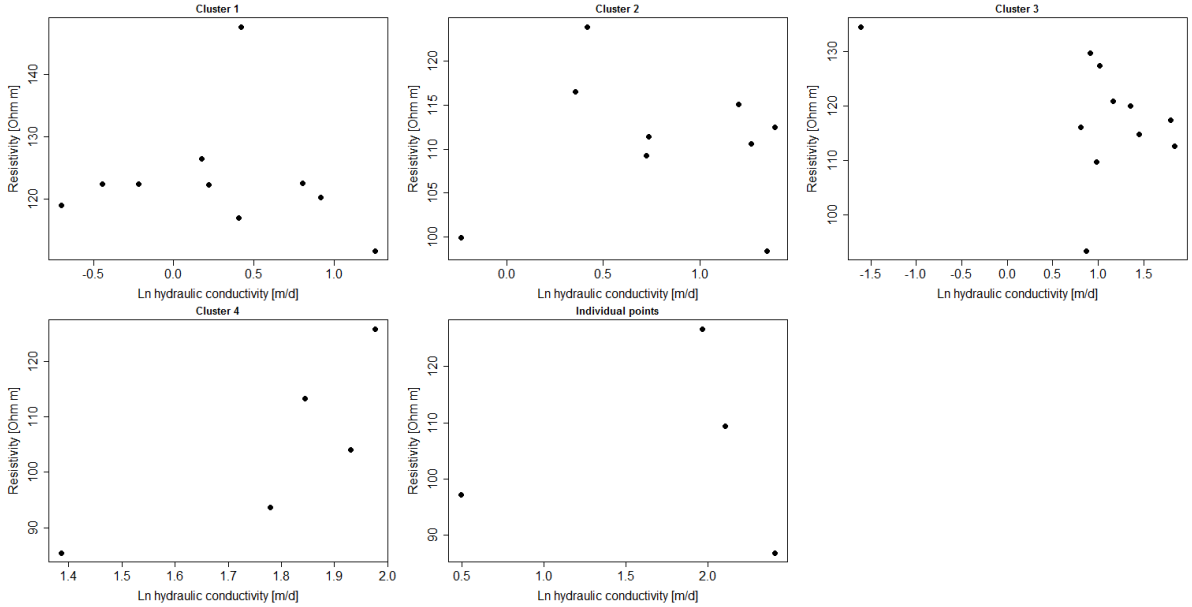

Figure 92 Scatterplots of ln(hydraulic conductivity) versus resistivity for data within the clusters, based on UPGMA clustering.

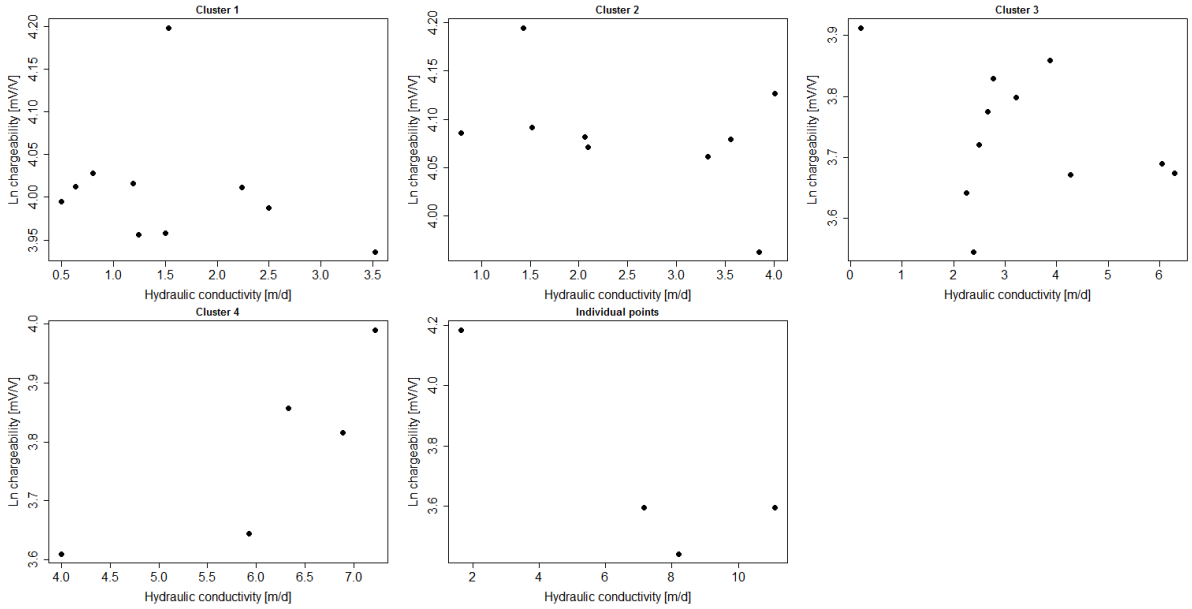

Figure 93 Scatterplots of hydraulic conductivity versus ln(chargeability) for data within the clusters, based on UPGMA clustering.

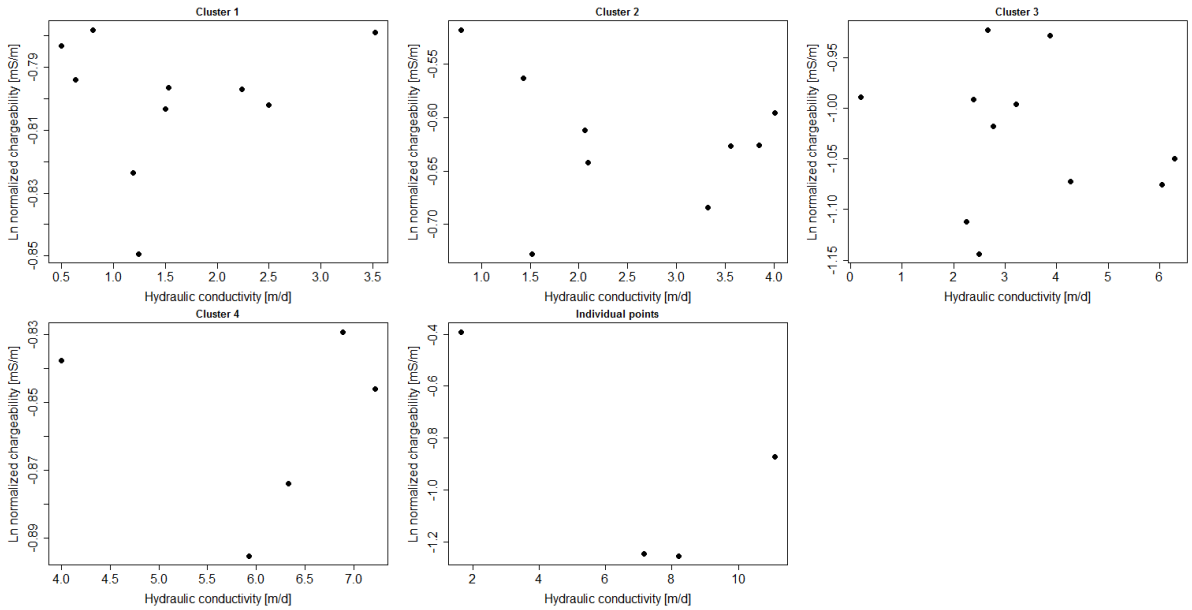

Figure 94 Scatterplots of hydraulic conductivity versus ln(normalized chargeability) for data within the clusters, based on UPGMA clustering.

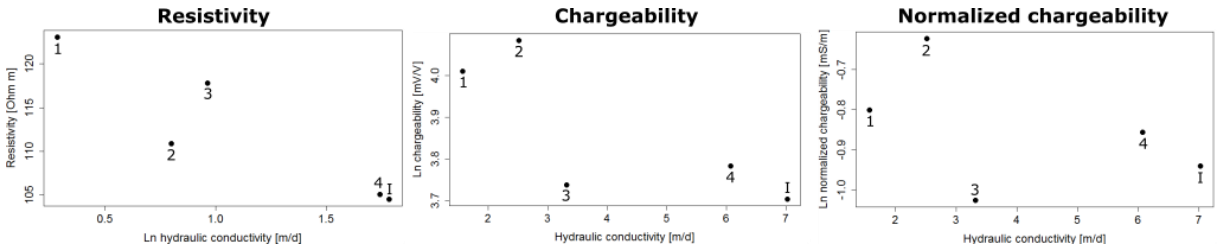

Figure 95 Scatterplots of the mean values of the parameters in the clusters, based on UPGMA clustering. The numbers indicate the number of the cluster. 'I' indicate the mean of the individual points, not included in a cluster.

AFDELING GEOLOGIE
Celestijnenlaan 200 E bus 2408
3001 LEUVEN, BELGIË
tel. + 32 16 32 64 60
fax + 32 16 32 29 80